



*Florida Department of Transportation
Central Structures Office*

**TEST AND ASSESSMENT OF NDT METHODS
FOR POST-TENSIONING SYSTEMS IN SEGMENTAL
BALANCED CANTILEVER CONCRETE BRIDGES**



DMJM HARRIS

February 15, 2003

Preface

Recent corrosion-related failures of post-tensioning tendons on various segmental concrete bridges, in the state of Florida, has risen a tremendous concern on the reliability and durability of these structures. As a result, the Florida Department of Transportation, in collaboration with the Federal Highway Administration, has taken the initiative to study various types of non-destructive testing (NDT) methods for internal post-tensioning systems of balanced cantilever concrete bridges. The object of the project is to test and assess their reliability and accuracy in detecting these types of problems. The project has also taken the advantage of examining an existing segmental cantilever bridge, located at the Fort Lauderdale International Airport, Fort Lauderdale, Florida, prior to its demolition due to the airports recent expansion design. The study has been managed by Mr. Larry Sessions, P.E., Senior Structures Design Engineer, FDOT Central Structures Office.

The non-destructive testing methods that were used in this program are as follows: Impulse Radar Testing, Impact Echo Testing, Magnetic Flux Leakage Method and the High Energy Linear Accelerator Inspection. Each of these testing methods were implemented on the Fort Lauderdale Airport segmental concrete bridge. The testing methods were monitored and the results investigated and verified through use of Endoscope Inspection, Core Drilling and visual inspection during the dismantling of the bridge.

A detailed explanation of each inspection method as well as a basic summary of the test method concept is herein reported along with the test results, pictures and field notes. Conclusions and recommendations for each of the NDT methods of this assessment program are included in this report. Based on the results of the testing program, recommendations are provided for inspecting segmental balanced cantilever bridges.

Acknowledgements

The authors wish to express their gratitude to William Nickas, FDOT Central Structures Office; Glen Washer and Habeeb Saleh, FHWA NDT Validation Center; Jorge Martos, Jose Quintana, Alberto Sardinias and Edwin Radson, FDOT District 4 Structures and Facilities; Scott Updegrave, PCL Civil Contractors; Aimee Yocca, O'Brien-Kreitzberg (URS) for their invaluable assistance in this project

Disclaimer

The information presented within this report represents research and development with regard to improving the inspection procedures of internally post-tensioned bridges in Florida. The use of the information within this report, other than as a guide to improve the inspection procedures of internal post-tensioning, can not be ensured. The opinions, findings and conclusions in this report are those of the authors and do not necessarily reflect the views of the FDOT, the FWHA, nor the individuals and organizations acknowledged above.

TEST AND ASSESSMENT OF NDT TESTING METHODS FOR POST-TENSIONING SYSTEMS IN SEGMENTAL BALANCED CANTILEVER CONCRETE BRIDGES

Table of Contents

Preface	1
Acknowledgement	1
Disclaimer	1
Executive Summary	Ex-1
Table of Contents	Co-1
Chapter 1 – Introduction	
1.1 Overview	Ch1-1
1.2 Project Description	Ch1-1
1.3 Bridge Description – Ramp D Fort Lauderdale-Hollywood International Airport	Ch1-2
Chapter 2 – Endoscope Inspection	
2.1 Introduction	Ch2-1
2.2 Description of Endoscope Inspection	Ch2-1
2.2.1 Locating Tendon Ducts	Ch2-6
2.2.2 Performing Endoscope Inspection	Ch2-6
2.2.3 Endoscope Inspection Results	Ch2-8
2.3 Summary and Conclusion	Ch2-9
Chapter 3 – Impulse Radar Testing	
3.1 Introduction	Ch3-1
3.2 Impulse Radar Concept	Ch4-1
3.3 Field Testing	Ch3-1
3.4 Summary and Conclusions	Ch3-2
Chapter 4 – Impact Echo Testing	
4.1 Introduction	Ch4-1
4.2 Basic Theory on Stress Wave Propagation	Ch4-1
4.3 Impact-Echo Testing Applied to Testing of Bonded Post-tensioned Tendons	Ch4-3
4.4 Field Testing	Ch4-6
4.5 Constructions Technology Laboratories, Inc. (CTL) Impact-Echo Testing	Ch4-6
4.6 Professor Al Ghorbanpoor Impact Echo Testing	Ch4-11
4.7 Summary and Conclusions	Ch4-14

Chapter 5 – Magnetic Flux

5.1	Introduction	Ch5-1
5.2	Magnetic Flux Leakage Concept	Ch5-1
5.3	Testing Equipment	Ch5-3
5.4	Laboratory Study	Ch5-5
5.5	Field Testing	Ch5-6
5.6	Summary and Conclusions	Ch5-9

Chapter 6 – High Energy Linear Accelerator Inspection

6.1	Introduction	Ch6-1
6.2	Equipment	Ch6-2
6.3	Testing Procedure	Ch6-2
6.4	Film Processing and Results	Ch6-3
6.5	Summary and Conclusions	Ch6-5

Chapter 7 – Bridge Demolition and Inspection of Existing Ramp D Structure

7.1	Introduction	Ch7-1
7.2	Ramp D Demolition Description	Ch7-1
7.3	Evaluation of Existing Ramp D Structure	
7.3.1	Visual Inspection	Ch7-5
7.3.2	Endoscope Inspection	Ch7-7
7.3.3	Inspection of Remains	Ch7-8
7.3.4	Inspection of Segments	Ch7-9
7.4	Evaluation of Segment Epoxy Joint Quality	Ch7-12

Chapter 8 – Conclusions and recommendations

8.1	Conclusions	Ch8-1
8.1.1	Endoscope Inspection	Ch8-1
8.1.2	Impulse Radar Testing Method	Ch8-1
8.1.3	Impact-Echo Testing Method	Ch8-1
8.1.4	Magnetic Flux Leakage Method	Ch8-2
8.1.5	High Energy Linear Accelerator	Ch8-2
8.2	Recommendations	Ch8-3

References

Appendix A – Endoscope Results	A1
Appendix B – Damage Induced to Post-Tensioning Tendons	B1
Appendix C – Core-Drilling Results	C1
Appendix D – Forensic Investigation of Dismantled Bridge	D1
Appendix E – CTL Report	E1

Appendix F – Professor Al Ghorbanpoor Report

F1

Appendix G – HESCO Report

G1

Executive Summary

The failure of several post-tensioning tendons in the Niles Channel and Mid-Bay bridges in Florida due to poor workmanship and inadequate grouting has raised questions about the integrity of post-tensioning tendons in existing concrete segmental bridges. The need to assess the condition of post-tensioning tendons in existing Florida bridges has prompted the Florida Department of Transportation to fund a study, with collaboration from the FHWA, on the accuracy of several Non-Destructive Testing (NDT) methods in a real case scenario. The program involves the use of selected NDT methods to assess the status of the top slab post-tensioning tendons of Ramp D located in the interchange at the Fort Lauderdale-Hollywood International Airport. This precast balanced cantilever concrete box girder bridge is being demolished as part of the airport expansion thus permitting the verification of the NDT findings via dissection of the concrete segments. The NDT methods to be examined are: Impulse Radar, Impact-Echo, Magnetic Flux Leakage and High-Powered X-Ray Imaging. The tests were performed in late March 2002 by three independent sub-consultants with overall project management provided by DMJM+HARRIS. This report will provide a description of the procedures used by the sub-consultants to utilize these NDT methods to evaluate an existing concrete bridge, and will present conclusions on the accuracy of the NDT findings. The accuracy of the NDT findings have been evaluated by core drilling in the deck and visually inspecting the tendons.

The assessment of the NDT methods provided the following conclusions:

Endoscope Inspection

The use of the endoscope to evaluate the condition of top slab tendons was found, in this testing program, to be a reliable testing method. Testing, at a given point in the deck, was done in an average of 10 minutes and required a four-person crew. The endoscope inspection should be preceded by more economical NDT testing methods that locate areas where tendon flaws (void, corrosion, loss of section, etc) are most likely to exist. Also, it is critical for drilling to be done with much care in order to avoid damaging the tendons at the time of inspection. The use of special concrete drills capable to detect the steel duct and stop before damaging it is recommended. And finally, after inspection, drilled holes should be appropriately patched to avoid any future maintenance and durability problems.

Impulse Radar Testing Method

The impulse radar testing method provided quick and accurate location of the tendons. The method requires small size equipment that can be operated by a two-person crew. A test at a given point can be done in less than one minute. Although the location of the tendons at the segment joints was performed accurately based on the contract drawings information, the location of these tendons between segment joints could not be ascertained based on this information only. At these locations Impulse Radar was 80% reliable in locating the tendons. The method can provide not only the horizontal location

of the tendon but also the depth into the concrete, which can be of tremendous value in the interpretation of the Impact Echo results.

Impact-Echo Testing Method

The Impact-Echo testing method was found to be a reliable method to identify grout voids in tendon ducts provided that a combination of techniques including impulse radar and rebar locators are used. In addition, invasive endoscopy tests are required to correlate the interpretation of the signals with the existing conditions (deck 3-D geometry, nearby tendons and mild steel, etc.). The reliability of the method (defined as detecting large voids) was found to be higher than 60% in this testing program. Locating the testing point and performing the test can be done in less than 3 minutes with very small equipment operated by a two-person crew. The method is effective in providing a clear indication of a sudden discontinuity in material properties and distinguishing whether this discontinuity represents a void or a stiffer material (the tendon). However, the size of the void, (an essential factor in assessing its importance and possible consequences), is difficult to ascertain.

Magnetic Flux Leakage Method

The testing performed using the MFL method was, for practical purposes, found inadequate to identify losses of tendon area. The method failed to locate the tendons with the induced flaws in anchor trumpets. The reason being that the equipment used, did not have magnets strong enough to magnetically saturate the tendons and consequently, produce the flux to leak. The method, as this stage, does not provide the necessary confidence in the method (in its current condition) for practical applications. The MFL method is fast in terms of data acquisition. However, it requires careful and expert interpretation of the test record. A major drawback of this method is that it requires a very accurate depiction of the tendon path at the roadway surface, which, in turn, requires the extensive use of another testing methods such as Impulse Radar.

High Energy Linear Accelerator

This procedure was found to have the potential to be a very effective method for locating flaws in tendons deeply embedded in the concrete. It provided a relatively clear view of the elements inside the concrete. To be most effective, the interpretation of the film should be performed by an expert in both concrete bridges and x-rays. At this moment, the method is very expensive, very cumbersome to use, and requires a large amount of heavy equipment and a large crew size. In addition, the scatter of the x-ray beam requires that a large radius around the testing area to be evacuated to avoid health issues. In the future, if more compact equipment is developed for use in bridges, this method could be a valuable tool for the inspection of post-tensioned bridges.

Based on the results of the study, the authors recommend the following steps for the inspection of tendon in existing balanced cantilever concrete box girder bridges:

- Step 1 –** Examination of existing records and information, such as Contract Plans, Shop Drawings, As-built Plans and previous inspection reports.

- Step 2 –** Perform a detailed visual inspection of the bridge. The recommendations stated in the Florida Department of Transportation document titled “Post Tensioned Bridges Walk Through Inspections”, can be used for this purpose.
- Step 3 –** Depending on the results of the visual inspection the following scenarios are possible:
- a) If the visual inspection does not reveal deficiencies that may affect the integrity of the post-tensioning system, no further action is needed. On the other hand, if the bridge has been in service for a number of years (say 10) and an in-depth inspection is warranted, then prepare a plan for inspecting the bridge using a combination of NDT testing (Impulse Radar and Impact-Echo) and invasive techniques (Endoscopy Inspection). The testing should be done on a representative sample of the tendons, at most 10%, 2002. The tendons to be tested and the test location on the tendons should be based on their structural importance.
 - b) If the visual inspection reveals significant deficiencies such as water leakage at segment joints, efflorescence, concrete cracking or spalling; prepare an inspection plan combining impact echo an endoscopy inspection. In this case, however, the areas with significant deficiencies should be inspected in detail and, if deemed necessary, all tendons should be inspected. Other areas should be inspected following the 5% rule stated above.
- Step 4 -** If an inspection combining NDT testing techniques and invasive techniques is deemed necessary, then proceed as follows:
- a) Use a combination of as-built plans, impulse radar and rebar locators to locate the embedded steel components including both reinforcing steel and post-tensioning tendons. Mark the location of the embedded steel on the concrete surface.
 - b) Artificially divide the tendons in sections (approximately five feet long each) and select a sample based on an statistically-based method like those employed in quality control programs.
 - c) Investigate the selected sample for tendon voids using the Impact-Echo method. Calibrate the signal interpretation using the knowledge of embedded steel components and deck 3-D geometry with drilling and endoscopy. Using the calibrated signal interpretation complete the inspection of the selected samples. If the inspection does not reveal

significant deficiencies and a high percentage of the test locations (say 95%) indicate no relevant voids, take no further actions. If other conditions exist, verify void relevance and strand integrity by drilling and inspecting with a flexible shaft endoscope.

- d) If the flexible shaft endoscope inspection find significant voids and strand corrosion, then expand the sample size.
- e) At each drilled hole determine the volume of the void by using a vacuum or a pressure device. If this volume is large then repair the void using vacuum grouting.
- f) Upon completion of the inspection clean the hole and repair the drilled hole with a fluid epoxy for the repair of old structures (like FDOT Type E).

Chapter 1 – Introduction

1.1 Overview

Florida is one of the leading states in the construction of post-tensioned bridges, especially in segmental concrete bridges. Recently, corrosion-related failures of post-tensioning tendons have been found in several major segmental bridges. In the spring of 1999, a corrosion related failure of an external tendon was found in the Niles Channel Bridge near Key West, Florida. Similarly, in August 2000, one failed external tendon and one partially failed external tendon (5 failed strands out of 19) were found in the Mid-Bay Bridge near Destin, Florida. Subsequent inspections of this bridge resulted in the removal and replacement of nine additional tendons. These problems appear to be related to lack of corrosion protection due to the absence of grout at the tendon anchorages. In addition to these cases in September 2000, corrosion damage was found in two vertical external tendons in one of the piers of the Sunshine Skyway Bridge near Tampa, Florida. At the I-75/I-595 Sawgrass Interchange, composed of fourteen precast box girder segmental cantilever bridges with bonded internal tendons, the Florida Department of Transportation found efflorescence at some of the anchor blocks and water leakage at some joints. During the repair process of some of these tendon ducts, it was found that some of them did not contain any grout. The above-mentioned problems have therefore raised a tremendous concern about the durability and structural performance of these types of structures.

1.2 Project Description

These grouting related problems prompted the Florida Department of Transportation (FDOT) to fund a field study (with the collaboration of the Federal Highway Administration) to evaluate the capability of several Non-Destructive Testing (NDT) methods to detect grout voids and strand corrosion of internal post-tensioning tendons. The NDT methods examined are: Impulse Radar, Impact-Echo, Magnetic Flux Leakage and High-Powered X-Ray Imaging. The results of this study will assist the FDOT to develop recommendations for appropriate inspection methods of internal tendons.

The project participants are as follows:

- **Funding** **FDOT Central Structures Design Office**
Tallahassee, FL
FHWA , NDE Validation Center
McLean, VA

- **Project Manager** **DMJM+HARRIS, Inc.**
Tallahassee, FL

- **Consultants**
 - Construction Technology Laboratories, Inc**
Skokie, Ill
 - Al Ghorbanpoor, Ph.D., P.E. Consulting Engineer**
Milwaukee, WI
 - High Energy Services Corporation**
La Honda, CA

In addition, the **FDOT District Four Structures and Facilities Department** provided substantial manpower and equipment during all testing and maintenance of traffic phases. Coordination with the Fort Lauderdale Airport and field construction was accomplished with the assistance of **O'Brien Kreitzberg (URS)**, the airport consultant; and of **PCL Civil Contractors**, the contractor for the airport roadway expansion, which also provided equipment for X-Ray testing.

To develop conclusions about the capabilities of the NDT methods, they need to be applied to a real structure under real field conditions and their findings be compared with visual inspection of the dissected tendons at the test locations. The opportunity to perform the study under very real field conditions presented itself with the work to be performed during the expansion of the Fort Lauderdale-Hollywood International Airport. A critical component of airport infrastructure expansion is the improvements to the terminal area roadways to provide basic circulation capacity. In order to develop this enhanced access, the plan included the construction of eight cantilever concrete segmental bridges and the demolition of three of the existing cantilever concrete segmental bridges. This allowed the FDOT to use one of the bridges to be demolished (Ramp D Bridge) as a testing ground without the future consequences caused by the damage induced in the structure during the dissection of the tendon locations tested.

1.3 Bridge Description – Ramp D Fort Lauderdale-Hollywood International Airport

The Ramp D Bridge is a curved continuous balanced cantilever concrete segmental box girder superstructure consisting of seven spans, ranging from 87 feet to 145.5 feet in length (Fig. 1.1 and 1.2). The NDT evaluation was limited to the post-tensioning cantilever tendons in the top slab in Spans 5, 6, and 7, with span lengths of 125.8, 145.5, and 97.5 feet, respectively.



Figure 1.1 - Aerial photo of the Fort Lauderdale-Hollywood International Airport before Expansion. Ramp D Bridge is shown at the left above U.S. 1.

The bridge was erected using the balanced cantilever construction method with precast concrete boxes that were post-tensioned with internal longitudinal and transverse tendons. The longitudinal post-tensioning tendons generally consisted of 12 – ½ inch diameter 270 ksi low relaxation strands that were placed inside of galvanized ducts with 2 5/8 inches diameter. The available structural drawings indicate that the deck thickness over the wing and between the webs of each box varies between 8 and 9 inches. The distance between the center of each duct and the top of the deck was 5.25 inches. Ten to fourteen longitudinal tendons were located in the deck at the vicinity of each web of the box cross section. Each tendon is anchored at a segment face in the vicinity of the web. The Plan and Elevation, Typical Section and Top Tendon Layout contract drawings of the Ramp D bridge are presented below in Figures 1.3, 1.4 and 1.5, respectively.



Figure 1.2 - View of Ramp D Bridge Span 6 over U.S. 1.

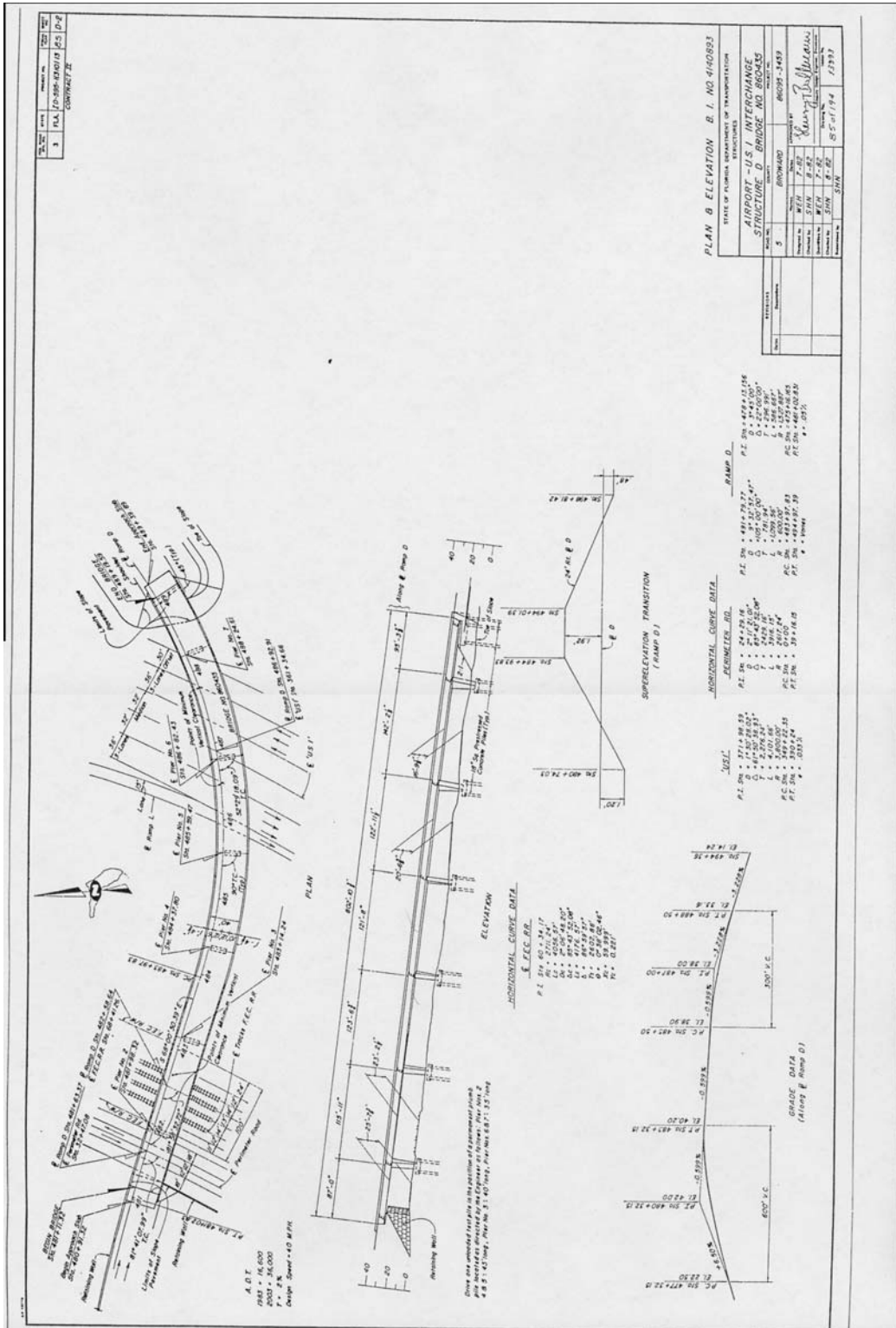


Figure 1.3 – Plan and Elevation

Chapter 2 – Endoscope Inspection

2.1 Introduction

Prior to commencing the implementation of the Non-Destructive Testing Methods of this program an assessment of the actual conditions of the top slab post-tensioning tendons was performed. Through this assessment an initial record of the type and magnitude of the tendon flaws were obtained (grout voids in the ducts and corrosion of the strands). This information was initially used to plan and organize the Non Destructive Testing Program as well as to verify the results obtained from the various testing methods.

2.2 Description of the Endoscope Inspection

A set of testing points in the top slab cantilever tendons and their anchors at Spans 5, 6 and 7 were inspected using a flexible endoscope to locate areas where tendons contain voids and other flaws. The Florida Department of Transportation, District 4 Structures and Facilities Department provided the equipment and the personnel to perform the inspection work, while the consultant provided a structural engineer to oversee and direct the inspection operation; like, locating the tendons, evaluating the video images, and taking notes of the findings and making decisions regarding to the need for further inspection.

Figures 2.1a and 2.1b show a schematic layout of the top tendons (cantilever tendons) at Spans 5, 6 and 7, along with the location of the endoscope inspection points. As shown in these figures, the inspection was performed at Segments 54, 56, 57, 58 and 64 in Span 5. In Span 6, the inspection points are within Segments 69, 71, 72, 76, 79 and 81, while at Span 7 the segments inspected were 86, 88 and 89. The inspections were performed on both wings (left and right).

No as-built drawings associated with the bridge were available. Therefore, the information in the contract drawings was used to locate the tendons. Still, the tendon layout information shown in the contract drawings was contradictory. On one hand, the top tendon layout drawing (drawing No. 117, Figure 2.2) shows that the tendons transition from the tendon anchor located at the web to the actual tendon position over the piers by transitioning one duct hole per segment. On the other hand, the details of the top tendon geometry (drawing No. 160, Figure 2.3) show a different tendon transition arrangement. The transition, in this case, is done in a shorter distance, skipping some of duct holes between segments. As this drawing (drawing No. 160) had a more recent date it was decided to use this information to locate the tendons. The contract drawing illustrates the cantilever tendons consisting of 12-1/2"Ø low-relaxation strands with an ultimate strength of 270 ksi. Metallic ducts, with a diameter of 2 3/8", are shown approximately 4" from the top surface of the deck.

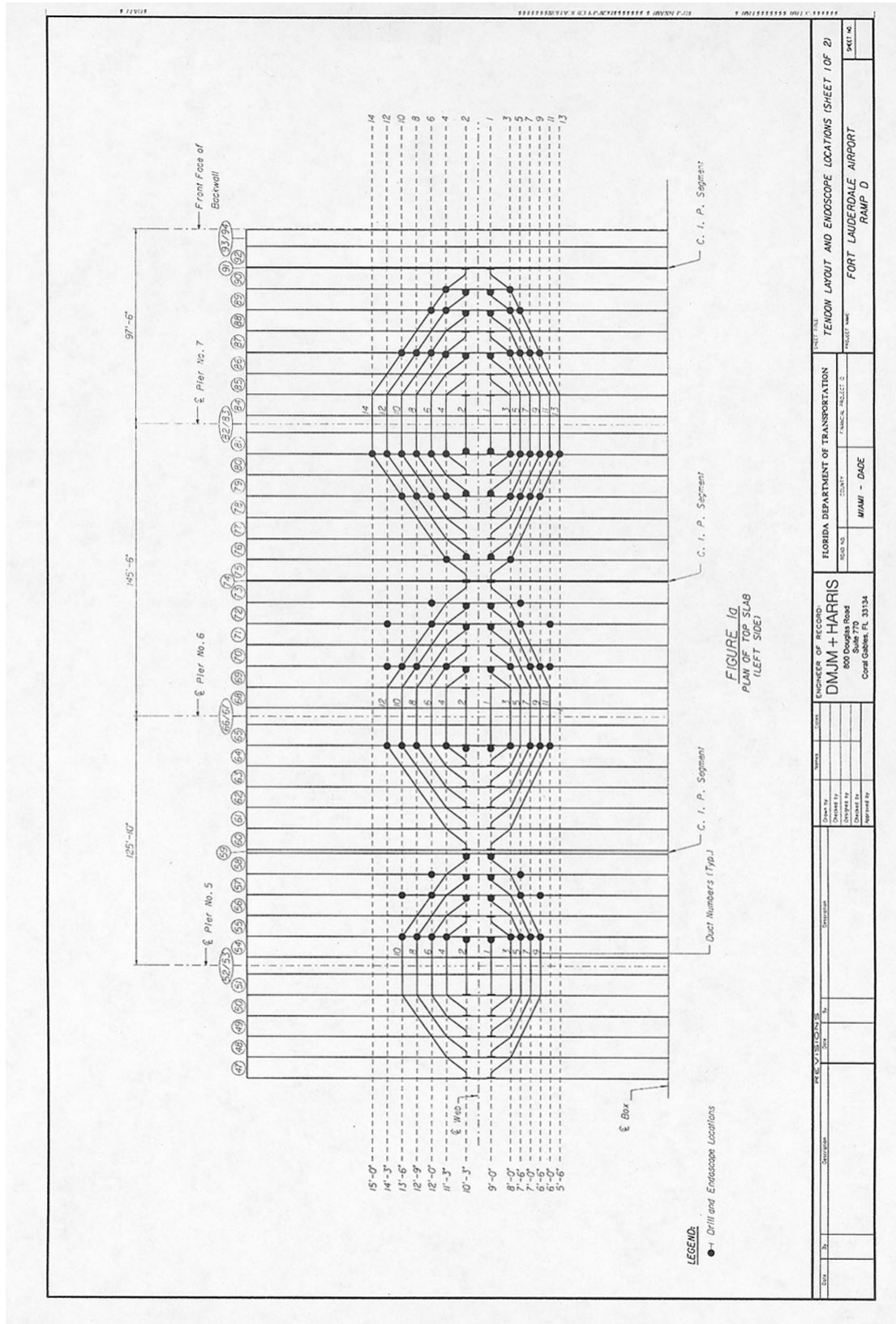


Figure 2.1a – Endoscope Inspection Points

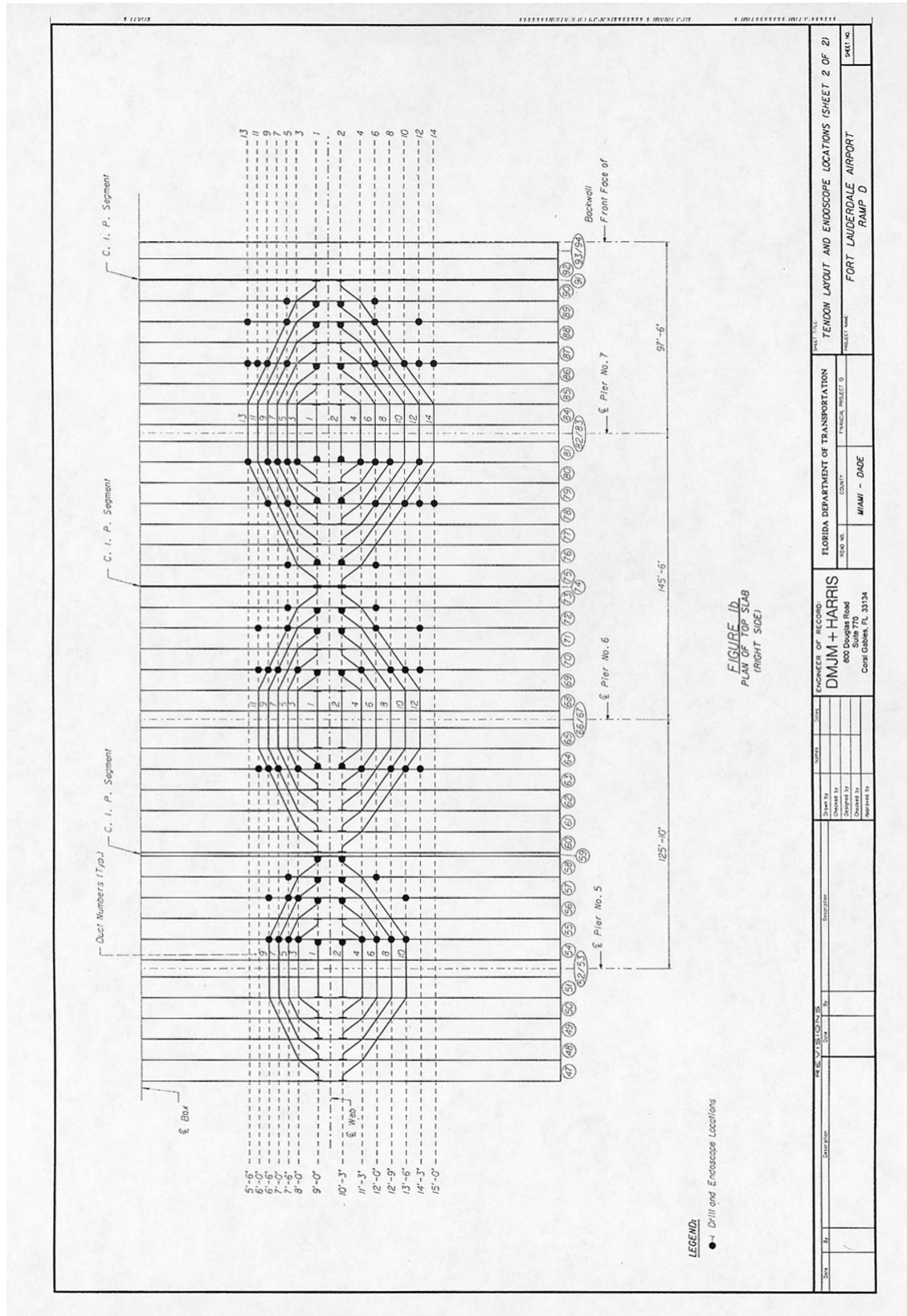


Figure 2.1b – Endoscope inspection points

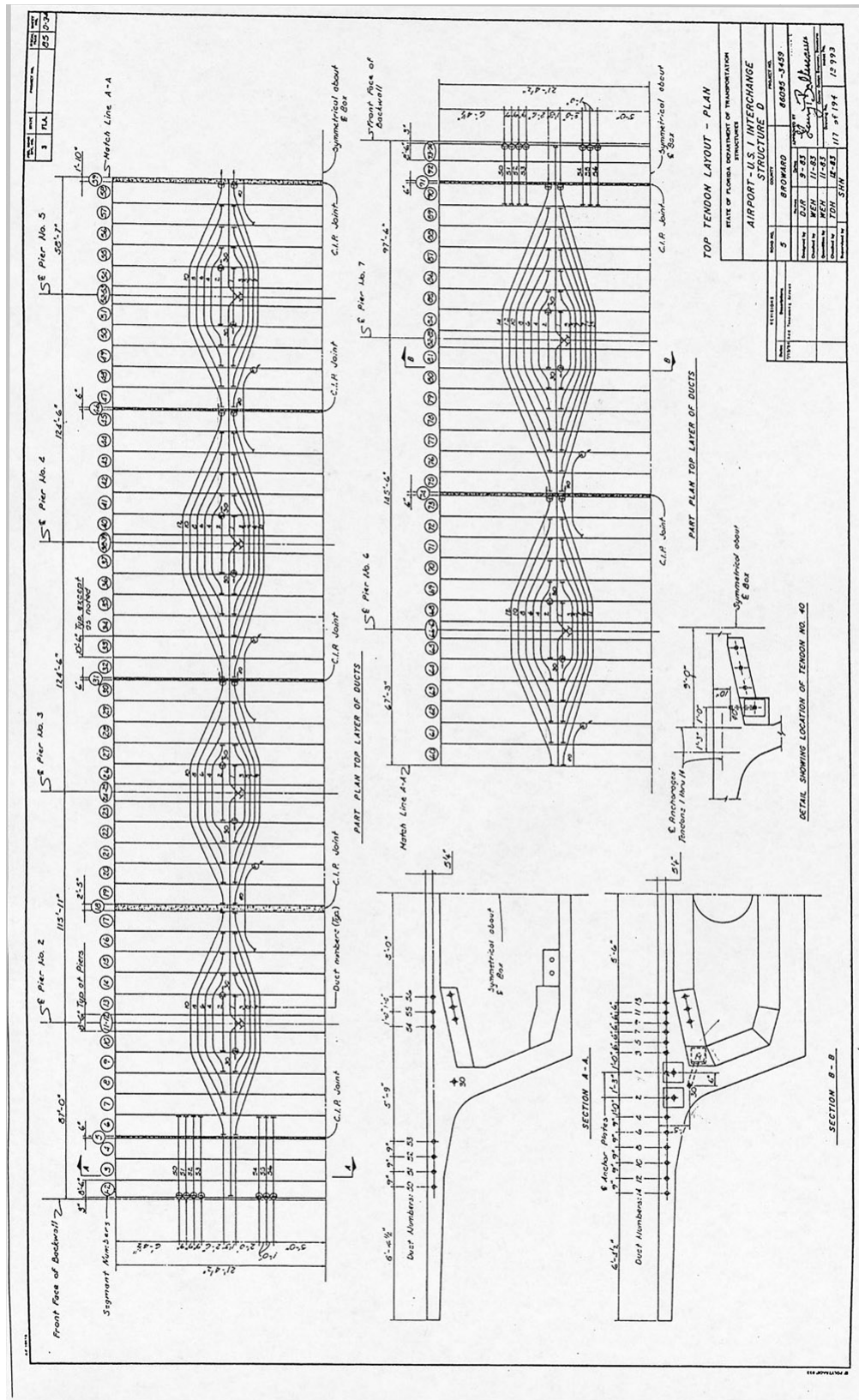


Figure 2.2 – Contract Drawing 117

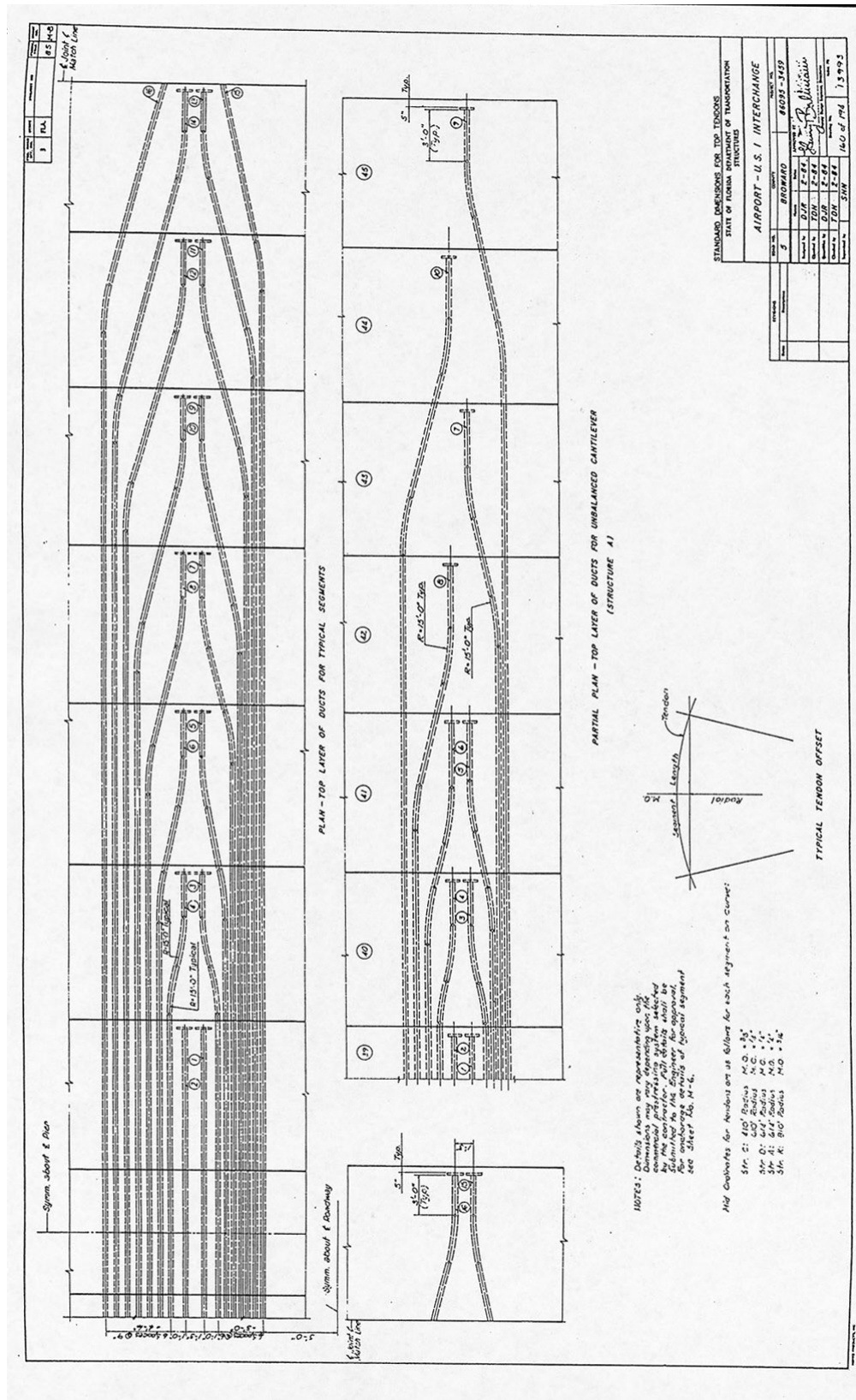


Figure 2.3 – Contract Drawing 160

2.2.1 Locating Tendon Ducts

The tendons were located in the field by first identifying the segments. This was done without much difficulty, since the segment joints were clearly visible along the bridge deck. Once the segment was identified the location of the tendon was found by measuring its offset from the centerline of the box. The centerline of the box was located from the remains of the original hairpin stirrups in the concrete deck that were used for the horizontal geometric control of the bridge construction. The inspection points were located at 1½” from the segment joints in order to avoid conflicts with the segment reinforcing bars. This distance was increased to 12” at tendon anchor locations. Figure 2.4 shows a photograph that illustrates the process of locating the tendon in the field.



Figure 2.4 – Locating the tendons in the top deck

2.2.2 Performing Endoscope Inspection

Once the tendon locations were marked on the deck surface, ¾”Ø holes were drilled into the deck. Drilling was typically required to a depth of 4” before reaching the tendon duct. In most cases, the tendon ducts were located by determining the difference in resistance to drilling provided by the tendon grout or tendon void as compared to drilling in the segment concrete. After the drilling operation was complete, the holes were cleaned with pressurized air.



Figure 2.5 – Viewing the Endoscope video

A typical inspection team consisted of an inspector that operated the endoscope in the drilled hole, and an inspector controlling the video recording equipment. Two or three other members of the team provided support services like drilling and cleaning the holes, moving the light stands, etc. The consultant engineer kept a written log documenting the inspection including the depth and length of voids, conditions of the strands if they were visible, etc. Figure 2.5 shows a photograph of the endoscope inspection operation while Figure 2.6 shows photographs of an endoscope inspection of different tendons.

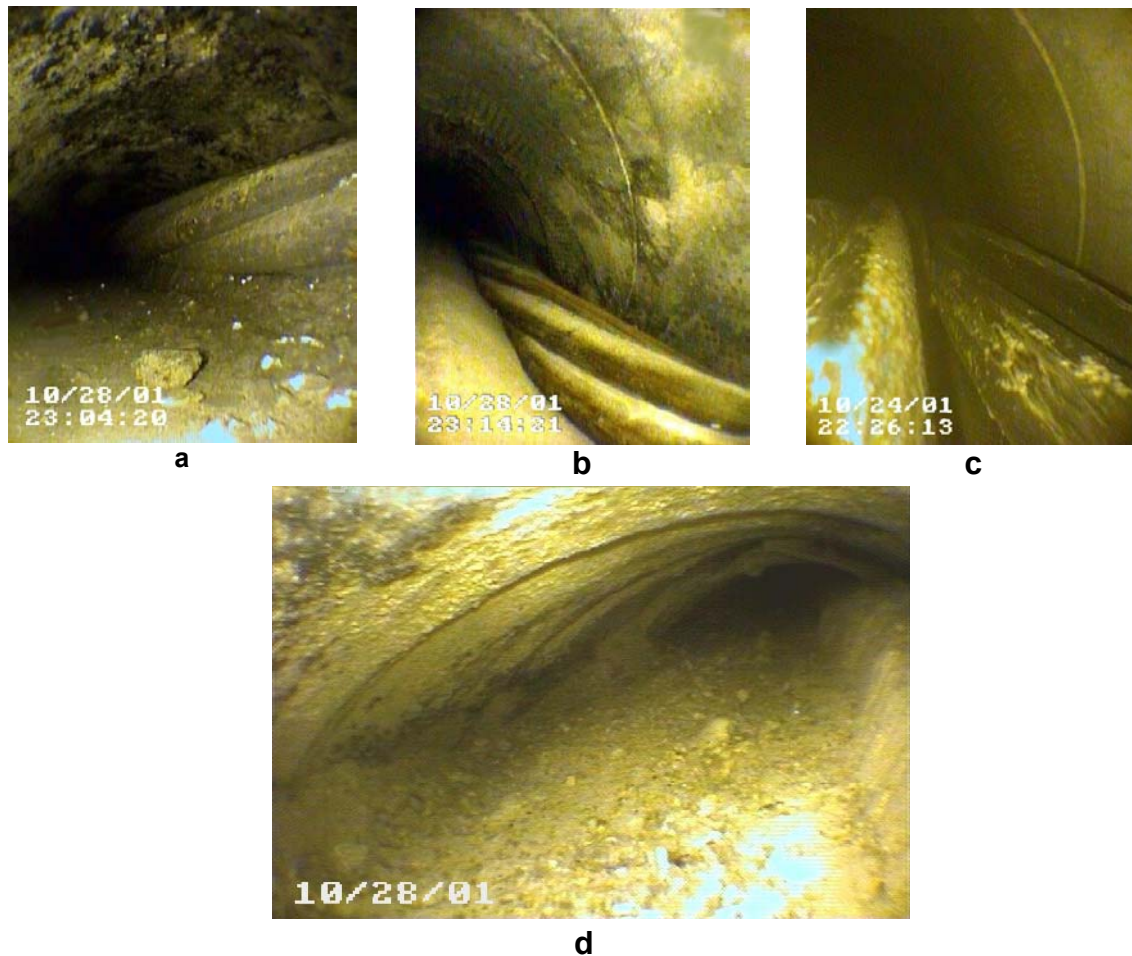


Figure 2.6 – Photos a and b show duct partially grouted with strand exposure. Photo c shows voided duct with strands fully exposed. Photo d shows partially grouted duct, no strands exposed.

During the inspection a number of tendons could not be located, which indicated the possibility that the actual tendon layout did not follow the geometry indicated in contract drawing No. 160. During the last day of inspection, the tendons were located using the geometry indicated in contract drawing No. 117 (transition from anchor to actual tendon location by transitioning one duct hole per segment). That day all tendons were located. This indicated that the actual tendon layout most likely followed the geometry in drawing No. 117.

2.2.3 Endoscope Inspection Results

The results of the inspection are shown graphically in Figures 2.7, 2.8a and 2.8b. A summary of the results is as follows:

Tendon locations inspected:	198
Fully grouted tendons	95
Voided tendons	61
Small voids	48
Large voids with exposed tendons	10
Voids with water present	3
Drilled, but not located	42

It appears that the small voids were the result of bleed water accumulation and subsequent evaporation. The large voids with exposed tendons were the obvious result of poor grouting procedure. In most of these locations the strands presented moderate signs of superficial corrosion. Voids with water present were probably due to deck cracks at duct joint locations, and in these cases it was not possible to assess the conditions of the strands (exposure and signs of corrosion) due to the difficulties of using the endoscope in a humid environment.

The inspections were performed at night during the week of October 21, 2001. The total inspection operation was completed in 5 nights. The work was performed with traffic in the bridge. The FDOT District Four Structures and Facilities Department provided the maintenance of traffic which consisting in blocking the half portion of the roadway where the inspection was being performed. The field logs of the endoscope inspection along with photographs taken within the voided tendons are shown in Appendix A.

In general, the procedure of locating the tendons based on the offset from the centerline of the box, as indicated in the contract drawings, was very precise. This is due to the fact that the points inspected were located very close to the joints and, consequently, the as-built conditions presented only insignificant discrepancies from the locations shown in the contract drawings. However, of the 198 locations inspected, the tendons were only located at 156 locations or 79% of the total location inspected. This was due mainly to the confusion created by the contradictory information shown in the contract drawings related to the layout of the tendons.

During the first night of the inspection, weather conditions (heavy rain) did not allow much to be accomplished. Therefore, considering 32 effective hours of work, the production rate was 1 testing point per 10 minutes (considering the total number of locations inspected) or 12 minutes per testing point (considering only the locations in which the tendons were correctly located). Furthermore, it should be indicated that the flexible endoscope lens is a very delicate and sensitive piece of equipment. During the

inspection, on several occasions, the lens did not work properly and required repairs that consequently delayed the inspection.

2.3 Summary and Conclusions

The results of the endoscope inspection revealed that approximately 40% of the inspected locations were voided. However, most of these voids were small and in most of the cases, the strands were not exposed. Approximately 7% of the testing locations corresponded to large voids in which a large portion, if not all, of the duct's cross section was ungrouted. But, even in these situations, the strands were found to be in good condition and with no significant signs of corrosion or section loss.

In general it can be stated that the endoscope inspection is a reliable method for assessing the conditions of the post-tensioning tendons. The method is invasive, but the damage induced to the tendons and deck is minimal, provided that proper procedures are used to repair the holes. This method should be used to validate and corroborate the findings of more economical NDT procedures.

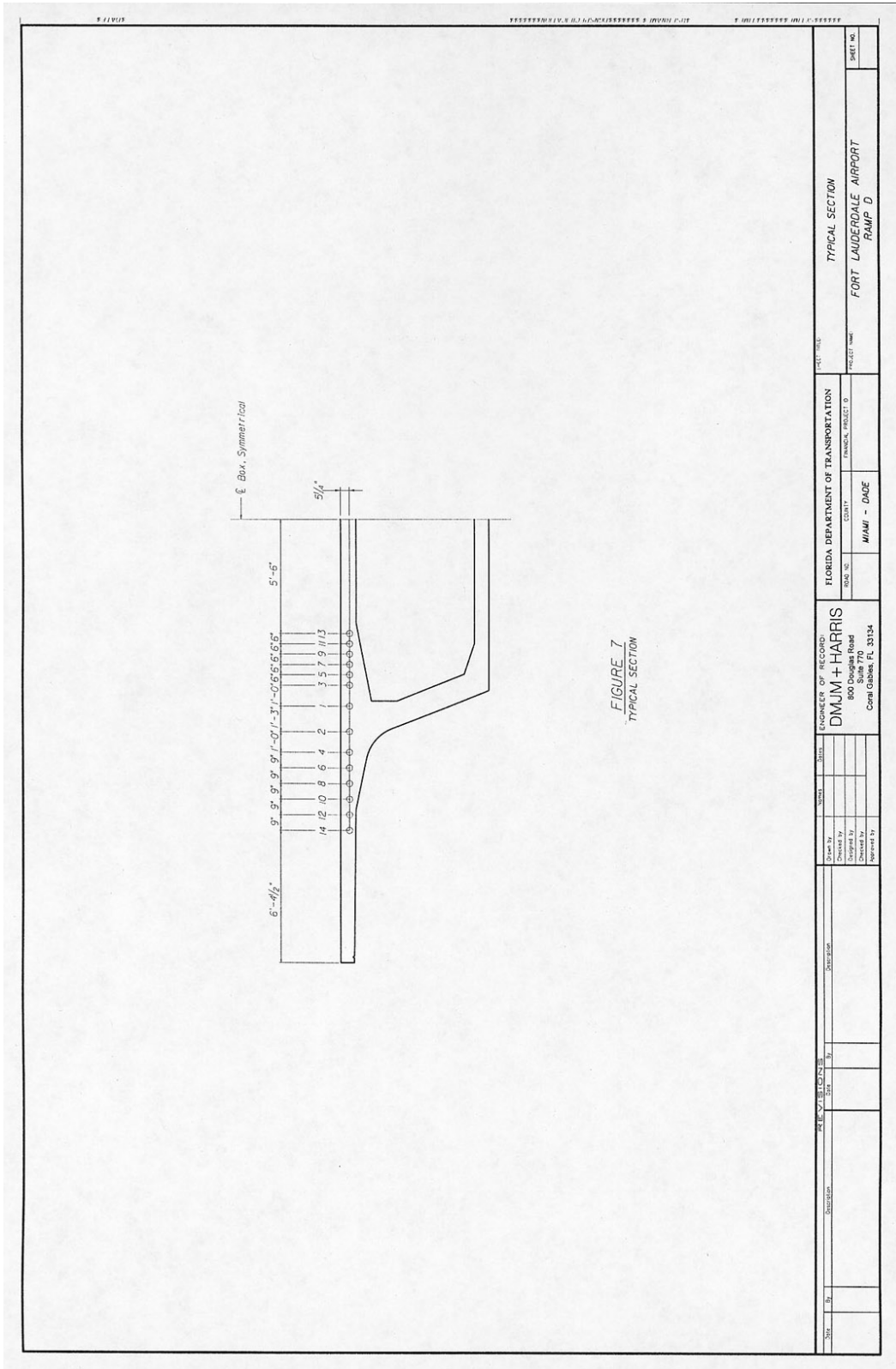


Figure 2.7 – Tendon locations

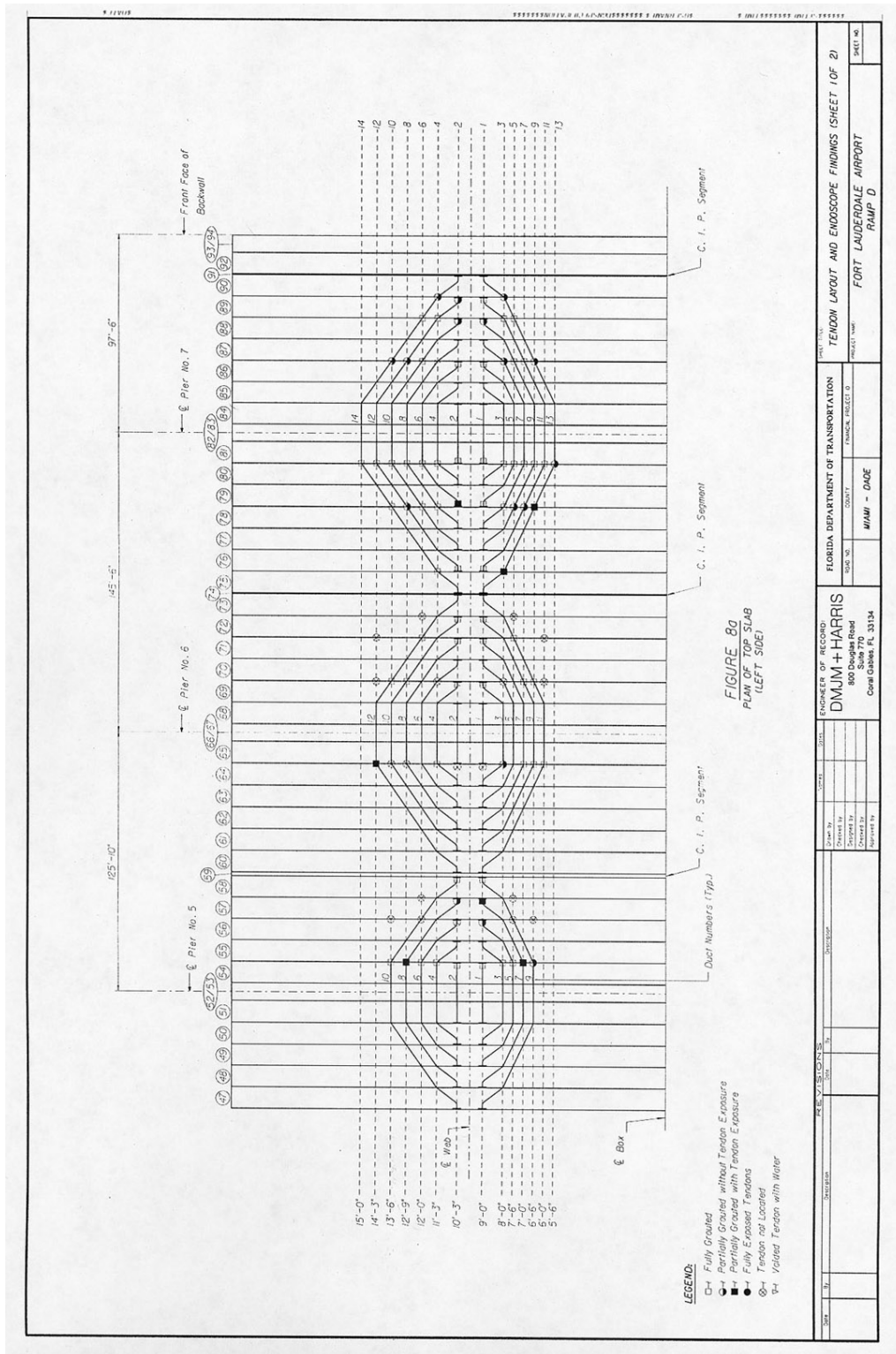


Figure 2.8a – Endoscope inspection findings

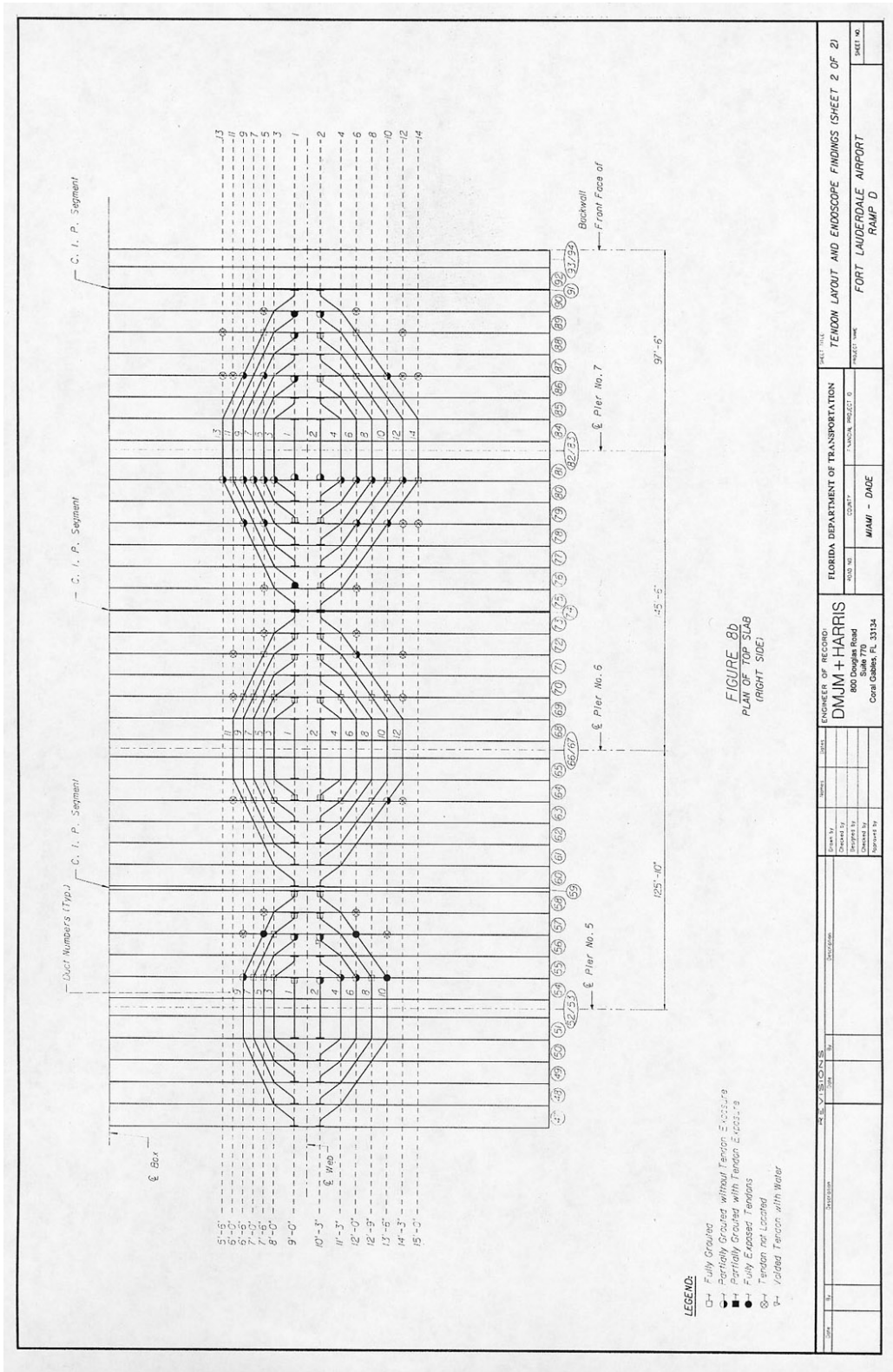


Figure 2.8b – Endoscope inspection findings

Chapter 3 – Impulse Radar Testing

3.1 Introduction

The Impulse Radar testing method (or ground penetration radar testing) was employed in this program by Construction Technology Laboratories, Inc. (CTL) to locate the top slab tendons. While the endoscope testing program indicated that the contract drawings could provide the location of the tendons in the top slab at the segment joints, the location of the ducts at locations between segment joints could not be ascertained with sufficient precision for use in the assessment of the Impact Echo, the Magnetic Flux and the High Energy Linear Accelerator non-destructive tests.

3.2 Impulse Radar Concept

The impulse radar is a valuable method to quickly evaluate large concrete areas and qualitatively provide information about the existence of reinforcing steel, tendon ducts and voids. The principles of impulse radar are similar to those for the radar used in air traffic control or when the police detect the speed of a car. A signal is transmitted from an antenna which, in turn, is partially reflected back to the antenna by objects in its path. Then, the reflected signal is analyzed immediately to provide an image of the objects encountered. The signal, for concrete applications, is formed by FM waves typically in the range of 500 MHz to 1.5GHz. The image can be viewed in either a 2-D or 3-D mode on a computer screen.

3.3 Field Testing

CTL's scope of work included the use of impulse radar testing to locate and layout the tendon ducts along the top flange of Spans 5, 6 and 7. This step would speed up the testing process using the Magnetic Flux Leakage equipment. Locating the tendon ducts resulted in a time consuming operation. It took approximately 40% of CTL's testing time. CTL mapped the location of all the ducts with spray paint along the top of the deck on the southern section of the ramp, while only spotting locations across each segment on the northern section of the deck.



Figure 3.1 - Impulse Radar Testing



Figure 3.2 - Impulse Radar Testing Equipment

Figures 3.1 and 3.2 illustrate the impulse radar testing and equipment used. Typically, half of a span, on the northern or southern portion of the deck, would contain 12 to 14 tendons which were located and mapped on the structure in approximately 1.5 to 2 hrs, thus resulting in a production rate of approximately 15 minutes per 100 ft of tendon. Details of the testing can be found in CTL's report.

An assessment of the accuracy of the Impulse Radar Testing to locate tendon ducts can be made by examining the results of the core-drilling program described in Appendix C. The data involved a total of 50 cores drilled at points where CTL had performed Impact-Echo. Of these 50 locations, which were initially located using the Impulse Radar, the core drilling inspection found 40 (80% of the 50 total) ducts associated with longitudinal tendons. At 7 additional locations, the program located transverse tendons, which can be considered a failure of the method and finally, at two locations no ducts were found and at one point the core was left unfinished due to lack of time.

3.4 Summary and Conclusions

The Impulse Radar Testing method is a quick and economical technique to locate tendons embedded in the concrete. This method not only provides information on the horizontal location of the tendon, but also the depth at which the tendon is located. The results of the tests performed at Ramp D indicated that the Impulse Radar Testing has a high degree of accuracy. This method would serve as a valuable tool in an in-depth bridge inspection program.

Chapter 4 - Impact-Echo Testing

4.1 Introduction

The Impact-Echo test method is a nondestructive testing technique currently used to test the structural conditions of concrete and masonry structures. This method uses transient stress waves generated by a mechanical impact on the surface of the structure being tested. The stress waves induced by the impact propagate through the structure and are reflected from external boundaries and discontinuities inside the medium. The surface displacements or accelerations caused by the passage and the reflections of the stress waves are monitored at a location near the impact point and are used to find the depth of interfaces and boundaries. The method has been used in a variety of applications such as, measuring member thicknesses, identification of concrete delamination, cracks, honeycombing, poor quality concrete and the location of air voids within tendon ducts of grouted post-tensioned structures.

In order to understand the principles involved in the Impact-Echo testing method some background on stress wave propagation is necessary.

4.2 Basic Theory on Stress Wave Propagation

When a disturbance (displacement or force) is suddenly applied at a point within an unbounded solid, such as by sudden impact, the disturbance propagates through the solid in the form of two different types of waves: an extensional wave or primary wave (P-wave), and a shear or secondary wave (S-wave). The two waves propagate along a spherical wave front. In the case of P-waves the particle movement is in the direction of wave propagation (normal stresses) while, for the S-wave the particles move in a plane normal to the direction of wave propagation (shear stresses). In an isotropic elastic medium the P-wave speed, V_p , is related to the Elasticity modulus, E , Poisson's ratio, ν , and the density, ρ , as follows (Timoshenko and Goodier, 1970):

$$V_p = \sqrt{\frac{E(1-\nu)}{\rho(1+\nu)(1-2\nu)}} \quad (\text{Eq. 4.1})$$

The S-wave propagates at a slower speed given by:

$$V_s = \sqrt{G/\rho} \quad (\text{Eq. 4.2})$$

where $G = E/2(1+\nu)$ is the shear modulus of elasticity. The ratio between the P-wave speed to the S-wave speed is given by:

$$\frac{V_s}{V_p} = \sqrt{\frac{1-2\nu}{2(1+\nu)}} \quad (\text{Eq. 4.3})$$

This ratio is equal to 0.61 for a Poisson's ratio of 0.2, which is the typical value for concrete.

For the case of an isotropic, elastic, half-space medium, subject to an impact load at the surface (Figure 4.1), there is, in addition to the body waves (P-waves and S-waves) that propagates along a hemispherical wave front, a surface wave that propagates along a cylindrical wave front confined to the surface of the solid and with a speed smaller than the S-wave. The surface wave, called Rayleigh wave or R-wave, resembles gravitational surface waves in liquids. The particle trajectory is an ellipse with the minor axes in the direction of wave propagations and the particle displacements attenuate exponentially with depth. The speed of the R-wave for a material with Poisson's ratio equal to 0.2 is about 92% of the S-wave speed.

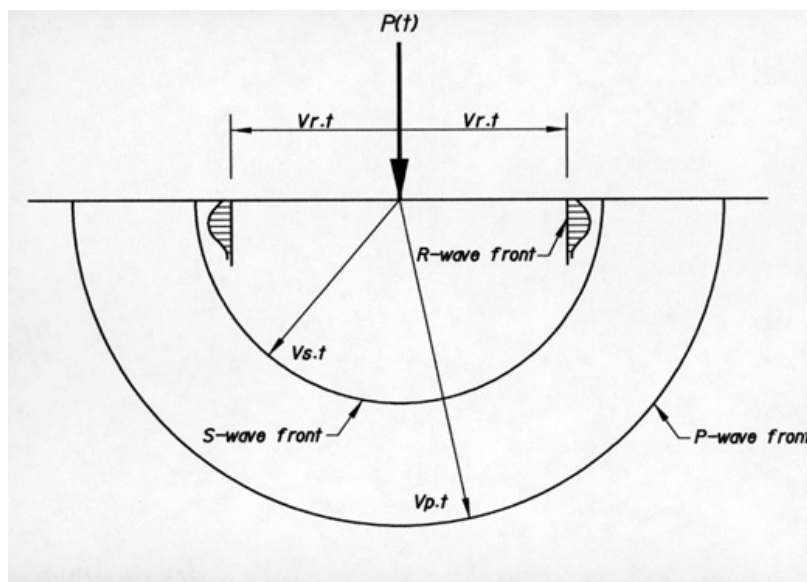


Figure 4.1 - Stress wave-fronts at time "t" due to an impulsive load.

When interfaces exist, like the presence of two materials with different stiffnesses and densities, the incident waves are reflected and refracted and additional waves traveling along the interface may be generated. In general, the amplitude of the reflected and refracted waves depends upon the angle of incidence and on the acoustic impedance of the materials (wave speed times the material density). Two extreme cases are of practical interest; first, the reflections from a free boundary, and second, the reflections from a rigid boundary. These correspond to cases in which the second medium has acoustic impedance's of zero and infinity respectively. Generally, an incident P-wave will generate a reflected P-wave and a reflected S-wave. This is also true for an incident S-wave. When the angle of incidence is normal to the surface, then the reflected wave is of the same type as the incident wave and an incident compressional wave will be reflected as a tension wave at a free surface (the surface is stress free), and as a compressional wave when impinging on a rigid boundary (the displacement at the interface is zero). These differences are important in the Impact-Echo method for distinguishing between reflections from a concrete-air interface and from a concrete-steel interface.

4.3 Impact-Echo Testing Applied to Testing of Bonded Post-tensioned Tendons

A diagram of the Impact-Echo test is shown in Figure 4.2. A transient stress pulse is introduced into the structure by tapping a small steel sphere against the concrete surface. As previously discussed, impact on the surface produces P- and S-waves that travel through the structure and a surface wave (R-wave) that travels away from the impact point. These waves are reflected by internal defects or external boundaries. A receiver transducer measures the time history of surface displacements or accelerations. This signal would contain the response of the system to the passage of the transient stress pulse plus the reflected waves. When the geometry of the structure being tested is simple, like the plate structure shown in the figure, P-wave echoes will dominate the response at points close to the impact point.

The graph on the right side of Figure No. 4.2 shows the pattern of vertical surface displacements that would occur. The large downward displacement at the beginning of the waveform is caused by the R-wave, and the series of repeating downward displacements of lower amplitude are due to the arrival of the P-wave as it undergoes multiple reflections between the surface and the internal void. The periodicity of the reflected waves, which are used to evaluate the integrity of the structure or to determine the location of flaws, can be easily identified by transforming the time history response to the frequency domain and plotting the amplitude of the response against frequency. The resonance peaks in this spectrum are the key elements for the interpretation of the Impact-Echo test.

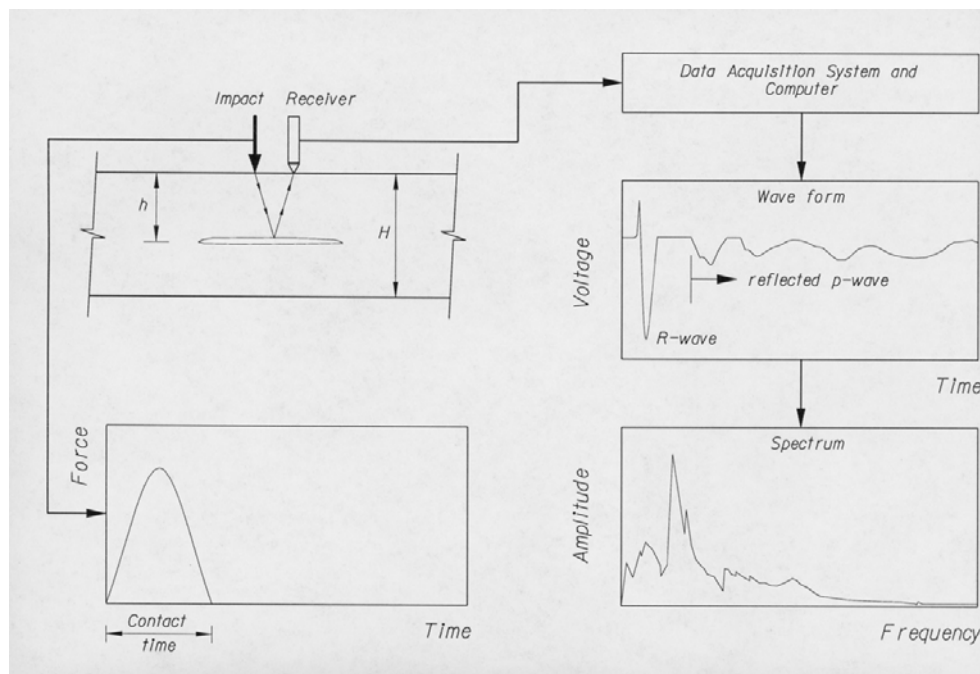


Figure 4.2 - Diagram of the Impact-Echo method

In general, the response of a three dimensional structure subject to a transient pulse is a complicated analytical task that can be solved using numerical techniques like the finite element method. When testing plate like structures using the Impact-Echo, the response at points very close to the receiver can be treated as a one dimensional wave propagation problem involving reflection of only P-waves; this fact is what makes the results of the Impact-Echo testing method very simple to interpret.

Figure 4.3 illustrates the use of Impact-Echo test to detect tendon voids of three different plates with its corresponding qualitative response spectra. In Figure 4.3a, a plate with no voids is tested. In this case, the compressional P-wave due to the impact is reflected at the bottom boundary as a tension wave, which will also be reflected at the top surface as a compression wave. Consequently, the waves must travel a distance of $2H$, where H is the plate thickness, in order to complete a cycle. In such a case, the wave period (T_{plate}) can be approximated by using the following equation:

$$T_{plate} \approx \frac{2H}{V_p} \quad (\text{Eq. 4.4})$$

The frequency, which is the inverse of the wave period, is given by,

$$f_{plate} \approx \frac{V_p}{2H} \quad (\text{Eq. 4.5})$$

In this case, since no voids exist, the response spectrum will show a single peak corresponding to resonant plate frequency given by Eq. 4.5.

Next, a plate with a ungrouted duct is examined (Figure 4.3b). In this case, the frequency corresponding to the plate thickness is shifted to a lower value. Upon impact, the waves will be diffracted by the empty duct, taking a longer time to complete a cycle. The frequency corresponding to the reflection from the empty duct is given by,

$$f_{void} \approx \frac{V_p}{2h} \quad (\text{Eq. 4.6})$$

Where h is the distance from top of plate to top of duct. In this case the amplitude frequency spectrum will show two resonant peaks.

Finally, Figure 4.3c shows a case in which the duct is fully grouted. In this case, the frequency corresponding to the plate thickness will be almost identical to the frequency of the plate without the duct. The waves reflected from the tendon steel will need to travel a total distance of $4h$ in order to complete a cycle. A compression wave will be reflected by the tendon steel as a compression wave and reflected as a tension wave at the surface. Then, the tension wave will be reflected as a tension wave at the tendon steel and converted back to a compression wave when being reflected from the surface. In this case, the amplitude frequency spectrum, will also result in two resonant peaks. The resonant frequency from waves reflected from the tendon steel is given by,

$$f_{steel} \approx \frac{V_p}{4h} \quad (\text{Eq. 4.7})$$

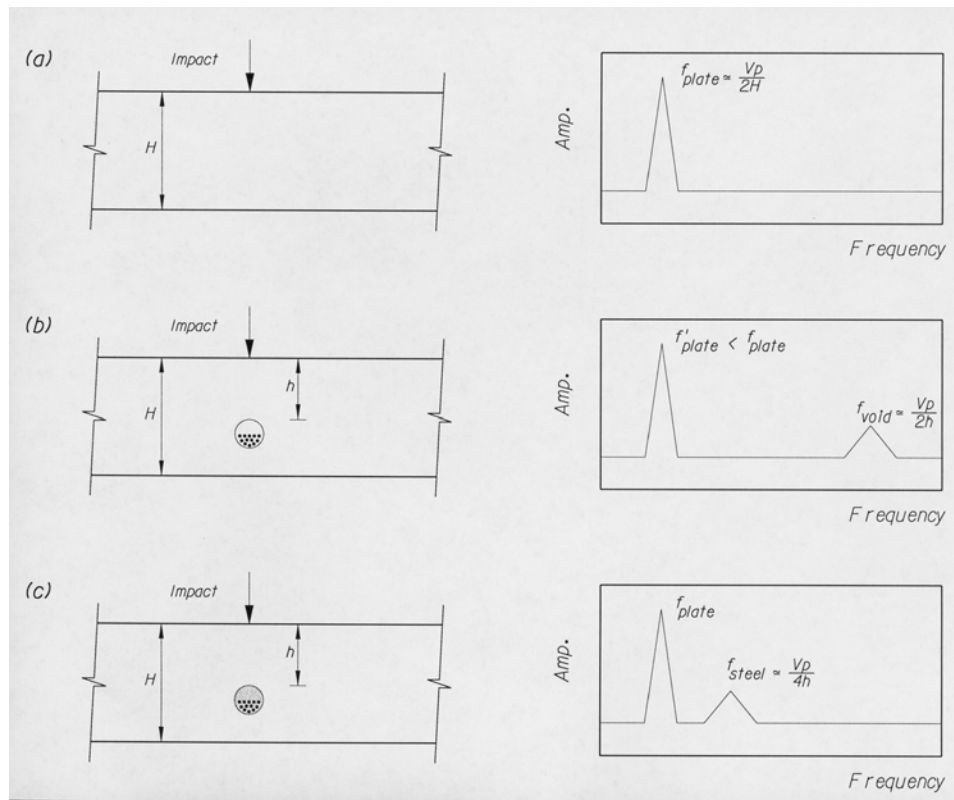


Figure 4.3 - Typical Impact-Echo test frequency spectrum for (a) solid plate, (b) plate containing an ungrouted post-tensioning duct and (c) plate containing a grouted duct.

In order to excite the resonant frequencies given by Equations 4.5, 4.6 and 4.7, the frequency spectrum of the transient impulse should generate enough energy at these frequencies. This is directly related to the pulse contact time, which is also related to the size of the steel ball impactor. Smaller impactors have smaller contact time and higher frequency components.

The reliability of the Impact-Echo method to evaluate the presence of voids in longitudinal tendon ducts is very much affected by the interference effects of transverse post-tensioning and reinforcement in the testing area that influence the interpretation of the results. In addition, the complex geometry of the bridge concrete deck (web blisters, chamfers, etc) can interfere with the interpretations of the results. Therefore, the use of the Impact-Echo method should be associated with additional work including mapping of the tendon and mild steel locations and some limited invasive proving (drilling and endoscopy) to adequately correlate the impact-echo signals with the existing duct conditions.

4.4 Field Testing

The Impact-Echo was performed on the Ramp D Bridge of the Fort Lauderdale Airport Interchange. This test was conducted in order to identify grout voids within the longitudinal cantilever tendons along the top flange of Spans 5, 6 and 7 of the bridge structure. The testing program was performed by Construction Technology Laboratories, Inc. (CTL) and, to a minor degree, by professor Al Ghorbanpoor from the University of Wisconsin in Milwaukee, Wisconsin.

4.5 Construction Technology Laboratories, Inc. (CTL) Impact-Echo Testing

CTL performed the Impact-Echo test from March 18, 2002 to March 22, 2002. This section of the report presents a summary of the testing process including information on production rates. CTL's complete report is presented in Appendix E. CTL's findings were compared with the results obtained from the core borings that were performed to corroborate the test results and with the visual inspection performed during the deconstruction of the bridge structure.

CTL's scope of work included the use of Impulse Radar testing to locate and layout the tendon ducts along the top flange of Spans 5, 6 and 7. This step was required in order to also perform the Magnetic Flux Leakage Test, which is reported in Chapter 5 of this report. Locating the tendon ducts was a time consuming operation. It took approximately 40% of CTL's testing time. CTL mapped the location of all the ducts with spray paint along the top of the deck on the southern section of the ramp, while only spotting locations across each segment on the northern section of the deck.

CTL started the testing at the Northern section of segment 52-53, over Pier 5. The contract drawings show 10 tendons, at this location, out of a maximum of 14 tendons. CTL's staff believed that the additional 4 ducts were ungrouted and could be used for Impact-Echo calibration purposes. Unfortunately this was not the case, as was confirmed by impulse radar testing. Duct locations were marked on the deck as per contract drawings. Then, the Impulse Radar (I-R) test was used to locate the actual locations of the ducts. The I-R test revealed that most ducts were located as shown on contract drawings. The sample Impulse Radar test is shown in Figure B.1 of CTL's report (Appendix E).

Afterwards, CTL performed a series of Impact-Echo calibration tests to obtain a typical base reflection and to measure the compression wave velocity of the concrete applicable to the testing program. The tests were performed at the cantilever wing section where the slab thickness is a constant 8 inches (per contract documents), which was confirmed by direct measurement at some drainage openings. The base frequency found from the calibration tests was approximately 8.8 kHz, which corresponds to a P-wave propagation speed of 11,700 ft/s. This value can also be found using Equation 4.1, using the following parameters,

$$E = 0.9 \times 57000 \times \sqrt{f'c} = 0.9 \times 57 \times \sqrt{5500} = 3804.5ksi = 547849ksf$$

The concrete strength was assumed as 5,500 psi with a 0.9 factor to account for the weakness of the limerock aggregate. Using a specific concrete specific weight of 145 pcf (22.8 kN/m³, FDOT Structures Design Guidelines) and a Poisson's ratio of 0.2, the P-wave speed was calculated at:

$$V_p = \sqrt{\frac{547849 \times (1 - 0.2) \times 32.2}{0.145 \times (1 + 0.2)(1 - 2 \times 0.2)}} = 11,627 \text{ ft/sec}$$

This value is comparable with the P-wave speed found using Impact-Echo testing.

The peak frequencies expected in the amplitude spectrum for the case of a fully grouted duct and for a completely ungrouted (voided) duct are in the range of 10kHz and 20kHz respectively (determined by Eq. 4.7 and 4.6 with $V_p=11,700$ ft/sec and h , equal to 3.5 in). Also, as a result from the calibration, the proper size of steel impact ball that would excite these frequencies was selected.

Once the testing points were located using Impulse Radar, Impact-Echo tests were performed. Normally three Impact-Echo tests were performed at each location. The operator will look at the result of each test, which includes the time history and the frequency spectrum of amplitudes and accept or disregard the test. In the event that background noise or double impact of the impactor ball had interfered with the results, the test is disregarded. Once three acceptable tests are obtained, an average result is compounded from the three. If there was good correlation between the three signals, the average result was accepted, otherwise the tests were repeated. Figures 4.4, 4.5 and 4.6 depict the actual Impact-Echo testing process. Typically, the average production rate was approximately 20 test points per hour or a test point every 3 minutes.



Figure 4.4 - Impact-Echo testing.



Figure 4.5 - Impact-Echo testing, impact application and receiver.



Figure 4.6 - Impact-Echo testing, computer screen showing the time history of the signal and its frequency amplitude spectrum

Most of the tested tendons are located in places in which the slab is of varying thickness; where the bottom surface is inclined or over the webs. In these cases, the plate resonant frequency cannot be determined using a simplistic model of one-dimensional wave propagation (Eq. 4.5) since the response will be very complex due to interactions between reflected P- and S-waves but, still, it will be the first resonant peak in the spectrum. The resonant peaks due to reflections from a voided duct or a fully grouted duct will not be affected by the conditions at the bottom of the plate.

A total of 290 duct points were tested. From the 290 duct points tested, CTL reports (CTL's report, Table C.1), that voids were identified in 103 of the test points. This represents 35.5% of the total tested points. Twenty-nine (29) test points were reported as

small voids representing 10% of the total number of test points. CTL’s report classifies the Impact-Echo results as a small void (sv) or a void (v) (CTL’s report, Table C.1). This classification is determined by evaluating the frequency spectrum. CTL explains that a significant peak in the spectrum is classified as a “significant void”. However, the degree of voiding and the possible exposure of strands is not determined.

In order to corroborate the findings of the Impact-Echo testing program, core drilling of the tendons was performed. The results of the core drilling are presented in Appendix C. A total of 50 cores were drilled at locations in which CTL reported a small or large void. Four additional cores were drilled at segments 54, 55 and 56, to corroborate Professor Ghorbanpoor Impact-Echo testing results. CTL did not perform tests at these last four locations.

A comparison between the core drilling findings and the ones reported by CTL is as follows:

<u>Core findings</u>	<u>Corresponding CTL findings</u>
Grouted = 17	Void = 16 Small void = 1
Small Voids = 21	Void = 21
Void = 2	Void = 2
Not Performed = 10	Void = 10

As reflected in the comparison of CTL’s Impact-Echo test results to the core drilling results, a significant peak in the frequency spectrum is not necessarily considered a “significant” void in practice. In general, during the core drilling inspection, voids smaller than ½” were reported as small voids, and the strands were found mostly grouted. Assuming that the grout surface in these small voids is horizontal, for a void ½” deep, the horizontal dimension along the chord is 2.12” (duct diameter is 2.75”); while for a void ¼” deep the chord is 1.58”. This corresponds to 77% and 57% of the duct diameter, respectively. Consequently, these voids will provide a reflecting boundary that will clearly be detected in the Impact-Echo amplitude frequency spectrum of the time signal and will be reported as a significant void when in fact they may be acceptable and considered insignificant in practice.

Sansalone and Streett, 1997, provide recommendations for the smallest voids that can be detected within ducts. They state that, “voids with width-to-depth ratios greater than ¼

can be detected, while voids having width-to-depth ratios greater than $1/3$ can be clearly identified". In our case, with a concrete cover of 3.5", the ratios of width-to-depth of $1/4$ and $1/3$ corresponds respectively to voids of 0.875" and 1.167" wide and depths of voids of 0.071" ($\sim 1/16$ ") and 0.129" ($\sim 1/8$ "). This implies, that in our case, voids with depths greater than $1/8$ " will be clearly identified.

From the previous discussion, we can state that even small voids will provide a reflecting surface that will clearly be detected with the Impact-Echo test. CTL's effort was effective in detecting voids of various sizes. Their process was able to detect 60% of all the voids found during the core drilling operation.

In addition to core drilling, a total of nine segments from Spans 5 and 6 were inspected after their disassembly (See Chapter 7 and Appendix D). Most of the bridge was demolished using a concrete crushing machine that demolished the concrete segments in their original place. Only sections of the bridge on Spans 5 and 6 were disassembled by cutting across the bridge cross section at the segment joints using a wire cutting machine. Some of these segments were visually inspected prior to demolition. A disassembled bridge segment is shown in Figure 4.7. Figure 4.8 shows a tendon duct with a small void, which was typically found in most of the ducts. Documentation of these inspections, including pictures of each of the inspected tendon ducts, is included in Appendix D. A total of 216 points were visually inspected in the following segments: Segments 63, 64, and 65 of Span 5, and Segments 68, 69, 70, 71, 75 and 76 of Span 6. As previously noted, voids smaller than $1/2$ " deep were reported as small voids. The statistics of this inspection shows that approximately 70% of the locations were classified as small voids, 10% as voids and 20% as fully grouted ducts. It should be noted that the strands in the ducts with small voids were mostly encased within the grout.



Figure 4.7 - Bridge segment after removal.



Figure 4.8 - View of duct with void

The large percentage of ducts with small voids, as compared to those found during the endoscopy inspection and the core drilling, could be explained as follows:

1. Small voids are difficult to detect with the sole use of drilling procedures, and
2. The drilling operation can deform the ducts and possibly collapse them into the voids.

In addition, the visual inspection of a segment in which the endoscopy testing was also performed revealed that the drilling conducted for the endoscope testing did not penetrate the duct surface. Therefore, at this particular location the duct was rendered as fully grouted when, in fact, it had a small void. These arguments serve to infer that, to locate voids in a concrete bridge structure, the Impact-Echo testing method, as used by CTL in this particular bridge, results to be more efficient than previously reported.

4.6 Professor Al Ghorbanpoor Impact-Echo Testing

Professor Ghorbanpoor performed Impact-Echo testing at four areas of the bridge deck in Spans 5, 6 and 7. He performed calibration tests at three different locations on the structure, where no longitudinal post-tensioning tendons were present and where the slab was of constant thickness. The speed of longitudinal wave propagation was computed based on these calibration tests (resonance frequency of the plate). This speed was found to be 140,000 in/sec, which coincides with the value reported by CTL.

The results of the Impact-Echo tests performed in four different locations are as follows:

The first test location was at Tendons 8 and 10, close to the joint between Segments 86 and 87, in the Northern portion of the bridge. At this location Professor Ghorbanpoor reports evidence of voids in the grout at Tendon 8, and "no conclusive evidence" in Tendon 10. During the endoscope inspection, Tendon 10 was found fully grouted, and

Tendon 8 was found to have voids. However, the extent of the void was not established. Trapped water was also identified inside the duct.

The second test location was at Tendon 4 at Segment 69 in the Northern portion of the bridge. At this location CTL not only found voids within the duct, but also found that the tendon was exposed and located at a depth greater than 5", which exceeds the expected 3 1/2" of concrete cover. Nevertheless, only a small void was found at the top of the duct. At this location, Professor Ghorbanpoor also reports evidence of grout voids and indicates that the duct at a depth of 5.7" from the surface, which corresponds with CTL's findings.

The third test location was at Segment 69, on the Southern portion of the bridge, where ten tendons were tested. Approximately 4 to 5 testing points were per tendon; for a total of 58 testing points. Both, CTL and Professor Ghorbanpoor performed tests at all these testing points. Professor Ghorbanpoor reports that no significant voids were observed at Tendons 9, 10, 11 and 12. Ghorbanpoor's findings correspond with the endoscopy inspections, which found these tendons fully grouted. The subsequent visual inspection of this segment found that these tendon ducts were either fully grouted or with a very small voids. Professor Ghorbanpoor reports indications of grout voids in Tendons 3, 4, 5, 6, 7 and 8 based on the frequencies reported in Table 1 of the Appendix F report. These frequency values correspond to the void findings show in the table below.

Test Points	Tendon ID No.									
	3	4	5	6	7	8	9	10	11	12
1 (1' - 4")		void	void	void	void	void				
2 (4' - 4")	void	void	void	void	void	void				Void ?
3 (6' - 8")	void	void	void	void	void	void				
4 (8' - 8")		void		void				Void?		
5 (10')			void	void						

Table 4-1 – Indications of voids for IE test points in Segment 69

Several of these points were inspected during the Core-drilling program. The results are presented below:

<u>Tendon</u>	<u>Test Point</u>	<u>I-E Finding</u>	<u>Core-drilling finding</u>
6	1	Void	Grouted
6	4	Void	Small Void
7	1	Void	Grouted
8	1	Void	Small Void
8	2	Void	Small Void
8	4	Grouted	Small Void
12	1	Grouted	Small Void

The above table shows that Dr. Ghorbanpoor reports voids in locations where the core-drilling indicates grouted tendons (2 of 7 or 29%). It accurately reports voids in 3 of 7 (43%) and reports incorrect results (no voids in voided ducts) in 2 cases (29%). This last result was not found in the case of the testing performed by CTL. Given the small number of testing locations, the success or failure of the method, as performed by Dr. Ghorbanpoor, may not be conclusively ascertained.

The last test location was at Tendon 10 in Segments 54, 55 and 56 in the Southern portion of the bridge (a total of 22 points were tested). This tendon was found completely voided during the endoscopy inspection. Core drilling was performed at 2 locations in Segment 56, and at one location in Segments 55 and 54. At all these locations the tendon was found completely voided, with no trace of any grout. This was confirmed during the deconstruction process. Figure 4.9 shows this tendon at the hole drilled in Segment 54. The strands can clearly be seen with no sign of grout. However, although this tendon was completely ungrouted, no signs of corrosion were found. In this location professor Ghorbanpoor performed 22 Impact-Echo tests and he reported evidence of grout voids in Segment 56 and no strong indications of any significant voids in Segment 55. For Segment 54, Professor Ghorbanpoor reports partial voids within the first 5 feet of tendon, away from the joint between Segments 53 and 54. In this testing area the testing points were marked along the deck based on the information shown on the original contract drawings by measuring the offset of the tendon duct from the centerline of the section at the segment joints and by interpolating linearly in between these points. In general, this method of locating tendons is not as accurate as using the Impulse Radar method, especially for points in between the segment joints and in regions where the tendon has a transition curve or a sharp angle, which is the case at the joint between Segments 54 and 55. It is possible that the testing points in this area were not located exactly over the

tendon ducts. This would explain why no clear wave reflections from the voided ducts were found in some areas.



Figure 4.9 - Tendon 10, core drilled at Segment 54.

With respect to the locations where the testing method did not detect the presence of existing voids, rather than attributing this to a failure in the testing methodology, factors like proper location of the ducts may have affected the end result. Overall, the Impact-Echo test method performed by Professor Ghorbanpoor was shown to have limited success in detecting the presence of voids.

4.7 Summary and Conclusions

With the combined use of highly skilled testing professionals and on-site calibration of the output signals, the application of the Impact-Echo Testing Method to identify the existence of voids in the grout filling the ducts of the post-tensioned tendons in this project can be considered successful. When the results are compared with the findings of the core drilling inspections performed, the Impact-Echo method results to be approximately 60% reliable. In most of the cases, the voids found were relatively small and generally located in the top part of the ducts. However, these small voids occupied a great percentage of the section diameter when looked in plan view. Consequently, these small voids provided a reflecting surface, which was clearly detected by the test and appeared in the Impact-Echo frequency spectrum as the second resonant peak. During the forensic evaluation of the dismantled segments it was found that 80% of the inspected ducts were voided; with 70% of them being small voids. Being a coarse procedure, the core drilling operation was apparently unable to detect some of these small voids. Consequently, one can assess that the reliability of this method to be higher than 60%.

The Impact-Echo method may provide a clear indication of a sudden discontinuity in material properties and distinguishes whether this discontinuity represents a void or a

stiffer material (the tendon). The size of the void, which is an essential factor in assessing its importance and possible consequences, is, however, difficult to ascertain. This is specially true when testing tendons located on the top part of the deck in which the interpretation of the test is based almost exclusively in the reflections from the tendon duct (second resonant peak in the frequency spectrum). The first resonant peak in the frequency spectrum is not used because it is difficult to assess what the theoretical resonant frequency will be since the deck is of varying thickness and/or the effect of the webs is relevant. Consequently, one dimensional wave propagation cannot be applied in those cases. Nevertheless, if the test is performed in the box bottom slab, which is normally of constant thickness, then, plate like behavior can be applied and the first resonant frequency, which is associated with the slab thickness, will be shifted due to the presence of a void. The amount of shifting, which is directly related to the size of the void will provide indication of the relative void size as reported by Abraham and Côte, 2002.

The Impact-Echo testing procedure is simple and the equipment is light, requiring a very small crew (2 persons) to perform the test. CTL's and Professor Ghorbanpoor production rates were approximately 3 minutes per testing point. This includes the time needed to locate accurately the tendon. Higher production rates can be obtained provided that the testing points are located in advance to the actual testing. In practice the test would need to be complemented by invasive techniques, such as endoscopy, to assess the relative importance of the identified voids and also to assess the actual conditions of the tendon strands. In addition, the interpretation of the results should take into account the possible interferences from nearby tendons and mild steel; the possible changes in duct vertical and horizontal location; and the deck geometry. To perform a dependable testing program, the output signal interpretation should be based on the results of a correlation analysis between a series of impact-echo results and their associated endoscopy results.

Chapter 5 - Magnetic Flux Leakage (MFL) Testing

5.1 Introduction

The purpose of the Magnetic Flux Leakage (MFL) test is to identify the loss of the tendon cross sectional area due to corrosion. The MFL testing was performed on the post-tensioned tendons, within the top of the concrete decks, at Spans 5, 6 and 7. Prior to performing this test endoscope inspections were performed at these locations in order to identify the actual condition of the tendons. In most of the cases, the tendon strands were completely encased within the grout, and, in cases in which the strands were exposed, no sign or only minimal signs of corrosion were found. These results were later confirmed during the bridge demolition and the forensic investigation of dismantled bridge sections. Since no significant sign of corrosion were found, the decision was made to induce damage in the tendon strands in order to effectively evaluate the test. The range of sectional areas cut for testing was determined based on the MFL testing research and field experience available. Ducts were exposed and wires were cut at nine locations ranging from 1.5 to 3 strands that represent 12.5% and 25% of the total tendon area respectively. Several other ducts were opened but wires were not cut to mask damaged tendons. Appendix B presents the description of the damage induced to the post-tensioned tendons.

Professor Al Ghorbanpoor, from the University of Wisconsin, Milwaukee, Wisconsin, performed the testing. Professor Ghorbanpoor has been involved in the research and the practical application of the MFL system since the early 1990's and recently he performed the evaluation of the external post-tensioned tendons of the Mid-Bay bridge. In this case the MFL system was able to identify losses of cross sectional area in the order of 0.3 %.

5.2 Magnetic Flux Leakage Concept

By applying an external magnetic field to a ferromagnetic component, such as a post-tensioning tendon, a constant directional flow of magnetic flux will be introduced in the component. If the magnetic flux encounters a flaw such as a corroded region or fracture in the component, some or all of the flux will leak out of the component. This magnetic flux leakage is detected by a series of sensors that produce electrical voltage proportionate to the field amplitude at a specific location. The signals detected by the sensors are then analyzed to determine the extent or severity of the flaw that caused the magnetic flux leakage.

The applied magnetic field strength has a dominant influence on the concentration of the flux within ferromagnetic materials and subsequently on the extent of the flux leakage. Adequate flux leakage must take place at the location of a flaw or discontinuity in the steel so appropriate sensors, which have their inherent limitations in terms of sensitivity, signal-to-noise ratio, etc., can measure it. The field strength, consequently, must be large enough to overcome problems due to noise, distance between the magnetic field source and the ferromagnetic material, and the masking effect of large quantities of steel found in many prestressed and reinforced concrete members. Figure 5.1 schematically

illustrates the magnetic flux leakage concept: a magnet inducing a strong magnetic field in a ferromagnetic material. In the presence of a flaw, a magnetic flux leakage field is formed at the flaw location. An array of sensors is positioned between the magnet poles to detect the flux leakage. The sensors are usually Hall-effect devices.

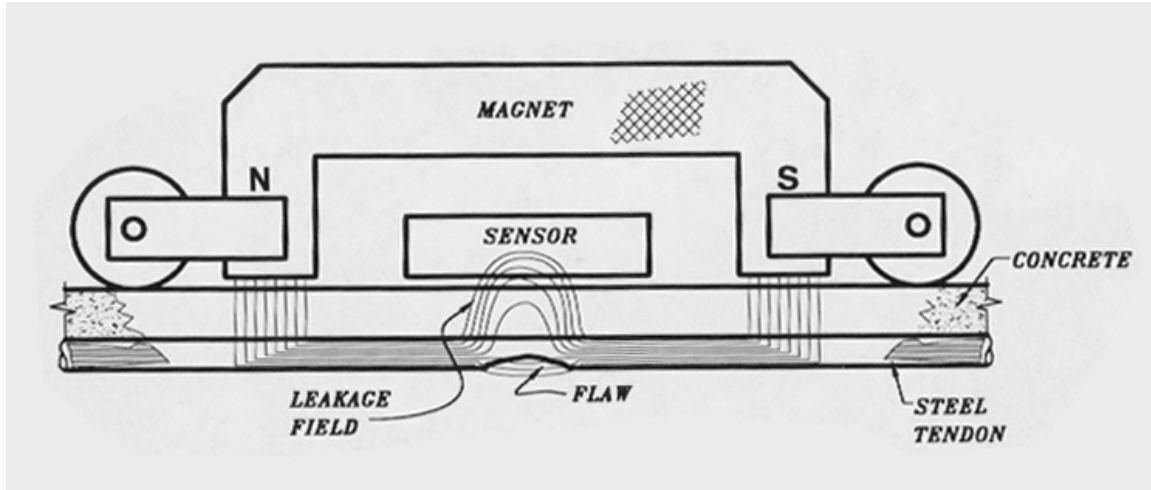


Figure 5.1 - Magnetic Flux Leakage Testing concept

It should be noted that the effect of the concrete on the magnetic field is insignificant, or it may be stated that concrete is generally transparent to the field. All ferro-magnetic materials have a limited ability to carry flux. When they reach this limit they are saturated and behave like transparent materials (like air or concrete). Below the level of saturation, a ferromagnetic material will substantially contain the flux lines passing through it. As saturation approaches, the flux lines will follow the path of greatest permeance or lowest reluctance and, as flux lines flowing in the same direction repel each other, the flux lines may travel as readily through the air or concrete as through the material.

Figure 5.2 illustrates the effect of the magnet strength on the applied field. To detect flaws in the ferromagnetic material the magnet strength must be strong enough to saturate the material so that a flaw will cause flux to leak. For a given magnet strength, an increase in the distance between the magnet and the ferromagnetic material reduces the magnetic field significantly (approximately to the power of 3). Additionally an increase in the sectional area of the material will decrease the flux density in the material.

The MFL concept has been in practice for a long time in the oil industry, mainly for examination of oil and natural gas pipelines. However, the first instrumentation for inspection of prestressed concrete bridges using the MFL concept was developed in the late 1970's. Improvements on the initial equipment were performed in the 1980's. Although these initial efforts showed excellent potential in the detection of flaws in prestressing steel, there were several limitations related to the operation and speed of testing (heavy equipment), data acquisition, and data processing.

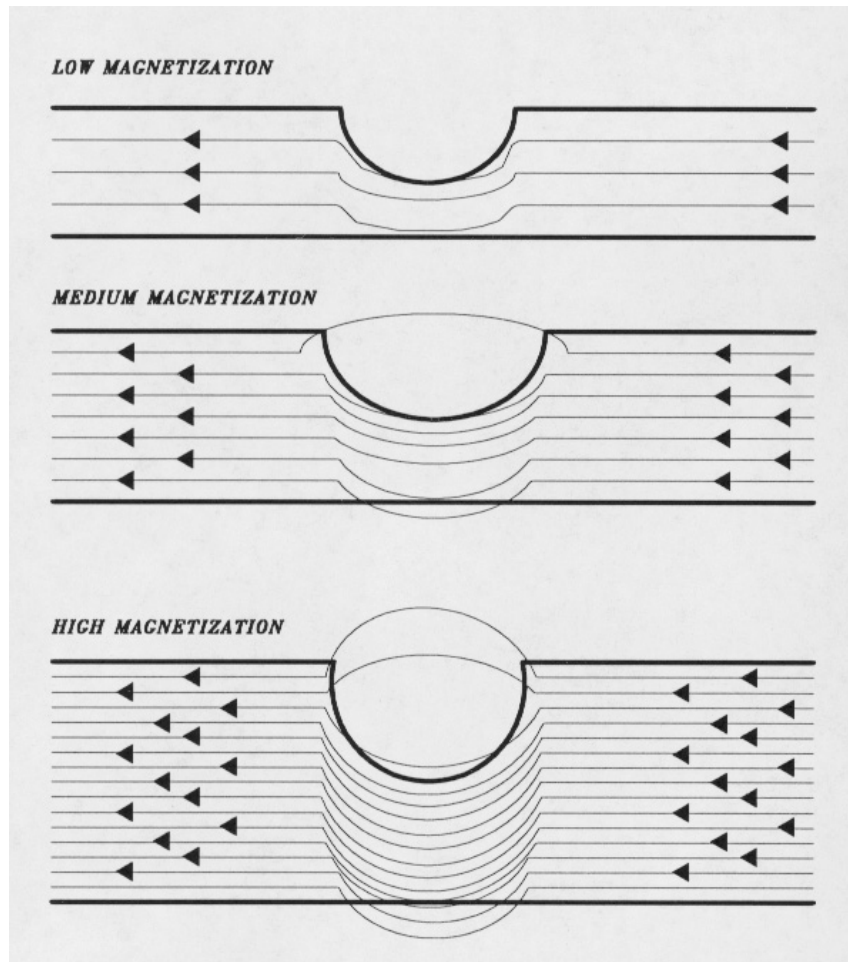


Figure 5.2 - Flux Leakage at different magnetization levels.

In 1995, the Federal Highway Administration funded a study on “Magnetic-Based system for NDE of Prestressing Steel in Pre-Tensioned and Post-Tensioned Concrete Bridges”. As a result of this research effort, a new system that overcomes the shortcomings mentioned previously was developed. The new system, designed to find the conditions of prestressing strands in concrete girders, was tested both in the laboratory and in the field. It was found that the MFL system is capable of detecting a 7 percent or larger reduction in the cross-sectional area of the strands. This capability was demonstrated for strands placed at a distance of up to 5 inches from the system’s magnet and sensor assembly. A more comprehensive discussion on the development of the referenced MFL system, and its theoretical basis and application to bridge structures, can be found in Ghorbanpoor et. al., 2000.

5.3 Testing Equipment

The equipment especially configured for testing of internal post-tensioned tendons in a bridge deck is shown in Figure 5.3. The testing equipment consists of an aluminum push-cart frame that supports a pair of strong magnets and a series of Hall-effect sensors, a

computer, a data acquisition unit, and a DC power source. A detailed description of this equipment and the testing procedure as well as the results can be found in Professor Ghorbanpoor’s report included in Appendix F. The cart is rolled on its rubber wheels along the tendon lines that are marked on the surface of the concrete deck. During the test, a constant distance of 0.25 inch is maintained between the magnet/sensor assembly and the concrete deck surface. This is a very important factor since the magnitude of the MFL data is proportional to the distance between the magnet/sensors assembly and the steel tendon within the deck. The sensors are positioned 1 inch on centers in both horizontal and vertical directions. This layout is shown in Figure 5.4. During the test, the equipment is guided such that an alignment of sensors 4 and 9, located on the equipment’s centerline, is maintained with the centerline of the tendon along its length. The output signals from these four sensors are displayed in the form of graphs of flux leakage amplitude vs. longitudinal travel distance of the magnets/sensors assembly from the starting point of the test.



Figure 5.3 – Photograph of the MFL equipment as configured for testing internal P-T tendons in a bridge deck

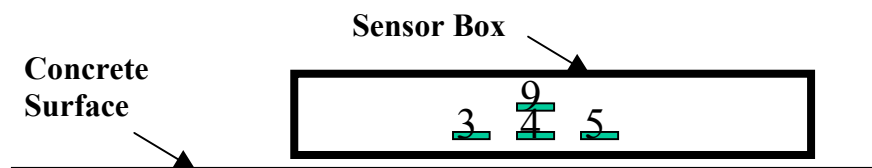


Figure 5.4 – Layout of Hall-Effect sensors in the MFL equipment

5.4 Laboratory Study

Professor Ghorbanpoor performed a brief laboratory study prior to the field-testing. In this study the conditions to be encountered at the field were approximately reproduced, that is, the laboratory tendon had 12 one-half inch diameter seven-wire strands. The tendon was positioned at a distance of 5.5 inches from the test surface. Transverse No. 4 reinforcing steel bars were installed at 2 inches below the test surface and at a spacing of 17 inches on center to simulate the actual bridge post-tensioning and reinforcement. The frequently repeated indications with large amplitudes in the output of each sensor, as shown in the Figure 5.5, are from the effects of transverse reinforcing steel bars that are located closer to the test surface (at 2.0 inches). As the signal diminishes rapidly with distance, it can be seen that the response at sensor No. 9 is weaker than the ones closer to the deck.

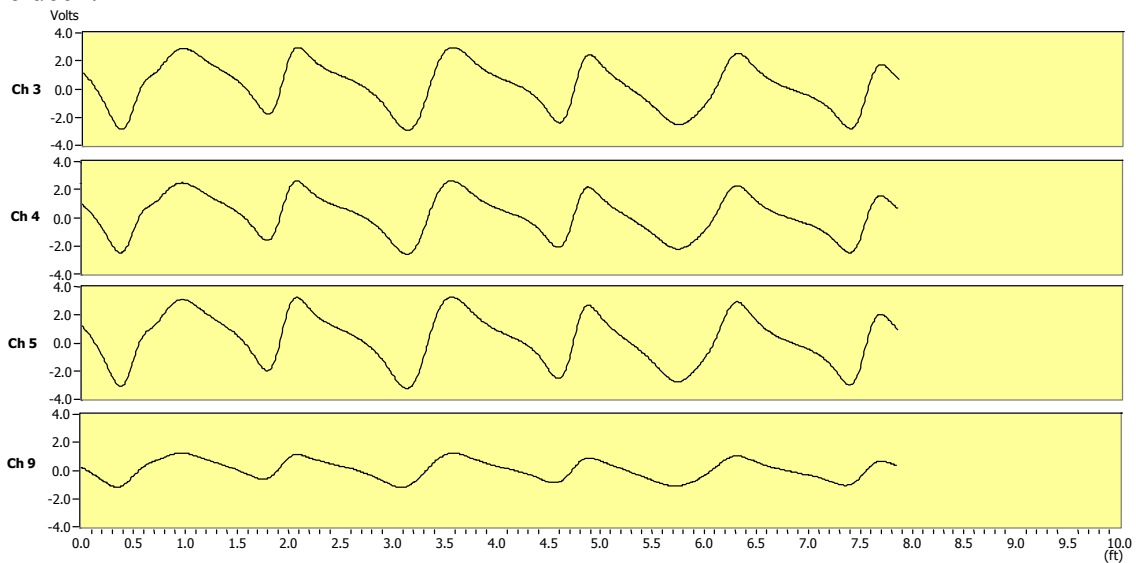


Figure 5.5 – Typical MFL data (four sensors) for an 8-ft long tendon without flaws

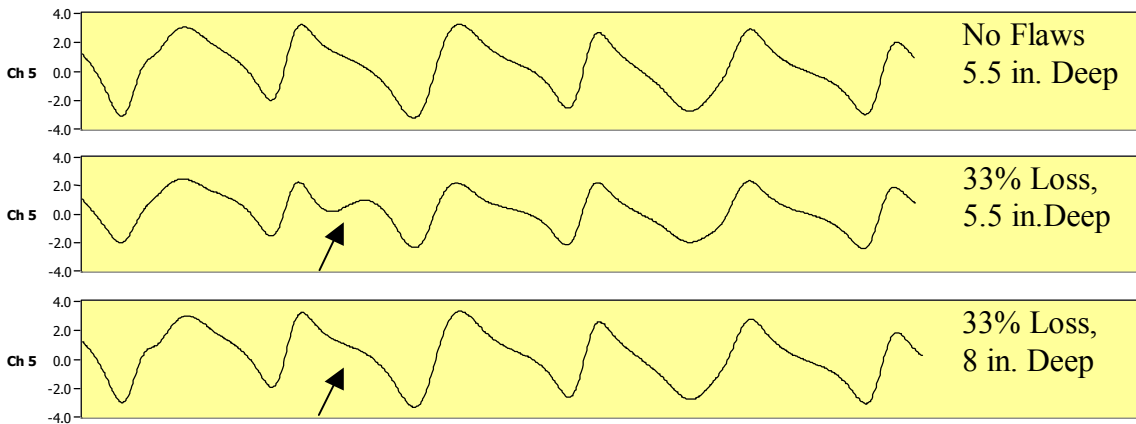


Figure 5.6 – MFL data from one sensor (Ch. 5) for the 8-ft long tendon for three conditions, no flaws (5.5” deep), 33% loss (5.5” deep), and 33% loss (8” deep)

Professor Ghorbanpoor studied the feasibility of identifying losses of cross sectional by cutting some strands in the tendon. Figure 5.6 compares the MFL data from one sensor for a tendon with no flaw, a tendon with a 33% loss in cross sectional area located at 5.5 inches from the surface, and a tendon with a 33% loss located at 8 inch from the surface. The MFL laboratory test for the tendon at 5,5 inches from the surface clearly identified the flaw on the tendon. However, the flaw on the tendon located at 8 inches from the surface is not clearly recognized. As a result of this study, Professor Ghorbanpoor concluded that using this specific equipment, the MFL test would only recognize major flaws (losses in cross sectional area larger than 33%) at the tendons of the Ramp D Bridge.

5.5 Field Testing

Prior to the MFL field testing, the location of the tendons within the top of the concrete deck at Spans 5, 6 and 7 were marked with spray paint. The tendons were located using ground penetration radar in the South part of the bridge. The operation involved locating 4 or 5 points per segment in each one of the tendons and spray painting along the points by linear interpolation without using any straight edge or similar assistance. This last operation resulted in an imprecise location of the tendon path, as can be seen by the waviness of the tendon paths shown in Figure 5.7. In the North part of the bridge, the tendons were located by measuring the offset of the tendon duct from the centerline of the section at the segment joints, and interpolating linearly in between these points. In this case, previous to the spray painting a straight line was marked with a chalk line. Offsets were obtained from the available Ramp D Bridge contract drawings. The accurate location of the tendon is essential for the successful application of the MFL test, since the magnetic flux in the tendon is very sensitive to the distance between the tendon and the magnets and sensors.



Figure 5.7 – Spray painted tendon paths

Professor Ghorbanpoor performed the test during the period of March 27 to March 30, 2002. A technician provided by the consultant assisted him. In addition to the MFL testing his scope of work also included performing impact-echo testing. During the testing period all marked tendons in Spans 5, 6 and 7 were tested. The effective time to

perform this operation was approximately 2.5 days and, in this time frame, a total of 52 post-tensioned tendons were tested. The length of each tendon varied from approximately 30 feet to 150 feet. The starting point for the test was either at the anchored end of the tendon or at the centerline of a pier (half-length of the tendon). In general, the actual test was performed quickly. The operator guided the equipment along the marked tendon walking at a normal pace. During the test the MFL data was displayed on the computer screen monitored by the operator. The MFL data collected at each location was then saved in the computer for post-processing and analysis. This procedure was repeated at each tendon location.

At the end of the testing program Professor Ghorbanpoor performed an overall evaluation of the MFL data recorded in the field. He indicated to the consultant that the data did not reveal any obvious indication of the presence of major flaws. However, as previously determined in his laboratory tests, the equipment used could only detect a major flaw of at least 33% loss of the tendon cross sectional area. Consequently, the induced flaws ranging from 12.5% to 25% were not detected.

Since Professor Ghorbanpoor could not identify any flaws from his initial inspection of the test results, the consultant requested him to re-examine the results. However, this time the test was performed with additional information. The consultant requested for a comparative analysis of the recorded MFL data to be conducted on pairs of tendons. Each pair would consist of one tendon with induced flaws and one without induced flaws. The consultant provided Professor Ghorbanpoor with a list of the pair of tendons to be compared (the control tendon and the one with the induced flaw). This list identified the segment number in which the flaw was located and if the flaw was in the trumpet region or the duct region.

The first three locations were in the trumpet region of the tendons. Professor Ghorbanpoor indicated that no reliable MFL interpretation could be made in these areas. As previously noted, a tendon must be magnetic flux saturated in order for a flaw to leak flux. However, at these locations the tendons were located deep into the concrete at approximately 8 inches from the surface of the concrete deck. Thus, magnetic flux saturation could not be achieved with the magnets used. In addition to the problem of the strength of the magnet, the trumpet regions of the tendons are generally difficult to evaluate due to the high congestion of reinforcement steel (spiral and stirrups) and the end anchor plate, which produces signals difficult to interpret.

The fourth location provided was not used since the MFL testing was not conducted on the tendon. The next four pairs of tendons were located in duct regions. At these locations, Professor Ghorbanpoor provided a comparison between the signals of the pair of tendons and identified the flawed tendons. He indicated that the test interpretation was pushing the capability of the system for this application to its limits. He indicated that the factor contributing to this difficulty are variations and uncertainties in the location of the tendons, greater than expected depth of the tendons in the deck and smaller than 33% cross sectional losses in the tendon. The results of his comparison study are as follows:

Location 5: Two strands were cut in Tendon 7 (16.7% of tendon area) in the North (left) part of the bridge at the upstation edge of Segment 89. Tendon 9 was chosen as the control tendon. In this case, the starting point for the test was the centerline of Pier 7. Figures 5.9 and 5.10 graphically display the MFL data for Tendons 7 and 9, respectively. The data shown represents the 10 ft length beginning at a distance of 30 ft from the starting point of the test. Professor Ghorbanpoor explains that the data for Tendon 7 reflects an indication for the possible presence of a flaw at approximately 35 ft from the starting point of the test. This point corresponds exactly to the location of the induced flaw. He indicates that the signal amplitude pattern at that location is similar to that observed in the laboratory tests (Figure 5.6). He also indicates that the MFL data for tendon does not reveal a pattern associated with a flaw. The results of his comparative analysis correctly identify the flawed and control tendon.

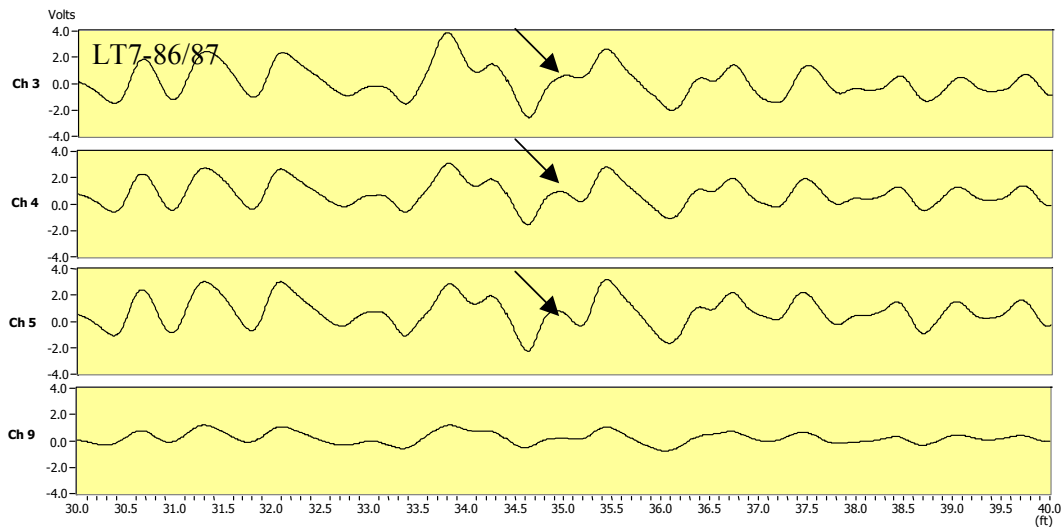


Figure 5.9 – MFL signals (4 channels) for Tendon 7 between Segments 86 and 87 (data for 5 feet of the tendons on both sides of the joint between Segments 86 and 87)

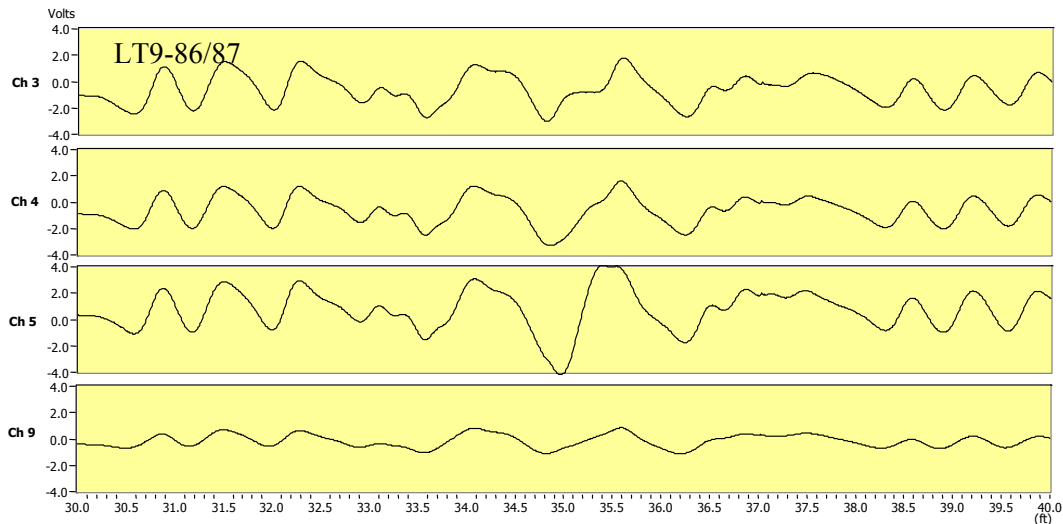


Figure 5.10 – MFL signals (4 channels) for Tendon 9 between Segments 86 and 87 (data for 5 feet of the tendon on both sides of the joint between Segments 86 and 87)

Location 6: One and a half strands were cut in Tendon 13 (12.5% of tendon area) in the North (left) part of the bridge at the up station edge of Segment 86. Tendon 11 was chosen as the control tendon. The flawed and control tendon were correctly identified.

Location 7: One and a half strands were cut in Tendon 13 (12.5% of tendon area) in the North (left) part of the bridge at the down station edge of Segment 79. Tendon 11 was chosen as the control tendon. The flawed and control tendon were correctly identified.

Location 8: Two strands were cut in Tendon 13 (16.6% of tendon area) in the North (left) part of the bridge at the down station edge of Segment 76. Tendon 14 was chosen as the control tendon. The flawed and control tendon were correctly identified.

Professor Ghorbanpoor was able to identify the tendons with the induced flaws and their exact positions at all of these locations (Locations 5-8). The MFL data for these tendons revealed characteristic variations of signal amplitudes similar to the ones observed at flaw locations in the laboratory tests.

5.6 Summary and Conclusions

The Magnetic Flux Leakage Testing performed to assess the conditions of the top slab post-tensioning tendons, was unable to identify losses of tendon area under truly blind conditions. The method failed to locate the tendons with the induced flaws in trumpets. The reason being that the equipment used did not have magnets strong enough to magnetically saturate the tendons and, consequently, produce the flux to leak. In laboratory test studies resembling the conditions encountered in Ramp D Bridge (tendons positioned at a distance of 5.5 inches from the test surface) Professor Ghorbanpoor, indicated that his equipment was able to detect only major flaws (in the range of 33% of the section area). He indicated that equipment with stronger magnets, which will be able to magnetically saturate the tendons in conditions similar to the ones encounter in Ramp D Bridge, could be fabricated. Unfortunately, this was outside of his scope of work in this project.

Upon a more detailed re-examination of the test data requested by the consultant, in which the data was compared for a pair of tendons (one tendon with and one without induced flaws), Professor Ghorbanpoor was able to correctly identify the tendons and the location of the induced flaw (only when flaws were located outside of the trumpet region of the tendons). The magnetic flux leakage signal due to the induced flaws, although weak, were recognized in the MFL signals of the bottom MFL sensors.

As the method is very sensible to the distance between the magnet and the tendon, a precise description of the tendon path painted on the deck is required. This task can be performed using the Impulse Radar Testing method and can be a very time consuming operation. The testing itself is performed in a quick manner requiring the operator to guide the equipment along the marked tendons walking at a normal pace. Consequently, large areas of the bridge deck can be tested in very little time.

The MFL method has been applied with success to test the conditions of externally post-tensioned tendons (Mid Bay Bridge) and the conditions of prestressing strands in concrete girder bridges. It seems that the MFL method could be applied successfully to assess the conditions of the post-tensioned tendons in segmental bridges with internal tendons, provided that the equipment used has magnets strong enough to magnetically saturate the tendons and the tendons are precisely located. However, even with the use of stronger magnets, it appears that the conditions of the tendons located in the trumpet areas will be difficult to assess. This is primarily due to the fact that these tendons are located deep within the concrete deck and also due to the magnetic disturbance created by the anchor plates and the local anchorage reinforcement, such as the spirals.

Chapter 6 – High Energy Linear Accelerator Inspection

6.1 Introduction

X-ray inspection is currently being used as a non-destructive testing method on post-tensioned concrete structures to determine defects and flaws in the post-tensioning system. This non destructive testing method was applied to the post-tensioning system of Ramp D Bridge at the Fort Lauderdale International Airport. It was performed in March of 2002 by High Energy Service Corporation (HESCO). The goal was to determine its accuracy in the identification of defects or flaws in post-tensioned structures. The consultant (DMJN+HARRIS, INC) determined 16 testing points in the last three spans (approximately 300') of the bridge prior to the arrival of HESCO. These points were marked on the top of deck (Figure 6.1) and inside of the box girder (Figure 6.2). The X-Ray testing locations were determined based on the findings during Endoscope Inspection, Impact-Echo testing, and areas where damage was induced to strands for the Magnetic Flux testing procedure.



Figure 6.1 – Location at the top of deck for X-Ray inspection



Figure 6.2 – Location at the inside of the Box for X-Ray inspection

6.2 Equipment

The HESCO equipment used for this procedure consisted of a portable linear accelerator. The Contractor (PCL) provided HESCO with a forklift for the mobility of the testing equipment (Figure 6.3). A portable film developing company was hired by HESCO to develop the film onsite during the testing procedure. The remaining equipment, provided by FDOT District 4 Facilities, consisted of an under-bridge inspection vehicle (snooper truck), a power generator and night lighting. Also, the Florida Highway Patrol provided traffic control of the roadway traveling underneath the bridge during the testing procedure to prevent radiation exposure to the traveling public.



Figure 6.3 – Linear Accelerator suspended by the forklift

6.3 Testing Procedure

The testing took place at night to minimize the amount of traffic traveling underneath the bridge. The procedure was conducted with two technicians: one technician operated the x-ray equipment and the other set the film on the inside of the box girder. Inside the bridge, multiple 14”x17” sheets of film were arranged at each shot location to ensure that the picture was captured. This was a consequence of the uncertainty that the top shot location coincided exactly with the placement of the film inside of the box. The film was held in place by telescoping poles and duct tape. The film for each shot location was identified and marked with lead lettering to coincide with the consultants point labeling convention (see Figure 6.4). At the same time, the x-ray source equipment was set-up on top of the deck using the provided forklift (as seen in Figure 6.3). Once the equipment and film was set-up, people were cleared from the testing location and the traffic traveling on the roadway underneath the bridge was stopped outside a radius of about two hundred feet centered at the bridge. The time it took to take each shot varied from approximately 3 to 15 minutes depending on the thickness of the slab at the testing location.

6.4 Film Processing & Results

A film processing truck was hired for onsite film developing during the time of testing. The truck developed the film in a short period of time and provided a good light source for inspecting the pictures. Viewing the pictures onsite enabled the technicians to determine if the film was located in the correct position, and to determine if another shot at the same testing location was required. The viewing was accurate with flaws and defects easily detectable (Figure 6.5). Defects detected with the x-ray consisted of voids, damaged strands, damaged ducts, and flaws induced in the concrete. However, areas where the deck was saw cut and patched showed defects that required an additional level of interpretation.

Due to the nighttime work limitations and the initial set-up time of the equipment, only 12 of the 18 points could be completed. HESCO's final report is presented in Appendix G. Within their report, HESCO provides a table indicating their findings at every testing point. These results were compared with the consultant's findings and are shown in Table 6.1. Note that some defects identified by HESCO within the report are not a clear interpretation of the actual defects. Therefore, it is recommended that for future x-ray inspection of post-tensioned structures, the technician should analyze the pictures with the assistance of a structural engineer to clarify the defects or flaws.

A brief review of the literature on this subject reveals that in some cases a quantitative view of the picture could be performed by scanning the picture and drawing the film density along different lines of the picture. This procedure helps in the identification of the defects and flaws. In this case, a similar procedure was not used and the interpretation was only based on looking at the picture.

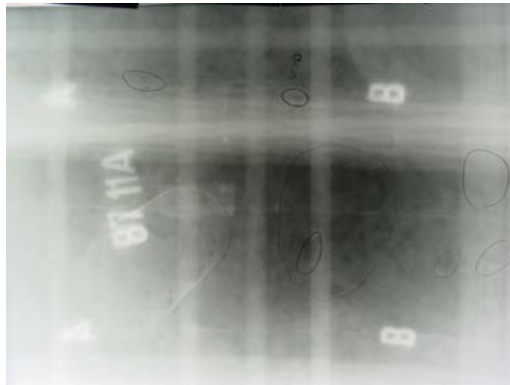


Figure 6.4 X-ray film after development

Table 6.1

Seg.	Hole I.D.	Defects Reported by HESCO	Defects Reported by Consultant
89	S1	Broken and cut strands, voids in grout	A 10"x8" saw cut in deck was made at trumpet location, trumpet was cut open and 21 wires (3 strands) were cut.
88	SS1	Voids in grout, ground strands	An 8"x6" saw cut in deck was made at trumpet location, trumpet was cut open and 11 wires (1.5 strands) were cut.
88	13C	Voids in conduit at left, voids in concrete	Void reported by Impact-Echo.
88	13D	Voids in grout, ground strands, strands have been separated, broken conduit casing	Point tested with Impact-Echo and void was not evident.
87	11A	1" x 1/2" void in center of film w/smaller 1/4" voids surrounding, possible broken cable B-B, coil of wire	Void reported by Impact-Echo.
86	SS3	Cable has been ground/cut in two, partial pcs of rebar, pulled back conduit sheeting is visible	An 8"x6" saw cut in deck was made at duct location, duct was cut open and 14 wires (2 strands) were cut.
86	SS9	Cable conduit on right contains large void and is ground and cut, cable in center of view is ground and cut, missing sections of cable, strands of center cables or broken at bottom of view. Partial pcs of rebar, large "staple" in lower left also electrical wire, voids in grout	An 8"x6" saw cut in deck was made at duct location, duct was cut open and 10 wires (1.5 strands) were cut.
85	5A	Film moved, not readable	Void reported by Impact-Echo.
79	SS9	Saw cut from A to A, cable conduit and some cable cut, missing section of rebar, saw cut from B to B, voids in concrete	An 8"x6" saw cut in deck was made at duct location, duct was cut open and 10 wires (1.5 strands) were cut.
79	5B	Small voids in grout	Void reported by Impact-Echo.
79	13A	Large void in concrete by wire IQI, breaks in conduit wall, broken cable strand below "B" on right, voids in grout	Void reported by Impact-Echo.
77	11B	Voids in concrete, cable in center has large strands	Void reported by Impact-Echo.
76	S1	Not tested	A 12"x8" saw cut in deck was made at trumpet location, trumpet was cut open and 21 wires (3 strands) were cut.
76	SS3	Not tested	An 8"x6" saw cut in deck was made at duct location, duct was cut open and 14 wires (2 strands) were cut.
69	11B	Not tested	Point tested with Impact-Echo and void was not evident.
56	S5	Not tested	An 8"x6" saw cut in deck was made at duct location, duct was cut open and 21 wires (3 strands) were cut.

6.5 Summary and Conclusions

The procedure needs refinement to be a cost effective testing procedure for civil structures. The issue with the high-energy testing procedure, as it is presently implemented, is that it is a time consuming and expensive testing method. The equipment used is big and bulky requiring machinery such as a forklift to maneuver it into position. Also, it needs access to the underside of the shot location which requires an under bridge inspection vehicle (snooper truck) for bridge structures. The testing procedure produces high levels of radiation, which is hazardous to the health of the surrounding public. Therefore, the procedure requires the shut down of traffic on the structure and the roadways or waterways below and around it. Consequently, on high capacity highway structures the testing task must include a maintenance of traffic scheme. A film processing crew is needed at the site to handle film development to insure a satisfactory shot of the location under investigation. The time to investigate each location includes maintenance of traffic on the bridge for maneuvering the equipment, setting of the linear accelerator, placement of the film on the underside of the deck, maintenance of traffic of roadways or waterways below the bridge during the X-Ray procedure and the processing of the film. This testing method, at this stage, is very time consuming and costly for the department.

This procedure can be very useful if used as a supplement to other non-destructive testing procedures. Problem areas in a bridge should be identified by other means prior to the X-Ray testing. For example, if significant voids have been detected by Impact-Echo or if cross-section loss has been determined by Magnetic Flux Leakage, X-Ray testing at these locations can be used to verify the extent of these post-tensioning deficiencies. The testing procedure produces accurate images of the post-tensioning defects that, if properly interpreted by the combination of an x-ray technician and a structural engineer, can provide accurate information about the health of the bridge.

Chapter 7 – Bridge Demolition and Inspection of Existing Ramp D Structure

7.1 Introduction

The Ramp D Bridge was demolished while maintaining the traffic on the roadways and railroad below. Due to the complexity of the structure and existing constraints, the demolition was done in phases, requiring various types of heavy machinery including a concrete saw, a concrete crushing machine, a pneumatic punching machine, a wire saw, cranes and several stability towers. The evaluation of Non-Destructive Testing Techniques Program was performed in parallel with the bridge demolition, which required substantial coordination with the Contractor. This program focused on the last three spans of the bridge, which, consequently, were the last spans demolished. Prior to the demolition and throughout the monitoring of the demolition, the structure was thoroughly inspected. The inspection was performed to evaluate the overall condition of the structure and to determine the condition of the internal post-tensioning system.

7.2 Ramp D Demolition Description

Demolition of the existing bridge began once traffic was shifted to a newly built ramp. The first stage of the demolition began by saw cutting five feet of the cantilevered wings, as shown on Figure 7.1, in order to reduce the weight of the segments as well as provide a convenient edge on which to effectively use the concrete crushing machine or wire cutting saw. This, however, did not compromise the integrity of the structure in the longitudinal direction since longitudinal tendons were not affected.



Figure 7.1 – View of a partially demolished cantilever with wings saw cut.

The bridge was demolished in reverse order of its original construction (balanced cantilever). A typical demolition sequence of one of the cantilevers proceeded as follows. First, a temporary tower was installed at the pier. The tower was supported on the existing footing and the superstructure was shimmed against the temporary tower (the first segment away from the pier segment). If the pot bearing was identified as an expansion bearing, the bearing was fixed by welding the sliding plates against the masonry plates. The next step was to cut the segment closure pours and isolating the pier and the portion of the superstructure between the cuts from the rest of the bridge. The

demolition proceeded by either, demolishing the segments using the concrete crushing machine or, by cutting the segments using the wire cutter. The demolition of each segment continued as alternate segments from each side of the cantilever were removed in such a way as to minimize the unbalanced force.

In some cases a heavy counterweight was used to allow having a couple of unbalanced segments and, consequently, reducing the mobilization of the equipment from one side of the cantilever to the other side. This demolition process proceeded until the pier segment was reached. This segment was dismantled using the crane. Once the isolated superstructure was completely demolished, the pier column was wire cut at the base and tilted over using the concrete crushing machine. Lastly, the footing was buried in place. This typical procedure was used throughout the demolition of the entire bridge structure except for the first and last spans where certain constraints existed. The demolition process used at these two locations is explained later in this section.

The most challenging part of this demolition procedure was the cutting of the closure pour segment as shown in Figure 7.2. Since a clear biting edge was not available at the junction between the top slab and the web, additional steps were required. One step was the opening of holes by a pneumatic puncher on the top slab (see Figure 7.3). This would facilitate the concrete crushing machine with a better edge to work with in demolishing the closure pour. Another step was the torch cutting of the (continuity and positive moment) tendons that were passing through the closure pour. Finally, once the closure pour was cut, the demolition of the segments proceeded in a faster pace. Approximately four segments were demolished each day using the crushing machine (the contractor-preferred way of demolition). Figures 7.4 through 7.7 depict the demolition process and equipment used.



Figure 7.2 – Cutting the closure pour at mid span with the concrete crusher



Figure 7.3 – Punching holes in top slab to facilitate concrete crusher machine operation



Figures 7.4 and 7.5 – Details of concrete crusher demolition method



Figures 7.6 and 7.7 – Details of concrete crusher demolition method

The concrete crushing machine worked well for most areas of the bridge. However, in areas where the bridge crossed over roadways in operation, such as US-1, perimeter road and railroads, a different demolition method was used. In these areas, a wire cutting procedure was used in order to minimize the amount of debris that could affect the roadways (still in operation) beneath the bridge. In order to use the wire cutter, holes were made at the top and bottom slab. This allowed the wire to wrap around the web, the

bottom and top slab and the cantilevered wing, cutting half of the section at a time. In order to proceed with this operation, the equipment needed to be anchored to the top slab.

The main problem that occurred during this demolition process was that the wire would continually break. This complication caused several delays. The work was performed mainly at night to minimize the maintenance of traffic. The production rate for the wire sawing process varied from one segment to four segments per night. Figures 7.8 through 7.11 illustrate the operation of the wire cutting operation.



Figure 7.8 and 7.9 – Details of wire cutting demolition method



Figure 7.10 and 7.11 – Details of segment removal and storage

The demolition of the first and last span presented additional complications and required another alternate demolition method. One of the complications that existed was that the first span crossed the perimeter road, which required traffic to be maintained at all times. Another constraint was that a railroad track was located just to the east of Pier 2. Consequently, the crane had to be located to the east of these tracks. But at this location the crane was not able to reach the segments in the first span. As a result, falsework spanning from the abutment up to the first pier (Pier 2) was installed. Finally, segments were wire cut and then rolled back onto the abutment, from where they were lowered and demolished.

The last span (Span 7) was a curved span with a 5% super elevation and was located just east of US-1 North. The contractor's intent was to tilt the entire span onto the ground. But one of the constraints at this location was that the whole span needed to fall towards the outer side of the curve (away from US-1), opposite direction of the 5% super elevation grade.

The contractor approached this task by providing temporary supports at the quarter points of the last span closest to the pier. Then, the cantilevered segments on Span 6 were demolished using the concrete crushing machine. Next, in order to tilt the entire span, the temporary stability towers supporting the outer side of the curved span were removed. However, the span did not fall. As a result, seven of the twelve prestressed concrete piles at the abutment, located towards the outside of the curved span, were broken. At the end, the concrete crushing machine was used to push the span toward the opposite side of curvature. The entire span successfully fell to the ground as a rigid body as shown in Figure 7.12. Surprisingly, the impact only produced minor cracks. Lastly, the concrete crushing machine was used to pulverize the entire span, completing the demolition of the bridge.



Figure 7.12 – Demolition of Span 7

7.3 - Evaluation of Existing Ramp D Structure

7.3.1 Visual Inspection

A visual inspection of the inside and outside of the box girder structure while the bridge was still in service showed that the bridge was in very good service condition. Concrete deficiencies detectable by a visual inspection include cracking, spalling, pop-outs, leaching or efflorescence, scaling, honeycombing, and surface wear on the deck. Other detectable defects from a visual inspection include water leakage at the segment joints, anchor pourback deficiencies, distress on bearings and distress on expansion devices. There were not any relevant deficiencies of this kind noted during this inspection.

The top of deck was transversely grooved to provide a safe riding surface for the traveling public and did not show any relevant deficiencies. The bridge had a superelevation transition with a maximum cross-slope of 5%. Drainage scuppers were

placed on the low side of the cross-section to remove rainwater runoff from the bridge deck. These scuppers adequately drained the bridge and no ponding was evident on the deck during heavy rains. The riding surface was in good condition and provided a pleasantly smooth ride. The exterior faces of the bridge including the box girder and the piers had a coated finish that provided an aesthetically pleasing structure. A visual inspection of the exterior of the bridge was performed from below the bridge (Figure 7.13) and an inspection of the inside was performed from the inside of the girder (Figure 7.14). There were no evident signs of concrete deficiencies or distress present.

The bridge was constructed with the balanced cantilever method of erection, which requires wet joints (epoxy at the segment joints). These joints had epoxy present and did not present any signs of water leakage (Figure 7.15). Water leakage at the joints can allow water to seep into the post-tensioning ducts creating corrosion. Since the bridge was constructed by balanced cantilever method of erection with internal post-tensioning, the only pour backs remaining exposed were for the bottom slab and web continuity tendons. These could be seen from the inside of the box girder and were in very good condition (Figure 7.16). Pot bearings at Pier 6 were checked with the snoopers and were found in very good condition and showed no signs of distress (Figure 7.17 & Figure 7.18). The modular expansion devices did not show any sign of distress.



Figure 7.13 and 7.14 – Exterior and interior view of structure



Figure 7.15 and Figure 7.16 – Segment joint and post-tensioning pourbacks



Figure 7.17 and Figure 7.18 – Pot bearings at Pier 6

7.3.2 Endoscope Inspection

As part of the evaluation of the different non-destructive testing methods an endoscope inspection was performed in the last three spans of the bridge prior to the testing. The endoscope inspection is described in detail in Chapter 2 of this report. This was performed to determine the condition of the internal post-tensioning before the non-destructive testing took place. This inspection also gave a good ground of comparison for the results of the different non-destructive testing methods. This inspection indicated that the overall condition of the post-tensioning was very good. The tendons in most cases were fully grouted with a small bleed water void at the top of the duct (Figure 7.19). The grout encasing the post-tensioning strands was in very good condition. It was sound with no signs of deficiencies such as moisture, efflorescence or cracking. In few testing locations, mainly trumpet locations, voids were found with tendon exposure. The duct had a double curvature transition into the anchor locations, which may have been causing a lack of grout in these areas. The tendons that were found exposed due to lack of grout were also in very good condition. The exposed tendons did not show any relevant deficiencies. In the worst case there was minor surface corrosion (Figure 7.20). This is a good indication that the ducts and the wet joints were properly sealed preventing corrosion of the post-tensioning steel.



Figure 7.19 and 7.20 – Endoscopy inspection

Focusing only on the relevant flaws (large grout voids or ungrouted ducts), the endoscope inspection revealed that only 13 of 156 locations tested (8.3%) had inadequate strand protection.

7.3.3 Inspection of Remains

As described in Section 7.2 of this report, two methods were used to demolish the bridge. Most of the bridge was demolished using a concrete crushing machine. This was the most effective method of deconstruction for the contractor. However, the nature of this demolition method did not allow inspectors to perform a forensic investigation of the segments post-tensioning system for voids in the tendon ducts. For the portions of the bridge that were dismantled by crushing, the steel remains were separated from the concrete, which permitted an evaluation of the post-tensioning remains (Figures 7.21 and 7.22). This was achieved by climbing through the steel remains and performing a hands-on inspection of fully intact anchor systems (Figures 7.23, 7.24, 7.25), post-tensioning strands (Figures 7.26), the ducts and grout within the ducts (Figures 7.27). This inspection of the remains allowed a detailed evaluation of the structures post-tensioning system. In some cases there was a fully intact tendon with the anchoring system, strands and portions of the duct still intact with the grout (Figures 7.28). An overall condition of the post-tensioning remains (including anchoring system, strands, grout and duct) were found to be very good, with no deficiencies noted except minor surface rust that developed after days of being exposed to environment (Figures 7.29 and 7.30).



Figure 7.21 and 7.22 – Steel remains of crushed segments



Figure 7.23 and 7.24 – Intact anchor systems in remains



Figure 7.25 and 7.26 – Post-tensioning anchor and strands



Figure 7.27 and 7.28 – Fully grouted duct with strands



Figure 7.29 and 7.30 – Surface corrosion on remains after exposure to environment

7.3.4 Inspection of Segments

In areas where the bridge spanned over roadways and the railroad in operation, a wire-cutting machine was used to remove individual segments. The three areas in which this technique was used include US-1, Perimeter Road and the CSX railroad. The detail of this operation was described in Section 7.2 of this report. In the non-destructive testing

area (last three spans of the bridge), part of Spans 5 and 6 were located over US-1 and were dismantled by wire cutting each of the segments. This provided a good opportunity to assess the condition of the post-tensioning ducts in these areas. In the beginning of the wire cutting operation 5' of the cantilever wing was removed to reduce the segment weight (Figure 7.31). At this time the transverse tendons at these locations were visually inspected. The transverse post-tensioning was in very good condition and showed no signs of corrosion (Figure 7.32). The transverse ducts inspected were fully grouted and the grout showed no signs of deficiencies. A total of nine dismantled segments were investigated. The inspected segments were; Segments 63, 64, and 65 in Span 5, and Segments 68, 69, 70, 71, 75 and 76 in Span 6. These segments were placed on the ground next to the structure for the forensic investigation of the tendons. A total of 216 ducts at the segments faces were inspected. Each segment was inspected on its down station and up station face (Figure 7.33). The condition of each one of the tendon ducts was documented and a photo was taken to show the final condition of the post-tensioning. This information is provided within Appendix D of this report.

A statistical analysis was performed of the voids found on the top (cantilever) tendons during the forensic investigation. This was based on describing a void as ½" deep or larger, a small void as less than ½" deep (bleed water void) and grouted as no void. The recorded statistics are, approximately, 70% small voids, 9% voids and 21% fully grouted. It should be noted that the strands in the ducts with small voids were mostly encased within the grout and overall the strands were in good conditions. These findings (9% relevant flaws) are consistent with the endoscope findings (8.3% of relevant flaws). One testing area, which was not included in this forensic evaluation, was the segments adjacent to Pier 5. These segments were crushed before the forensic investigation could be performed. These areas showed significant voids in the top tendons (Figures 7.34 and 7.35), although the core drilling shows that the tendons had no signs of corrosion (Figure 7.36).

In all cases the bottom ducts were found completely grouted (Figure 7.37). Only the tendon ducts running through the webs (continuity tendons) and anchored at the pier segment diaphragms were found completely ungrouted at the pier diaphragm segment and the adjacent segment (Figure 7.38). This can be explained by the significant change in geometry of the duct at this location. At these locations the tendons were found in good condition, without signs of any corrosion. Also, during the visual inspection a case was found in which the segment was cut at the same location where the endoscopy was performed. There it was noticed that in two locations the endoscopy reached the duct surface but did not penetrate the duct (Figure 7.39). At these particular locations the ducts were previously rendered as fully grouted when, in reality, they had a small void.



Figure 7.31 and 7.32 – Removal of portion of cantilever and transverse post-tensioning



Figure 7.33 and 7.34 – Forensic inspection procedure showing voided ducts



Figure 7.35 and 7.36 – UngROUTED tendon



Figure 7.37 and 7.38 –Tendons in bottom slab and continuity tendon in web



Figure 7.39 - Endoscopy inspection location not penetrating duct

7.4 - Evaluation of Segment Epoxy Joint Quality

The leaking joints in the I-75/I-595 Sawgrass Interchange, just a few miles away from Ramp D, prompted the FDOT to evaluate the quality of the top slab epoxied joints between segments in the airport bridges. A total of ten (10) cores were taken from Bridge A of the Fort Lauderdale-Hollywood International Airport before its demolition. Inspection of the cores (see Appendix C) revealed a 96% bonded area between segments. Additionally, 4 cores were selected and tested following the requirements of the Split Cylinder Test Method (ASTM C496-96). The minimum tensile stress computed from the test results was 636 psi (see Appendix C), which indicates an excellent bond between segments and an excellent quality of the epoxy application during construction.

Chapter 8 – Conclusions and Recommendations

8.1 Conclusions

General conclusions for each of the different NDT testing techniques used to assess the quality of the internal post-tensioned tendons at Ramp Bridge D of the Fort Lauderdale International Airport Interchange are reported below:

8.1.1 Endoscope Inspection

The use of the endoscope to evaluate the condition of top slab tendons was found, in this testing program, to be a reliable testing method. Testing, at a given point in the deck, was done in an average of 10 minutes and required a four-person crew. The endoscope inspection should be preceded by more economical NDT testing methods that locate areas where tendon flaws (void, corrosion, loss of section, etc) are most likely to exist. Also, it is critical for drilling to be done with much care in order to avoid damaging the tendons at the time of inspection. The use of special concrete drills capable to detect the steel duct and stop before damaging it is recommended. And finally, after inspection, drilled holes should be appropriately patched to avoid any future maintenance and durability problems.

8.1.2 Impulse Radar Testing Method

The impulse radar testing method provided quick and accurate location of the tendons. The method requires small size equipment that can be operated by a two-person crew. A test at a given point can be done in less than one minute. Although the location of the tendons at the segment joints was performed accurately based on the contract drawings information, the location of these tendons between segment joints could not be ascertained based on this information only. At these locations Impulse Radar was 80% reliable in locating the tendons. The method can provide not only the horizontal location of the tendon but also the depth into the concrete, which can be of tremendous value in the interpretation of the Impact Echo results.

8.1.3 Impact-Echo Testing Method

The Impact-Echo testing method was found to be a reliable method to identify grout voids in tendon ducts provided that a combination of techniques including impulse radar and rebar locators are used. In addition, invasive endoscopy tests are required to correlate the interpretations of the signals with the existing conditions (deck 3-D geometry, nearby tendons and mild steel, etc). The reliability of the method (defined as detecting large voids) was found to be higher than 60% in this testing program. Locating the testing point and performing the test can be done in less than 3 minutes with very small equipment operated by a two-person crew. The method is very effective in providing a clear indication of a sudden discontinuity in material properties and distinguishing whether this discontinuity represents a void or a stiffer material (the

tendon). However, the size of the void, (an essential factor in assessing its importance and possible consequences), is difficult to ascertain.

It seems that the method can be enhanced by first a more accurate analysis procedure (modeling more accurately the actual geometry of the problem instead of the simplified one dimensional wave propagation concepts used presently) and second providing one or more extra receivers along the length of the tendons which would provide extra information that would help to identify the size of the void.

Since this method currently fails to identify the size of the void and the possible exposure on the strands, the Impact-Echo test should be complemented by invasive techniques, such as Endoscope Inspection, to clearly identify the relative importance of the voids and to find the actual conditions of the tendon strands.

8.1.4 Magnetic Flux Leakage Method

The testing performed using the MFL method was, for practical purposes, found inadequate to identify losses of tendon area. The method failed to locate the tendons with the induced flaws in anchor trumpets. The reason being that the equipment used, did not have magnets strong enough to magnetically saturate the tendons and consequently, produce the flux to leak. Upon a more detailed analysis of the test data, performed by comparing pairs of tendons (a tendon with induced flaws and a tendon without induced flaws), the analyst was able to correctly identify the tendons and the location of the man-made flaws, when located outside of the trumpet region of the tendons. However, this does not provide the necessary confidence in the method (in its current condition) for practical applications.

It seems that equipment with magnets strong enough to magnetically saturate the tendons in conditions similar to the ones encountered in balance cantilever segmental construction, can now be fabricated. However, it appears that even with new equipment the tendons located in the trumpet areas will be difficult to assess. This is primarily due to the fact that these tendons are located deep within the concrete deck as well as to the magnetic disturbance created by the anchor plates and the local anchorage reinforcement, such as the spirals.

The MFL method is fast in terms of data acquisition. However, it requires careful and expert interpretation of the test record. A major drawback of this method is that it requires a very accurate depiction of the tendon path at the roadway surface, which, in turn, requires the extensive use of another testing methods such as Impulse Radar.

8.1.5 High Energy Linear Accelerator

This procedure was found to have the potential to be a very effective method for locating flaws in tendons deeply embedded in the concrete. It provided a relatively clear view of the elements inside the concrete. To be most effective, the interpretation of the film should be performed by an expert in both concrete bridges and x-rays. At this moment,

the method is very expensive, very cumbersome to use, and requires a large amount of heavy equipment and a large crew size. In addition, the scatter of the x-ray beam requires that a large radius around the testing area to be evacuated to avoid health issues. In the future, if more compact equipment is developed for use in bridges, this method could be a valuable tool for the inspection of post-tensioned bridges.

8.2 Recommendations

The recommendations regarding the NDT methods to be used to assess the conditions of internally post-tensioned tendons for balanced cantilever bridges stated below are based on the specific results found in the testing program performed at Ramp D Bridge at the Fort Lauderdale International Airport Interchange. Many other NDT procedures like those listed in ACI 228.2R-98 “*Nondestructive Test Methods for Evaluation of Concrete in Structures*” have not been considered in this testing program. Furthermore, it is important to keep abreast of advancements in NDT Technologies, as well as improvements to existing NDT technologies when considering the inspection of these types of structures. If these new and improved technologies become economical and reliable methods, they too may be incorporated into the inspection plan recommended below.

As a result of this program, the following steps to inspect the conditions of the post-tensioning systems of segmental balanced cantilever bridges are recommended:

- Step 1 –** Examination of existing records and information, such as Contract Plans, Shop Drawings, As-built Plans and previous inspection reports.
- Step 2 –** Perform a detailed visual inspection of the bridge. The recommendations stated in the Florida Department of Transportation document titled “Post Tensioned Bridges Walk Through Inspections”, can be used for this purpose.
- Step 3 –** Depending on the results of the visual inspection the following scenarios are possible:
 - a) If the visual inspection does not reveal deficiencies that may affect the integrity of the post-tensioning system, no further action is needed. On the other hand, if the bridge has been in service for a number of years (say 10) and an in-depth inspection is warranted, then prepare a plan for inspecting the bridge using a combination of NDT testing (Impulse Radar and Impact-Echo) and invasive techniques (Endoscopy Inspection). The testing should be done on a representative sample of the tendons, at most 10%. The tendons to be tested and the test location on the tendons should be based on their structural importance.

- b) If the visual inspection reveals significant deficiencies such as water leakage at segment joints, efflorescence, concrete cracking or spalling; prepare an inspection plan combining impact echo an endoscopy inspection. In this case, however, the areas with significant deficiencies should be inspected in detail and, if deemed necessary, all tendons should be inspected. Other areas should be inspected following the 10% rule stated above.

Step 4 - If an inspection combining NDT testing techniques and invasive techniques is deemed necessary, then proceed as follows:

- a) Use a combination of as-built plans, impulse radar and rebar locators to locate the embedded steel components including both reinforcing steel and post-tensioning tendons. Mark the location of the embedded steel on the concrete surface.
- b) Artificially divide the tendons in sections (approximately five feet long each) and select a sample based on an statistically-based method like those employed in quality control programs.
- c) Investigate the selected sample for tendon voids using the Impact-Echo method. Calibrate the signal interpretation using the knowledge of embedded steel components and deck 3-D geometry with drilling and endoscopy. Using the calibrated signal interpretation complete the inspection of the selected samples. If the inspection does not reveal significant deficiencies and a high percentage of the test locations (say 95%) indicate no relevant voids, take no further actions. If other conditions exist, verify void relevance and strand integrity by drilling and inspecting with a flexible shaft endoscope.
- d) If the flexible shaft endoscope inspection find significant voids and strand corrosion, then expand the sample size.
- e) At each drilled hole determine the volume of the void by using a vacuum or a pressure device. If this volume is large then repair the void using vacuum grouting.
- f) Upon completion of the inspection clean the hole and repair the drilled hole with a fluid epoxy for the repair of old structures (like FDOT Type E).

Additionally, if the visual inspection reveals significant deficiencies that may affect the integrity of the post-tensioning system, a structural analysis of the bridge may be useful. This analysis should consider the as-built conditions of the bridge to develop a bridge load rating in which parametric studies can be performed to assess the relative importance of the different tendons. This will be extremely helpful in the planning of an

inspection plan that focuses only on the relevant tendons. If during the inspection, significant losses of tendon area due to corrosion are found, the structural analysis will most definitely be required to assess the structural integrity of the structure.

Appendix A – Endoscope Results

FORT LAUDERDALE AIRPORT STRUCTURE "D"
LIST OF TOP DECK CANTILEVER TENDONS INSPECTED

Segment 54: Top Tendons Left of CL of Box Looking Upstation (L)

Hole Id	Distance from Center of Box ft	Tendon No.	Comments
54 - L - 1	9'-0"	1	Trumpet. Drilling performed 1 ft from edge of upstation joint. Trumpet was fully grouted.
54 - L - 2	10'-3"	2	Trumpet. Drilling performed 1 ft from edge of upstation joint. Trumpet was fully grouted.
54 - L - 3	8'-0"	3	Drilling performed 1.5" from edge of upstation joint. Tendon was fully grouted.
54 - L - 4	11'-3"	4	Drilling performed 1.5" from edge of upstation joint. Tendon was fully grouted.
54 - L - 5	7'-6"	5	Drilling performed 1.5" from edge of upstation joint. Tendon was fully grouted.
54 - L - 6	12'-0"	6	Drilling performed 1.5" from edge of upstation joint. Tendon was fully grouted.
54 - L - 7	7'-0"	7	Drilling performed 1.5" from edge of upstation joint. Tendon was mostly grouted (slightly exposed) - a small void on the top of duct. Picture L1
54 - L - 8	12'-9"	8	Drilling performed 1.5" from edge of upstation joint. Tendon was mostly grouted (slightly exposed) - a small void on the top of duct. Picture L2
54 - L - 9	6'-6"	9	Drilling performed 1.5" from edge of upstation joint. Tendon was mostly grouted - a small void on the top of duct.
54 - L - 10	13'-6"	10	Drilling performed 1.5" from edge of upstation joint. Tendon was fully grouted.

Segment 54: Top Tendons Right of CL of Box Looking Upstation (R)

Hole Id	Distance from Center of Box ft	Tendon No.	Comments
54 - R - 1	9'-0"	1	Trumpet. Drilling performed 1 ft from edge of upstation joint. Trumpet was fully grouted.
54 - R - 2	10'-3"	2	Trumpet. Drilling performed 1 ft from edge of upstation joint. Trumpet was mostly grouted - a small void on the top of duct.
54 - R - 3	8'-0"	3	Drilling performed 1.5" from edge of upstation joint. Tendon was fully grouted.
54 - R - 4	11'-3"	4	Drilling performed 1.5" from edge of upstation joint. Tendon was mostly grouted - a small void on the top of duct.
54 - R - 5	7'-6"	5	Drilling performed 1.5" from edge of upstation joint. Tendon was fully grouted.
54 - R - 6	12'-0"	6	Drilling performed 1.5" from edge of upstation joint. Tendon was mostly grouted - a small void on the top of duct.
54 - R - 7	7'-0"	7	Drilling performed 1.5" from edge of upstation joint. Tendon was fully grouted.
54 - R - 8	12'-9"	8	Drilling performed 1.5" from edge of upstation joint. Tendon was fully grouted.
54 - R - 9	6'-6"	9	Drilling performed 1.5" from edge of upstation joint. Tendon was mostly grouted - a small void on the top of duct.
54 - R - 10	13'-6"	10	Drilling performed 1.5" from edge of upstation joint. No grout was found in tendon - strands fully visible. Strands were slightly corroded. Void in duct is over 5 ft in length (full length of endoscope inserted). Void was in upstation direction from drill point - downstation was grouted. Picture R1 & R2.

Segment 56: Top Tendons Left of CL of Box Looking Upstation (L)

Hole Id	Distance from Center of Box ft	Tendon No.	Comments
56 - L - 1	9'-0"	5	Drilling performed 1.5" from edge of upstation joint. Tendon was mostly grouted - a small void on the top of trumpet. Picture L3.
56 - L - 2	10'-3"	6	Unable to locate duct. Several adjacent holes were drilled to locate trumpet with no success.
56 - L - 3	8'-0"	7	Not Drilled.
56 - L - 4	11'-3"	8	Not Drilled.
56 - L - 5	7'-6"	9	Unable to locate duct. Several adjacent holes were drilled to locate ducts with no success.
56 - L - 6	12'-0"	10	Unable to locate duct. Several adjacent holes were drilled to locate ducts with no success.
56 - L - 7	7'-0"	-	
56 - L - 8	12'-9"	-	
56 - L - 9	6'-6"	*	Unable to locate duct. Several adjacent holes were drilled to locate ducts with no success.
56 - L - 10	13'-6"	*	Unable to locate duct. Several adjacent holes were drilled to locate ducts with no success.

* These locations were drilled to locate tendons 9 and 10 according to the contract drawing No. 160.

Segment 56: Top Tendons Right of CL of Box Looking Upstation (R)

Hole Id	Distance from Center of Box ft	Tendon No.	Comments
56 - R - 1	9'-0"	5	Trumpet. Drilling performed 1 ft from edge of upstation joint. Trumpet was mostly grouted - a void present on top. Water was encountered in duct but strands were grouted (protected). Water was clear - no rust. Picture R3.
56 - R - 2	10'-3"	6	Trumpet. Drilling performed 1 ft from edge of upstation joint. Trumpet was mostly grouted - a small void on the top of duct. Picture R4.
56 - R - 3	8'-0"	7	*** Additional hole drilled because of suspicion that plan layout of ducts is not correct. This would explain why some ducts are missing. Evidence of duct found at this location (small pocket void a couple of inches from surface - but not as large as the other voids found in ducts) but nothing conclusive. If duct present, it is fully grouted.
56 - R - 4	11'-3"	8	Not Drilled.
56 - R - 5	7'-6"	9	Drilling performed 1.5" from edge of upstation joint. Little grout was found in tendon - strands fully visible. Strand could be seen with flashlight from deck surface. Strands were moderately corroded (surface corrosion). Void in duct is over 3 ft in length. Void was in upstation direction from drill point - downstation was grouted. Picture R5.
56 - R - 6	12'-0"	10	Drilling performed 1.5" from edge of upstation joint. No grout was found in tendon - strands fully visible - moisture encountered. Strands were moderately to severely corroded. Void is over 5 ft in length (full length of endoscope inserted). Void was in upstation direction from drill point - downstation was grouted. Picture R6.
56 - R - 7	7'-0"	-	
56 - R - 8	12'-9"	-	
56 - R - 9	6'-6"	*	No Duct Found
56 - R - 10	13'-6"	*	No Duct Found

* These locations were drilled to locate tendons 9 and 10 according to the contract drawing No. 160.

Segment 57: Top Tendons Left of CL of Box Looking Upstation (L)

Hole Id	Distance from Center of Box ft	Tendon No.	Comments
57 - L - 1	9'-0"	7	Trumpet. Drilling performed 1 ft from edge of upstation joint. Location of duct was shifted, therefore the side of the duct was penetrated. Trumpet was mostly grouted with a small void at the top. Slight exposure of tendon. Picture L4.
57 - L - 2	10'-3"	8	Trumpet. Drilling performed 1 ft from edge of upstation joint. Trumpet was mostly grouted with small void at the top. Location of the duct was at approximately 5" deep. Approximately 1' on center from adjacent trumpet. Picture L5.
57 - L - 3	8'-0"	9	Not Drilled.
57 - L - 4	11'-3"	10	Not Drilled.
57 - L - 5	7'-6"	*	No Duct Found
57 - L - 6	12'-0"	*	No Duct Found
57 - L - 7	7'-0"	-	
57 - L - 8	12'-9"	-	
57 - L - 9	6'-6"	-	
57 - L - 10	13'-6"	-	

* These locations were drilled to locate tendons 9 and 10 according to the contract drawing No. 160.

Segment 57: Top Tendons Right of CL of Box Looking Upstation (R)

Hole Id	Distance from Center of Box ft	Tendon No.	Comments
57 – R - 1	9'-0"	7	Trumpet. Drilling performed 1 ft from edge of upstation joint. Trumpet was fully grouted.
57 – R - 2	10'-3"	8	Trumpet. Drilling performed 1 ft from edge of upstation joint. Trumpet was fully grouted.
57 – R - 3	8'-0"	9	Not Drilled.
57 – R - 4	11'-3"	10	Not Drilled.
57 – R - 5	7'-6"	*	No Duct Found
57 – R - 6	12'-0"	*	No Duct Found
57 – R - 7	7'-0"	-	
57 – R - 8	12'-9"	-	
57 – R - 9	6'-6"	-	
57 – R - 10	13'-6"	-	

* These locations were drilled to locate tendons 9 and 10 according to the contract drawing No. 160.

Segment 58: Top Tendons Left of CL of Box Looking Upstation (L)

Hole Id	Distance from Center of Box ft	Tendon No.	Comments
58 - L - 1	9'-0"	9	Trumpet. Drilling performed 1 ft from edge of upstation joint. Trumpet was fully grouted.
58 - L - 2	10'-3"	10	Trumpet. Drilling performed 1 ft from edge of upstation joint. Trumpet was fully grouted.
58 - L - 3	8'-0"	-	
58 - L - 4	11'-3"	-	
58 - L - 5	7'-6"	-	
58 - L - 6	12'-0"	-	
58 - L - 7	7'-0"	-	
58 - L - 8	12'-9"	-	
58 - L - 9	6'-6"	-	
58 - L - 10	13'-6"	-	

Segment 58: Top Tendons Right of CL of Box Looking Upstation (R)

Hole Id	Distance from Center of Box ft	Tendon No.	Comments
58 - R - 1	9'-0"	9	Trumpet. Drilling performed 1 ft from edge of upstation joint. Trumpet was fully grouted. Tendon was exposed during drilling operation, but this was because of drilling depth - duct was grouted.
58 - R - 2	10'-3"	10	Trumpet. Drilling performed 1 ft from edge of upstation joint. Trumpet was fully grouted.
58 - R - 3	8'-0"	-	
58 - R - 4	11'-3"	-	
58 - R - 5	7'-6"	-	
58 - R - 6	12'-0"	-	
58 - R - 7	7'-0"	-	
58 - R - 8	12'-9"	-	
58 - R - 9	6'-6"	-	
58 - R - 10	13'-6"	-	

Segment 64: Top Tendons Left of CL of Box Looking Upstation (L)**Drilling was performed at the upstation side of segment 64.**

Hole Id	Distance from Center of Box ft	Tendon No.	Comments
64 - L - 1	9'-0"	1	Drilling was performed on upstation side of Segment 64, therefore the trumpet was not located. See attached drawings with drilling locations.
64 - L - 2	10'-3"	2	Drilling was performed on upstation side of Segment 64, therefore the trumpet was not located. See attached drawings with drilling locations.
64 - L - 3	8'-0"	3	Drilling was performed on upstation side of Segment 64, duct was located with small void at top. Picture L6.
64 - L - 4	11'-3"	4	Drilling was performed on upstation side of Segment 64. Duct was located and fully grouted.
64 - L - 5	7'-6"	5	Not Drilled.
64 - L - 6	12'-0"	6	Not Drilled.
64 - L - 7	7'-0"	7	Drilling was performed on upstation side of Segment 64. Duct was located and fully grouted.
64 - L - 8	12'-9"	8	Drilling was performed on upstation side of Segment 64. Unable to locate duct.
64 - L - 9	6'-6"	9	Drilling was performed on upstation side of Segment 64. Duct was located and fully grouted.
64 - L - 10	13'-6"	10	Drilling was performed on upstation side of Segment 64. Unable to locate duct.
64 - L - 11	6'-0"	11	Drilling was performed on upstation side of Segment 64. Duct was located and fully grouted.
64 - L - 12	14'-3"	12	Drilling was performed on upstation side of Segment 64. Duct was located with small void at top with slight strand exposure. Picture L7.

Segment 64: Top Tendons Right of CL of Box Looking Upstation (R)

Hole Id	Distance from Center of Box ft	Tendon No.	Comments
64 - R - 1	9'-0"	3	Trumpet. Drilling performed 1 ft from edge of upstation joint. Trumpet was fully grouted.
64 - R - 2	10'-3"	4	Trumpet. Drilling performed 1 ft from edge of upstation joint. Trumpet was fully grouted.
64 - R - 3	8'-0"	5	Drilling performed 1.5" from edge of upstation joint. Tendon was fully grouted.
64 - R - 4	11'-3"	6	Drilling performed 1.5" from edge of upstation joint. Tendon was fully grouted.
64 - R - 5	7'-6"	7	Not Drilled.
64 - R - 6	12'-0"	8	Not Drilled.
64 - R - 7	7'-0"	9	Drilling performed 1.5" from edge of upstation joint. Tendon was fully grouted.
64 - R - 8	12'-9"	10	Drilling performed 1.5" from edge of upstation joint. Tendon was fully grouted.
64 - R - 9	6'-6"	11	Drilling performed 1.5" from edge of upstation joint. Tendon was fully grouted.
64 - R - 10	13'-6"	12	Drilling performed 1.5" from edge of upstation joint. Tendon was mostly grouted - a small void on the top of duct.
64 - R - 11	6'-0"	*	Drilling performed 1.5" from edge of upstation joint. Unable to locate duct.
64 - R - 12	14'-3"	*	Drilling performed 1.5" from edge of upstation joint. Unable to locate duct.

* These locations were drilled to locate tendons 11 and 12 according to the contract drawing No. 160.

Segment 69: Top Tendons Left of CL of Box Looking Upstation (L)

Hole Id	Distance from Center of Box ft	Tendon No.	Comments
69 - L - 1	9'-0"	3	Trumpet. Drilling performed 1 ft from edge of upstation joint. Trumpet was fully grouted.
69 - L - 2	10'-3"	4	Trumpet. Drilling performed 1 ft from edge of upstation joint. Trumpet was full of water. Endoscope was inserted in water, but visibility was poor due to cloudy water. An additional hole was drilled approx. 2' from joint and air pressure was applied to try and drain water. This was unsuccessful and tendon could not be inspected. It is recommended that this location should be revisited in the future.
69 - L - 3	8'-0"	5	No Duct Found. Picture L8.
69 - L - 4	11'-3"	6	No Duct Found
69 - L - 5	7'-6"	7	Not Drilled.
69 - L - 6	12'-0"	8	Not Drilled.
69 - L - 7	7'-0"	9	Drilling performed 1.5" from edge of upstation joint. Tendon was fully grouted.
69 - L - 8	12'-9"	10	Drilling performed 1.5" from edge of upstation joint. Tendon was fully grouted.
69 - L - 9	6'-6"	11	Drilling performed 1.5" from edge of upstation joint. Tendon was fully grouted.
69 - L - 10	13'-6"	12	Drilling performed 1.5" from edge of upstation joint. Tendon was fully grouted.
69 - L - 11	6'-0"	*	No Duct Found
69 - L - 12	14'-3"	*	No Duct Found. Picture L9.

* These locations were drilled to locate tendons 11 and 12 according to the contract drawing No. 160.

Segment 69: Top Tendons Right of CL of Box Looking Upstation (R)

Hole Id	Distance from Center of Box ft	Tendon No.	Comments
69 - R - 1	9'-0"	3	Trumpet. Drilling performed 1 ft from edge of upstation joint. Trumpet was fully grouted.
69 - R - 2	10'-3"	4	Trumpet. Drilling performed 1 ft from edge of upstation joint. Trumpet was fully grouted.
69 - R - 3	8'-0"	5	Drilling performed 1.5" from edge of upstation joint. Tendon was fully grouted.
69 - R - 4	11'-3"	6	Drilling performed 1.5" from edge of upstation joint. Tendon was fully grouted.
69 - R - 5	7'-6"	7	Not Drilled.
69 - R - 6	12'-0"	8	Not Drilled.
69 - R - 7	7'-0"	9	Drilling performed 1.5" from edge of upstation joint. Tendon was fully grouted.
69 - R - 8	12'-9"	10	Drilling performed 1.5" from edge of upstation joint. Tendon was fully grouted.
69 - R - 9	6'-6"	11	Drilling performed 1.5" from edge of upstation joint. Tendon was fully grouted.
69 - R - 10	13'-6"	12	Drilling performed 1.5" from edge of upstation joint. Tendon was fully grouted.
69 - R - 11	6'-0"	*	No Duct Found
69 - R - 12	14'-3"	*	No Duct Found

* These locations were drilled to locate tendons 11 and 12 according to the contract drawing No. 160.

Segment 71: Top Tendons Left of CL of Box Looking Upstation (L)

Hole Id	Distance from Center of Box ft	Tendon No.	Comments
71 - L - 1	9'-0"	7	Trumpet. Drilling performed 1 ft from edge of upstation joint. Trumpet was fully grouted.
71 - L - 2	10'-3"	8	Trumpet. Drilling performed 1 ft from edge of upstation joint. Trumpet was fully grouted.
71 - L - 3	8'-0"	9	Not Drilled.
71 - L - 4	11'-3"	10	Not Drilled.
71 - L - 5	7'-6"	11	Drilling performed 1.5" from edge of upstation joint. Tendon was fully grouted.
71 - L - 6	12'-0"	12	Drilling performed 1.5" from edge of upstation joint. Tendon was fully grouted.
71 - L - 7	7'-0"	-	
71 - L - 8	12'-9"	-	
71 - L - 9	6'-6"	-	
71 - L - 10	13'-6"	-	
71 - L - 11	6'-0"	*	No Duct Found
71 - L - 12	14'-3"	*	No Duct Found

* These locations were drilled to locate tendons 11 and 12 according to the contract drawing No. 160.

Segment 71: Top Tendons Right of CL of Box Looking Upstation (R)

Hole Id	Distance from Center of Box ft	Tendon No.	Comments
71 - R - 1	9'-0"	7	Trumpet. Drilling performed 1 ft from edge of upstation joint. Trumpet was fully grouted.
71 - R - 2	10'-3"	8	Trumpet. Drilling performed 1 ft from edge of upstation joint. Trumpet was fully grouted.
71 - R - 3	8'-0"	9	Not Drilled.
71 - R - 4	11'-3"	10	Not Drilled.
71 - R - 5	7'-6"	11	Drilling performed 1.5" from edge of upstation joint. Tendon was fully grouted.
71 - R - 6	12'-0"	12	Drilling performed 1.5" from edge of upstation joint. Tendon was mostly grouted - a small void on the top of duct.
71 - R - 7	7'-0"	-	
71 - R - 8	12'-9"	-	
71 - R - 9	6'-6"	-	
71 - R - 10	13'-6"	-	
71 - R - 11	6'-0"	*	No Duct Found
71 - R - 12	14'-3"	*	No Duct Found

* These locations were drilled to locate tendons 11 and 12 according to the contract drawing No. 160.

Segment 72: Top Tendons Left of CL of Box Looking Upstation (L)

Hole Id	Distance from Center of Box ft	Tendon No.	Comments
72 – L - 1	9'-0"	9	Trumpet. Drilling performed 1 ft from edge of upstation joint. Trumpet was fully grouted.
72 – L - 2	10'-3"	10	Trumpet. Drilling performed 1 ft from edge of upstation joint. Trumpet was fully grouted.
72 – L - 3	8'-0"	11	Not Drilled.
72 – L - 4	11'-3"	12	Not Drilled.
72 – L - 5	7'-6"	*	No Duct Found
72 – L - 6	12'-0"	*	No Duct Found
72 – L - 7	7'-0"	-	
72 – L - 8	12'-9"	-	
72 – L - 9	6'-6"	-	
72 – L - 10	13'-6"	-	
72 – L - 11	6'-0"	-	
72 – L - 12	14'-3"	-	

* These locations were drilled to locate tendons 11 and 12 according to the contract drawing No. 160.

Segment 72: Top Tendons Right of CL of Box Looking Upstation (R)

Hole Id	Distance from Center of Box ft	Tendon No.	Comments
72 - R - 1	9'-0"	9	Trumpet. Drilling performed 1 ft from edge of upstation joint. Trumpet was fully grouted.
72 - R - 2	10'-3"	10	Trumpet. Drilling performed 1 ft from edge of upstation joint. Trumpet was fully grouted.
72 - R - 3	8'-0"	11	Not Drilled.
72 - R - 4	11'-3"	12	Not Drilled.
72 - R - 5	7'-6"	*	No Duct Found
72 - R - 6	12'-0"	*	No Duct Found
72 - R - 7	7'-0"	-	
72 - R - 8	12'-9"	-	
72 - R - 9	6'-6"	-	
72 - R - 10	13'-6"	-	
72 - R - 11	6'-0"	-	
72 - R - 12	14'-3"	-	

* These locations were drilled to locate tendons 11 and 12 according to the contract drawing No. 160.

Segment 76: Top Tendons Left of CL of Box Looking Upstation (L)

Hole Id	Distance from Center of Box ft	Tendon No.**	Comments
76 - L - 1	9'-0"	11	Trumpet. Drilling performed 1 ft from edge of upstation joint. Trumpet was fully grouted.
76 - L - 2	10'-3"	12	Trumpet. Drilling performed 1 ft from edge of upstation joint. Trumpet was fully grouted.
76 - L - 3	8'-0"	13	Drilling performed 1.5" from edge of up station joint. Tendon was partially grouted; one strand is completely exposed and present signs of superficial corrosion. The endoscope went 4' in both directions (up and down station). The void was probably 3/4" deep. Picture L10 - L13.
76 - L - 4	11'-3"	14	Drilling performed 1.5" from edge of upstation joint. Tendon was fully grouted.
76 - L - 5	7'-6"	-	
76 - L - 6	12'-0"	-	
76 - L - 7	7'-0"	-	
76 - L - 8	12'-9"	-	
76 - L - 9	6'-6"	-	
76 - L - 10	13'-6"	-	
76 - L - 11	6'-0"	-	
76 - L - 12	14'-3"	-	
76 - L - 13	5'-6"	-	
76 - L - 14	15'-0"	-	

** Tendon numbers from original spreadsheet are changed to reflect the actual location in which tendons were found (the pattern follows what is shown on the contract drawings, sheet No. D-34)

This Note is valid for segments 76 thru. 89 at the left of the CL of box

Segment 76: Top Tendons Right of CL of Box Looking Upstation (R)

Hole Id	Distance from Center of Box ft	Tendon No.	Comments
76 - R - 1	9'-0"	11	12" from joint. Strands are fully exposed for more than 12" length with a trace of corrosion. Very little grout is present.
76 - R - 2	10'-3"	12	12" from joint. Fully grouted.
76 - R - 3	8'-0"	13	Not Drilled.
76 - R - 4	11'-3"	14	Not Drilled.
76 - R - 5	7'-6"	*	1 1/2" from joint. Not found.
76 - R - 6	12'-0"	*	1 1/2" of joint. Not found.
76 - R - 7	7'-0"	-	
76 - R - 8	12'-9"	-	
76 - R - 9	6'-6"	-	
76 - R - 10	13'-6"	-	
76 - R - 11	6'-0"	-	
76 - R - 12	14'-3"	-	
76 - R - 13	5'-6"	-	
76 - R - 14	15'-0"	-	

* These locations were drilled to locate tendons 11 and 12 according to the contract drawing No. 160.

Segment 79: Top Tendons Left of CL of Box Looking Upstation (L)

Hole Id	Distance from Center of Box ft	Tendon No.	Comments
79 - L - 1	9'-0"	5	Trumpet. Drilling performed 1 ft from edge of upstation joint. Trumpet was fully grouted.
79 - L - 2	10'-3"	6	Trumpet. Drilling performed 1 ft from edge of upstation joint. Small void, a strand can be partially seen (seems that drilling exposed some of the wires). Picture L14.
79 - L - 3	8'-0"	7	1 1/2" from joint. Fully grouted.
79 - L - 4	11'-3"	8	1 1/2" from joint. Fully grouted.
79 - L - 5	7'-6"	9	1 1/2" from joint. Mostly grouted with minimal void on top side of duct. Picture L15.
79 - L - 6	12'-0"	10	1 1/2" from joint. Fully grouted.
79 - L - 7	7'-0"	11	1 1/2" from joint. Mostly grouted with minimal void on top side of duct, the endoscope went 1' upstation. Picture L16.
79 - L - 8	12'-9"	12	1 1/2" from joint. Mostly grouted with minimal void on top side of duct, the endoscope couldn't get in. Picture L19.
79 - L - 9	6'-6"	13	Drilling performed 1.5" from edge of up station joint. Tendon was partially grouted; one strand is clearly visible and present signs of superficial corrosion. The endoscope went almost all its length (5') in upstation direction, downstation the tendon was completely grouted. Picture L17 & L18.
79 - L - 10	13'-6"	14	1 1/2" from joint. Fully grouted.
79 - L - 11	6'-0"	-	
79 - L - 12	14'-3"	-	
79 - L - 13	5'-6"	-	
79 - L - 14	15'-0"	-	

Segment 79: Top Tendons Right of CL of Box Looking Upstation (R)

Hole Id	Distance from Center of Box ft	Tendon No.	Comments
79 - R - 1	9'-0"	5	12" from joint. Fully grouted.
79 - R - 2	10'-3"	6	12" from joint. Fully grouted.
79 - R - 3	8'-0"	7	Not Drilled.
79 - R - 4	11'-3"	8	Not Drilled.
79 - R - 5	7'-6"	9	1 1/2" from joint. Mostly grouted with minimal void on top side of duct.
79 - R - 6	12'-0"	10	1 1/2" from joint. Mostly grouted with minimal void on top side of duct.
79 - R - 7	7'-0"	11	Not Drilled.
79 - R - 8	12'-9"	12	Not Drilled.
79 - R - 9	6'-6"	13	1 1/2" from joint. Mostly grouted with minimal void on top side of duct.
79 - R - 10	13'-6"	14	1 1/2" from joint. Mostly grouted with minimal void on top side of duct.
79 - R - 11	6'-0"		Not drilled.
79 - R - 12	14'-3"	*	1 1/2" from joint. Not found
79 - R - 13	5'-6"		Not drilled.
79 - R - 14	15'-0"	*	1 1/2" from joint. Not found.

* These locations were drilled to locate tendons 12 and 14 according to the contract drawing No. 160.

Segment 81: Top Tendons Left of CL of Box Looking Upstation (L)

Hole Id	Distance from Center of Box ft	Tendon No.	Comments
81 - L - 1	9'-0"	1	Trumpet. Drilling performed 1 ft from edge of upstation joint. Trumpet was fully grouted.
81 - L - 2	10'-3"	2	Trumpet. Drilling performed 1 ft from edge of upstation joint. Trumpet was fully grouted.
81 - L - 3	8'-0"	3	1 1/2" from joint. Fully grouted.
81 - L - 4	11'-3"	4	1 1/2" from joint. Fully grouted.
81 - L - 5	7'-6"	5	1 1/2" from joint. Fully grouted.
81 - L - 6	12'-0"	6	1 1/2" from joint. Fully grouted.
81 - L - 7	7'-0"	7	1 1/2" from joint. Fully grouted.
81 - L - 8	12'-9"	8	1 1/2" from joint. Fully grouted.
81 - L - 9	6'-6"	9	1 1/2" from joint. Fully grouted.
81 - L - 10	13'-6"	10	1 1/2" from joint. Fully grouted.
81 - L - 11	6'-0"	11	1 1/2" from joint. Fully grouted.
81 - L - 12	14'-3"	12	1 1/2" from joint. Fully grouted.
81 - L - 13	5'-6"	13	1 1/2" from joint. Small void in downstation direction but strands are grouted. Picture L20.
81 - L - 14	15'-0"	14	1 1/2" from joint. Fully grouted.

Segment 81: Top Tendons Right of CL of Box Looking Upstation (R)

Hole Id	Distance from Center of Box ft	Tendon No.	Comments
81 - R - 1	9'-0"	1	12" from joint. Mostly grouted with minimal void on top side of duct.
81 - R - 2	10'-3"	2	12" from joint. Mostly grouted with minimal void on top side of duct.
81 - R - 3	8'-0"	3	1 1/2" from joint. Mostly grouted with minimal void on top side of duct.
81 - R - 4	11'-3"	4	1 1/2" from joint. Mostly grouted with minimal void on top side of duct.
81 - R - 5	7'-6"	5	1 1/2" from joint. Mostly grouted with minimal void on top side of duct.
81 - R - 6	12'-0"	6	1 1/2" from joint. Mostly grouted with minimal void on top side of duct.
81 - R - 7	7'-0"	7	1 1/2" from joint. Mostly grouted with minimal void on top side of duct.
81 - R - 8	12'-9"	8	1 1/2" from joint. Mostly grouted with minimal void on top side of duct.
81 - R - 9	6'-6"	9	1 1/2" from joint. Mostly grouted with minimal void on top side of duct.
81 - R - 10	13'-6"	10	1 1/2" from joint. Fully grouted.
81 - R - 11	6'-0"	11	1 1/2" from joint. Fully grouted.
81 - R - 12	14'-3"	12	1 1/2" from joint. Mostly grouted with minimal void on top side of duct.
81 - R - 13	5'-6"	13	1 1/2" from joint. Mostly grouted with minimal void on top side of duct.
81 - R - 14	15'-0"	14	1 1/2" from joint. Fully grouted.

Segment 86: Top Tendons Left of CL of Box Looking Upstation (L)

Hole Id	Distance from Center of Box ft	Tendon No.	Comments
86 – L - 1	9'-0"	5	Trumpet. Drilling performed 1 ft from edge of downstation joint. Trumpet was fully grouted.
86 – L - 2	10'-3"	6	Trumpet. Drilling performed 1 ft from edge of downstation joint. Trumpet was fully grouted.
86 – L - 3	8'-0"	7	1 1/2" from joint. Small void in downstation direction but strands are grouted, endoscope went 3' in this direction. Upstation the duct was fully grouted. Picture L21.
86 – L - 4	11'-3"	8	Drilling performed 1.5" from edge of downstation joint. Significant amount of water came out of the duct, and additional hole was drilled at the trumpet location of this duct (11' downstation), again water was found. Air pressure was applied to drain the water, but it seems that there was still water coming from downstation. Endoscope was inserted in water, but visibility was poor due to cloudy water. The extent of the void (in cross section) and the conditions of the strands couldn't be established. It is recommended that this location should be revisited in the future.
86 – L - 5	7'-6"	9	1 1/2" from joint. Fully grouted.
86 – L - 6	12'-0"	10	1 1/2" from joint. Fully grouted.
86 – L - 7	7'-0"	11	1 1/2" from joint. Fully grouted.
86 – L - 8	12'-9"	12	1 1/2" from joint. Almost fully grouted, small void looking upstation. Picture L22.
86 – L - 9	6'-6"	13	1 1/2" from joint. Almost fully grouted, 1 strand is visible, void is aprox. 0.5" to 0.75" deep. Picture L23.
86 – L - 10	13'-6"	14	1 1/2" from joint. Small void in upstation direction but strands are fully grouted. No voids in downstation direction.
86 – L - 11	6'-0"	-	
86 – L - 12	14'-3"	-	
86 – L - 13	5'-6"	-	
86 – L - 14	15'-0"	-	

Segment 86: Top Tendons Right of CL of Box Looking Upstation (R)

Hole Id	Distance from Center of Box ft	Tendon No.	Comments
86 - R - 1	9'-0"	5	12" from joint. Mostly grouted with minimal void on top side of duct.
86 - R - 2	10'-3"	6	12" from joint. Fully grouted.
86 - R - 3	8'-0"	7	Not Drilled.
86 - R - 4	11'-3"	8	Not Drilled.
86 - R - 5	7'-6"	9	1 1/2" from joint. Mostly grouted with minimal void on top side of duct.
86 - R - 6	12'-0"	10	1 1/2" from joint. Fully grouted.
86 - R - 7	7'-0"	11	Not Drilled.
86 - R - 8	12'-9"	12	Not Drilled.
86 - R - 9	6'-6"	13	1 1/2" from joint. Mostly grouted with minimal void on top side of duct.
86 - R - 10	13'-6"	14	1 1/2" from joint. Mostly grouted with minimal void on top side of duct.
86 - R - 11	6'-0"	*	1 1/2" from joint. Not found.
86 - R - 12	14'-3"	*	1 1/2" from joint. Not found.
86 - R - 13	5'-6"	*	1 1/2" from joint. Not found.
86 - R - 14	15'-0"	*	1 1/2" from joint. Not found.

* These locations were drilled to locate tendons 11, 12, 13 and 14 according to the contract drawing No. 160.

Segment 88: Top Tendons Left of CL of Box Looking Upstation (L)

Hole Id	Distance from Center of Box ft	Tendon No.	Comments
88 - L - 1	9'-0"	9	Trumpet. Drilling performed 1 ft from edge of downstation joint. Small void, the endoscope went 8" in upstation direction and 3' downstation. No strands were visible. Picture L24 & L25.
88 - L - 2	10'-3"	10	Trumpet. Drilling performed 1 ft from edge of downstation joint. Small void, the endoscope went 4" in upstation direction and 4' downstation. No strands exposed. Picture L26.
88 - L - 3	8'-0"	11	1 1/2" from joint. Fully grouted.
88 - L - 4	11'-3"	12	1 1/2" from joint. Fully grouted.
88 - L - 5	7'-6"	13	1 1/2" from joint. Fully grouted.
88 - L - 6	12'-0"	14	1 1/2" from joint. Fully grouted.
88 - L - 7	7'-0"	-	
88 - L - 8	12'-9"	-	
88 - L - 9	6'-6"	-	
88 - L - 10	13'-6"	-	
88 - L - 11	6'-0"	-	
88 - L - 12	14'-3"	-	
88 - L - 13	5'-6"	-	
88 - L - 14	15'-0"	-	

Segment 88: Top Tendons Right of CL of Box Looking Upstation (R)

Hole Id	Distance from Center of Box ft	Tendon No.	Comments
88 - R - 1	9'-0"	9	12" from joint. A medium size void for approximately 9" length. No tendons exposed.
88 - R - 2	10'-3"	10	12" from joint. Fully grouted.
88 - R - 3	8'-0"	11	Not Drilled.
88 - R - 4	11'-3"	12	Not Drilled.
88 - R - 5	7'-6"	13	1 1/2" from joint. Fully grouted.
88 - R - 6	12'-0"	14	1 1/2" from joint. Fully grouted.
88 - R - 7	7'-0"	-	
88 - R - 8	12'-9"	-	
88 - R - 9	6'-6"	-	
88 - R - 10	13'-6"	-	
88 - R - 11	6'-0"	-	
88 - R - 12	14'-3"	*	1 1/2" from joint. Not found.
88 - R - 13	5'-6"	*	1 1/2" from joint. Not found.
88 - R - 14	15'-0"	-	

* These locations were drilled to locate tendons 13 and 14 according to the contract drawing No. 160.

Segment 89: Top Tendons Left of CL of Box Looking Upstation (L)

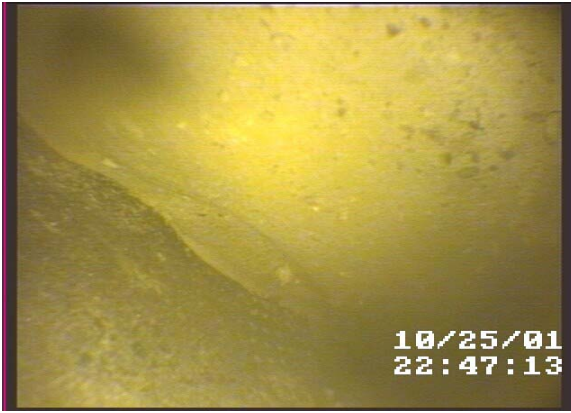
Hole Id	Distance from Center of Box ft	Tendon No.	Comments
89 - L - 1	9'-0"	11	Trumpet. Drilling performed 1 ft from edge of downstation joint. Fully grouted.
89 - L - 2	10'-3"	12	Trumpet. Drilling performed 1 ft from edge of downstation joint. Small void, the endoscope went 4" in upstation direction and 4' downstation. No strands exposed.
89 - L - 3	8'-0"	13	Drilling performed 1.5" from edge of downstation joint. Tendon was mostly grouted - a small void on the top of duct. Picture L27.
89 - L - 4	11'-3"	14	Drilling performed 1.5" from edge of downstation joint. Tendon was mostly grouted - a small void on the top of duct.
89 - L - 5	7'-6"	-	
89 - L - 6	12'-0"	-	
89 - L - 7	7'-0"	-	
89 - L - 8	12'-9"	-	
89 - L - 9	6'-6"	-	
89 - L - 10	13'-6"	-	
89 - L - 11	6'-0"	-	
89 - L - 12	14'-3"	-	
89 - L - 13	5'-6"	-	
89 - L - 14	15'-0"	-	

Segment 89: Top Tendons Right of CL of Box Looking Upstation (R)

Hole Id	Distance from Center of Box ft	Tendon No.	Comments
89 - R - 1	9'-0"	11	12" from joint. Tendons are completely exposed, very little grout is present for more than 5 feet. Tendons have some stains of green and yellow colors. Picture R7 & R8.
89 - R - 2	10'-3"	12	12" from joint. Mostly grouted with minimal void on top side of duct.
89 - R - 3	8'-0"	13	Not Drilled.
89 - R - 4	11'-3"	14	Not Drilled.
89 - R - 5	7'-6"	*	1 1/2" from joint. Not found.
89 - R - 6	12'-0"	*	1 1/2" from joint. Not found.
89 - R - 7	7'-0"	-	
89 - R - 8	12'-9"	-	
89 - R - 9	6'-6"	-	
89 - R - 10	13'-6"	-	
89 - R - 11	6'-0"	-	
89 - R - 12	14'-3"	-	
89 - R - 13	5'-6"	-	
89 - R - 14	15'-0"	-	

* These locations were drilled to locate tendons 13 and 14 according to the contract drawing No. 160.

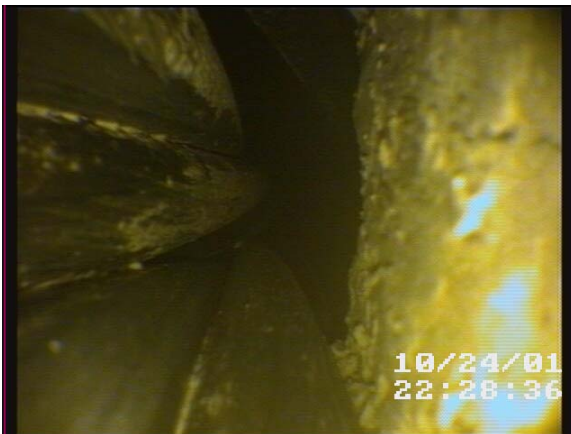
Segment 54 Endoscope Pictures



Picture L1 – Hole 54-L-7



Picture I2 – Hole 54-L-8

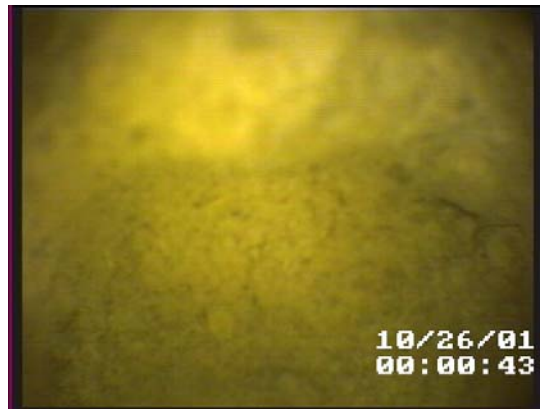


Picture R1 – Hole 54-R-10

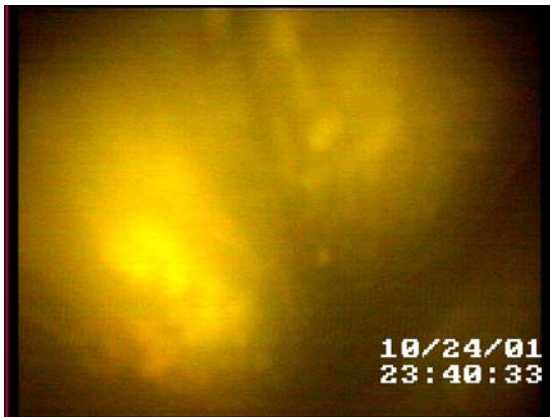


Picture R2 – Hole 54-R-10

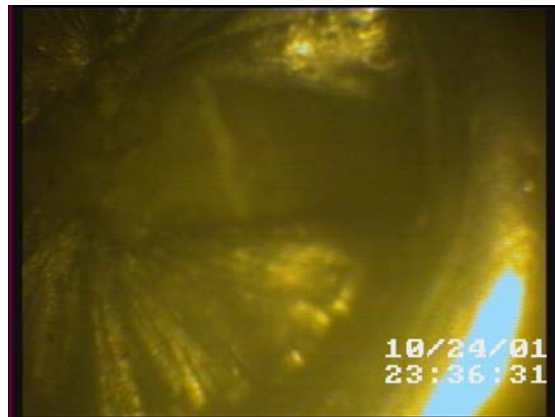
Segment 56 Endoscope Pictures



Picture L3 – Hole 56-L-1



Picture R3 – Hole 56-R-1



Picture R4 – Hole 56-R-2



Picture R5 – Hole 56-R-5



Picture R6 – Hole 56-R-6

Segment 57 Endoscope Pictures



Picture L4 – Hole 57-L-1



Picture L5 –Hole 57-L-2

Segment 64 Endoscope Pictures



Picture L6 – Hole 64-L-3

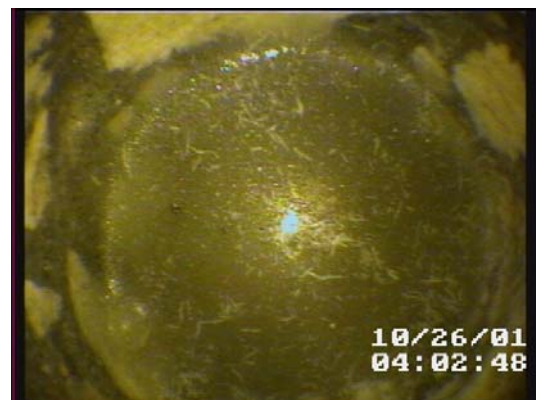


Picture L6 – Hole 64-L-12

Segment 69 Endoscope Pictures



Picture L8 – Hole 69-L-3

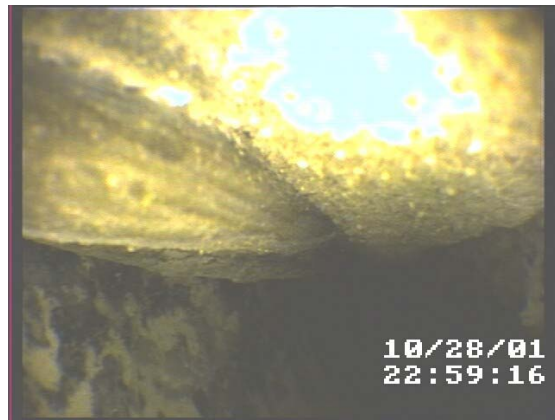


Picture L9 – Hole 69-L-12

Segment 76 Endoscope Pictures



Picture L10 – Hole 76-L-3



Picture L11 – Hole 76-L-3

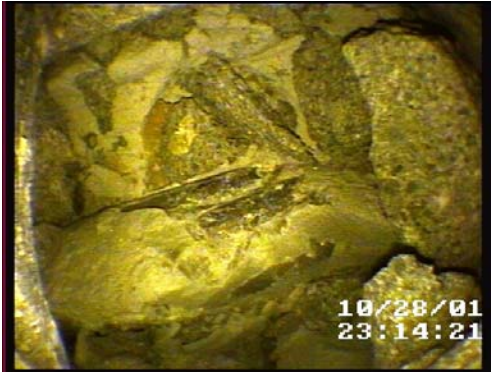


Picture L12 – Hole 76-L-3



Picture L13 – Hole 76-L-3

Segment 79 Endoscope Pictures



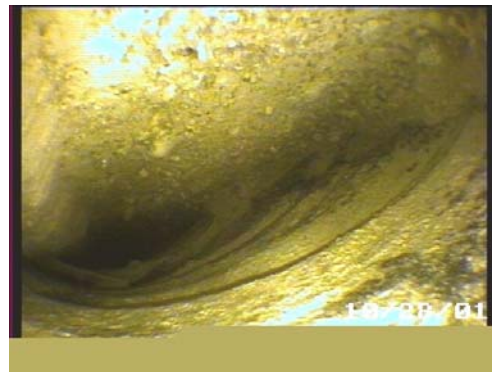
Picture L14 – Hole 79-L-2



Picture L15 – Hole 79-L-5



Picture L16 – Hole 79-L-7



Picture L19 – Hole 79-L-8

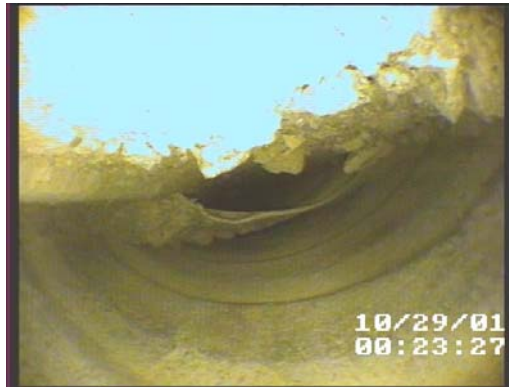


Picture L17 – Hole 79-L-9



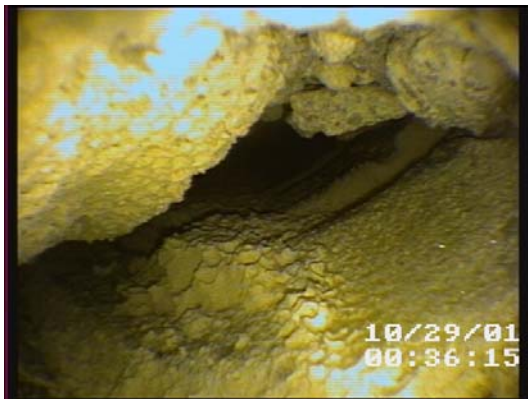
Picture L18 – Hole 79-L-9

Segment 81 Endoscope Pictures

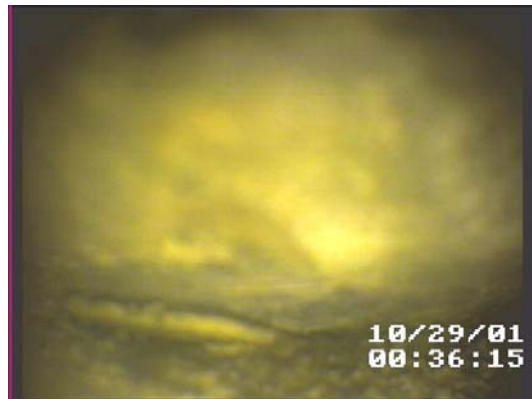


Picture L20 – Hole 81-L-13

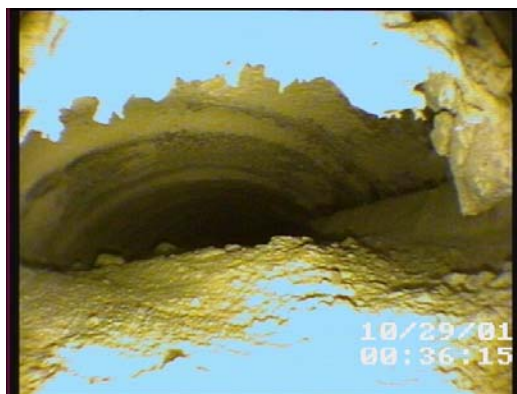
Segment 86 Endoscope Pictures



Picture L21 – Hole 86-L-3



Picture L22 – Hole 86-L-8

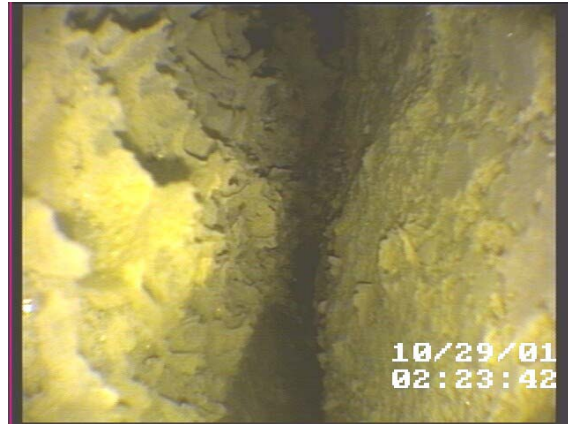


Picture L23 – Hole 86-L-9

Segment 88 Endoscope Pictures



Picture L24 – Hole 88-L-1



Picture L25 – Hole 88-L-1



Picture L26 – Hole 88-L-2

Segment 89 Endoscope Pictures



Picture L27 – Hole 89-L-3



Picture R7 – Hole 89-R-1



Picture R8 – Hole 89-R-1

Appendix B –Damage Induced to Post-Tensioning Tendons**Introduction**

The Endoscope Inspection of the bridge did not provide any cases of strand loss of section that could be used to evaluate the Magnetic Flux testing method and the High-Energy Linear Accelerator inspection. Therefore, it was decided to induce strand damage at certain location in the top slab tendons and to create dummy holes to mask the test locations. The work took place March 11, 2002 and March 12, 2002. As in the case of the Endoscope Inspection, the activity took place with traffic in the bridge. The personal and equipment was provided by the FDOR District Four Facilities.

In March 11, 2002, the team worked on the right hand side of the bridge (the left lane was open to traffic) during the morning, in this side the following tendons were damaged:

Hole ID 89-R-1

This location is a trumpet in Segment 89, in Tendon 11 located 9 feet from the center of the box. A 10"x 8" hole located at 1'-9" from the joint was open using a concrete saw cut and chipping the concrete with a pneumatic hammer. The drilling depth was approximately 5", the spiral reinforcement was found. All tendons were exposed, there was not grout in the trumpet and the tendons presented a little bit of corrosion. However, no reduction of cross sectional area was noticed. The tendon wires were cut using a chisel with the pneumatic hammer, 21 wires were cut. The hole was patch using a fast curing grout, the strands were covered with paper and the grout used can be exposed to traffic 1.5 hours after its application. The whole operation took approximately 1 hour 15 minutes, which was also typical at the other locations.

Hole ID 76-R-1

This location is a trumpet in Segment 76, in Tendon 11 located 9 feet from the center of the box. A hole 1 ft by 8 inches was made at 1'-6" from the joint. Most of the strands were fully exposed and little grout was present. The strands were a little bit corroded but without loss of cross sectional area. Eight wires were cut using the hammer, the other ones were difficult to cut due to bouncing of the hammer, which indicated that the strands were not grouted for a significant length and the wires were just vibrating when they were hammered and consequently it was difficult to cut them. The additional wires were cut using a torch; in this case the operation was performed very carefully trying to avoid damage to the other strands, as this method was much quicker than the mechanical cutting done with the hammer. Twenty-one wires were cut.

Hole ID 56-R-5

The damage was performed in the duct of Tendon 11 in Segment 56 at 7'-6" from the center of the deck. A hole 8"x 6" was made adjacent to the Segment joint. The tendons were completely exposed and no grout was found. The strands did not show signs of corrosion. Eight strands were cut using mechanical means while the other ones were cut torched due to the same reasons explained previously.

The operation for the above holes took from 8:20 A.M to 12:30 A.M. Then, It was decided not to perform the dummy holes (for masking) and continue in the afternoon on the left side of the bridge. The traffic was then shifted to the left side at 2:30 PM and two additional locations were worked.

Hole ID 76-L-3

This location is in the duct of Tendon 13 in Segment 76 at 8 feet from the center of the box. A hole 8"x 6" was made adjacent to the segment joint. The drilling exposed partially the duct. The duct was partially grouted but most of the strands were exposed. However, they didn't present signs of corrosion. When the wires were cut they separated 2" indicating that they were ungrouted for a significant distance. Fourteen wires were cut, half of them mechanically and the other half using a torch.

Hole ID 79-L-9

The damage was performed in the duct of Tendon 13 at Segment 79 at 6'-6" from the center of the box. A hole 8"x 6" was made adjacent to the segment joint. The duct was partially grouted with some of the strands exposed. However, they didn't present signs of corrosion. When the exposed strand was cut, the wires separated 2.5" indicating that they were ungrouted for a significant distance. Ten wires were cut, 7 of them mechanically and 3 using a torch.

This operation was finished around 4:15 P.M. and the team marked the additional locations for the next day of work. Also, some additional locations were marked (eight total) to create some dummy holes. All work performed on March 12, 2002 took place on the left side of the bridge.

Hole ID 86-L-9

This location relates to the duct of Tendon 13 in Segment 86 at 6'-6" from the center of the box. A notch, approximately 8"x 6", was cut out of the concrete and located adjacent to the segment joint. The duct was partially grouted (small void at the top of the duct) with no exposure of the tendon. Two strands were exposed by simply chipping the grout away with a hammer and a chisel. Once the strands were exposed, 10 wires were cut (1.5 strands). 8 wires were cut with a mechanical chipping hammer and 2 were cut with an acetylene torch. This completed the induced damage procedure and the hole was patched.

Hole ID 86-L-3

A notch, approximately 8"x 6", was cut out of the concrete and located adjacent to the Segment 86 joint at a distance of 8 feet from the center of the box. The duct of Tendon 7 was partially grouted (small void at the top of the duct) with no exposure of the tendon. Two strands were exposed by simply chipping the grout away with a hammer and a chisel. Once the strands were exposed, 14 wires were cut (2 strands). 10 wires were cut with a mechanical chipping hammer and 4 were cut with an acetylene torch. This completed the induced damage procedure and the hole was patched.

Hole ID 86-L-4

The damage was created in the duct of Tendon 8 in Segment 86 at a distance of 11'-3" from the center of the box. A notch, approximately 8"x 6", was cut out of the concrete located adjacent to the segment joint. The duct was partially grouted (void at the top of the duct) with partial exposure of the tendon. Previously water was found within this duct, but there was no water at this time. There were signs of surface corrosion (no loss of cross sectional area) in the tendon. The three strands were fully exposed by simply chipping the grout away with a hammer and a chisel. Once the strands were exposed, 21 wires were cut (3 strands); 17 wires were cut with a mechanical chipping hammer and 4 were cut with an acetylene torch. When these strands broke, there was a separation of approximately 2". Also, when these strands were cut a vibration was felt and heard on top of the bridge (downstation). This was a good indication of the void with water previously found. This completed the induced damage procedure and the hole was patched. Two additional dummy holes were created within Segment 86.

Hole ID 88-L-1

This location is a trumpet in Segment 88, in Tendon 11 located 9 feet from the center of the box. A notch, approximately 8"x 6", was cut out of the concrete located adjacent to the segment joint. There was no indication of a duct present, but the tendon was fully grouted. Two strands were exposed by simply chipping the grout away with a hammer and a chisel. Once the strands were exposed, 11 wires were cut (1.5 strands). 8 wires were cut with a mechanical chipping hammer and 3 were cut with an acetylene torch. This completed the induced damage procedure and the hole was patched. An additional dummy hole was also created within Segment 88.

Summary and Conclusions

The techniques, Endoscope Inspection and core drilling, used to assess the state of the top slab tendons indicated that, although some tendons had voids, a few of them were ungrouted, the strands did not show any significant signs of corrosion or section loss. The program also indicated that these techniques, specially the Endoscope Inspection, can quickly, economically and accurately evaluate the state of the tendons in the bridge without inducing substantial long term damage to the structure. They do not require extensive equipment or crew size and can be used without major disruptions to the traffic in or around the bridge.

Appendix C – Core-Drilling Results

**FORT LAUDERDALE AIRPORT: STRUCTURE "D"
REPORT OF CORE DRILLING TO VERIFY IMPACT-ECHO TEST
RESULTS**

Legend: g=duct fully grouted, sv=small void, v=void, N/A=no data

Segment 89 South: Distance west from 90/89 joint

Duct No.	Test I.D.	Distance	IE-Test Results	Core Findings	Comments	Picture ID
13	C	6'-1"	sv	g	First drill performed. A 4 inch diameter drill was used. The duct was located at 4-7/8" from the deck surface. The tendon was fully grouted, the concrete core shows a porous structure (voids of up to 3/8" were found). Rebar crossing transversely the hole was found at approx. 2-1/2".	N/A
12	C	7'-1"	v	g	The duct was found at a depth of 5-1/2". Strands are completely grouted. Longitudinal and transverse rebar crossing the drilled hole at a depth of approx. 3".	30
14	A	3'-0"	v	sv	A small void of approximately 1/4 to 1/8 of an inch was found. The strands are completely grouted Tendon cover approx. 4-1/2".	31
14	C	6'-5"	v	N/A	Drilling was stopped, transverse tendon found almost on top of testing point.	N/A

Note: Tendon Ids reported by CTL are shown incorrectly. CTL Tendons 14, 12, 11 and 13 correspond to actual Tendons 12, 14, 13 and 11.

Segment 88 South: Distance west from 89/88 joint

Duct No.	Test I.D.	Distance	IE-Test Results	Core Findings	Comments	Picture ID
10	B	2'-6"	v	sv	Tendon cover approx. 4". Small void on top of tendon (1/16" to 1/8" deep). Strands are completely grouted. Two transverse rebars just on top of the tendon.	32
12	B	3'-4"	v	sv	Tendon cover approx. 4". Small void on top of tendon (1/8" to 1/4" deep). Strands are completely grouted. Two transverse rebars just on top of the tendon.	N/A
12	C	4'-4"	v	sv	Tendon cover approx. 4". Small void on top of tendon (1/8" to 1/4" deep). Strands are completely grouted. One transverse rebar just on top of the tendon.	N/A
13	C	4'-6"	v	g	Tendon cover approx. 4". Fully grouted, no voids.	33
9	C	4'-6"	v	v	Tendon cover approx. 4-1/2". Partially voided. A 3/4" void on one side of the duct was found. The strands are completely grouted.	N/A

Segment 87 South: Distance west from 88/87 joint

Duct No.	Test I.D.	Distance	IE-Test Results	Core Findings	Comments	Picture ID
11	A	2'-1"	v	sv	Tendon cover approx. 4". Small void on top of tendon (1/16" to 1/8" deep) extending down the duct. The tendon was grouted, but the grout was found moist and brittle. A strand was exposed and showed moderate signs of corrosion.	34,35, & 36
12	C	5'-6"	v	g	Tendon cover approx. 4". Fully grouted.	N/A

Segment 86 South: Distance west from 87/86 joint

Duct No.	Test I.D.	Distance	IE-Test Results	Core Findings	Comments	Picture ID
12	B	3'-8"	v	sv	Tendon cover approx. 4 1/2". Small void on top of tendon (1/16" to 1/8" deep). Strands are completely grouted.	37
8	A	2'-4"	v	sv	Tendon cover approx. 5". Small void on top of tendon (1/16" to 1/8" deep). Strands are completely grouted, but a strand was slightly exposed due to the core drilling operation.	38

Segment 85 South: Distance west from 86/85 joint

Duct No.	Test I.D.	Distance	IE-Test Results	Core Findings	Comments	Picture ID
10	A	2'-5"	v	sv	Tendon cover approx. 4". Test point location was off center with the duct. The core drilling/chipping operation penetrated the side of the duct. Small void on top of tendon (1/16" to 1/8" deep). Strands are completely grouted.	39
8	A	2'-5"	v	sv	Tendon cover approx. 4 3/4". Small void on top of tendon (1/16" to 1/8" deep). Strands are completely grouted.	40
4	B	2'-4"	v	N/A	Tendon cover approx. 4". Lapped bars were located above the duct at the testing location. This could have been disturbing the testing and giving misleading results. Core drilling was terminated due to time constraints.	41
4	C	3'-8"	v	g	Concrete cover on duct was greater than 6". The duct seemed to be deviating down. Maybe under transverse PT. Due to the deviating duct, the tendon was located at the top of the duct. This made it very difficult to penetrate the top of the duct. The side of the duct was penetrated to inspect. The tendon was found fully grouted.	46 & 47
3	C	3'-8"	v	g	Concrete cover on duct was greater than 6". The duct seemed to be deviating down. Maybe under transverse PT. Due to the deviating duct, the tendon was located at the top of the duct. This made it very difficult to penetrate the top of the duct. The side of the duct was penetrated to inspect. The tendon was found fully grouted.	48 & 49
5	A	2'-3"	v	sv	Tendon cover approx. 5". Small void on top of tendon (1/16" to 1/8" deep). Strands are completely grouted. Tendon was slightly exposed due to the core drilling and hammering operation.	50
7	C	5'-7"	v	g	Tendon cover approx. 5 1/4". Tendon was completely grouted with no indication of void.	51

Segment 69 South: Distance west from 70/69 joint

Duct No.	Test I.D.	Distance	IE-Test Results	Core Findings	Comments	Picture ID
12	A	10"	v	sv	Tendon cover approx. 4 ". Small void on top of tendon (1/4" deep). Strands are completely grouted. Concrete core had a rather large void. This could be disturbing the testing and giving misleading results.	53 & 54
8	A	10"	v	sv	Tendon cover approx. 4 1/2". Small void on top of tendon (< 1/8" deep). Strands are completely grouted.	55
8	B	2'-2"	v	sv	Tendon cover approx. 4 3/4". Small void on top of tendon (< 1/8" deep). Strands are completely grouted.	56, 57 & 58
7	A	10"	v	g	Tendon cover approx. 4". Tendon was fully grouted with no indication of void. For further verification the duct was cut and peeled back to view grout. This indicated a fully grouted tendon.	59
8	D	5'-4"	v	sv	Tendon cover approx. 5 1/4". Small void on top of tendon (> 1/8" deep). Strands are completely grouted.	60
7	D	5'-4"	v	g	Testing location was not over the longitudinal PT, but was partially over the transverse PT. The longitudinal PT was located more to the center of the box (approx. 2") by drilling and chiseling. The side of the duct was penetrated and there was no indication of voids.	66, 68 & 69
11	C	4'-0"	v	N/A	Testing location was directly above Transverse PT. The drilling was terminated when the Transverse PT was identified.	67
6	A	10"	v	g	Tendon cover approx. 4 1/2". Tendon was completely grouted with no indication of void.	78
6	D	5'-4"	v	sv	Tendon cover approx. 5 1/2". Small void on top of tendon (1/16" to 1/8" deep). Tendon was completely grouted.	82
4	D	5'-4"	v	N/A	This was an area where the tendon was transitioning to the anchor. At the testing location, there were lapped bars found at approx. 4". These bars were cut to try and locate the duct. Drilling continued to approx. 7" and the tendon was not located.	80
10	E	9'-4"	v	N/A	Testing location was directly above Transverse PT. The drilling was terminated when the Transverse PT was identified.	79
3	E	9'-4"	v	N/A	Drilled to approx. 7 1/2" and the duct was not located.	81

Segment 70 South: Distance west from 71/70 joint

Duct No.	Test I.D.	Distance	IE-Test Results	Core Findings	Comments	Picture ID
10	C	4'-9"	v	sv	Tendon cover approx. 4 1/4". Small void on top of tendon (1/8" deep). Strands are completely grouted. Tendon was slightly exposed by drilling / chiseling procedure.	70
8	C	4'-9"	v	g	Tendon cover approx. 4 ". Tendon was completely grouted with no indication of void.	71
6	C	4'-9"	v	g	Tendon cover approx. 5 1/2". The duct seemed to be deviating down. Maybe under transverse PT. Also there was a lap splice in this location above the duct. Due to the deviating duct the tendon was located at the top of the duct. This made it very difficult to penetrate the top of the duct. Strands are completely grouted.	72
12	B	2'-9"	v	sv	Tendon cover approx. 4". Small void on top of tendon (approx. 1/4" deep). The tendon was fully grouted.	77

Segment 56 South: Distance west from 56/57 joint

Tendon No.	Test I.D.	Distance	IE-Test Results	Core Findings	Comments	Picture ID
13	A	1'-10 1/2"	v	v	Tendon cover approx. 4". Duct was opened and was completely voided.	83
13	B	4'-7"	v	v	Tendon cover approx. 4 1/4". Duct was opened and was completely voided.	84

Segment 55 South: Distance west from 55/56 joint

Tendon No.	Test I.D.	Distance	IE-Test Results	Core Findings	Comments	Picture ID
13	A	5'-9"	v	v	Tendon cover approx. 4 3/4". Duct was opened and was completely voided.	85

Segment 54 South: Distance west from 54/53 joint

Tendon No.	Test I.D.	Distance	IE-Test Results	Core Findings	Comments	Picture ID
13	A	5"	v	v	Tendon cover approx. 3 1/2". Duct was opened and was completely voided.	86

Segment 79 South: Distance west from 79/80 joint

Duct No.	Test I.D.	Distance	IE-Test Results	Core Findings	Comments	Picture ID
13	A	1'-4"	v	g	Tendon cover approx. 3 3/4 ". Tendon was completely grouted with no indication of void.	87 & 88
13	C	3'-11"	v	sv	Tendon cover approx. 4 1/4". Small void on top of tendon (approx. 1/8" deep). The tendon was fully grouted.	89
13	B	2'-10"	v	sv	Tendon cover approx. 3 3/4". Small void on top of tendon (approx. 1/8" deep). The tendon was fully grouted.	90
11	B	2'-10"	v	g	Tendon cover approx. 4". When duct was penetrated tendons were found at the top of duct. There was no indication of a void.	91
7	B	2'-10"	v	sv	Tendon cover approx. 4". Small void on top of tendon (approx. 1/8" deep). The tendon was fully grouted.	92 & 93
5	B	2'-10"	v	N/A	The duct was not found at the testing location. Drilling was performed up to approx. 7". An additional hole was drilled 6" from 7B which was already located. The tendon was still not located.	94
5	A	1'-4"	v	N/A	Testing location was directly above transverse PT. Accidentally cored through the transverse PT, but could not locate longitudinal PT. Cored to an approx. depth of 7".	96

Segment 77 South: Distance west from 77/78 joint

Duct No.	Test I.D.	Distance	IE-Test Results	Core Findings	Comments	Picture ID
9	B	6'-10"	v	N/A	Testing location was directly above transverse PT. Drilling was halted.	N/A
11	B	6'-10"	v	g	Tendon cover approx. 4 1/4". Duct was peeled back and tendon was located at the top of the duct. Tendon seemed fully grouted, but grout broke away during peeling. Also, the grout seemed moist (maybe due to drilling operation).	97
13	B	6'-10"	v	g	Tendon cover approx. 4". The tendon was fully grouted with no indication of a void.	98
14	C	8'-7"	v	sv	Tendon cover approx. 4". The testing location was off center of the duct. The side of the duct was penetrated and a small void (approx. 1/4") was found at the top of the duct	99
12	B	6'-10"	v	N/A	Testing location was directly above transverse PT. Drilling was halted.	N/A
11	C	8'-7"	v	g	The tendon was found at the top of the duct with no indication of void. The tendon was slightly exposed due to the drilling procedure.	100
10	C	8'-7"	v	v	Duct was completely empty. There was signs of slight corrosion (pitting) on tendon.	101, 102, 103 & 104

Comparison of Core Findings and CTL Findings

Core Findings	CTL Findings
Grouted = 17	Void = 16 Small Void = 1
Small Void = 21	Void = 21
No Data = 10	Void = 10

Core Drilling Pictures



Picture 30



Picture 31



Picture 32



Picture 33



Picture 34



Picture 35



Picture 36



Picture 37



Picture 38



Picture 39



Picture 40



Picture 41



Picture 46



Picture 47



Picture 48



Picture 49



Picture 50



Picture 51



Picture 53



Picture 54



Picture 55



Picture 56



Picture 57



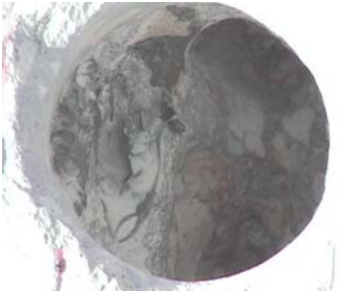
Picture 58



Picture 59



Picture 60



Picture 66



Picture 67



Picture 68



Picture 69



Picture 70



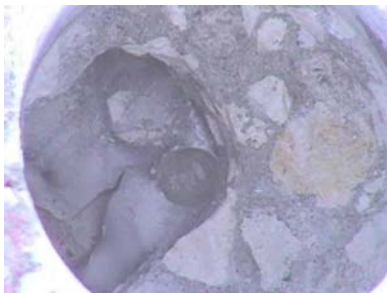
Picture 71



Picture 72



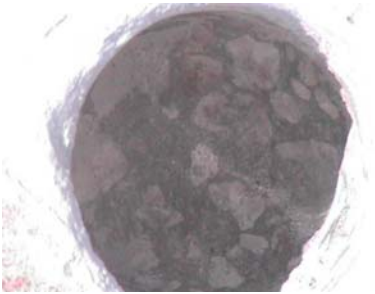
Picture 77



Picture 78



Picture 79



Picture 80



Picture 81



Picture 82



Picture 83



Picture 84



Picture 85



Picture 86



Picture 87



Picture 88



Picture 89



Picture 89



Picture 90



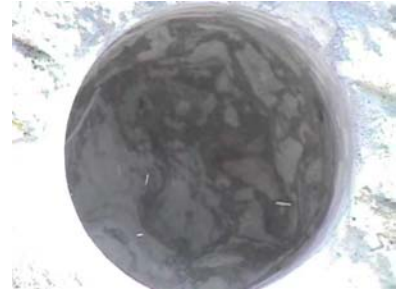
Picture 92



Picture 93



Picture 94



Picture 96



Picture 97



Picture 98



Picture 99



Picture 100



Picture 101



Picture 102



Picture 103



Picture 104

**FORT LAUDERDALE AIRPORT: STRUCTURE "A"
REPORT OF CORE DRILLING TO EVALUATE EPOXY IN SEGMENT
JOINTS**

Core No.	Length	Bonded Length	Unbonded Length	Split Tensile Test Stress	Comments	Picture ID
1	12"	12"				
2	12"	12"		831 psi		
3	9 ³ / ₄ "	9 ³ / ₄ "				
4	10"	10"			Good Joint. Contains Duct	
5	12 ¹ / ₂ "	12.5" Side1 10.5" Side2	0" 2"		Note: 100% at Top	
6	12"	12"		663 psi		
7	7 ¹ / ₄ "	7 ¹ / ₄ "				
8	8 ⁵ / ₈ "	8 ⁵ / ₈ "		636 psi	Cylinder Broken	
9	8 ³ / ₄ "	8 ³ / ₄ "				
10	10 ¹ / ₂ "	10 ¹ / ₂ "		763 psi	Contains Shear Key	

Total 103.375" 99.375"

Percent Bonded = 96.190

Split Tensile Test Performed According to ASTM C496-96
Core Size 2³/₄" Ø 5¹/₂" Long
Epoxy Joint Runing Vertical at Centerline of Core

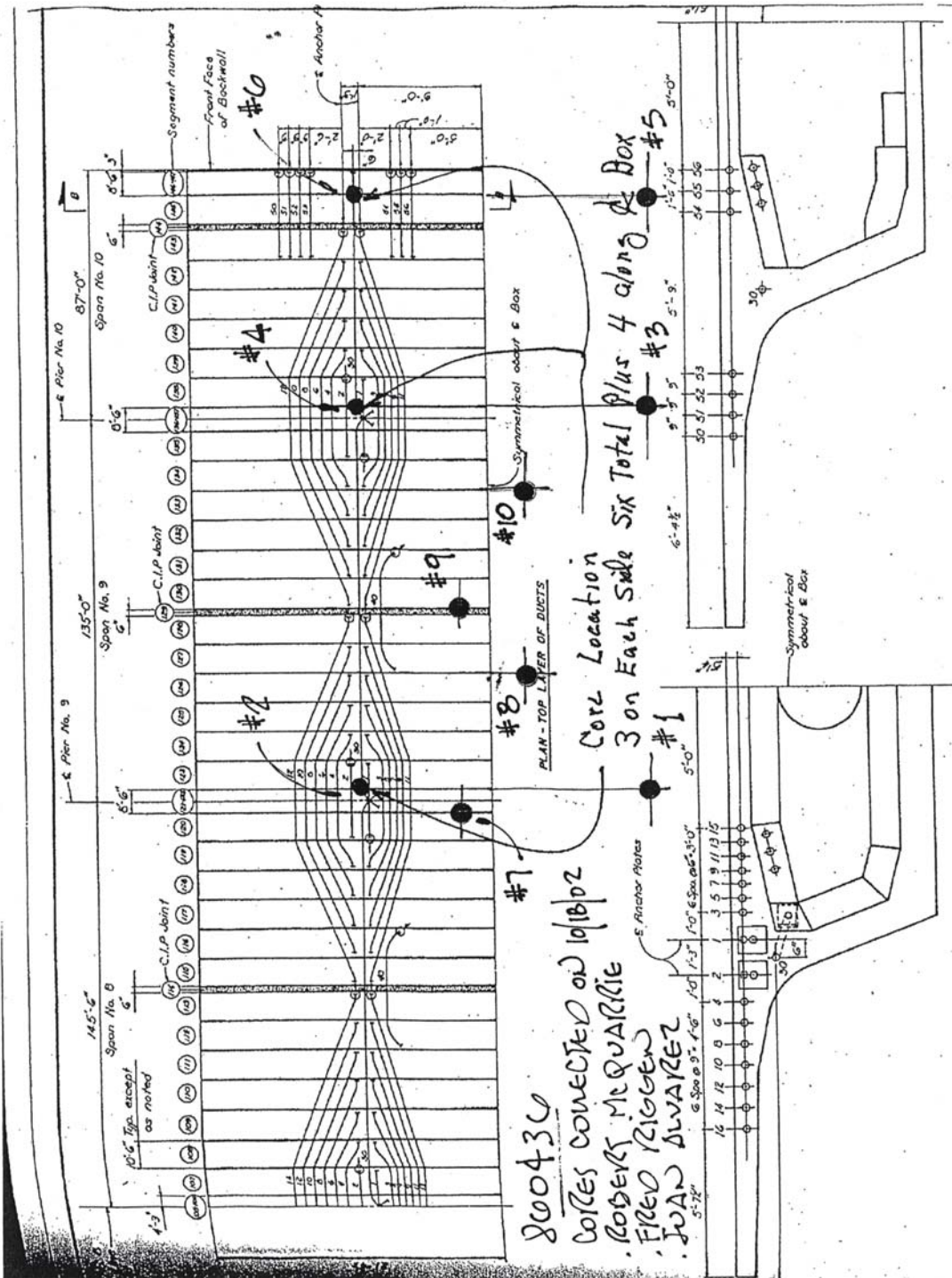


Figure 1 – Location of Cores



Designation: C 496 – 96

Standard Test Method for Splitting Tensile Strength of Cylindrical Concrete Specimens¹

This standard is issued under the fixed designation C 496; the number immediately following the designation indicates the year of original adoption or, in the case of revision, the year of last revision. A number in parentheses indicates the year of last reapproval. A superscript epsilon (ϵ) indicates an editorial change since the last revision or reapproval.

This standard has been approved for use by agencies of the Department of Defense.

1. Scope

1.1 This test method covers the determination of the splitting tensile strength of cylindrical concrete specimens, such as molded cylinders and drilled cores.

NOTE 1—For methods of molding cylindrical concrete specimens, see Practice C 192 and Practice C 31. For methods of obtaining drilled cores see Test Method C 42.

1.2 The values stated in inch-pound units are to be regarded as the standard.

1.3 *This standard does not purport to address all of the safety concerns, if any, associated with its use. It is the responsibility of the user of this standard to establish appropriate safety and health practices and determine the applicability of regulatory limitations prior to use.*

2. Referenced Documents

2.1 ASTM Standards:

- C 31 Practice for Making and Curing Concrete Test Specimens in the Field²
- C 39 Test Method for Compressive Strength of Cylindrical Concrete Specimens²
- C 42 Test Method for Obtaining and Testing Drilled Cores and Sawed Beams of Concrete²
- C 192 Practice for Making and Curing Concrete Test Specimens in the Laboratory²
- C 670 Practice for Preparing Precision and Bias Statements for Test Methods for Construction Materials²

3. Summary of Test Method

3.1 This test method consists of applying a diametral compressive force along the length of a cylindrical concrete specimen at a rate that is within a prescribed range until failure occurs. This loading induces tensile stresses on the plane containing the applied load and relatively high compressive stresses in the area immediately around the applied load.

¹ This test method is under the jurisdiction of ASTM Committee C-9 on Concrete and Concrete Aggregates and is the direct responsibility of Subcommittee C09.61 on Testing Concrete for Strength.

Current edition approved Jan. 10, 1996. Published March 1996. Originally published as C 496 – 62. Last previous edition C 496 – 90.

² Annual Book of ASTM Standards, Vol 04.02.

Tensile failure occurs rather than compressive failure because the areas of load application are in a state of triaxial compression, thereby allowing them to withstand much higher compressive stresses than would be indicated by a uniaxial compressive strength test result.

3.2 Thin, plywood bearing strips are used so that the load is applied uniformly along the length of the cylinder.

3.3 The maximum load sustained by the specimen is divided by appropriate geometrical factors to obtain the splitting tensile strength.

4. Significance and Use

4.1 Splitting tensile strength is simpler to determine than direct tensile strength.

4.2 Splitting tensile strength is used to evaluate the shear resistance provided by concrete in reinforced lightweight aggregate concrete members.

5. Apparatus

5.1 *Testing Machine*—The testing machine shall conform to the requirements of Test Method C 39 and may be of any type of sufficient capacity that will provide the rate of loading prescribed in 7.5.

5.2 *Supplementary Bearing Bar or Plate*—If the diameter or the largest dimension of the upper bearing face or the lower bearing block is less than the length of the cylinder to be tested, a supplementary bearing bar or plate of machined steel shall be used. The surfaces of the bar or plate shall be machined to within ± 0.001 in. (0.025 mm) of planeness, as measured on any line of contact of the bearing area. It shall have a width of at least 2 in. (51 mm), and a thickness not less than the distance from the edge of the spherical or rectangular bearing block to the end of the cylinder. The bar or plate shall be used in such manner that the load will be applied over the entire length of the specimen.

5.3 *Bearing Strips*—Two bearing strips of nominal $\frac{1}{8}$ in. (3.2 mm) thick plywood, free of imperfections, approximately 1 in. (25 mm) wide, and of a length equal to, or slightly longer than, that of the specimen shall be provided for each specimen. The bearing strips shall be placed between the specimen and both the upper and lower bearing blocks of the testing machine or between the specimen and supplemental bars or plates, if

Figure 2a – Splitting Tensile Test

C 496

used (see 5.2). Bearing strips shall not be reused.

6. Test Specimens

6.1 The test specimens shall conform to the size, molding, and curing requirements set forth in either Practice C 31 (field specimens) or Practice C 192 (laboratory specimens). Drilled cores shall conform to the size and moisture-conditioning requirements set forth in Test Method C 42. Moist-cured specimens, during the period between their removal from the curing environment and testing, shall be kept moist by a wet burlap or blanket covering, and shall be tested in a moist condition as soon as practicable.

6.2 The following curing procedure shall be used for evaluations of light-weight concrete: specimens tested at 28 days shall be in an air-dry condition after 7 days moist curing followed by 21 days drying at $73 \pm 3^\circ\text{F}$ ($23.0 \pm 1.7^\circ\text{C}$) and $50 \pm 5\%$ relative humidity.

7. Procedure

7.1 *Marking*—Draw diametral lines on each end of the specimen using a suitable device that will ensure that they are in the same axial plane (see Fig. 1, Fig. 2 and Note 2), or as an alternative, use the aligning jig shown in Fig. 3 (Note 3).

Note 2—Figs. 1 and 2 show a suitable device for drawing diametral lines on each end of the specimen in the same axial plane. The device consists of three parts as follows:

- (1) A length of 4-in. (100-mm) steel channel, the flanges of which have been machined flat,
- (2) A section of a tee bar, *B*, that is grooved to fit smoothly over the flanges of the channel and that includes a rectangular notch for positioning the vertical member of the tee bar assembly, and
- (3) A vertical bar, *C*, containing a longitudinal aperture (clef), *A*, for guiding a pencil.

The tee bar assembly is not fastened to the channel and is positioned at either end of the channel without disturbing the position of the specimen when marking the diametral lines.

Note 3—Fig. 4 is a detailed drawing of the aligning jig shown in Fig. 3 for achieving the same purpose as marking the diametral lines. The device consists of:

- (1) A base for holding the lower bearing strip and cylinder,
- (2) A supplementary bearing bar conforming to the requirements in Section 5 as to critical dimensions and planeness, and

- (3) Two uprights to serve for positioning the test cylinder, bearing strips, and supplementary bearing bar.

7.2 *Measurements*—Determine the diameter of the test specimen to the nearest 0.01 in. (0.25 mm) by averaging three diameters measured near the ends and the middle of the specimen and lying in the plane containing the lines marked on the two ends. Determine the length of the specimen to the nearest 0.1 in. (2.5 mm) by averaging at least two length measurements taken in the plane containing the lines marked on the two ends.

7.3 *Positioning Using Marked Diametral Lines*—Center one of the plywood strips along the center of the lower bearing block. Place the specimen on the plywood strip and align so that the lines marked on the ends of the specimen are vertical and centered over the plywood strip. Place a second plywood strip lengthwise on the cylinder, centered on the lines marked on the ends of the cylinder. Position the assembly to ensure the following conditions:

7.3.1 The projection of the plane of the two lines marked on the ends of the specimen intersects the center of the upper bearing plate, and

7.3.2 The supplementary bearing bar or plate, when used, and the center of the specimen are directly beneath the center of thrust of the spherical bearing block (see Fig. 5).

7.4 *Positioning by Use of Aligning Jig*—Position the bearing strips, test cylinder, and supplementary bearing bar by means of the aligning jig as illustrated in Fig. 3 and center the jig so that the supplementary bearing bar and the center of the specimen are directly beneath the center of thrust of the spherical bearing block.

7.5 *Rate of Loading*—Apply the load continuously and without shock, at a constant rate within the range 100 to 200 psi/min (689 to 1380 kPa/min) splitting tensile stress until failure of the specimen (Note 4). Record the maximum applied load indicated by the testing machine at failure. Note the type of failure and the appearance of the concrete.

Note 4—The relationship between splitting tensile stress and applied load is shown in Section 8. The required loading range in splitting tensile stress corresponds to applied total load in the range of 11 300 to 22 600 lbf (50 to 100 kN)/min for 6 by 12-in. (152 by 305-mm) cylinders.

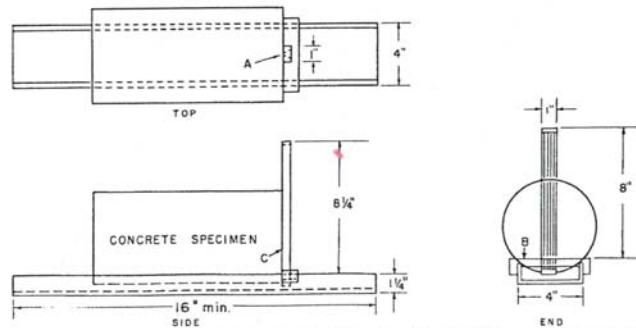
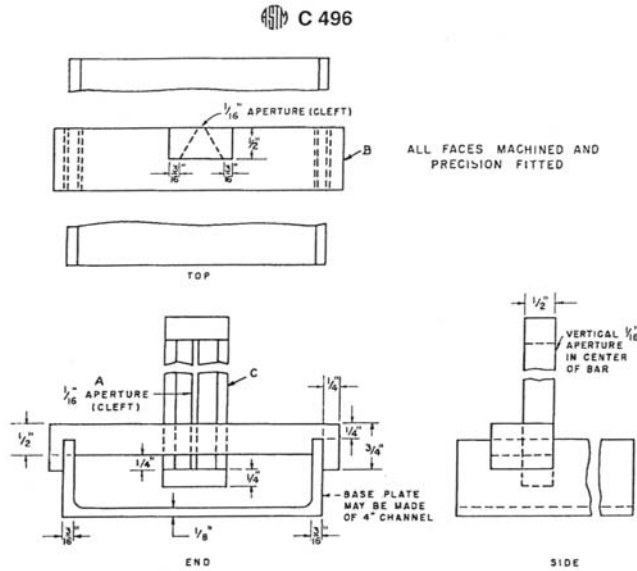


FIG. 1 General Views of a Suitable Apparatus for Marking End Diameters Used for Alignment of Specimen in Testing Machine

Figure 2b – Splitting Tensile Test



Metric Equivalents—Fig. 1, Fig. 2 and Fig. 3

in.	1/16	1/8	3/16	1/4	3/8	1/2	5/8	1	1 1/4	2	2 1/2	4	7 1/2	8	8 1/4	15	16
mm	1.6	3.2	4.8	6.4	13	19	25	32	50	65	100	190	200	205	375	400	

FIG. 2 Detailed Plans for a Suitable Apparatus for Marking End Diameters Used for Aligning the Specimen

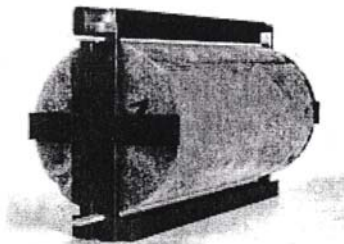


FIG. 3 Jig for Aligning Concrete Cylinder and Bearing Strips

8. Calculation

8.1 Calculate the splitting tensile strength of the specimen as follows:

$$T = 2P/\pi ld \tag{1}$$

where:

- T = splitting tensile strength, psi (kPa),
- P = maximum applied load indicated by the testing machine, lbf (kN),
- l = length, in. (m), and
- d = diameter, in. (m).

9. Report

9.1 Report the following information:

- 9.1.1 Identification number,
- 9.1.2 Diameter and length, in. (m),
- 9.1.3 Maximum load, lbf (kN),
- 9.1.4 Splitting tensile strength calculated to the nearest 5 psi (35 kPa),
- 9.1.5 Estimated proportion of coarse aggregate fractured during test,
- 9.1.6 Age of specimen,
- 9.1.7 Curing history,
- 9.1.8 Defects in specimen,
- 9.1.9 Type of fracture, and
- 9.1.10 Type of specimen.

10. Precision and Bias

10.1 *Precision*—An interlaboratory study of this test method has not been performed. Available research data,³ however, suggests that the within batch coefficient of variation is 5 % (see Note 5) for 6 × 12-in. (152 × 305-mm) cylindrical specimens with an average splitting tensile strength of 405 psi (2.8 MPa). Results of two properly conducted tests on the same material, therefore, should not differ by more than 14 % (see Note 5) of their average for splitting tensile strengths of about 400 psi (2.8 MPa).

NOTE 5—These numbers represent, respectively, the (1s %) and (d2s %) limits as defined in Practice C 670.

10.2 *Bias*—The test method has no bias because the splitting tensile strength can be defined only in terms of this test

Figure 2c – Splitting Tensile Test

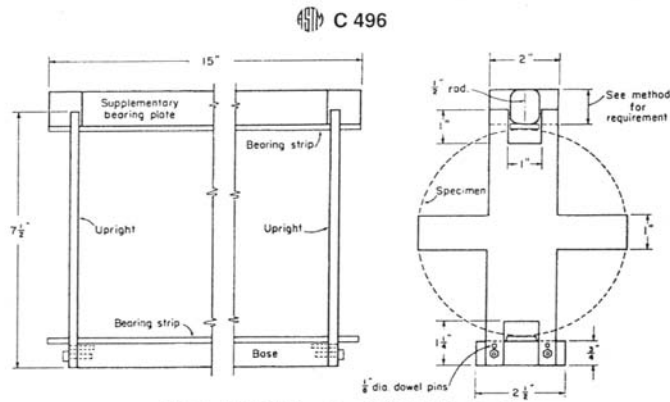


FIG. 4 Detailed Plans for a Suitable Aligning Jig

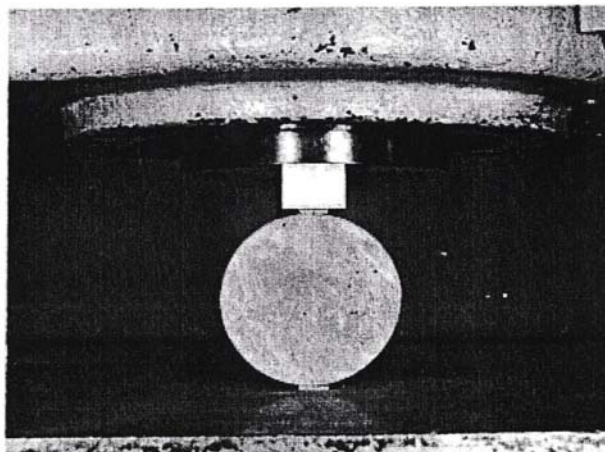


FIG. 5 Specimen Positioned in a Testing Machine for Determination of Splitting Tensile Strength

method.

11. Keywords

11.1 cylindrical concrete specimens; splitting tension; tensile strength

The American Society for Testing and Materials takes no position respecting the validity of any patent rights asserted in connection with any item mentioned in this standard. Users of this standard are expressly advised that determination of the validity of any such patent rights, and the risk of infringement of such rights, are entirely their own responsibility.

This standard is subject to revision at any time by the responsible technical committee and must be reviewed every five years and if not revised, either reapproved or withdrawn. Your comments are invited either for revision of this standard or for additional standards and should be addressed to ASTM Headquarters. Your comments will receive careful consideration at a meeting of the responsible technical committee, which you may attend. If you feel that your comments have not received a fair hearing you should make your views known to the ASTM Committee on Standards, 100 Barr Harbor Drive, West Conshohocken, PA 19428.

This standard is copyrighted by ASTM, 100 Barr Harbor Drive, West Conshohocken, PA 19428-2959, United States. Individual reprints (single or multiple copies) of this standard may be obtained by contacting ASTM at the above address or at 610-832-9585 (phone), 610-832-9555 (fax), or service@astm.org (e-mail); or through the ASTM website (http://www.astm.org).

Figure 2d – Splitting Tensile Test

Segment Joint Core Pictures



Picture 1 -Core #9



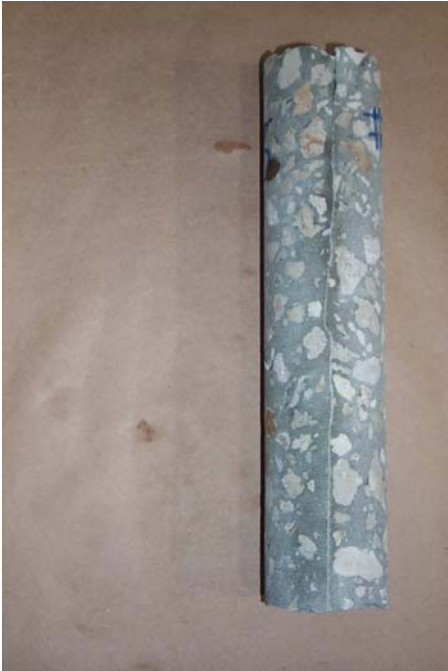
Picture 2 - Core #1



Picture 3 - Core #1



Picture 4 - Core #3



Picture 5 – Core #5



Picture 6 – Core #4



Picture 7 – Core #8



Picture 8 – Core#6 Split Cylinder
Cut from Middle



Picture 9 – Core #19 Split Cylinder Cut from Middle



Picture 10 – Core #7 Split Cylinder Cut from Middle



Picture 11 – Core #2 Split Cylinder



Picture 12 – Core #2 Core to be Split.



Picture 13 – Core#10 Core to be Split



Picture 14 – Core #6 Core to be Split



Picture 15 – Core#5 Core to be Split



Picture 16 – Split Tensile Test on Core #6



Picture 17 – Split Tensile Test on Core 6. Joint Vertical



Picture 18 – Split Tensile Test on Core 6



Picture 19 – Split Tensile Test on Core 6



Picture 20 –Split Tensile Test on Core 6



Picture 21 – Split Tensile Test on Core 6



Picture 22 – Split Tensile Test on Core #7. Joint Vertical



Picture 23 – Split tensile Test on Core #7



Picture 24 – Split Tensile Test on Core #2. Joint Vertical



Picture 25 – Split Tensile Test on Core #2.



Picture 26 – Split Tensile Test on Core #10. Joint Vertical



Picture 27 – Split Tensile Test on Core #10



Picture 28 – Split Tensile Test on Core #10

Appendix D – Forensic Investigation of Dismantled Bridge

Segment 63: Top Tendons Left of CL of Box Looking Upstation

Upstation Face

Downstation Face

Tendon No.	Comments	Picture No.	Tendon No.	Comments	Picture No.
12	Tendons are fully grouted with a small void (approx. 1/8") at the top.	63-1	12	Tendons are fully grouted with a small void (approx. 1/4") at the top.	63-2
11	Tendons are fully grouted with a small void (approx. 1/4") at the top.	63-3	11	Tendons are fully grouted with a small void (approx. 1/2") at the top.	63-4
10	Tendons are fully grouted with a small void (approx. 1/8") at the top.	63-5	10	Tendons are fully grouted with a small void (approx. 1/8") at the top.	63-6
9	Completely grouted with no evidence of void.	63-7	9	Fully Grouted	63-8
8	Tendons are fully grouted with a small void (approx. 1/8") at the top.	63-9	8	Tendons are fully grouted with a small void (approx. 1/8") at the top.	63-10
7	Completely grouted with no evidence of void.	63-11	7	Completely grouted.	63-12
6	Tendons are fully grouted with a small void (approx. 1/8") at the top.	63-13			
5	Tendons are fully grouted with a small void (approx. 1/4") at the top.	63-14			

Segment 63: Top Tendons Right of CL of Box Looking Upstation

Upstation Face

Downstation Face

Tendon No.	Comments	Picture No.	Tendon No.	Comments	Picture No.
12	Tendons are fully grouted with a small void (approx. 1/2") at the top.	63-15	12	Tendons are fully grouted with a small void (approx. 1/2") at the top.	63-16
11	Tendons are fully grouted with a small void (approx. 1/8") at the top.	63-17	11	Tendons are fully grouted with a small void (approx. 1/2") at the top.	63-18
10	Tendons are fully grouted with a small void (approx. 1/2") at the top.	63-19	10	Tendons are fully grouted with a small void (approx. 1/8") at the top.	63-20
9	Tendons are fully grouted with a small void (approx. 1/8") at the top.	63-21	9	Tendons are fully grouted with a small void (approx. 1/2") at the top.	63-22
8	Tendons are fully grouted with a small void (approx. 1/4") at the top.	63-23	8	Completely grouted with no evidence of void.	63-24
7	Tendons are fully grouted with a small void (approx. 1/8") at the top.	63-25	7	Tendons are fully grouted with a small void (approx. 1") at the top.	63-26
6	Tendons are fully grouted with a small void (approx. 1/2") at the top.	63-27			
5	Tendons are fully grouted with a small void (approx. 1/2") at the top.	63-28			

Segment 64: Top Tendons Left of CL of Box Looking Upstation

Upstation Face

Downstation Face

Tendon No.	Comments	Picture No.	Tendon No.	Comments	Picture No.
12	Completely grouted with no evidence of void.	64-1	12	Tendons are fully grouted with a small void (approx. 1/4") at the top.	64-2
11	Tendons are fully grouted with a small void (approx. 1/8") at the top.	64-3	11	Tendons are fully grouted with a small void (approx. 1/8") at the top.	64-4
10	Tendons are fully grouted with a small void (approx. 1/4") at the top.	64-5	10	Completely grouted with no evidence of void.	64-6
9	Tendons are fully grouted with a small void (approx. 1/8") at the top.	64-7	9	Completely grouted with no evidence of void.	64-8
8	Completely grouted with no evidence of void.	64-9	8	Completely grouted with no evidence of void.	64-10
7	Completely grouted with no evidence of void.	64-11	7	Completely grouted with no evidence of void.	64-12
6	Completely grouted with no evidence of void.	64-13	6	Tendons are fully grouted with a small void (approx. 1/8") at the top.	64-14
5	Tendons are fully grouted with a small void (approx. 1/8") at the top.	64-15	5	Tendons are fully grouted with a small void (approx. 1/4") at the top.	64-16
4	Tendons are fully grouted with a small void (approx. 1/4") at the top.	64-17			
3	Tendons are fully grouted with a small void (approx. 1/8") at the top.	64-18			

Segment 64: Top Tendons Right of CL of Box Looking Upstation
Upstation Face **Downstation Face**

Tendon No.	Comments	Picture No.	Tendon No.	Comments	Picture No.
12	Completely grouted with no evidence of void.	64-19	12	Tendons are fully grouted with a small void (approx. 1/8") at the top.	64-20
11	Tendons are fully grouted with a small void (approx. 1/8") at the top.	64-21	11	Tendons are fully grouted with a small void (approx. 1/4") at the top.	64-22
10	Tendons are fully grouted with a small void (approx. 1/4") at the top.	64-23	10	Tendons are fully grouted with a small void (approx. 1/8") at the top.	64-24
9	Tendons are fully grouted with a small void (approx. 1/8") at the top.	64-25	9	Tendons are fully grouted with a small void (approx. 1/8") at the top.	64-26
8	Tendons are fully grouted with a small void (approx. 1/4") at the top.	64-27	8	Completely grouted with no evidence of void.	64-28
7	Tendons are fully grouted with a small void (approx. 1/8") at the top.	64-29	7	Tendons are fully grouted with a small void (approx. 1/2") at the top.	64-30
6	Tendons are fully grouted with a small void (approx. 1/2") at the top.	64-31	6	Tendons are fully grouted with a small void (approx. 1/2") at the top.	64-32
5	Tendons are fully grouted with a small void (approx. 1/8") at the top.	64-33	5	Tendons are fully grouted with a small void (approx. 1/2") at the top.	64-34
4	Tendons are fully grouted with a small void (approx. 1/8") at the top.	64-35			
3	Tendons are fully grouted with a small void (approx. 1/8") at the top.	64-36			

Segment 65: Top Tendons Right of CL of Box Looking Upstation

Upstation Face

Downstation Face

Tendon No.	Comments	Picture No.	Tendon No.	Comments	Picture No.
12	Tendons are fully grouted with a small void (approx. 1/2") at the top.	23	12	Fully Grouted	24
11	Tendons are fully grouted with a small void (approx. 1/8") at the top.	25	11	Tendons are fully grouted with a small void (approx. 1/8") at the top.	26
10	Tendons are fully grouted with a small void (approx. 1/4") at the top.	27	10	Fully Grouted	28
9	Tendons are fully grouted with a small void (approx. 1/2") at the top.	29	9	Tendons are fully grouted with a small void (approx. 1/4") at the top.	30
8	Tendons are fully grouted with a small void (approx. 1/4") at the top.	31	8	Completely grouted.	32
7	Tendons are fully grouted with a small void (approx. 1/4") at the top.	33	7	Tendons are fully grouted with a small void (approx. 1/4") at the top.	34
6	Tendons are partially grouted, duct is half empty. No corrosion evident on tendons.	35	6	Tendons are fully grouted with a small void (approx. 1/2") at the top.	36
5	Tendons are fully grouted with a small void (approx. 1/4") at the top.	37	5	Tendons are fully grouted with a small void (approx. 1/4") at the top.	38
4	Tendons are fully grouted with a small void (approx. 1/4") at the top.	39	4	Tendons are fully grouted with a small void (approx. 1/8") at the top.	40
3	Tendons are fully grouted with a small void (approx. 1/4") at the top.	41	3	Completely grouted.	42
2	Tendons are fully grouted with a small void (approx. 1/8") at the top.	43			
1	Tendons are fully grouted with a small void (approx. 1/8") at the top.	44			

Note: Web tendons on the upstation face were completely grouted with no evidence of a void. Web tendons on the downstation face were completely grouted with no evidence of a void (pictures 6 & 19).

Segment 68: Top Tendons Left of CL of Box Looking Upstation

Upstation Face

Downstation Face

Tendon No.	Comments	*Picture No.	Tendon No.	Comments	*Picture No.
12	Tendons are fully grouted with a small void (approx. 1/8") at the top.	1	12	Tendons are fully grouted with a small void (approx. 1/4") at the top.	2
11	Tendons are fully grouted with a small void (approx. 1/8") at the top.	3	11	Tendons are fully grouted with a small void (approx. 1/8") at the top.	4
10	Tendons are fully grouted with a small void (approx. 1/8") at the top.	5	10	Tendons are fully grouted with a small void (approx. 1/8") at the top.	6
9	Tendons are fully grouted with a small void (approx. 1/8") at the top.	7	9	Tendons are fully grouted with a small void (approx. 1/2") at the top.	8
8	Tendons are fully grouted with a small void (approx. 1/8") at the top.	9	8	Tendons are fully grouted with a small void (approx. 1/8") at the top.	10
7	Tendons are fully grouted with a small void (approx. 1/8") at the top.	11	7	Completely grouted.	12
6	Tendons are fully grouted with a small void (approx. 1/8") at the top.	13	6	Tendons are fully grouted with a small void (approx. 1/8") at the top.	14
5	Tendons are fully grouted with a small void (approx. 1/8") at the top.	15	5	Tendons are fully grouted with a small void (approx. 1/8") at the top.	16
4	Tendons are fully grouted with a small void (approx. 1/8") at the top.	17	4	Completely grouted.	18
3	Tendons are fully grouted with a small void (approx. 1/4") at the top.	19	3	Tendons are fully grouted with a small void (approx. 1/4") at the top.	20
			2	Tendons are fully grouted with a small void (approx. 1/4") at the top.	21
			1	Completely grouted.	22

*Pictures have an incorrect notation showing segment 70. All pictures referenced are segment 68.

Segment 69: Top Tendons Left of CL of Box Looking Upstation

Upstation Face

Downstation Face

Tendon No.	Comments	Picture No.	Tendon No.	Comments	Picture No.
12	Tendons are fully grouted with a small void (approx. 1/2") at the top.	1	12	Tendons are fully grouted, no void.	2
11	Tendons are fully grouted with no voids.	3	11	Tendons are fully grouted with a small void (approx. 1/16") at the top.	4
10	Tendons are fully grouted with a small void (approx. 1/16") at the top.	5	10	Tendons are fully grouted with a small void (approx. 1/16") at the top.	6
9	Tendons are fully grouted with no voids.	7	9	Tendons are fully grouted with a small void (approx. 1/16") at the top.	8
8	Tendons are fully grouted with a small void (approx. 1/8") at the top.	9	8	Tendons are fully grouted with a small void (approx. 1/16") at the top.	10
7	Tendons are fully grouted with no voids.	11	7	Completely grouted.	12
6	Tendons are fully grouted with a small void (approx. 1/8") at the top.	13	6	Tendons are fully grouted, no void.	14
5	Tendons are fully grouted with no voids.	15	5	Tendons are fully grouted with a small void (approx. 1/8") at the top.	16
4	Anchor block, tendon is not visible		4	Completely grouted. Small void (approx. 1/8") at the top.	17
3	Anchor block, tendon is not visible		3	Tendons are fully grouted with a void (approx. 3/4") at the top. Significant amount of water was discharge, it seems that this water was trapped in the duct.	18 & 19

Segment 69: Top Tendons Right of CL of Box Looking Upstation

Upstation Face

Downstation Face

Tendon No.	Comments	Picture No.	Tendon No.	Comments	Picture No.
12	Tendons are fully grouted with a small void (approx. 1/16") at the top.	20	12	Tendons are fully grouted with a small void (approx. 1/8") at the top.	21
11	Completely grouted, no void.	22	11	Tendons are fully grouted with a small void (approx. 1/16") at the top.	23
10	Tendons are fully grouted with a small void (approx. 1/8") at the top.	24	10	Tendons are fully grouted with a small void (approx. 1/16") at the top.	25
9	Completely grouted, no void.	26	9	Tendons are fully grouted with void (approx. 3/4") at the top.	27
8	Tendons are fully grouted with a small void (approx. 1/16") at the top.	28	8	Tendons are fully grouted with no void.	29
7	Tendons are fully grouted with a small void (approx. 1/4") at the top.	30	7	Tendons are fully grouted with a void (approx. 1/2") at the top.	31
6	Tendons are partially grouted, duct is half empty. Strands exposed, but no corrosion evident on tendons.	32	6	Almost fully grouted, only top tendon exposed. Void (approx. 1/2") at the top.	33
5	Completely grouted, no void.	34	5	Tendons are fully grouted with a small void (approx. 1/16") at the top.	35
4	Anchor block, tendon is not visible		4	Partially grouted, most tendons are exposed, big void.	36
3	Anchor block, tendon is not visible		3	Tendons are fully grouted with a small void (approx. 1/16") at the top.	37

Segment 70: Top Tendons Left of CL of Box Looking Upstation

Upstation Face

Downstation Face

Tendon No.	Comments	Picture No.	Tendon No.	Comments	Picture No.
12	Tendons are fully grouted with a small void (approx. 1/4") at the top.	1	12	Tendons are fully grouted with a small void (approx. 1/2") at the top.	2
11	Tendons are fully grouted with a small void (approx. 1/8") at the top.	3	11	Tendons are fully grouted with a small void (approx. 1/2") at the top.	4
10	Tendons are fully grouted with a small void (approx. 1/16") at the top.	5	10	Tendons are fully grouted with a small void (approx. 1/8") at the top.	6
9	Tendons are fully grouted with a small void (approx. 1/16") at the top.	7	9	Tendons are fully grouted with a small void (approx. 1/8") at the top.	8
8	Tendons are fully grouted with a small void (approx. 1/8") at the top.	9	8	Tendons are fully grouted with a small void (approx. 1/8") at the top.	10
7	Completely grouted with no evidence of void.	11	7	Completely grouted with no evidence of void.	12
			6	Completely grouted with no evidence of void.	13
			5	Tendons are fully grouted with a small void (approx. 1/8") at the top.	14

Segment 70: Top Tendons Right of CL of Box Looking Upstation

Upstation Face

Downstation Face

Tendon No.	Comments	Picture No.	Tendon No.	Comments	Picture No.
12	Tendons are mostly grouted with a small void (approx. 1/2") at the top. One strand is exposed.	15	12	Tendons are fully grouted with a small void (approx. 1/2") at the top.	16
11	Tendons are fully grouted with a small void (approx. 1/8") at the top.	17	11	Completely grouted with no evidence of void.	18
10	Tendons are fully grouted with a small void (approx. 1/4") at the top.	19	10	Tendons are fully grouted with a small void (approx. 1/8") at the top.	20
9	Tendons are fully grouted with a small void (approx. 1/2") at the top.	21	9	Completely grouted with no evidence of void.	22
8	Tendons are fully grouted with a small void (approx. 1/2") at the top.	23	8	Tendons are fully grouted with a small void (approx. 3/4") at the top.	24
7	Completely grouted with no evidence of void.	25	7	Completely grouted with no evidence of void.	26
			6	Tendons are partially grouted. More than 50% of section is voided.	27
			5	Completely grouted with no evidence of void.	28

Note: Web tendons on the upstation face and downstation face were completely grouted with no evidence of a void (pictures 181, 191, 199 & 206)

Segment 71: Top Tendons Left of CL of Box Looking Upstation
Upstation Face **Downstation Face**

Tendon No.	Comments	Picture No.	Tendon No.	Comments	Picture No.
12	Tendons are fully grouted with a small void (approx. 1/4") at the top.	1	12	Tendons are fully grouted with a small void (approx. 1/8") at the top.	2
11	Completely grouted with no evidence of void.	3	11	Tendons are fully grouted with a small void (approx. 1/8") at the top.	4
10	Tendons are fully grouted with a small void (approx. 1/8") at the top.	5	10	Tendons are fully grouted with a small void (approx. 1/4") at the top.	6
9	Tendons are fully grouted with a small void (approx. 1/16") at the top.	7	9	Tendons are fully grouted with a small void (approx. 1/16") at the top.	8
			8	Tendons are fully grouted with a small void (approx. 1/4") at the top.	9
			7	Completely grouted with no evidence of void.	10

Segment 71: Top Tendons Right of CL of Box Looking Upstation
Upstation Face **Downstation Face**

Tendon No.	Comments	Picture No.	Tendon No.	Comments	Picture No.
12	Tendons are mostly grouted with a small void (approx. 1/4") at the top. One strand is exposed.	11	12	Tendons are fully grouted with a small void (approx. 1/4") at the top.	12
11	Completely grouted with no evidence of void.	13	11	Tendons are fully grouted with a small void (approx. 1/8") at the top.	14
10	Tendons are fully grouted with a small void (approx. 1/8") at the top.	15	10	Tendons are fully grouted with a small void (approx. 1/8") at the top.	16
9	Tendons are fully grouted with a small void (approx. 1/4") at the top. Grout was moist and brittle.	17	9	Tendons are fully grouted with a small void (approx. 1/4") at the top.	18
			8	Tendons are fully grouted with a small void (approx. 1/8") at the top.	19
			7	Completely grouted with no evidence of void.	20

Segment 75: Top Tendons Left of CL of Box Looking Upstation

Upstation Face

Downstation Face

Tendon No.	Comments	Picture No.	Tendon No.	Comments	Picture No.
14	Anchor block, tendon is not visible		14	Mostly ungrouted, most strands are exposed and some wires have recessed 1/2".	75-1
12	Anchor block, tendon is not visible		13	Completely grouted.	

Segment 75: Top Tendons Right of CL of Box Looking Upstation

Upstation Face

Downstation Face

Tendon No.	Comments	Picture No.	Tendon No.	Comments	Picture No.
14	Anchor block, tendon is not visible		14	Mostly ungrouted, most strands are exposed.	75-2
12	Anchor block, tendon is not visible		13	Completely grouted.	75-3

Note: Web tendons on the upstation face were completely ungrouted, on the downstation side right side was ungrouted. See pictures 75-4 & 75-5. Picture 75-6 shows the upstation face of the segment

Segment 76: Top Tendons Left of CL of Box Looking Upstation

Upstation Face

Downstation Face

Tendon No.	Comments	Picture No.	Tendon No.	Comments	Picture No.
14	Top void of approx. 1/2", strands are grouted.	76-1	14	Partially grouted, top strands are exposed	76-2
12	Top void of approx. 3/4", top strands are exposed.	76-3	12	Anchor block, tendon is not visible	
13	Big void, almost 50% of section is voided, top strands are exposed.	76-4 76-6	13	Partially grouted, top strands are exposed. At this location damage was induced during NDT testing phase.	76-5
11	Top void of approx. 3/4", strands are grouted.	76-7	11	Anchor block, tendon is not visible	

Segment 76: Top Tendons Right of CL of Box Looking Upstation

Upstation Face

Downstation Face

Tendon No.	Comments	Picture No.	Tendon No.	Comments	Picture No.
14	Top void of approx. 3/4", strands are grouted.	76-8	14	Almost completely ungrouted and almost all tendons are exposed.	76-9
12	Strands fully grouted, top void of approx. 1/2".	76-8	12	Anchor block, tendon is not visible	
13	Strands fully grouted, top void of approx. 1/2".	76-10	13	Strands are grouted, but small void at top of duct of approx. 1/2" deep.	76-11
11	Strands fully grouted, top void of approx. 3/4".	76-10	11	Anchor block, tendon is not visible	

Note: Right Web tendon is almost completely ungrouted, pictures 76-12 & 76-13

Segment 63 Pictures



Picture 63-1



Picture 63-2



Picture 63-3



Picture 63-4



Picture 63-5



Picture 63-6

Segment 63 Pictures



Picture 63-7



Picture 63-8



Picture 63-9



Picture 63-10



Picture 63-11



Picture 63-12

Segment 63 Pictures



Picture 63-13



Picture 63-14



Picture 63-15



Picture 63.16



Picture 63-17

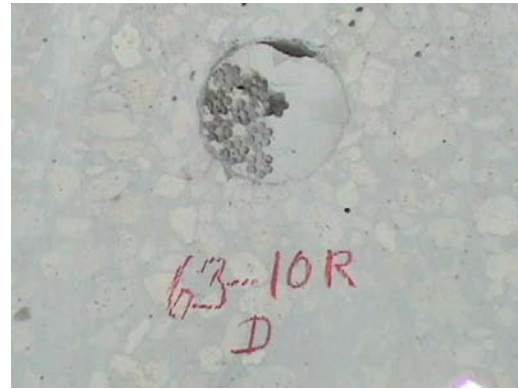


Picture 63-18

Segment 63 Pictures



Picture 63-19



Picture 63-20



Picture 63-21



Picture 63-22



Picture 63-23



Picture 63-24

Segment 63 Pictures



Picture 63-25



Picture 63-26



Picture 63-27



Picture 63-28

Segment 64 Pictures



Picture 64-1



Picture 64-2



Picture 64-3



Picture 64-4



Picture 64-5



Picture 64-6

Segment 64 Pictures



Picture 64-7



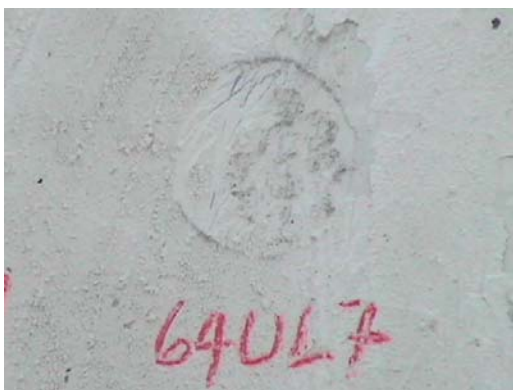
Picture 64-8



Picture 64-9



Picture 64-10



Picture 64-11



Picture 64-12

Segment 64 Pictures



Picture 64-13



Picture 64-14



Picture 64-15



Picture 64-16



Picture 64-17



Picture 64-18

Segment 64 Pictures



Picture 64-19



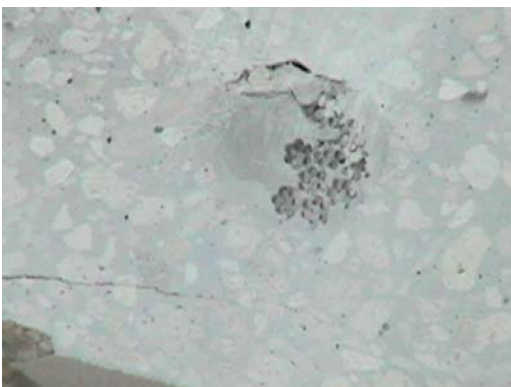
Picture 64-20



Picture 64-21



Picture 64-22



Picture 64-23



Picture 64-24

Segment 64 Pictures



Picture 64-25



Picture 64-26



Picture 64-27



Picture 64-28



Picture 64-29



Picture 64-30

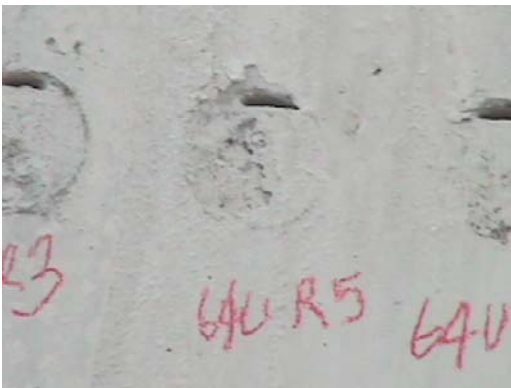
Segment 64 Pictures



Picture 64-31



Picture 64-32



Picture 64-33



Picture 64-34



Picture 64-35



Picture 64-36

Segment 65 Pictures



Picture 65-1



Picture 65-2



Picture 65-3



Picture 65-4



Picture 65-5



Picture 65-6

Segment 65 Pictures



Picture 65-7



Picture 65-8



Picture 65-9



Picture 65-10



Picture 65-11



Picture 65-12

Segment 65 Pictures



Picture 65-13



Picture 65-14



Picture 65-15



Picture 65-16



Picture 65-17



Picture 65-18

Segment 65 Pictures



Picture 65-19



Picture 65-20



Picture 65-21



Picture 65-22



Picture 65-23



Picture 65-24

Segment 65 Pictures



Picture 65-25



Picture 65-26



Picture 65-27



Picture 65-28



Picture 65-29



Picture 65-30

Segment 65 Pictures



Picture 65-31



Picture 65-32



Picture 65-33



Picture 65-34



Picture 65-35



Picture 65-36

Segment 65 Pictures



Picture 65-37



Picture 65-38



Picture 65-39



Picture 65-40



Picture 65-41



Picture 65-42

Segment 65 Pictures



Picture 65-43

Segment 68 Pictures



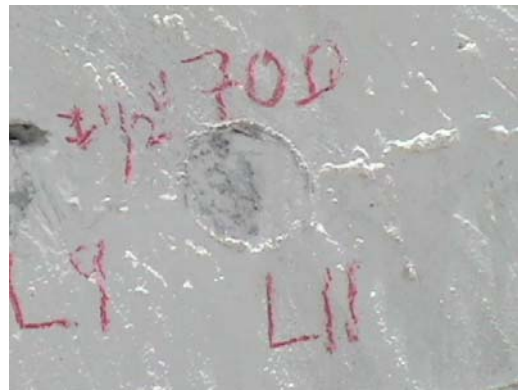
Picture 68-1



Picture 68-2



Picture 68-3



Picture 68-4



Picture 68-5



Picture 68-6

Segment 68 Pictures



Picture 68-7



Picture 68-8



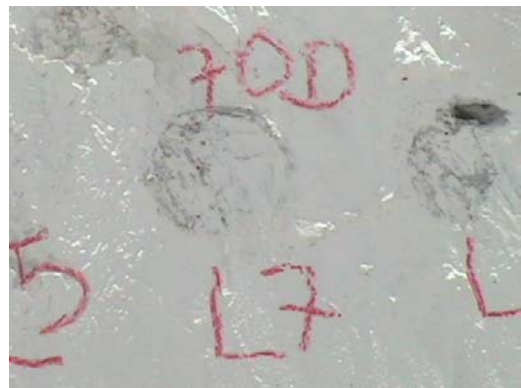
Picture 68-9



Picture 68-10



Picture 68-11



Picture 68-12

Segment 68 Pictures



Picture 68-13



Picture 68-14



Picture 68-15



Picture 68-16



Picture 68-17



Picture 68-18

Segment 68 Pictures



Picture 68-19



Picture 68-20



Picture 68-21



Picture 68-22



Picture 68-23



Picture 68-24

Segment 68 Pictures



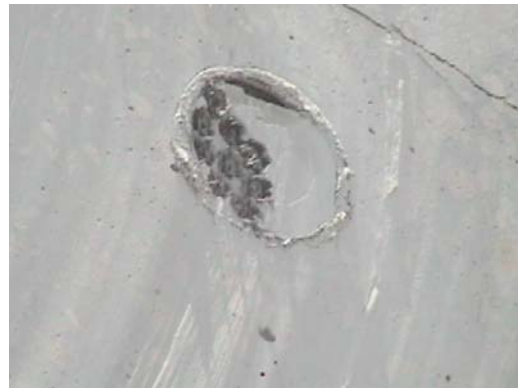
Picture 68-25



Picture 68-26



Picture 68-27



Picture 68-28



Picture 68-29



Picture 68-30

Segment 68 Pictures



Picture 68-31



Picture 68-32



Picture 68-33



Picture 68-34



Picture 68-35



Picture 68-36

Segment 68 Pictures



Picture 68-37



Picture 68-38



Picture 68-39



Picture 68-40



Picture 68-41



Picture 68-42

Segment 68 Pictures



Picture 68-43



Picture 68-44

Segment 69 Pictures



Picture 69-1



Picture 69-2



Picture 69-3



Picture 69-4



Picture 69-5



Picture 69-6

Segment 69 Pictures



Picture 69-7



Picture 69-8



Picture 69-9



Picture 69-10

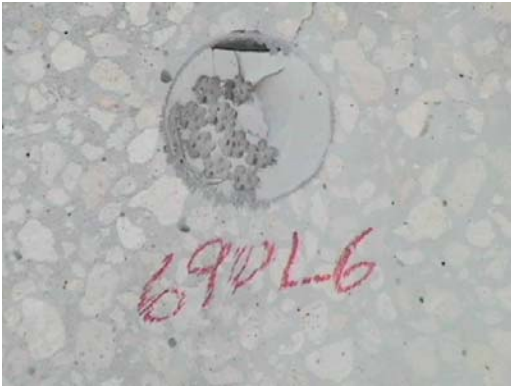


Picture 69-11



Picture 69-12

Segment 69 Pictures



Picture 69-13



Picture 69-14



Picture 69-15



Picture 69-16



Picture 69-19

Segment 69 Pictures



Picture 69-20



Picture 69-21



Picture 69-22



Picture 69-23



Picture 69-24



Picture 69-25

Segment 69 Pictures



Picture 69-26



Picture 69-27



Picture 69-28



Picture 69-29



Picture 69-30



Picture 69-31

Segment 69 Pictures



Picture 69-32



Picture 69-33



Picture 69-34



Picture 69-35



Picture 69-36



Picture 69-37

Segment 70 Pictures



Picture 70-1



Picture 70-2



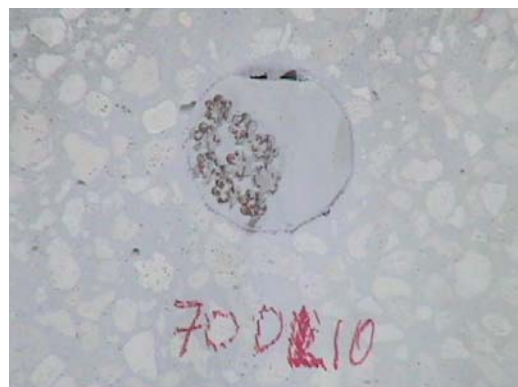
Picture 70-3



Picture 70-4



Picture 70-5



Picture 70-6

Segment 70 Pictures



Picture 70-7



Picture 70-8



Picture 70-9



Picture 70-10



Picture 70-11



Picture 70-12

Segment 70 Pictures



Picture 70-13



Picture 70-14



Picture 70-15



Picture 70-16



Picture 70-17



Picture 70-18

Segment 70 Pictures



Picture 70-19



Picture 70-20



Picture 70-21



Picture 70-22



Picture 70-23



Picture 70-24

Segment 70 Pictures



Picture 70-25



Picture 70-26

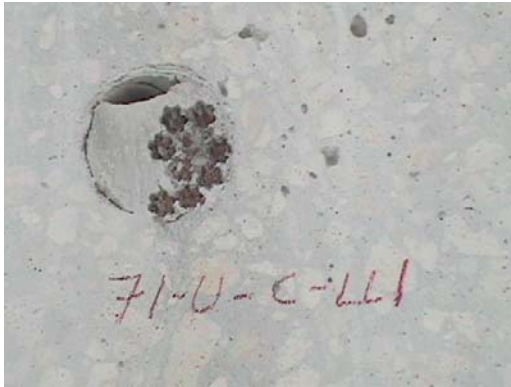


Picture 70-27



Picture 70-28

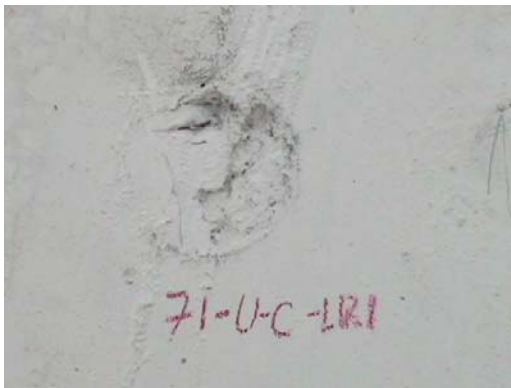
Segment 71 Pictures



Picture 71-1



Picture 71-2



Picture 71-3



Picture 71-4

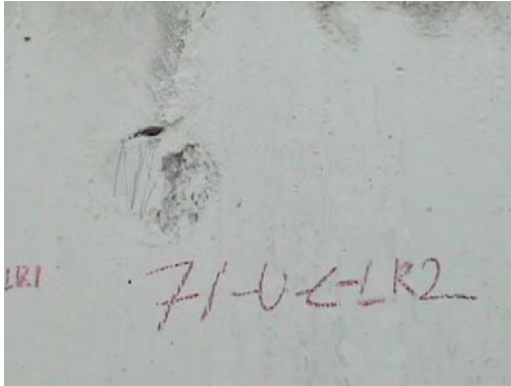


Picture 71-5



Picture 71-6

Segment 71 Pictures



Picture 71-7



Picture 71-8



Picture 71-9



Picture 71-10



Picture 71-11



Picture 71-12

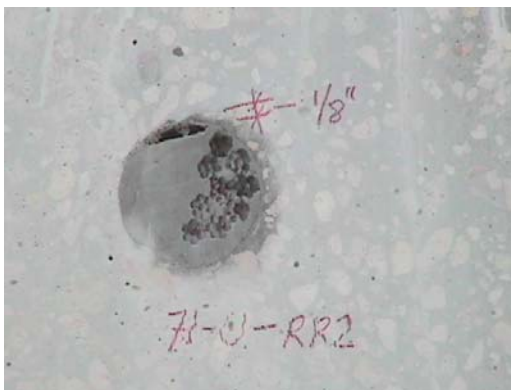
Segment 71 Pictures



Picture 71-13



Picture 71-14



Picture 71-15



Picture 71-16



Picture 71-17



Picture 71-18

Segment 71 Pictures



Picture 71-19



Picture 71-20

Segment 75 Pictures



Picture 75-1



Picture 75-2



Picture 75-3



Picture 75-4



Picture 75-5



Picture 75-6

Segment 76 pictures



Picture 76-1



Picture 76-2



Picture 76-3



Picture 76-4



Picture 76-5



Picture 76-6

Segment 76 Pictures



Picture 76-7



Picture 76-8



Picture 76-9



Picture 76-10



Picture 76-11



Picture 76-12



Picture 76-13

REPORT

PROJECT

NONDESTRUCTIVE EVALUATION OF POST-TENSIONING DUCTS
EXISTING RAMP D
FORT LAUDERDALE/HOLLYWOOD INTERNATIONAL AIRPORT
FLORIDA DOT CONTRACT No. C6912

CLIENT

DMJM + HARRIS
2056 CENTRE POINT LANE
TALLAHASSEE, FLORIDA 32308

Project No. 320233

APRIL 17, 2002

TABLE OF CONTENTS

1.0 INTRODUCTION

2.0 STRUCTURE DESCRIPTION

3.0 TEST PROGRAM

4.0 TEST RESULTS

4.1 Impulse Radar

4.2 Impact-Echo

4.3 Half-Cell Corrosion

5.0 DISCUSSION AND CONCLUSIONS

APPENDIX A: DESCRIPTION OF NONDESTRUCTIVE TEST METHODS

APPENDIX B: IMPULSE RADAR

Figure B.1: Impulse Radar Test Example

APPENDIX C: IMPACT-ECHO

Table C.1: Impact-Echo Test Locations and Findings

Table C.2: I-E Reflector Frequencies for Figures C.3 – C.8

Figures C.1 to C.8: Impact-Echo Test Examples

APPENDIX D: HALF-CELL POTENTIAL

Table D.1: Half-Cell Potential Readings

Figure D.1: Exposed Tendon in Void

Figure D.2: Borescope Image along Void in Figure D.1

**NONDESTRUCTIVE EVALUATION OF POST-TENSIONING DUCTS
EXISTING RAMP D
FORT LAUDERDALE/HOLLYWOOD INTERNATIONAL AIRPORT
FLORIDA DOT CONTRACT No. C6912**

1.0 INTRODUCTION

DMJM Harris of Tallahassee, Florida, has instructed Construction Technology Laboratories, Inc. (CTL) to perform nondestructive testing of selected post-tensioned reinforced concrete box girders at the Existing Ramp D at Fort Lauderdale/Hollywood International Airport.

CTL carried out testing between March 18 and 22, 2002. Nondestructive test methods used for this evaluation included Impulse Radar, the Impact-Echo (I-E) stress wave test and electric half-cell potential. This report describes the methods used and discusses the findings of the test program.

2.0 STRUCTURE DESCRIPTION

Ramp D includes seven spans comprised of post-tensioned reinforced concrete box girders. Each precast box segment is approximately 10 ft long by 43 ft wide by 7 ft high. Two segments make up the width of the bridge, and are suffixed S and N from south to north for identification purposes in this report. The area of interest for this test program comprised spans 5 through 7 inclusive. The post-tensioning ducts in the upper deck of each segment have been grouted from ports in the construction joint. The number of ducts in each box varies between 2 and 14, and their approximate locations are shown on Drawing No. 117 of 194 (Top Tendon Layout – Plan), State of Florida DOT, dated 7/19/84.

The metal ducts are 3 $\frac{3}{4}$ inches in diameter, with a nominal top concrete cover of approximately 3 $\frac{1}{2}$ inches. The thickness of the box flange increases from 8 inches at the outer edge to approximately 17 inches at 12 ft from the edge, close to the box web. Mild steel reinforcement is present above the ducts in both the transverse and longitudinal directions, at varying bar spacing.

3.0 TEST PROGRAM

The nondestructive Impulse Radar, Impact-Echo (I-E) and electric half-cell test methods were used in this program. These methods are described in Appendix A to this report, and are outlined in the American Concrete Institute Report ACI 228.2R-98, *“Nondestructive Test Methods for Evaluation of Concrete in Structures”*. Sansalone and Streett (Reference 1 Appendix A) describe the use of Impact-Echo testing for the detection of grouted or ungrouted tendon ducts.

Impulse Radar was used to locate the longitudinal alignment and depth of the ducts of interest, before I-E testing. It is essential that the ducts be located accurately before any stress wave testing is performed. In addition, the deck contains a considerable quantity of standard reinforcing steel, which has to be avoided during I-E testing. Ferro-magnetic devices such as covermeters are not adequate for this purpose, because of the concentration of different types of steel reinforcement and the depth of duct cover usually encountered. The location of all ducts in the southern half of the ramp was marked by spray paint on the deck. Spot locations across each box were also marked in the northern section of the deck.

The I-E compression wave velocity of the concrete was tested at drainage openings in the outer flange where the flange thickness could be confirmed.

Three I-E tests were made at each location, and the individual results stored on the computer. In addition, an average test result was compounded from the three tests, and processed according to the method outlined in Reference 2 in Appendix A. This process eliminates the influence of the Rayleigh wave on the result, and also minimizes any effect from background noise.

In order to assess the validity of electric half-cell potential testing on tendons in these ducts, two sections of duct were selected; one with air voids detected by the I-E test, and the second with a fully grouted I-E test response. In each case, the tendons were exposed by drilling through the concrete and cutting the steel duct. Half-cell tests were made on the concrete surface in the vicinity of the exposed tendons to estimate corrosion potential. At the same time, borescope images of the exposed void at one of the tendons were recorded.

4.0 TEST RESULTS

4.1 Impulse Radar

A typical radar test output is given in Appendix B, Figure B.1. This profile was run across unit No. 54 on the north side of the ramp, and shows the presence of post-tensioning ducts as well as reinforcing steel. The duct centerline locations obtained by radar for each test profile were marked on the deck surface with spray paint on the southern girder for boxes No 60 to 90, and marked at selected spots on the northern girder.

4.2 Impact-Echo

Preliminary I-E calibration tests were run at four drainage openings in the outer flanges, in order to obtain a typical base reflection and to measure the compression wave velocity of the concrete applicable to this test. I-E test results from two of these points are given in Figures C.1 and C.2, Appendix C. An average compression wave velocity, $C_p = 11,700$ ft/s was measured at these test points. This value is low for concrete normally encountered throughout the USA, and is a function of the aggregate type used in this construction. This value for C_p was used for all I-E tests on the ramp.

I-E tests were then run at selected points on the ramp. The test locations are given in Table C.1, Appendix C. A total of 290 duct points were tested. Examples of I-E test plots are shown in Figures C.3 – C.8 in Appendix C.

As described in Appendix A, when testing vertically above the ducts, if an air void occupies a large part of the horizontal duct section, it is impossible to determine if the void is partially or totally occupying the duct. However, the reflection from the air void varies in amplitude depending on the size of the void, so the analysis of the I-E data here includes a judgment on whether the void is large or small. Table C.1 includes this rating of the detected voids.

Table C.2 gives the principal reflector frequencies from selected test results as shown in Figures C.3 – C.8.

Of the 290 I-E test points, 100 showed full void responses from the top of the duct, with 29 partial void responses. The pattern of voiding was relatively random, with some adjacent test points showing voiding, whereas other test points with voids were isolated. Void location did not appear to be concentrated in the vicinity of anchor points.

4.3 Half-Cell Corrosion

In the case of Ramp D tested here, the purpose of the half-cell test was to measure the corrosion activity at the surface of the post-tension tendons embedded in grout inside metallic ducts. Therefore, the tendons had to be exposed and were directly connected to the voltmeter. It was assumed that tendons are not connected to the surrounding conventional reinforcing steel in the bridge, which is most likely the case in such structures. However, continuity between the tendons and reinforcing steel at the tested locations was checked to make sure that the tendon was isolated from the surrounding steel.

Location 1. The first tested location was near the joint between box girder 63 and 64, on tendon 4 in Box No. 64 North. At this location, no void was detected by the I-E test, and the duct was approximately 4.5 in. deep with the tendon at nearly 6 in. below the surface. The voltmeter terminal was connected to the tendon and half-cell measurements were taken on the concrete surface along the tendon at 1-foot intervals starting at the connection point. It should be mentioned that testing locations were wetted thoroughly with sponges prior to testing. The half-cell readings are given in Table D.1, Appendix D to this report.

These readings indicate that no corrosion activity is occurring at the surface of the tendon. Even though voids might have formed in the duct, corrosion is unlikely to have occurred if the voids were dry.

The voltmeter was then connected to conventional steel, and half-cell readings were taken at several points at the surface. Readings were close to readings taken at the tendons and they were less negative than -100 mV. No sign of corrosion was observed on exposed conventional steel.

Location 2. This location was on Tendon 4, Box No. 69 North, at I-E test point 4E. The I-E test located a void at this point, as well as at adjacent test further to the west. At this location, the duct was 5 in. deep and the tendon was at 6.5 in. A void was found when the duct was cut open. Lenses of water were found, typical of moisture formed by bleeding of the grout mixture or improper grouting practices. The voltmeter was connected to the tendon and half-cell measurements inside the cut (at approximately 2 in. above the duct) were taken. The half-cell potential was close to -280 mV. At this level of potential, corrosion is uncertain (ASTM C 876). However, this relatively high reading indicates an electrochemical activity at the level of the tendon, as a result of the presence of moisture. The surface of the tendon was closely examined, but no sign of rust was observed. Figure D.1 is a photograph of the exposed tendon.

When the voltmeter was connected to the conventional steel in the vicinity of the tendon, the half-cell reading above the bar was much less than that measured at the tendon. An average of -124 mV was measured.

Half-cell potential readings were taken on the surface of the concrete above the tendon (6 in. cover). Readings were much less than reading taken at 2 in. above the tendon. A pilot hole (1 in. in diameter and 2 to 3 in. deep) was drilled and half-cell readings were taken in the bottom of the hole after it had been wetted. The half-cell potentials were comparable with readings taken inside the hole (close to -240 mV). This indicates that the deep cover reduces the accuracy of the half-cell reading.

Borescope images were taken of the void developing along the upper portion of this tendon towards the west. The void was probed and found to be 3 ft. 5 in. long. A selected borescope picture of the void is presented in Figure D.1, Appendix D. It can be seen that this was a partial void, occupying the upper third of the duct.

5.0 DISCUSSION AND CONCLUSIONS

The nondestructive testing described in this report was able to identify the possible presence of fully grouted and voided ducts in the box segments of Ramp D at the Fort Lauderdale/Hollywood International Airport. Of the 290 Impact-Echo test points selected, 129 showed evidence of full or partial voiding in the top of the duct. Proof of the success of this methodology can only be achieved by exposing the tendons within the ducts at those specific test points. However, the two ducts exposed for half-cell potential testing did confirm the results from the Impact-Echo tests at those points.

In view of the very complex arrangement of the ducts in these elements (deviations in duct alignment, varying flange thickness, other steel reinforcement), we can only reiterate that it is essential to combine the use of Impulse Radar with Impact-Echo testing to reach a sensible interpretation of the I-E data.

It can be concluded from this study that half-cell potential can be used to measure corrosion activity in post-tensioned tendons, if voltmeter connection to the tendons is provided. In the case of deep cover, pilot holes can be drilled to a certain depth if feasible to obtain more accurate readings. Mini half-cells could be used in this case to minimize drill hole diameter. Obviously, the interpretation of the results is not straight forward as that for conventional steel. Discontinuity between tendons and conventional steel in the structure should be checked.

Allen G. Davis, Ph.D., P.E.
Senior Principal Engineer
Manager for Nondestructive Testing

April 17, 2002

Dr. Juan Goni
DMJM Harris
2056 Centre Pointe Lane
Tallahassee, Florida 32308

**RE: NONDESTRUCTIVE EVALUATION OF POST-TENSIONING DUCTS
EXISTING RAMP D FORT LAUDERDALE/HOLLYWOOD INTERNATIONAL AIRPORT
FLORIDA DOT CONTRACT No. C6912
CTL PROJECT No. 320233**

Dear Dr. Goni:

We have pleasure in presenting our report on the nondestructive testing of selected post-tensioned reinforced concrete box girders at the Existing Ramp D referenced above.

We sincerely appreciate the opportunity to work with you on this project. If you have any questions, please call us at 1-800-522-2CTL.

Respectfully:

CONSTRUCTION TECHNOLOGY LABORATORIES, INC.

Allen G. Davis, Ph.D., P.E.
Senior Principal Engineer
Manager for Nondestructive Testing

Attachments

APPENDIX A
NONDESTRUCTIVE TEST METHODS

THE IMPACT-ECHO TEST

The Impact-Echo (I-E) test uses stress waves to detect flaws within concrete structures. However, the frequency range used is considerably higher in the I-E test than the IR test, since much shorter wavelengths are required to detect smaller anomalies. Surface displacements caused by reflecting stress waves can be viewed versus time as a displacement waveform. The amplitude spectrum of this waveform is computed by FFT, as for the Impulse Response. This spectrum has a periodic nature, which is a function of the depth to the reflective boundary (either the back of the element, or some anomaly such as a crack in the element under test. The depth of a concrete/air interface (internal void or external boundary) is determined by:

$$T = v_c / 2f \quad (1)$$

T is the interface depth, v_c is the primary stress wave velocity and f is the frequency due to reflection of the P wave from the interface.

If the material beyond the reflective interface is acoustically stiffer than concrete (e.g. concrete/steel interface), then the following equation applies:

$$T = v_c / 4f \quad (2)$$

The difference in the acoustic impedance of the two materials at an interface is important because it determines whether the presence of an interface will be detected by an I-E test. For example, a concrete/grout interface gives no reflection of the stress wave because the acoustic impedance of concrete and grout are nearly equal. In contrast, at a concrete/air interface, nearly all the energy is reflected, since the acoustic impedance of air is very much less than concrete.

General Model for I-E testing of steel ducts

If the steel ducts in a concrete slab of a constant thickness are fully grouted, then the ducts will not affect the I-E thickness frequency. The majority of the P-wave will go through the steel duct containing the tendons and be reflected from the concrete base as if there were no cable duct between. As an example, for an 8-inch thick slab with a P-wave speed of 11,700 ft/s,

$$f = C_p / 2T = 11,700 \text{ ft/s} / (2 \times 8 \text{ in}) = 8.775 \text{ kHz}$$

The frequency over a fully injected duct would also be 8.775 kHz.

In addition, the P-wave will be reflected from the tendons inside the duct (if it contains a high-enough frequency content). Assuming a fully grouted duct with 3-½ inches concrete cover and with tendons close to the duct soffit, an additional peak will appear on the frequency spectrum at:

$$f = C_p / 4T_d = 11,700 \text{ ft/s} / (4 \times 3.5 \text{ in}) = 10.0 \text{ kHz}$$

On the other hand, if the cable duct is completely void of grout, the main part of the P-wave will run around the duct, resulting in a lengthened travel path. The solid frequency of 8.775 kHz would then drop, typically in this case by more than 2 kHz. Also, the P-wave in this event will be reflected from the air duct at a frequency of

$$f = C_p / 2T_d = 11,700 \text{ ft/s} / (2 \times 3.5 \text{ in}) = 20.0 \text{ kHz}$$

In the event of partial voiding in the duct, reflections from the air void will occur if the void is significant. The degree of significance of the void for reflection to occur is the critical issue, and will vary from case to case. If testing is carried out on the concrete surface vertically above the duct, then any air void is usually located in the top portion of the duct, and the reflection is clear. In this case, the degree of voiding cannot be determined; only that a significant air void exists. If testing is carried out on the concrete surface horizontally in line with the duct, the void size for identification is usually in excess of 40 % of the duct diameter.

References

1. Sansalone, M. and W.B. Streett, 1997, "Impact-Echo: nondestructive evaluation of concrete and masonry," Bullbrier Press, Ithaca, NY.
2. Abraham, M., C. Léonard, P. Côte and B. Piwakowski, 2000, "Time Frequency Analysis of Impact-Echo Signals: Numerical Modeling and Experimental Validation", ACI Materials Journal, V. 97, No. 6, Nov.-Dec. 2000, pp. 645-657.

IMPULSE RADAR METHODOLOGY

The impulse radar technique employs high-frequency electromagnetic energy for rapidly and continuously assessing a variety of characteristics of the subsurface being tested. The operating principle is based on scanning the reflections of electromagnetic waves from varying dielectric constant boundaries in the material being scanned. A single contacting transducer (antenna) is used for transmitting and receiving radar signals. High frequency, short pulse electromagnetic energy is transmitted into the concrete. Each transmitted pulse travels through the concrete element and is partially reflected when it encounters a change in dielectric constant such as a void, reinforcing steel, post-tensioning ducts, etc. The receiving sensor of the transducer detects the reflected pulses. Boundary depth is proportional to transmitted time. The data are then recorded on a computer hard drive for analysis in the field or in the office. For the purposes of this project, a 1.5GHz antenna was used for optimum signal interpretation.

HALF-CELL POTENTIAL:

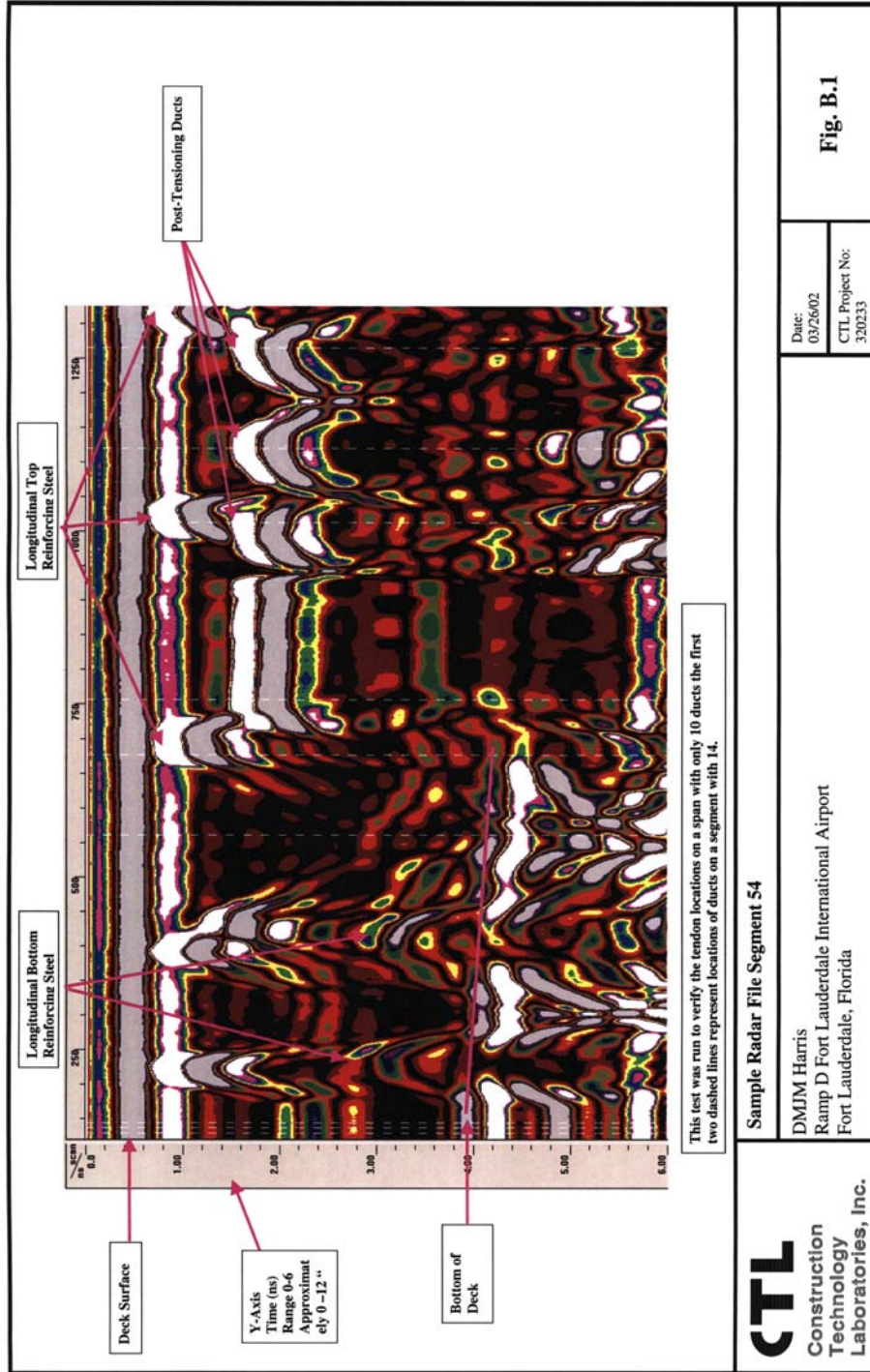
In order to evaluate the corrosion activity at selected locations on the Ft. Lauderdale airport bridge, the half-cell potential measurement technique was used. The half-cell is simply a piece of metal immersed in a solution of its own ions such as copper in copper sulfate. When a half-cell is connected to reinforcing steel embedded in concrete, it creates a complete electrical cell. A voltage will be then generated because the cell contains two different metals (copper and iron) that have different positions in the electrochemical series. When the cell is moved along a concrete surface, a change in the full cell is occurred due to the difference in condition of the steel surface below the moving half-cell. Potential measurement gives an indication of corrosion activities in the reinforcing steel embedded in concrete. A description of testing procedures is given in ASTM C 876 "Standard Test Method for Half-Cell Potentials of Uncoated Reinforcing Steel in Concrete."

Half-cell measurements are usually used to evaluate conventional reinforced concrete structures such as bridge decks with an average cover normally ranging from 2 to 4 in. In such cases, the voltmeter is connected to one point in the structure where the steel is usually electrically continuous across the structure, and the potential survey is conducted on its surface.

References

1. Broomfield, J.P., "Corrosion of Steel in Concrete, Understanding, Investigation and Repair," E&FN Spon, London, 238 pp., 1997.
2. Nagi, M, and Whiting, D., 'Corrosion of Prestressed Reinforcing Steel in Concrete Bridges: State-of-the-Art,' ACI SP-151, American Concrete Institute, Farmington Hills, Michigan, pp.1-17, 1994.

APPENDIX B
IMPULSE RADAR TEST EXAMPLE



APPENDIX C
IMPACT-ECHO TEST RESULTS

TABLE C.1 CTL IMPACT-ECHO TEST RESULTS
Fort Lauderdale Ramp "D"
Impact-Echo Test Points

v = void sv = small void steel = rebar

Segment 89 South: Distance west from 90/89 joint

Duct No	Test A	Test B	Test C	Test D
14	3'0"	5'8" steel	7'1" v	-
12	3'0" v	4'8"	6'5" v	7'4"
11	3'8"	5'1"	6'1" sv	7'0"
13	3'1"	5'1" sv	6'2"	7'0"

Segment 88 South: Distance west from 89/88 joint

Duct No	Test A	Test B	Test C	Test D
14	2'6" v	3'4"	4'4"	-
12	2'6"	3'4" v	4'4" v	-
10	1'4" v	2'6" v	3'0"	4'5"
9	1'6" sv	3'1"	4'6" v	-
11	3'1" v	4'6"	-	-
13	2'5"	3'2"	4'6" v	-

Segment 87 South: Distance west from 88/87 joint

Duct No.	Test A	Test B	Test C	Test D
14	2'4"	4'6" v	5'6"	-
12	2'4" sv	4'4" v	5'6" v	-
10	2'4" v	4'4" sv	5'6" sv	-
8	1'4"	2'5" v	4'4"	5'4"
7	1'2"	2'3"	4'3" v	4'10" v
9	2'1"	4'4"	5'4" sv	-
11	2'1" v	4'4"	5'4" v	-
13	2'1"	4'4"	5'4" v	-

Segment 86 South: Distance west from 87/86 joint

Duct No	Test A	Test B	Test C
14	2'4"	3'8"	5'8"
12	2'4"	3'8"	5'8" sv
10	2'4"	3'8"	5'8"
8	2'4" v	3'8"	5'8" sv

TABLE C.1 (continued)

Segment 85 South: Distance west from 86/85 joint

Duct No.	Test A	Test B	Test C	Test D
14	2'5"	3'6"	5'7"	-
12	2'5"	3'6" v	5'7"	-
10	2'5" v	3'6"	5'7"	-
8	2'5" v	3'6"	5'7"	-
6	2'5" sv	3'6"	5'7"	-
4	1'2'	2'4" v	3'8" v	5'7" sv
3	1'2'	2'4" v	3'8" v	5'7"
5	2'3" v	3'6"	5'7"	-
7	2'3"	3'6"	5'7" v	-
9	2'3" sv	3'6"	5'7" v	-
11	2'3" v	3'6"	5'7"	-
13	2'3" v	3'6"	5'7" v	-

Segment 81 South: Distance west from 82/81 joint

Duct No	Test A	Test B	Test C
4	5'7" v	6'10"	8'1" v
2	5'7" v	6'10" sv	8'1" v
1	5'7" v	6'10"	8'1"
3	5'7"	6'10"	8'1"

Segment 79 South: Distance west from 80/79 joint

Duct No	Test A	Test B	Test C
14	1'4" sv	2'10"	3'11" v
12	1'4"	2'10" v	3'11" v
10	1'4"	2'10" v	3'11"
8	1'4"	2'10" v	3'11"
6	1'4" v	2'10" v	3'11"
5	1'4" v	2'10" v	3'11" sv
7	1'4"	2'10" v	3'11"
9	1'4" v	2'10"	3'11"
11	1'4"	2'10" v	3'11"
13	1'4" v	2'10" v	3'11" v

TABLE C.1 (continued)**Segment 77 South: Distance west from 78/77 joint**

Duct No	Test A	Test B	Test C
14	-	6'10" sv	8'7" v
12	-	6'10" v	8'7" sv
10	-	6'10" sv	8'7" v
9	5'5"	6'10" v	8'7"
11	5'5" sv	6'10" v	8'7" v
13	5'5" v	6'10" v	8'7"

Segment 76 South: Distance west from 77/76 joint

Duct No	Test A	Test B	Test C	Test D
14	7'2" v	8'0" v	9'1" sv	10'4"
12	7'2" v	8'0" v	9'1"	-
11	7'2"	8'0" sv	9'1" (patch)	-
13	7'2"	8'0"	9'1"	10'4"

Segment 75 South: Distance west from 76/75 joint

Duct No	Test A	Test B	Test C
14	5'4"	7'2" v	8'4" v
13	5'4" sv	7'2" sv	8'4"

Segment 73 South: Distance west from 74/73 joint

Duct No	Test A	Test B	Test C
12	2'0"	3'7" v	5'2" v
11	2'0"	3'7"	5'2"

Segment 72 South: Distance west from 73/72 joint

Duct No	Test A	Test B	Test C
12	7'1" v	8'9" sv	10'3" v
10	7'1" sv	8'9" v	10'3" v
9	7'1"	8'9"	10'3" v
11	7'1"	8'9"	10'3"

TABLE C.1 (continued)

Segment 70 South: Distance west from 71/70 joint

Duct No	Test A	Test B	Test C
12	7" v	2'9" v	4'9"
10	-	2'9" v	4'9" v
8	7"	2'9"	4'9" v
6	-	2'9" v	4'9" v
5	-	2'9" v	4'9"
7	7"	2'9"	4'9"
9	7"	2'9" v	4'9"
11	7"	2'9"	4'9"

Segment 69 South: Distance west from 70/69 joint

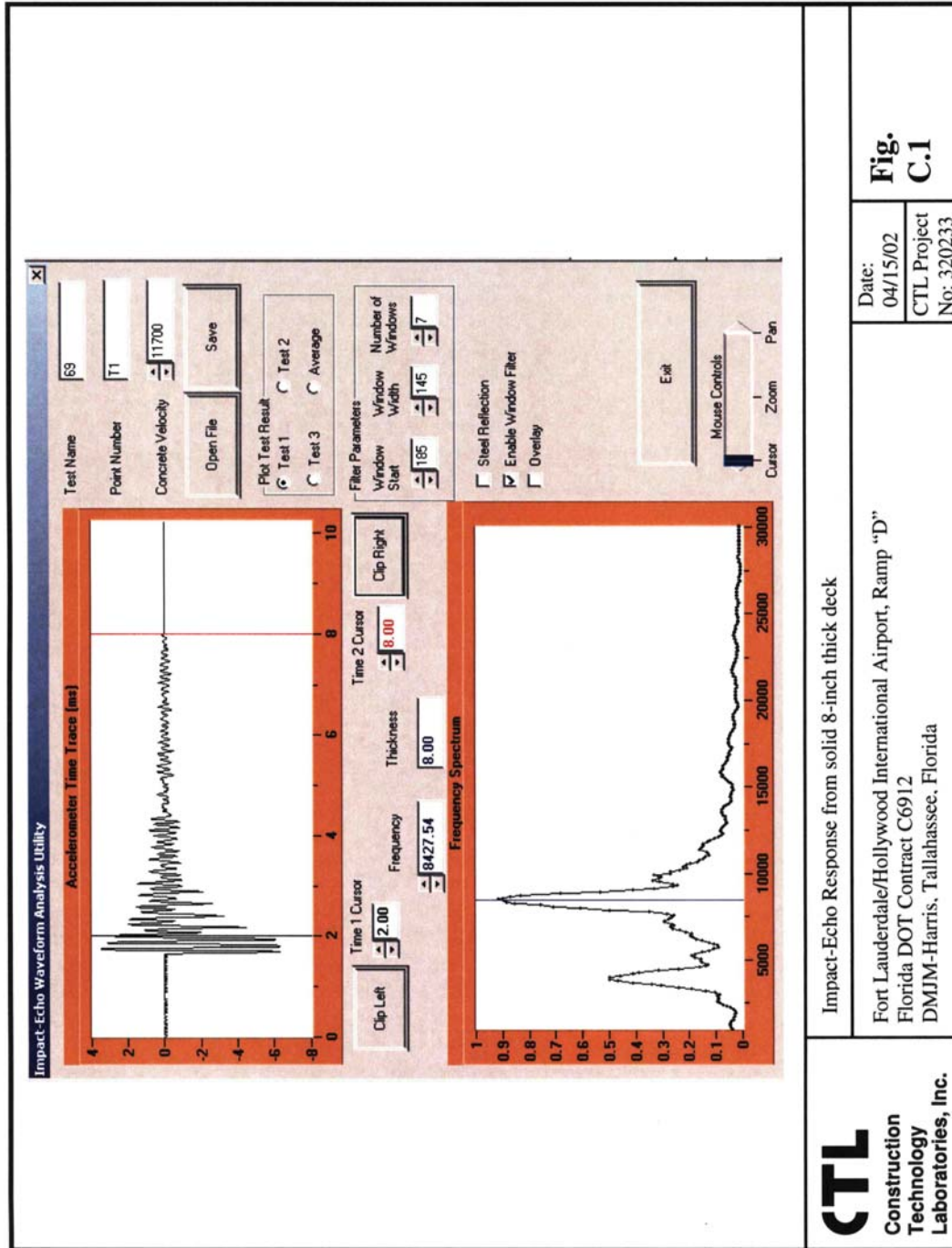
Duct No	Test A	Test B	Test C	Test D	Test E
12	10" v	2'2" v	-	5'4"	9'4"
10	10"	2'2"	-	5'4" sv	9'4" v
8	10" v	2'2" v	-	5'4" v	9'4"
6	10" v	2'2"	-	5'4" v	9'4"
4	-	2'2"	-	5'4" v	9'4"
3	-	2'2"	4'0"	5'4" sv	9'4" v
5	10"	2'2"	4'0"	5'4"	9'4"
7	10" v	2'2"	4'0" sv	5'4" v	9'4"
9	10"	2'2"	4'0"	5'4" v	9'4" sv
11	10"	2'2"	4'0" v	5'4"	9'4" sv

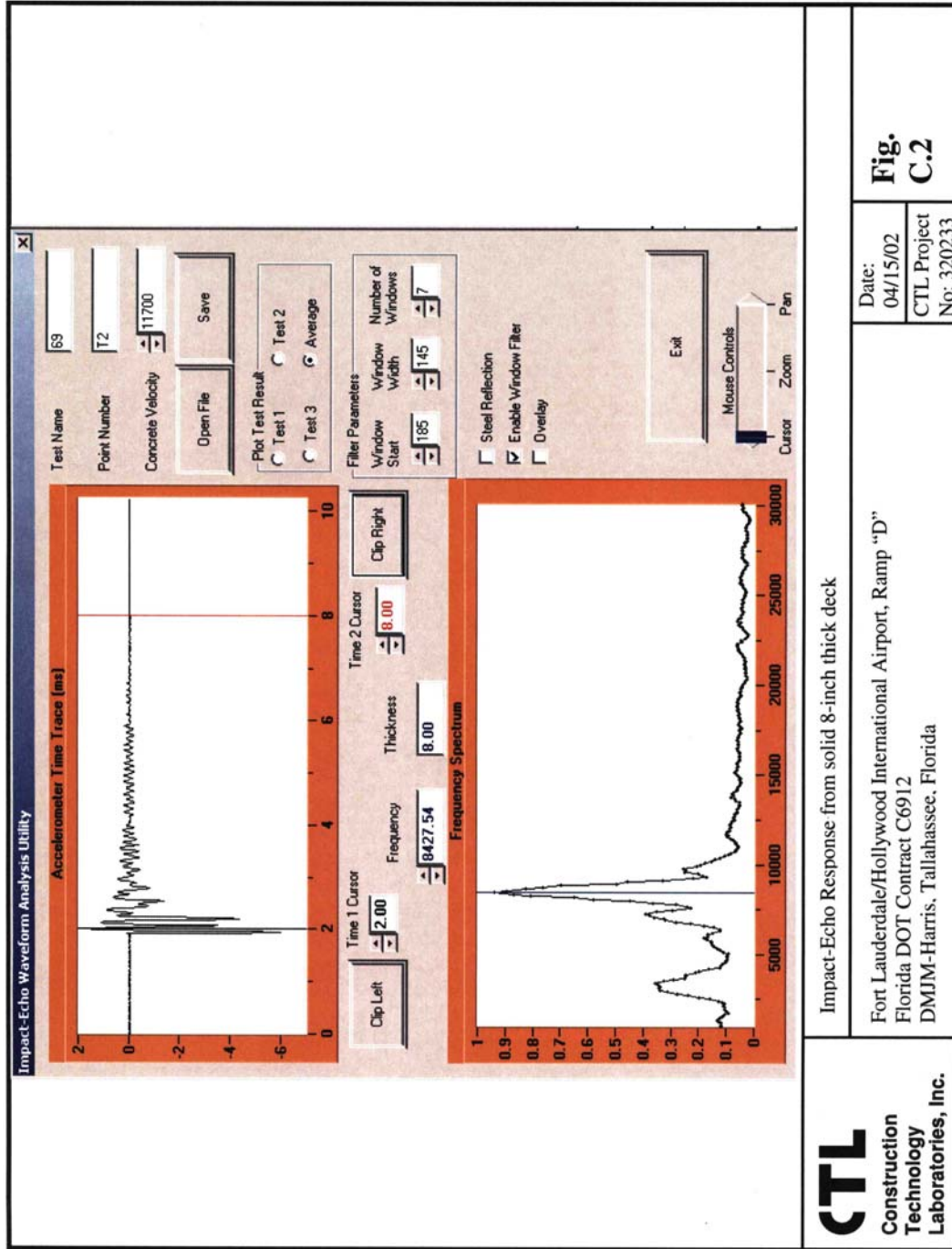
Segment 69 North: Distance west from 70/69 joint

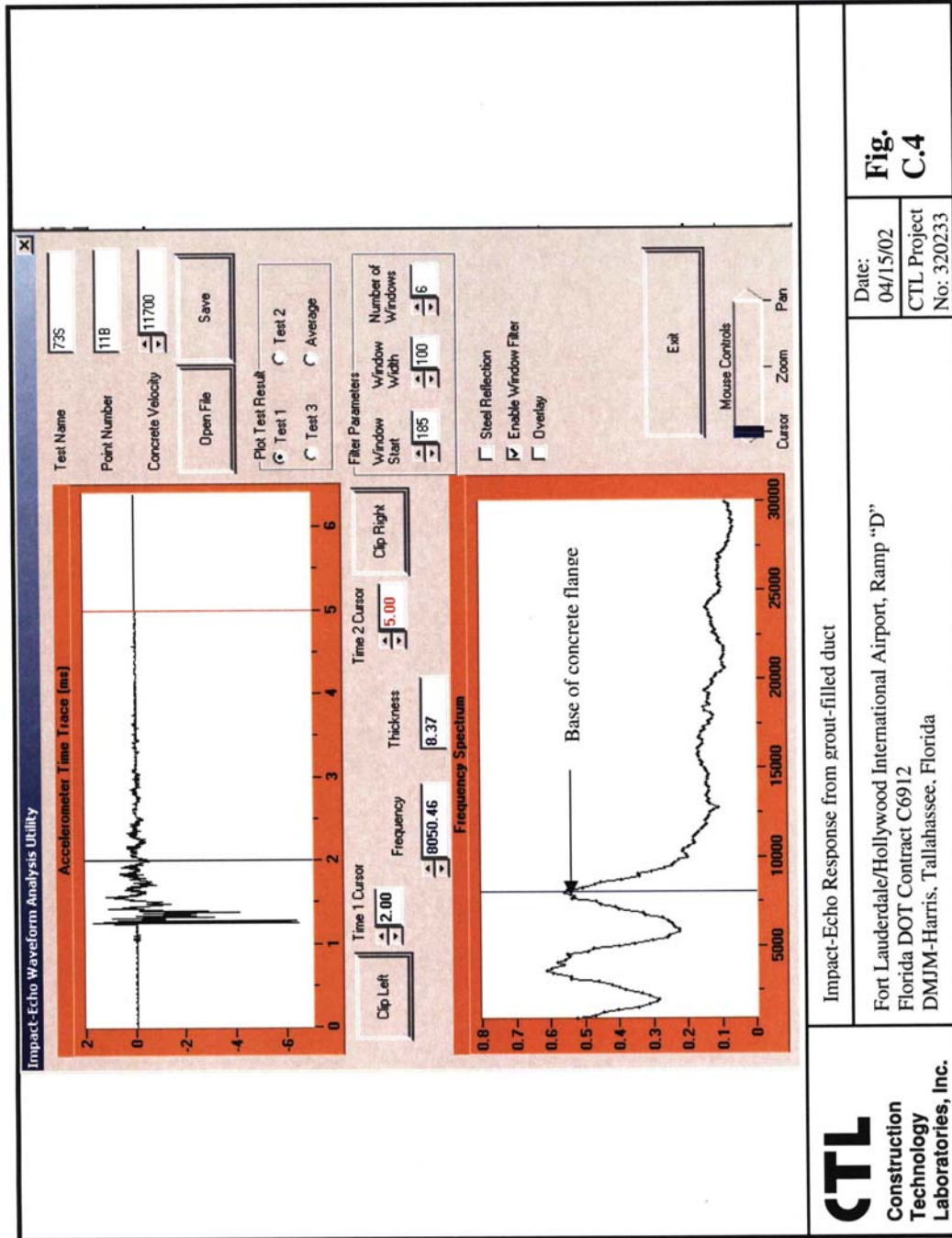
Duct No	Test A	Test B	Test C	Test D	Test E	Test F	Test G
T1 (thickness)	3" from edge						
6	-	-	-	-	6'0"	-	-
4	11"	3'5"	4'2"	5'0"	6'0" v	10'0" v	-
3	1'0"	3'6"	5'2"	6'4"	7'8"	8'10"	10'0"

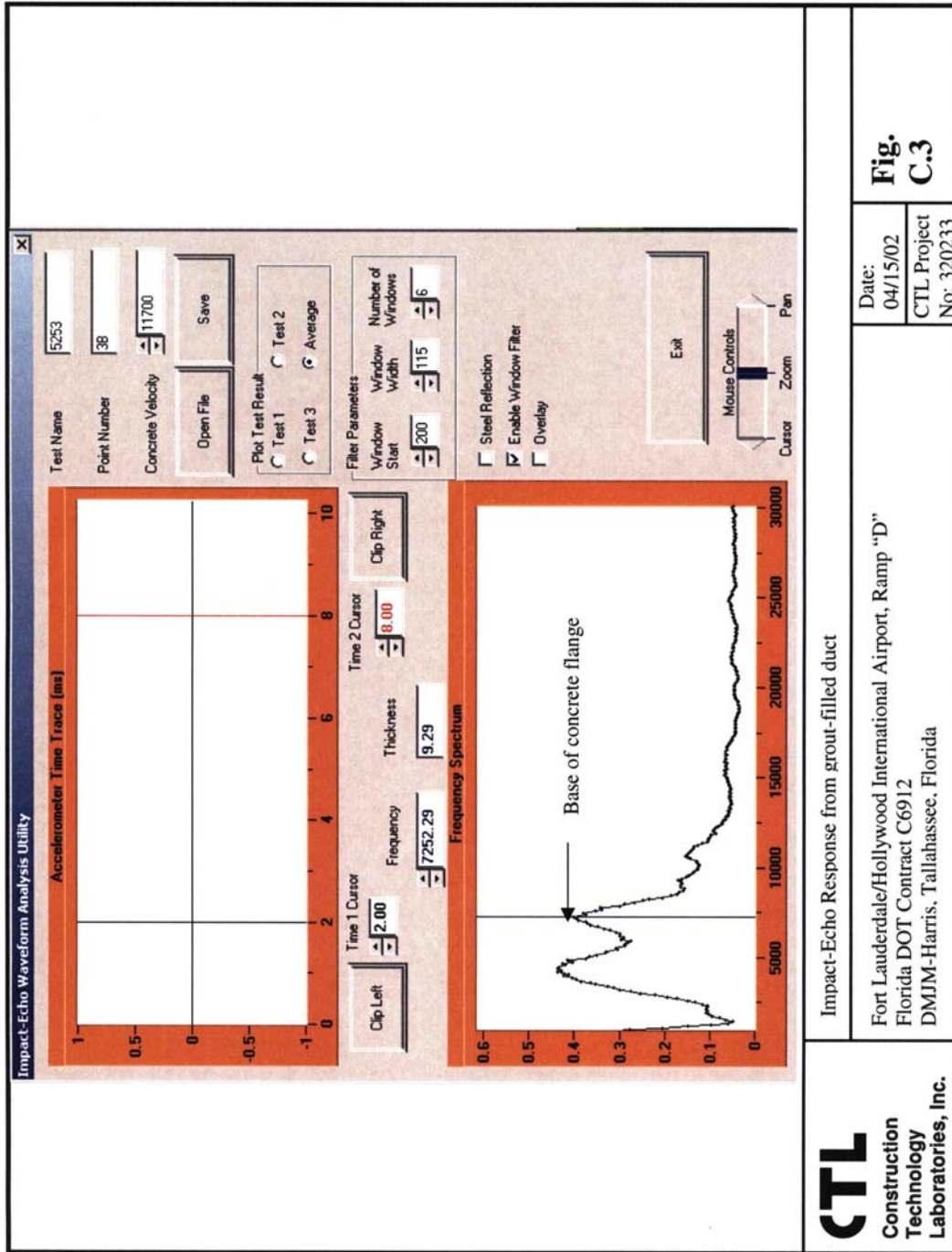
Table C.2

Test Box & I-E point	1st freq. (Hz)	2nd freq. (Hz)	3rd freq. (Hz)	4th freq. (Hz)	5th freq. (Hz)	Observations
Box 69N, T1	3930	8430				Calibration Test
Box 69N, T2	3530	8430				Calibration Test
Box 53N, 3B	4460	7250				Fully Grouted
Box 73S, 11B	3660	7980				Fully Grouted
Box 85S, 3C	3260	5990	11640	17630	25610	Void at 3.8"
Box 85S, 5A	3660	7120	12000	17300		Void at 3.9"
Box 79S, 13C	3730			20750		Void at 3.25"
Box 73S, 12B	3660	6720		17830		Small Void at 3.8"









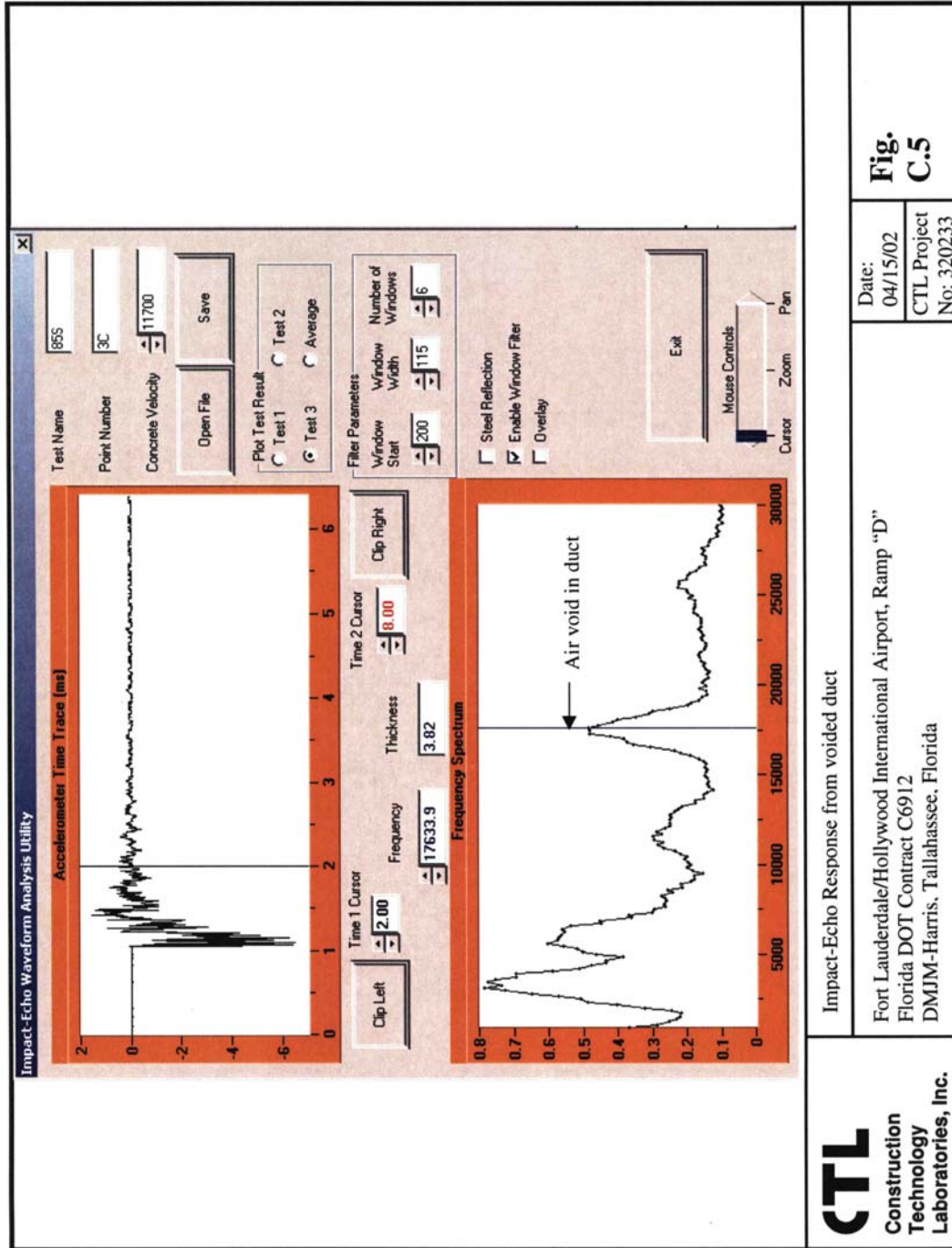
CTL
Construction
Technology
Laboratories, Inc.

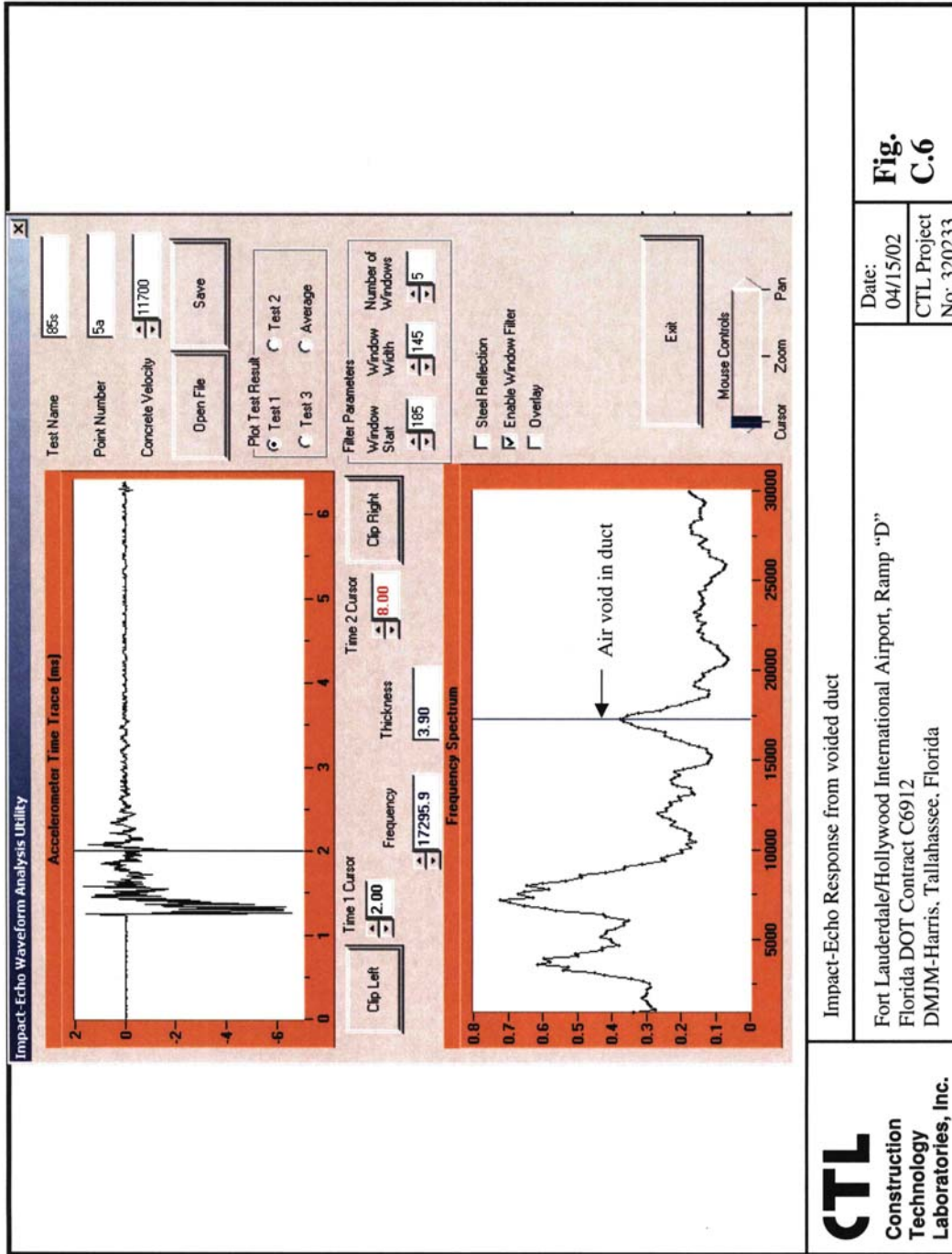
Impact-Echo Response from grout-filled duct

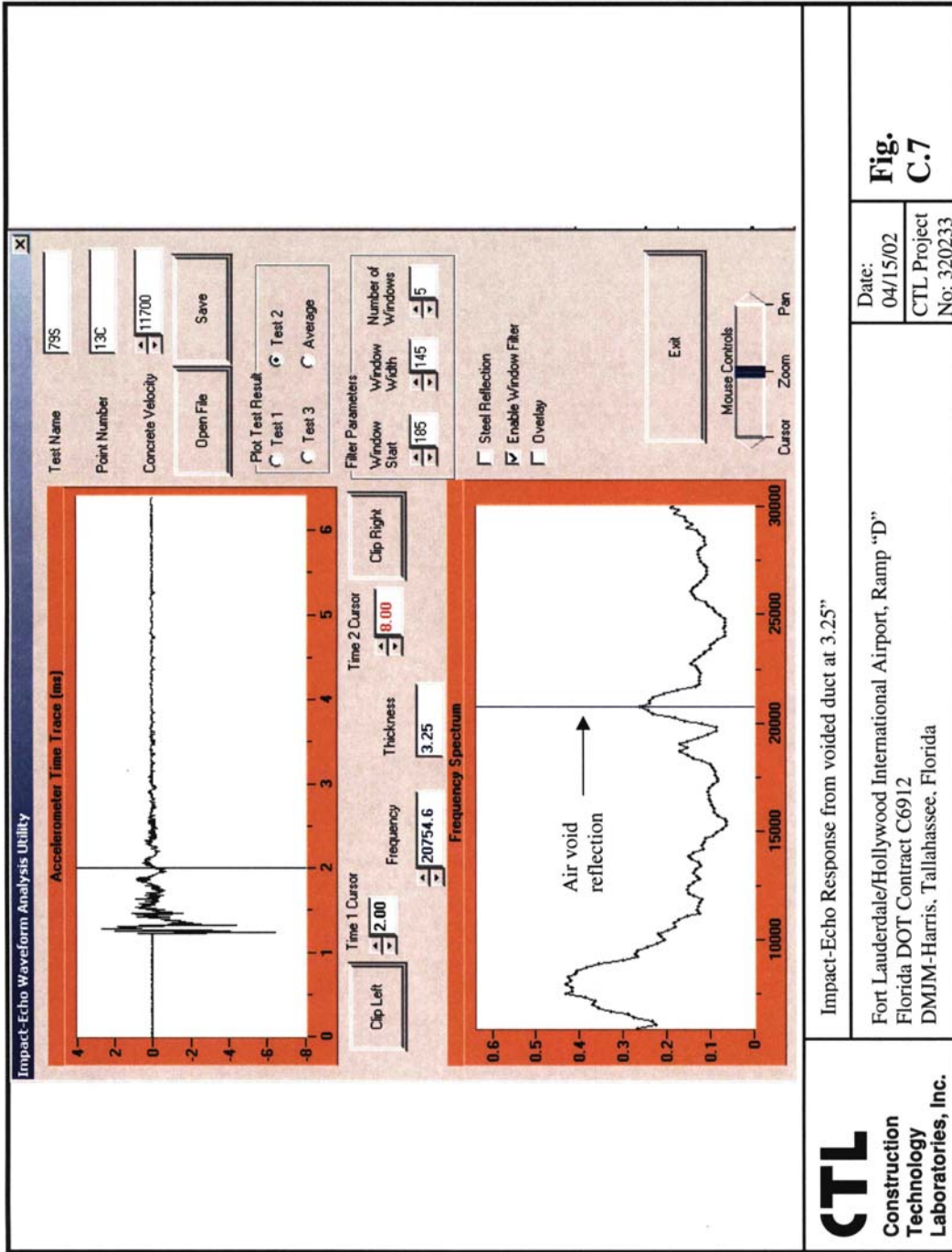
Fort Lauderdale/Hollywood International Airport, Ramp "D"
 Florida DOT Contract C6912
 DMJM-Harris, Tallahassee, Florida

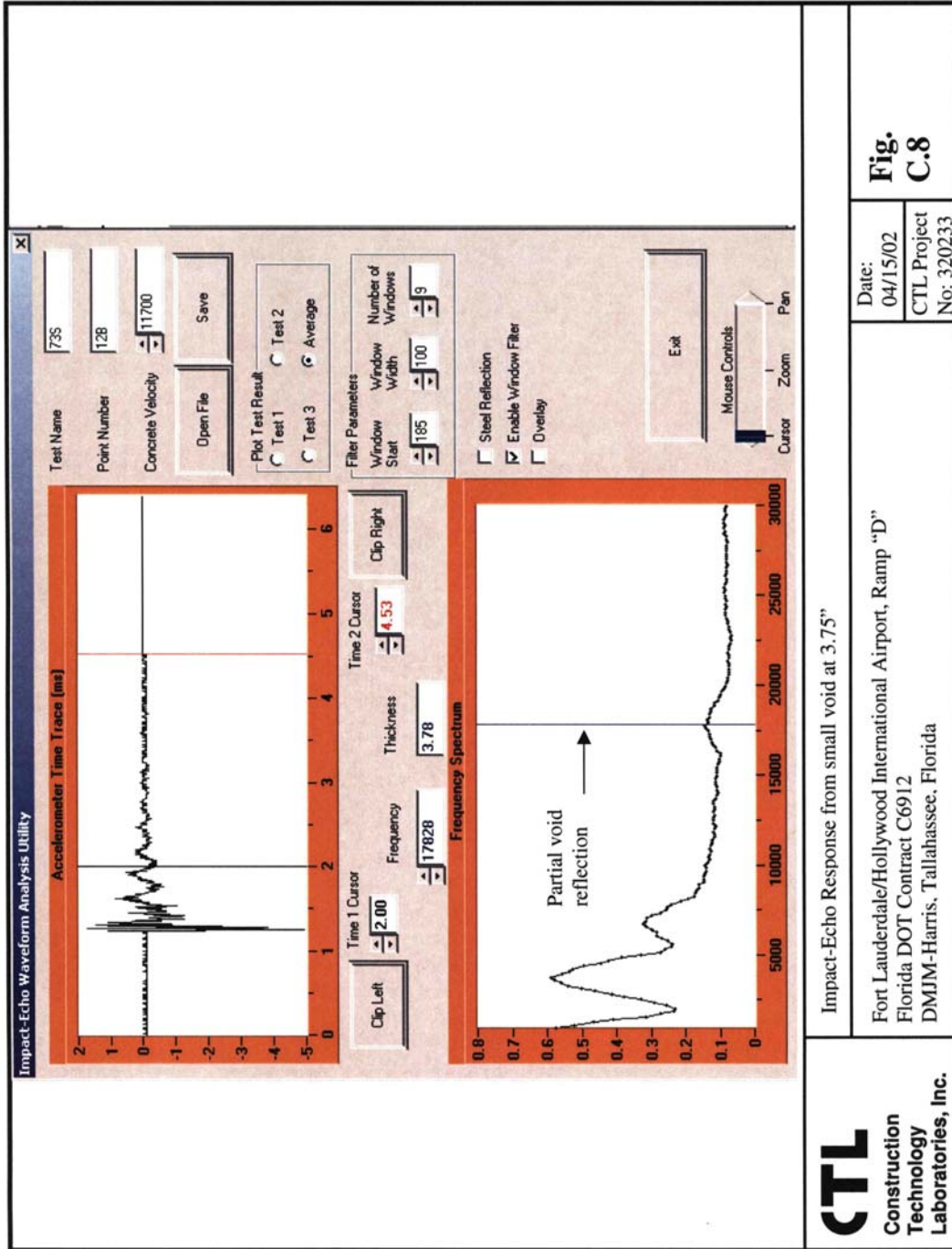
Date: 04/15/02
 CTL Project No: 320233

Fig. C.3










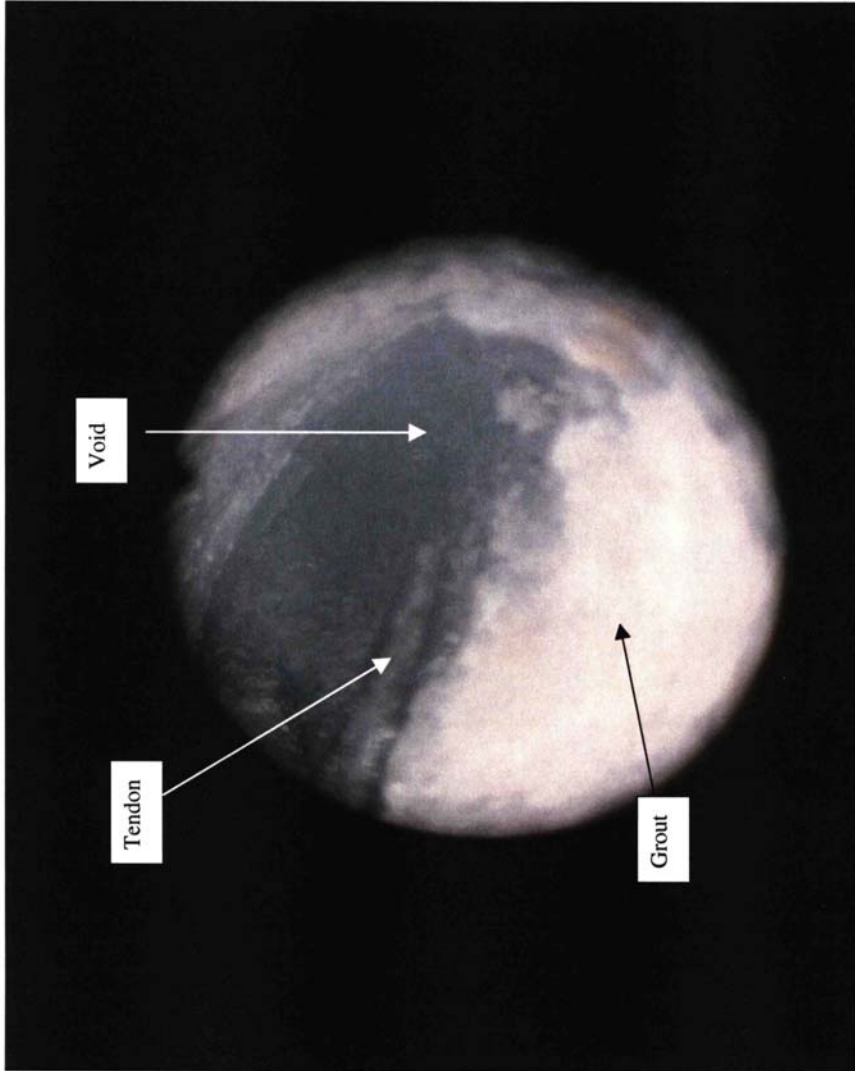

APPENDIX D

**CORROSION TEST RESULTS AND
BORESCOPE IMAGES, DUCT 4, BOX 69N**

Table D.1 Half-cell Potential Readings, Location 1, Box 64 North

Distance from Connecting Point (ft)	Half-Cell Potential (mV)
1	-114
2	-76
3	-45
4	-50
5	-35
6	-34
7	-41
8	-32
9	-57
10	-33
11	-49
12	-60
13	-46
14	-35
15	-29

	<p>Exposed tendon in voided duct, I-E test point 4D, Box 69 North Fort Lauderdale/Hollywood International Airport, Ramp "D" Florida DOT Contract C6912 DMJM-Harris, Tallahassee, Florida</p>	Date: 04/15/02	Fig. D.1
		CTL Project No: 320233	
			

	<p>Borescope Image of exposed tendon in voided duct, I-E test point 4D, Box 69 North</p>	Date: 04/15/02	Fig. D.2
		CTL Project No: 320233	
<p>Fort Lauderdale/Hollywood International Airport, Ramp "D" Florida DOT Contract C6912 DMJM-Harris, Tallahassee, Florida</p>			
			

Final Report

**MFL and IE Testing of Existing Ramp D, Ft. Lauderdale
International Airport Interchange**

by

Al Ghorbanpoor, P.E., Ph.D.
Consulting Engineer

May 2002

Final Report**MFL and IE Testing of Existing Ramp D, Ft. Lauderdale International Airport Interchange**

by

Al Ghorbanpoor, P.E., Ph.D.
Consulting Engineer**Introduction:**

Under a contract from DMJM+Harris, Inc., a non-destructive evaluation (NDE) of post-tensioning (P-T) tendons of the existing Ramp D Bridge located at the Fort Lauderdale International Airport Interchange, Fort Lauderdale, Florida, was made over the period of March 26 to 30, 2002. The NDE methods used in this work were based on the concept of magnetic flux leakage (MFL) and the Impact-Echo (IE) method. The NDE testing based on both the MFL and IE methods was conducted using equipment developed by Dr. Ghorbanpoor.

The existing Ramp D Bridge tested under this work is scheduled for removal since new replacement bridges have already been constructed. This provided a good opportunity for the Florida Department of Transportation (FLDOT) to secure the services of a consultant, DMJM+Harris, Inc., to coordinate a series of NDE experiments by this author and others to assess the capabilities and limitations of various test techniques relevant to condition assessment of the post-tensioning tendons of this bridge. The Ramp D Bridge consists of seven spans, each ranging from 87 feet to 145.5 feet in length. The NDE testing under this work was limited to the P-T tendons within the top concrete decks in spans 5, 6, and 7, that have span lengths of 125.8, 145.5, and 97.5 feet, respectively. The bridge is constructed of segmental concrete boxes that were post-tensioned with internal longitudinal and transverse tendons. The longitudinal post-tensioning tendons generally consisted of 12 – ½ inch diameter 270 K low relaxation strands that were placed inside of galvanized ducts with 2 and 5/8 inches diameter. The available structural drawings indicated that the deck thickness over the wing segments and between the webs of each box varied between 8 and 9 inches and the distance between the center of each duct and the top of the deck was 5.25 inches. Ten to fourteen longitudinal tendons were located in the deck and in the vicinity of each web of the segmental boxes. All longitudinal tendons were tapered (in pairs) at their ends towards the centerline of one of the two webs of the segmental boxes. Each tendon was anchored at each end at a larger depth within the thickened deck slab in the vicinity of the web. A typical layout of the tendons in one-half of the width of the bridge deck, as shown on available contract drawings, is shown in Figure 1.

Prior to conducting the MFL and IE tests, tendon locations were marked by others on top of the concrete decks for spans 5, 6, and 7. These locations were identified from either the results of ground penetration radar (GPR) tests or from the available information on existing contract drawings.

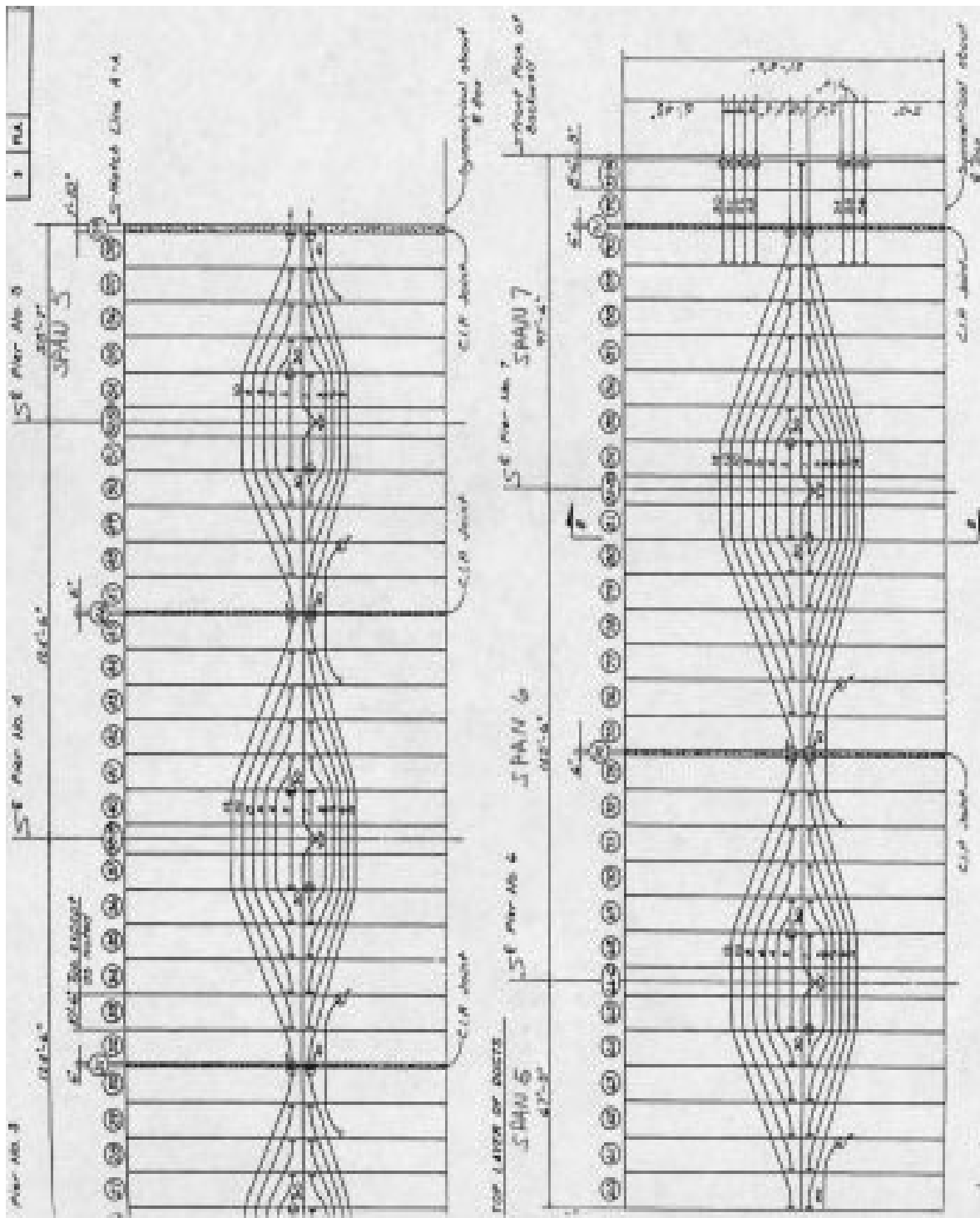


Figure 1 – Layout of post-tensioning tendons in the bridge decks for spans 5, 6, and 7 (one-half of the width)

A. Magnetic Flux Leakage (MFL) Testing:

By applying an external magnetic field to a ferromagnetic component, such as a post-tensioning tendon, a constant directional flow of magnetic flux will be introduced in the component. If the magnetic flux encounters a flaw such as a corroded region or fracture in the component, some or all of the flux will leak out of the component. This magnetic flux leakage is detected by a series of sensors that produce electrical voltage proportionate to the field amplitude at a specific location. The signals are analyzed to determine the extent or severity of the flaw that caused the magnetic flux leakage. This concept was recently used by the author to develop an equipment as well as an analysis capability to detect corrosion and fracture of prestressing steel strands in prestressed and post-tensioned concrete bridge members (Ref. 1).

Equipment Description - The equipment used for the field-testing of the P-T tendons in the Ramp D Bridge consists of a mechanical frame made of aluminum that supports a pair of strong permanent magnets and a series of Hall-Effect sensors. An encoder wheel is installed on the magnets/sensors assembly that rolls on the deck surface during the testing. Turning of the encoder wheel against the deck surface produces electrical pulses that are proportionate to the travel distance of the magnets/sensors assembly over the deck. By using the output of the encoder wheel, the precise position where the magnetic flux leakage occurs along the test subject can be determined. The magnets/sensors assembly has been fitted onto an aluminum push-cart that also supports a computer, a data acquisition unit, and a DC power source. Figure 2 shows a photograph of the MFL equipment as it is configured for testing internal P-T tendons in a bridge deck.



Figure 2 – Photograph of the MFL equipment as configured for testing internal P-T tendons in a bridge deck

The cart is rolled on its rubber wheels and along the tendon lines that are marked on the surface of the concrete deck. During each test, a constant distance of 0.25 inch is maintained between the magnets/sensors assembly and the concrete deck surface. This is accomplished through the use of a set of small contact wheels that are installed on the magnets/sensors assembly frame. Maintaining this constant distance is important since the amplitude of the MFL data is proportionate to the distance between the magnets/sensors assembly and the steel tendon within the deck. Data from four sensors is recorded and analyzed for the purpose of testing the P-T tendons in this work. The layout of the sensors in the system is shown in Figure 3. The sensors are positioned 1.0 inch on center in both horizontal and vertical directions.

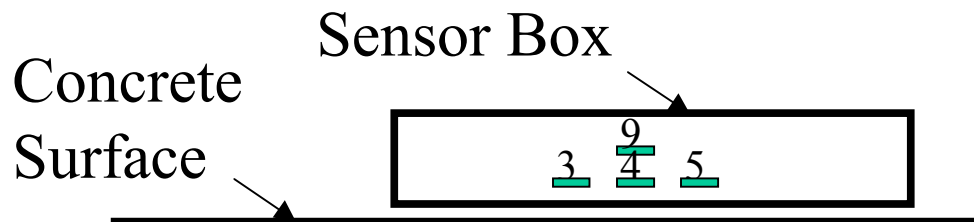


Figure 3 – Layout of Hall-Effect sensors in the MFL equipment

During each test, the operator attempts to guide the equipment so an alignment of sensors 4 and 9, located on the equipment's centerline, is maintained with the centerline of the tendon along its length. The output signals from these four sensors are displayed in the form of graphs of flux leakage amplitude vs. longitudinal travel distance of the magnets/sensors assembly from the starting point of the test. Data calibration based on the results of extensive previously performed laboratory investigations and the operator's experience are generally used to identify MFL indications that are produced from the presence of flaws vs. those from the effects of normal reinforcing steel components and other steel elements that are routinely used in concrete structural members. To facilitate data recording, displaying, and interpretation, a set of data acquisition and analysis software is developed and used in conjunction with the MFL equipment.

Laboratory Study - A brief laboratory study was conducted prior to the required field tests for this work to examine MFL data from partial fracture in a tendon similar to those present in the Ramp D Bridge. Figure 4a shows typical MFL amplitude graphs from the four sensors of the equipment for a test conducted on an 8-foot long P-T tendon without flaws in the laboratory. Similar to the longitudinal tendons of the Ramp D Bridge, the laboratory tendon has 12 one-half inch diameter seven-wire strands. The tendon was positioned at a distance of 5.5 inches from the test surface. Transverse # 4 reinforcing steel bars were installed at 2 inches below the test surface and at a spacing of 17 inches on center. The frequently repeated indications with large amplitudes in the output of each sensor, as shown in the figure, are from the effects of transverse reinforcing steel bars that are located closer to the test surface (at 2.0 inches).

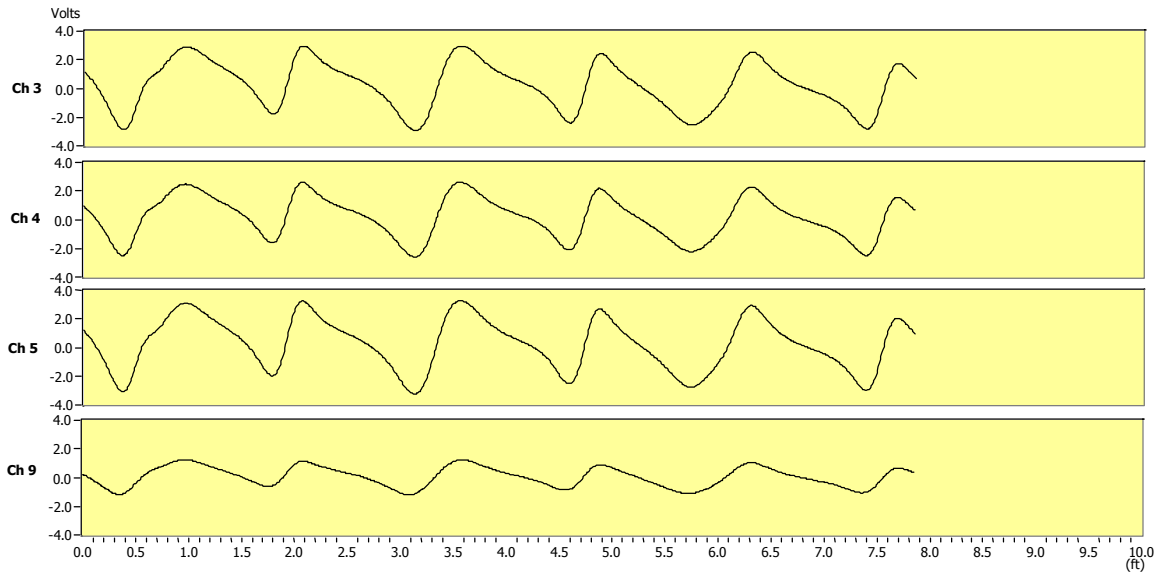


Figure 4a - Typical MFL data (four sensors) for an 8-ft long tendon without flaws

Figure 4b shows a display of MFL data for the same tendon as shown for Figure 4a but after a total of four strands in the tendon were cut (a 33% loss of cross sectional area of the tendon). The cut is at a distance of 2.75 feet from the starting point of the MFL test.

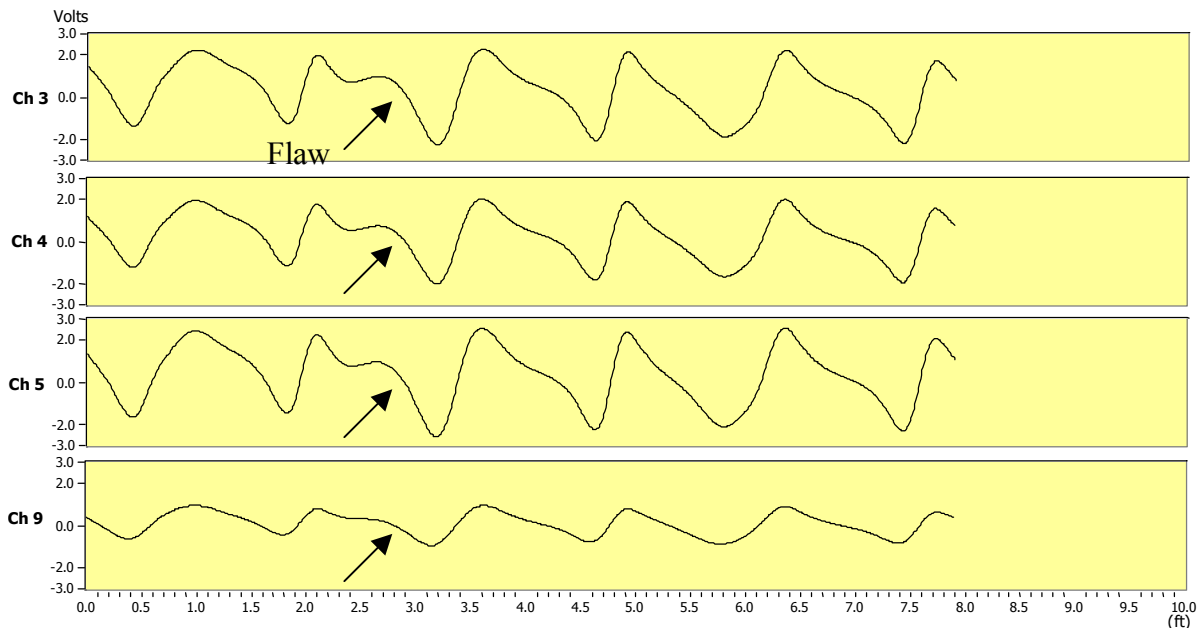


Figure 4b – MFL data for the 8-ft long tendon of Figure 4a but with a 33% loss of cross sectional area of the tendon at 2.75 feet from the starting point of the test

Distinct indications of the loss of the cross sectional area in the tendon can be seen in the graphs of Figure 4b at the specified location. The effect of the presence of the flaw can be easily noticed if a comparative evaluation of the data from the two figures is

performed. A point-by-point subtraction of the data from two tests is the most effective and reliable way that flaws can be detected in real structures with many reinforcing steel elements. When MFL data is available from only one test, the data must be examined with a goal of finding special features that could be associated with flaws. One feature of MFL data for a localized defect, such as a cut in a tendon, is that the signal amplitudes from different sensors are proportionate to their distance from the flaw. For example, sensors that are located closer to the flaw will produce larger amplitudes in comparison with the ones that are located farther. The presence of transverse bars and tendons can be easily distinguished by recognizing that signal amplitudes for all sensors (except sensor # 9) are the same since the sensors are positioned at the same distance from the bar or tendon.

The effectiveness of the MFL system for detection of flaws in P-T tendons is reduced as the tendon is located deeper in the concrete. Figure 4c shows MFL data from laboratory tests (only from one sensor) for the same tendon of Figures 4a and 4b with the addition of the data for the tendon when it is located at a depth of 8 inches (instead of 5.5 inches) from the test surface. As it can be seen from the figure, the distinct indication of the presence of the flaw is not noticeable as clearly for the tendon when it is located at the deeper position.

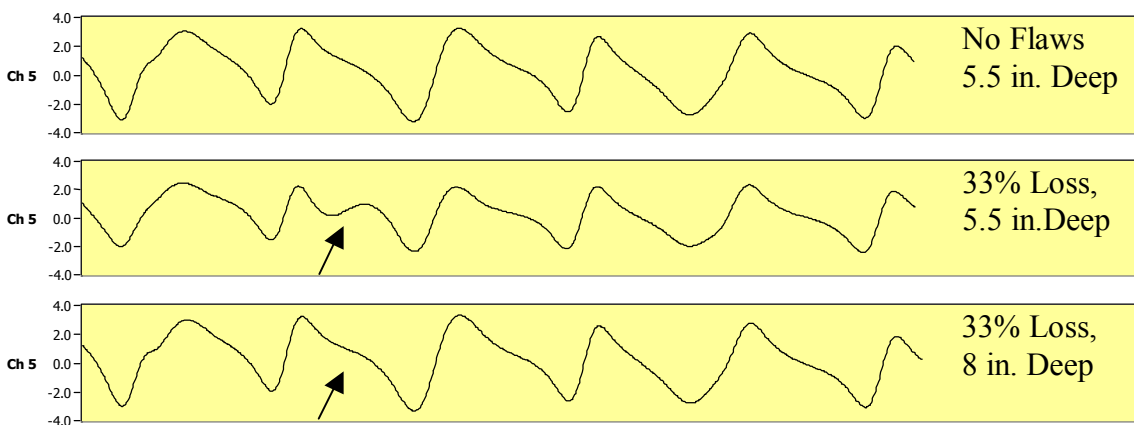


Figure 4c – MFL data from one sensor (Ch. 5) for the 8-ft long tendon for three conditions, no flaws (5.5” deep), 33% loss (5.5” deep), and 33% loss (8” deep)

All ferromagnetic components embedded in a concrete member affect the state of an induced magnetic field in the close vicinity of those components. Therefore, the interpretation of the MFL data could become difficult when numerous ferromagnetic components are present near the test surface and when there is no regularity in the positions of these elements within concrete. In such cases, the most effective and reliable data interpretation is achieved by performing a comparative analysis of data from two or more tests that are performed at different times. This analysis technique will allow reliable detection of any deterioration of steel within concrete for the period between the times the two tests were performed. A point by point digital subtraction of the recorded

data from the two tests would allow a reliable identification of small changes, due to corrosion or fracture, in P-T tendons within concrete.

Field Testing – The primary objective of this work was to demonstrate the applicability of the magnetic flux leakage concept in detecting corrosion and fracture of post-tensioning tendons within the concrete deck of the Ramp D Bridge at the Fort Lauderdale International Airport Interchange. Prior to the field testing, communications were made with the consultant, DMJM+Harris, Inc., to state the expected capabilities and limitations of the current MFL system for this application. It was stressed that the existing MFL system was designed to be effective for application to structural members such as external P-T tendons and prestressed bridge I-beams, where flaw detection in the steel located close to the magnets or to the test surface was intended. It was agreed by the author to modify the mechanical support components of the existing MFL equipment to allow application to bridge decks. Results from past laboratory and field studies have shown that defects as small as 0.3% of loss of the cross sectional area of an external post-tensioning tendon could be detected by the MFL system (Ref. 2).

The concept of the magnetic flux leakage evaluation of P-T tendons is based on saturating a steel tendon with a DC magnetic field and monitoring any changes in the magnetic field near the tendon due to fracture or corrosion of the tendon. The intensity of the magnetic field is reduced significantly (approximately to the power of 3) at larger distances from the test surface or the face of the magnet. Since the existing structural drawings for the Ramp D Bridge indicated that the centroid of each P-T tendon in the bridge deck is generally located at a distance of 5.25 inches or deeper from the deck surface, it was concluded that only major flaws (major cuts in the strands) could be detected with an acceptable degree of certainty when using the existing MFL system. Detection of smaller flaws could have been possible but the existing magnets in the system would have needed to be replaced by stronger magnets to allow magnetic saturation of the tendons at the larger distance from the magnets. As a part of this study, no modifications to the magnets were made since it was outside the scope and budget of the work. Limited laboratory tests were, however, performed prior to the field testing to determine the smallest loss of cross sectional area of a tendon similar to those in the bridge. Using the existing MFL system, it was found that a loss of cross sectional area equivalent to 33% or greater could be detected in P-T tendons under conditions similar to those for the Ramp D Bridge.

It was agreed by the consultant, DMJM+Harris, Inc., that the locations of all P-T tendons intended for the MFL testing would be identified accurately and marked on the bridge deck by other professionals prior to initiating the MFL testing. Accordingly, tendon locations were marked on the deck in spans 5, 6, and 7. Locations of some of the tendons were determined through using the ground penetrating radar (GPR) technique and the remaining tendons were located and marked on the deck based on the available information on the contract documents. It is important to note that a successful MFL test requires that all P-T tendons are accurately located and marked on the deck before the start of the test. Inaccurate determination of a tendon's location can cause larger distances between the magnets/sensors and the tendon that results in reduction of the

magnetic flux in the tendon and an increase in interferences from other ferromagnetic components in the deck. These adverse effects produce a diminishing of the magnetic responses from flaws or fracture in the tendon and make the flaw detection more difficult.

A total of 52 P-T tendons in the bridge deck of spans 5, 6, and 7 were tested during the MFL field investigation period. The length of each tendon varied from approximately 30 feet to 150 feet. The starting point of each test was either at the anchored end of the tendon or at the centerline of a pier was at is located at the half-length of the tendon. Testing for each tendon started from the West end of the tendon. For each test, the MFL equipment was positioned in such a way that the midpoint between the two magnets was aligned with the anchored end of the tendon as marked on the bridge deck. During each test, MFL data for each test was displayed on the computer screen and it was monitored by the operator. At the conclusion of each test the MFL data was stored in the computer for post-processing and analysis.

As indicated on the existing contract drawings, each tendon is gradually turned downward (deeper into the concrete) at its ends and it is anchored by heavy anchor plates at a depth of 8 inches or greater from the deck surface. Due to this additional depth of the tendons within the deck, a significant reduction of the magnetic flux intensity within the tendon resulted and therefore no conclusive indications could be observed for the presence of any flaws at the end of the tendon. An example of typical signals from the four sensors of the MFL system is shown in Figure 5 for tendon # 4 located between segments 80 and 85 on the left (North) side of the bridge.

As it is shown in the figure, MFL signals for the entire 50 feet length of the tendon are presented. High amplitude indications are usually present at the start and end points as well as at the joints between each two adjoining segments. These indications are due to the effects of heavy steel anchor plates at the tendon's ends and due to additional reinforcing steel at the joints between each two adjoining segments. Other frequently repeated MFL indications are from the effects of transverse reinforcing steel and transverse post-tensioning tendons. It is important to have a knowledge of locations or spacing of the existing reinforcing steel, post-tensioning steel and any other ferromagnetic elements such as end anchor plates, hold down devices, etc., in order to be able to interpret the MFL data in concrete structures. A majority of the MFL indications in the data shown in Figure 5 may be associated with the transverse reinforcing and post-tensioning steel at the approximate spacing distances that are specified on the existing contract drawings for the bridge. The data in Figure 5 is displayed in a compressed form for the entire length of the tendon (50 feet). Such displays make it more difficult to identify small changes in the magnetic field that could be related to flaws in steel. Normally, MFL data for a 10-foot length is displayed within the same frame as shown in Figure 5.

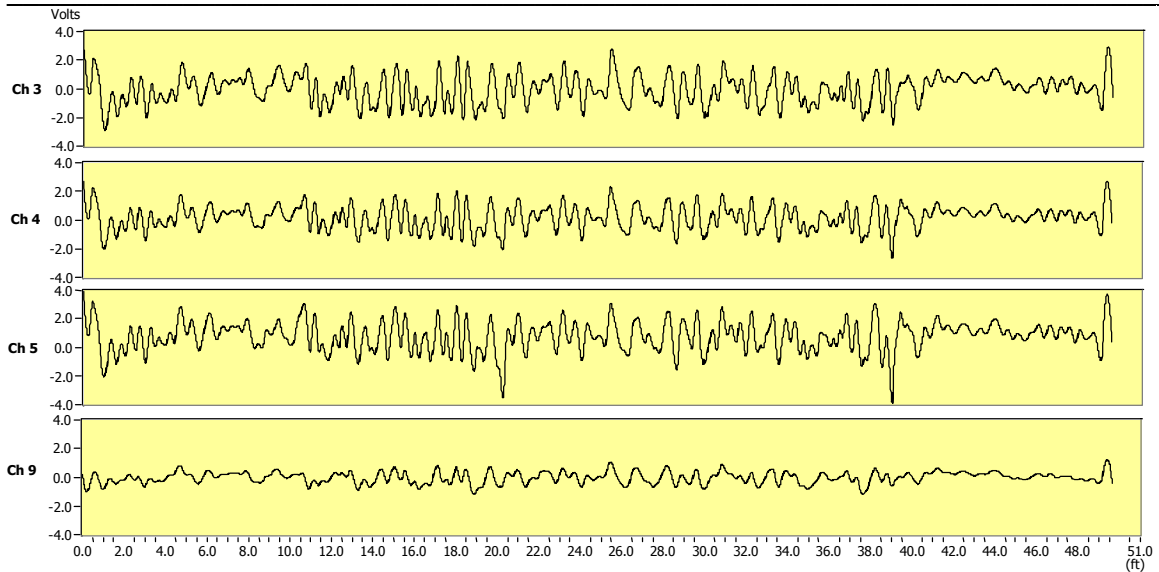


Figure 5 – MFL signals (4 channels) for tendon # 4 between segments 80 and 85

The MFL data for the first 10 feet of the tendon is shown in Figure 6. When data from each sensor is considered in Figure 6, one can easily determine that the spacing between the transverse reinforcing steel is about 7 inches on center. The signal amplitude from the effect of each transverse reinforcing steel varies depending on either the depth the steel is placed within the concrete deck or the extent of the offset of the moving MFL equipment from the centerline of the tendon during the test.

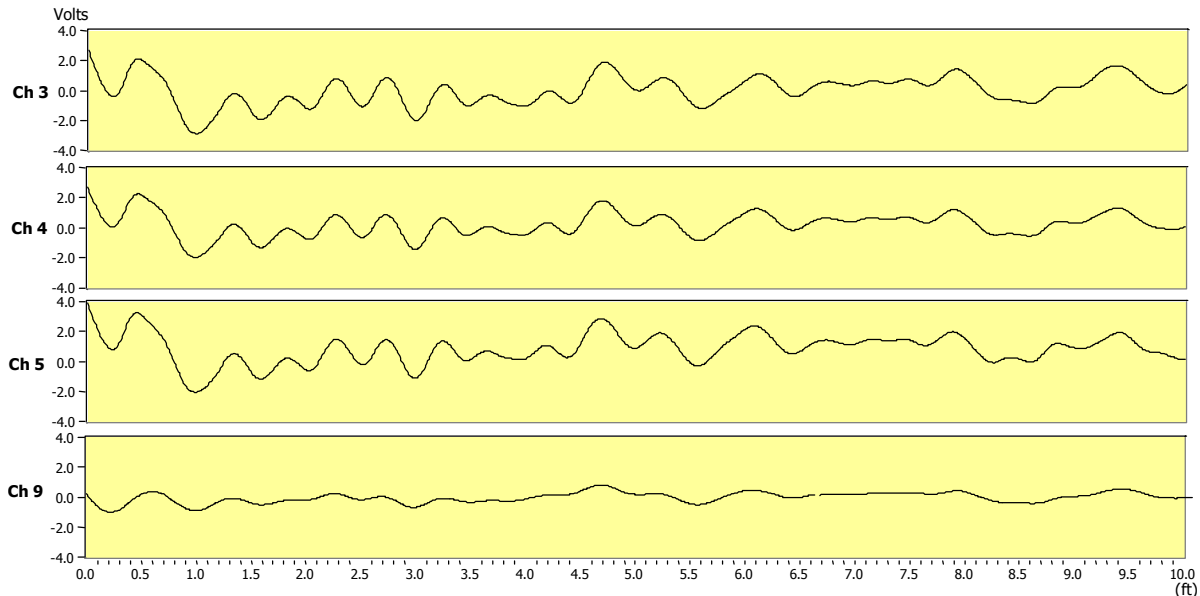


Figure 6 - MFL signals (4 channels) for tendon # 4 between segments 80 and 85 (First 10 feet of the tendon)

An overall evaluation of the MFL data recorded for the tendons of the Ramp D Bridge did not reveal any obvious indications for the presence of any major flaws (such as large cuts in excess of 33% of the cross sectional area of the total strands in each tendon). Since the tendons in the Ramp D Bridge were located relatively too deep within the concrete deck (5.25 inches from the deck surface), only large flaws were expected to be detected with the existing MFL system. After the completion of the MFL field tests, the consultant revealed to the author that several man-made flaws had been cut into the tendons to allow an evaluation of the capabilities of different NDE methods for the purpose of condition assessment of the tendons. These flaws had been introduced into some of the tendons prior to the initiation of the MFL and impact-echo tests. It was indicated that the man-made flaw sizes ranged from 5% to 25% of the cross sectional area of the tendons. As it was communicated to the consultant prior to the start of the MFL tests at the bridge site, only flaws with sizes larger than 33% of the cross sectional area of each tendon were expected to be detectable by the existing MFL system and under the existing field conditions. However, the consultant requested a comparative analysis of the recorded MFL data to be conducted for several pairs of tendons, where in each pair there was one tendon with and one without man-made flaws. The objective was to demonstrate that the tendon with the man-made flaws could be identified. The consultant identified several pairs of tendons at different locations for the comparative analysis. Only the consultant had the knowledge of the condition of each specific tendon in each pair. The pairs of tendons and their relevant locations that were identified as candidates for the comparative study were:

- 1) Tendons 11 and 12 on the right hand side (South) of the bridge and at the up station (East) edge of segment 89 (trumpet location)
- 2) Tendons 9 and 10 on the left hand side (North) of the bridge and at the up station edge of segment 88 (trumpet location)
- 3) Tendons 11 and 12 on the right hand side of the bridge and at the down station (West) edge of segment 76 (trumpet location)
- 4) Tendons 7 and 9 on the left hand side of the bridge and at the up station edge of segment 56 (duct location)
- 5) Tendons 7 and 9 on the left hand side of the bridge and at the up station edge of segment 86 (duct location)
- 6) Tendons 11 and 13 on the left hand side of the bridge and at the up station edge of segment 86 (duct location)
- 7) Tendons 11 and 13 on the left hand side of the bridge and at the down station edge of segment 79 (duct location)
- 8) Tendons 13 and 14 on the left hand side of the bridge and at the down station edge of segment 76 (duct location).

After reviewing and analyzing the recorded MFL data and as it was expected, it was concluded that no reliable MFL data interpretation could be made for the tendons included in the first three cases as shown above (where man-made flaws have been cut into the trumpet region of the tendons). The tendons in the trumpet regions are located

too deep into the concrete (at 8 inches or greater from the surface of the concrete deck) and a magnetic flux saturation of the tendons could not be achieved with the existing magnets to allow a reliable detection of tendon flaws with the specified sizes. In addition, no MFL test was scheduled by the consultant to be conducted in segment 56 for tendons 7 and 9 (item # 4 above) and, therefore, no data was available to use for the analysis. Recorded MFL data for the various pairs of tendons identified in items 5 to 8 above were analyzed and the findings are reported below. No opportunities for any physical or communicative verification of the findings reported here were available to the author. The consultant, DMJM+Harris, Inc., is expected to conduct a verification study for all of the NDE tests, including the MFL and IE tests, performed at the Ramp D Bridge. The results of the consultant's verification study will be made available in a future report.

Data from the MFL tests conducted for tendons 7 and 9 (item # 5 above) at segment 86 are presented in Figures 7 and 8, respectively. The data is shown for only a 10-ft length of the tendon in the vicinity of a possible man-made flaw located approximately at the joint between segments 86 and 87. As shown in the figures, the MFL data for both tendons is displayed for the 10-foot length beginning at a distance of 30 feet from the starting point of the test. For these tendons, the starting point of each test was at the centerline of Pier No. 7. An examination of the MFL data for the two tendons showed indications for the possible presence of flaws in tendon # 7 at approximately 35 feet from the starting point of the test. These flaw indications have been identified by arrow markers shown in Figure 7. A variation of the signal amplitudes for outputs of sensors 3, 4, and 5 can be seen in Figure 7 that suggests the presence of a flaw at specified point. This signal amplitude pattern is similar to that observed in the laboratory tests, see Figure 4b. An examination of the MFL data shown in Figure 8 reveals that a pattern associated with a flaw can not be found here. In spite of the flaw indications in Figure 7, one should consider other influencing factors before a conclusion can be made concerning the presence of flaws in these P-T tendons. For example, it must be noted that at the indicated location, tendon # 7 is located near the vicinity of the end anchor plate for tendon # 5. The end anchor plates are relatively heavy steel plates and their presence in close distances can produce signals that could make the data interpretation more difficult. As a result, flaw indication for tendon # 7 should be treated only as a strong possibility. However, there exists a flaw related signal pattern here since a local flaw is normally positioned at different distances from the three sensors. Therefore, the resulting signal amplitude from each sensor varies proportionately related to the distance of each sensor to the flaw.

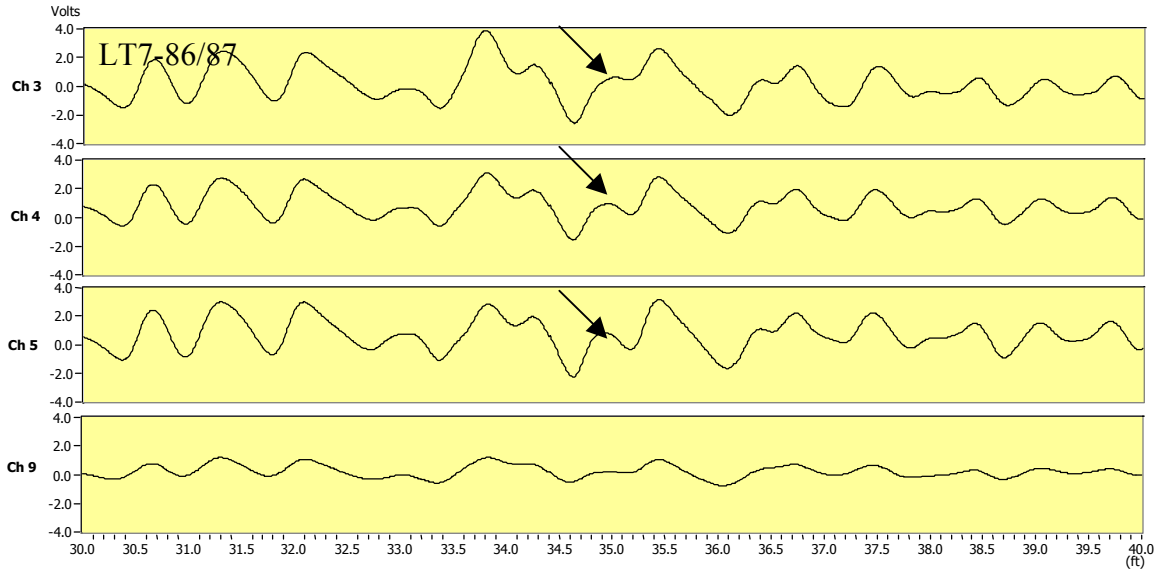


Figure 7 - MFL signals (4 channels) for tendon # 7 between segments 86 and 87 (data for 5 feet of the tendons on both sides of the joint between segments 86 and 87)

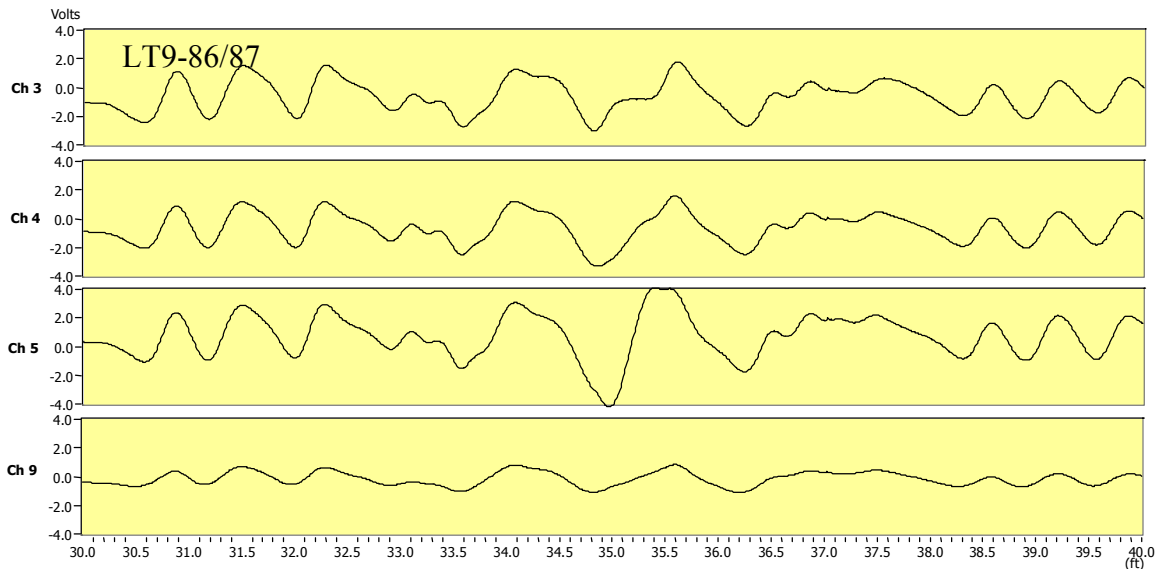


Figure 8 - MFL signals (4 channels) for tendon # 9 between segments 86 and 87 (data for 5 feet of the tendon on both sides of the joint between segments 86 and 87)

Results of the MFL field tests for tendons 11 and 13 (item 6 above) at segment 86 are shown in Figures 9 and 10, respectively. Again, the test results for both tendons are displayed for a 10-foot length beginning at a distance of 30 feet from the starting point of the test. For these tendons, the starting point of each test was also at the centerline of Pier No. 7. A review of the MFL data for the two tendons showed indications for the presence of flaws in tendon # 11 at approximately 35.5 feet from the starting point of the test.

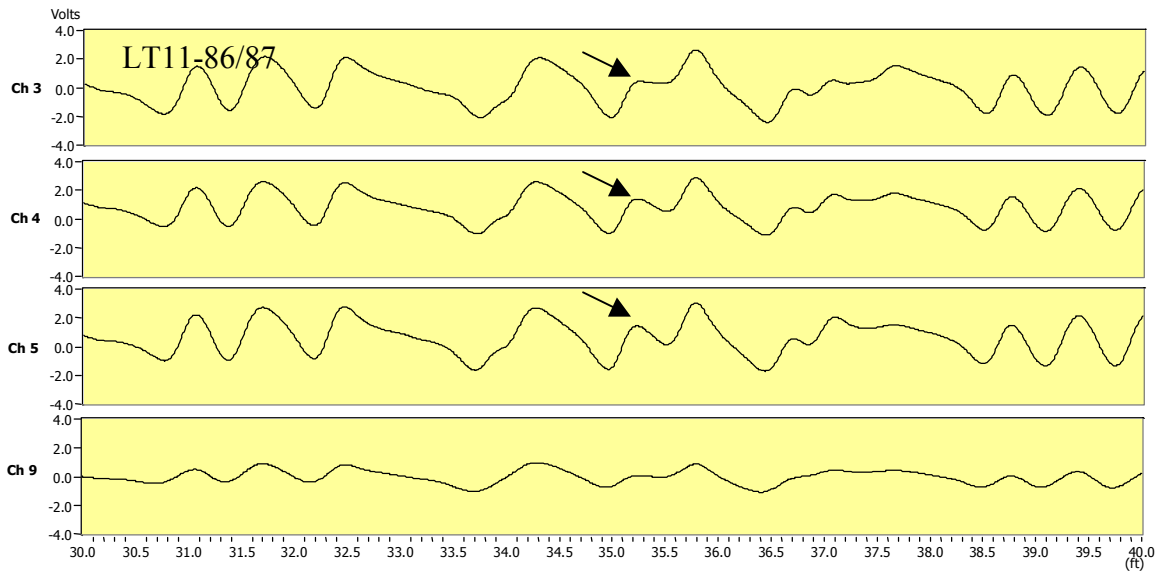


Figure 9 - MFL signals (4 channels) for tendon # 11 between segments 86 and 87 (data for 5 feet of the tendon on both sides of the joint between segments 86 and 87)

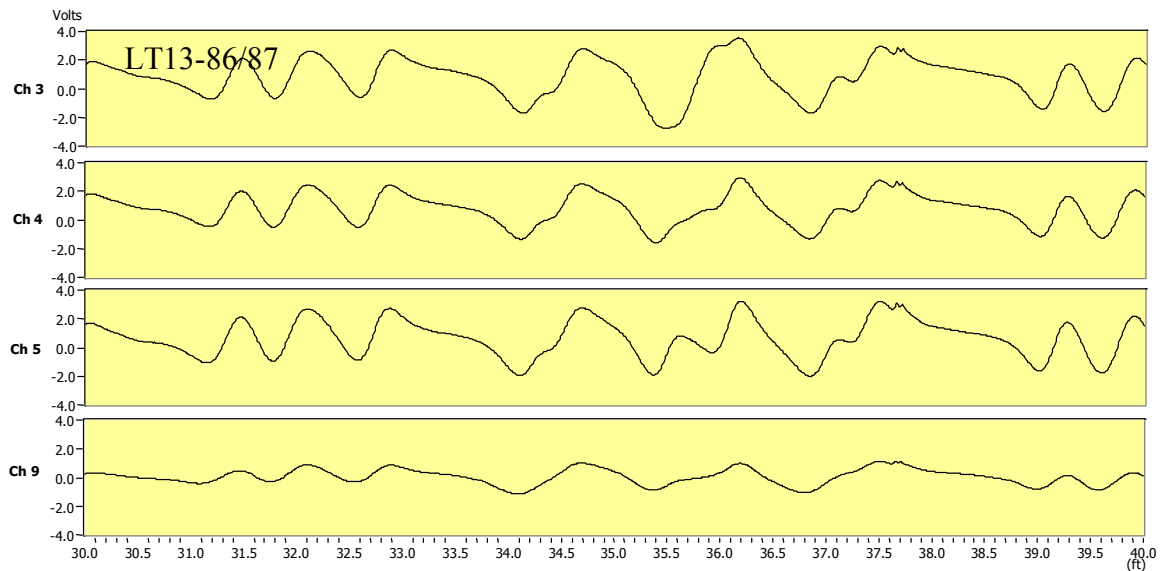


Figure 10 - MFL signals (4 channels) for tendon # 13 between segments 86 and 87 (data for 5 feet of the tendon on both sides of the joint between segments 86 and 87)

Figures 11 and 12 show the results of field tests for tendons 11 and 13, respectively, at segment 79 (item 7 above). Again, the data display is for a length of 10 feet for each tendon. The displayed data in each one of the two figures is for a five-foot tendon length on each side of the joint between segments 78 and 79. Flaw indications are shown in Figure 12 for tendon #13 at the specified location (41.5 feet from the starting point of the test or the West end of tendon # 13).

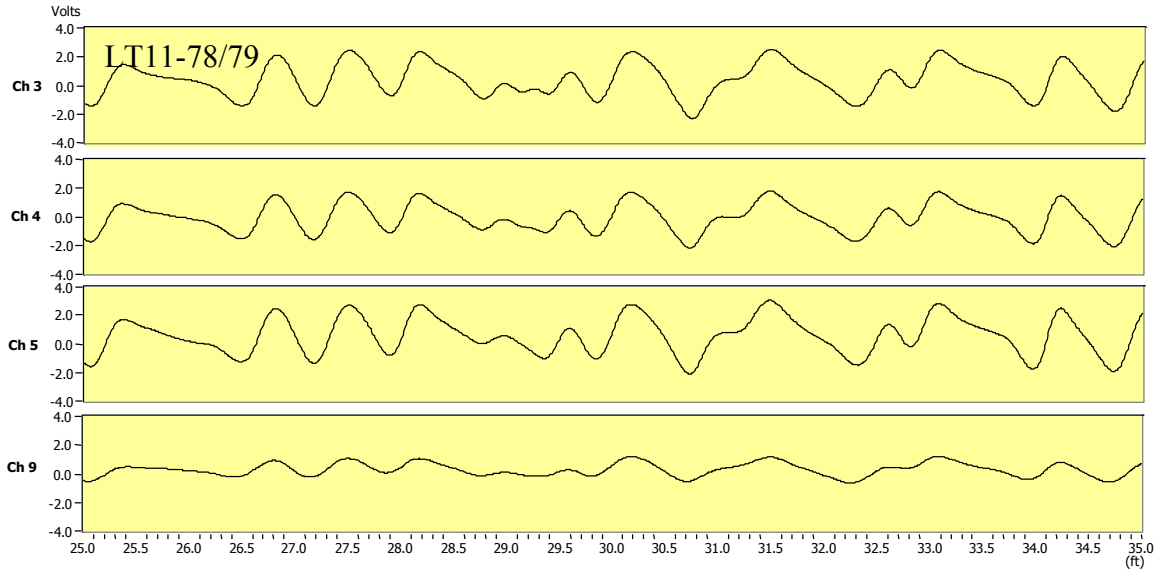


Figure 11 - MFL signals (4 channels) for tendon # 11 between segments 78 and 79 (data for 5 feet of the tendon on both sides of the joint between segments 78 and 79)

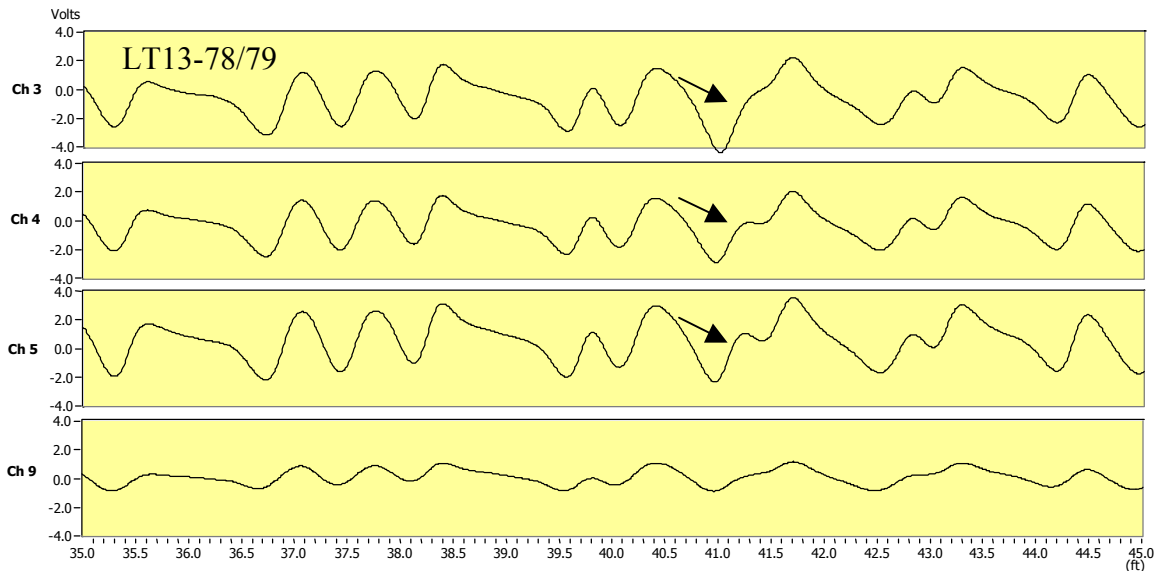


Figure 12 - MFL signals (4 channels) for tendon # 13 between segments 78 and 79 (data for 5 feet of the tendon on both sides of the joint between segments 78 and 79)

MFL tests were also performed to evaluate the condition of tendons # 13 and # 14 at the joint between segments 75 and 76. Figures 13 and 14 show the results of field tests for the two tendons, respectively. Again, the data display is for a length of 10 feet for each tendon. Approximately five feet of the MFL data for each tendon has been displayed on each side of the joint between segments 75 and 76. Flaw indications are shown in Figure 13 for tendon #13 at the specified location (10.1 feet from the starting

point of the test or the West end of tendon # 14). Due to the smaller signal amplitudes shown in Figure 13, it may be concluded that a smaller flaw is present at this location.

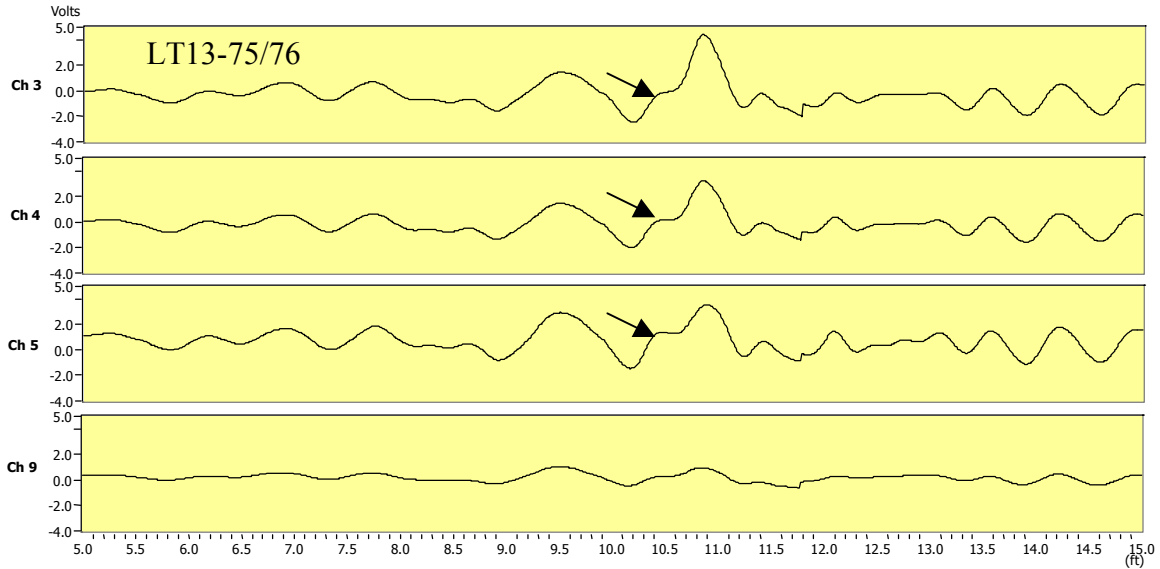


Figure 13 - MFL signals (4 channels) for tendon # 13 between segments 75 and 76 (data for 5 feet of the tendon on both sides of the joint between segments 75 and 76)

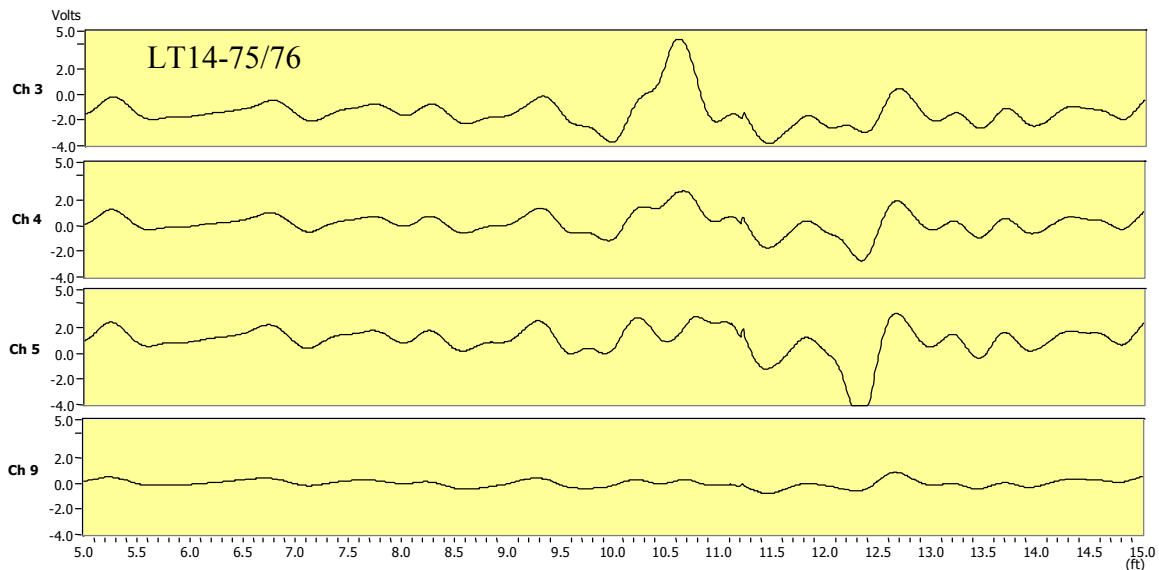


Figure 14 - MFL signals (4 channels) for tendon # 14 between segments 75 and 76 (data for 5 feet of the tendon on both sides of the joint between segments 75 and 76)

B. Impact-Echo (IE) Testing:

The Impact-Echo (IE) technique is a non-destructive test method that allows for accurate measurement of a member’s thickness as well as detection of internal defects such as voids in P-T ducts and in concrete, honeycombing, cracks, delamination, and poor quality concrete. An impact-echo test consists of introducing a small mechanical impact on the concrete surface and measuring and recording the resulting surface displacements close to the impact point. The small impact on the concrete surface results in stress pulses that propagate into the concrete along spherical wave fronts in the form of compression or P-waves and in a direction normal to the wave fronts. In addition, there are shear or S-waves that propagate inside the concrete in a direction perpendicular to the direction of the P-wave propagation. Also, surface waves, also named Rayleigh or R-waves, travel on the surface away from the impact point. The P- and S-waves travel through the material and are partly reflected back by internal interfaces, i.e., from defects, or external boundaries. The arrivals of these reflected waves at the surface, where the initial impact was generated, produce surface particle displacements, which are converted into electrical voltage by a receiving transducer. If the transducer is placed close to the impact point, the displacements will be dominated by the effect of the P-wave arrivals. However, the initial portion of the displacement waveform will also include a dominant R-wave displacement effect. This effect is easily identified and distinguished from the reflected P-wave arrivals by considering the difference in the propagation velocities and the resulting times for arrival of the P- and R-waves at the receiving transducer. The waveform may also be evaluated to determine the travel time, D_t , from the time of the impact to the arrival of the first reflected P-wave. If the P-wave propagation velocity, C_p , in the test object is known, the distance, T , to the reflecting interface can be calculated. The interpretation of the data in the time-domain, however, can be very time consuming and complex. A more effective approach is to construct a frequency spectrum of the time domain data and to evaluate the frequency values (or dominant frequency peaks) that correspond to reflections from certain interfaces inside concrete. The frequency, f_p , is calculated as:

$$f_p = C_p/2T \dots\dots\dots(1)$$

Where the term $2T$ in the above expression is the wave travel path for one full cycle (both the initial and reflected waves). If the propagation velocity and the frequency of arrivals (or reflections) of the P-wave in a concrete slab are known, then the thickness of the slab or the distance to the internal interface can be calculated as:

$$T = C_p/2f_p \dots\dots\dots(2)$$

The P-wave propagation velocity in the test object can usually be measured experimentally, through conducting a simple calibration procedure at the test site, and the frequency content of the recorded waveform is easily obtained using a Fast Fourier Transform (FFT) algorithm in a computer.

The instrumentation for the impact-echo test system is composed of three major elements: an impact source, a receiver, and a computerized data acquisition system with a

capability of waveform analysis both in the time and frequency domains. Normally, impact devices that have been used for IE testing are small steel balls. Each impact load applied on the concrete surface is assumed to be in a half-sine shape with loading duration from approximately 25 to 100 microseconds. Duration of the applied impact load influences the magnitude of the wavelength of the propagating wave within the material. Only flaws with lateral dimensions larger than the wavelength of the propagating wave may be detected by the impact-echo test. Therefore, it is important to apply an impact load with an appropriate duration value in order to be able to detect flaw sizes of interest. The receiver is normally a displacement sensor that converts mechanical surface displacement at a point on the concrete to an electrical voltage, or a signal, as a function of time. The data, or the signal, is normally transmitted to a data acquisition system for recording and analysis. The data acquisition and analysis system performs a conversion of the analog data into a digital format and it computes both the time and frequency information from the recorded data. Figure 15 shows typical time and frequency graphs for an impact-echo test.

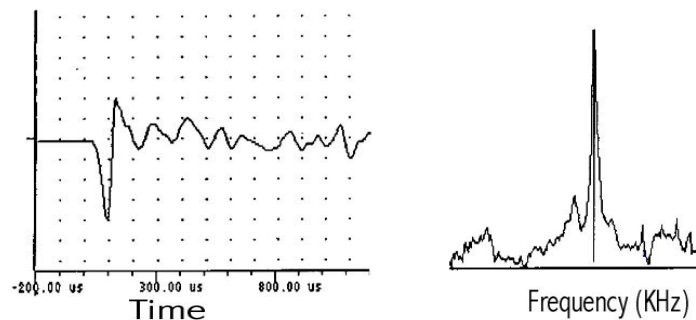


Figure 15 – Time and frequency graphs for an Impact-Echo test data

When a stress wave impinges on a boundary between two media, for the case of the normal incident, only the P-waves are generated. The amplitude of the reflected wave primarily depends on the difference between the magnitudes of the acoustic impedance (product of the wave speed and material density) values of the two media. When the acoustic impedance of the second medium is larger than that of the first, i.e., concrete/steel interface, the displacement amplitude from the reflected wave is of the same sign as that of the incident wave. Since, however, the direction of the propagation is reversed on the reflection, this corresponds to a phase change of 180 degrees in the vibrations of the surface particles. Consequently, the period of the vibrating surface particles due to the arrival of the reflected P-waves from a concrete/steel interface is twice as large as that for concrete/air interface. As a result, the frequency of the reflected P-waves generated at a concrete/steel interface is one-half of those generated at a concrete/air interface. This is a characteristic feature that may be used to identify frequency components corresponding to wave reflections from reinforcing steel bars or elements in concrete structures.

Laboratory and field studies have been performed to evaluate the condition of grout and to detect grout voids inside of P-T tendons (Ref. 3). In the laboratory studies, concrete samples with partially grouted P-T tendons were fabricated and tested with impact-echo equipment. From these tests, it was concluded that grout voids inside of P-T ducts could be detected reliably.

IE Field Testing – The impact-echo equipment developed by the author was used to evaluate a selected number of P-T tendons in the Ramp D Bridge at the Fort Lauderdale International Airport Interchange. The Impact-Echo tests were conducted for test points located directly over marked lines indicating the locations of the post-tensioning ducts in the top slab of the bridge. These tendon locations were determined by others using either the ground penetrating radar technique or by physical measurement based on available information on contract drawings and documents for the bridge. In this work, it was assumed that each IE test for a P-T tendon was conducted at a test point that was located directly over the tendon's centerline. Therefore, it should be understood that the accuracy of the IE test results reported herein hinges on the correctness of the identification and accuracy of the marking of the tendon's locations on the bridge deck. Furthermore, the IE test results could sometimes be difficult to clearly interpret when there are several interfering elements, such as reinforcing steel, nearby P-T tendons, or close boundaries, inside and around the concrete. The resulting wave reflections from these elements produce additional peaks in the frequency spectrum of each test that could make the interpretation of the results more difficult. In general, in an IE test of an internal P-T tendon that is located in the close vicinity of interfering elements, the operator will attempt to detect ungrouted tendons by identifying two features in the frequency spectrum that is constructed for the test data. First, a frequency peak in the spectrum that is associated with the location of the duct needs to be identified. Second, a specific frequency peak pattern should be found in the spectrum that will help to minimize the effects of the interfering elements present in the concrete. Furthermore, in order to identify a tendon duct as whether fully grouted or not, the results of tests from more than one location need to be examined.

The IE testing for the Ramp D Bridge was conducted in four areas. In addition to these four areas, IE tests were conducted in three local areas of the top slab with known thickness (from direct measurement or from information on contract documents) to establish the longitudinal wave propagation velocity for the purpose of equipment and test calibration. The calibration test points were chosen in areas where no longitudinal P-T tendons were present. The three calibration sites on the bridge deck were:

- 1) A test point located on segment 69, about 45 inches from the inside edge of the South side parapet and about 51 inches to the East of the joint with segment 68,
- 2) A test point located on segment 50, about 38 inches from the inside edge of the North side parapet and about 68 inches to the East of the joint with segment 49, and
- 3) A test point located on segment 86, about 48 inches from the inside edge of the North side parapet and about 78 inches to the East of the joint with segment 85.

The slab thickness at the calibration test point located in segment 50 was determined to be 9.0 inches as it was verified by a direct thickness measurement. The direct measurement of the slab thickness was possible at this point since it was near the wing part of the segment that was cut as a part of the scheduled bridge removal effort. The slab thickness at the other two calibration test points was assumed to be also 9.0 inches. This assumption was based on the available information that is shown on contract documents for the bridge. Considering the known slab thickness at the calibration sites, a longitudinal wave propagation velocity of approximately 140,000 in/sec was calculated. This wave propagation velocity value was used for all subsequent calculations required for the IE tests at the bridge site. Figure 16 shows the time and frequency graphs that are constructed from the response of the IE transducer at the calibration test point located in segment 50. Similar graphs were obtained when IE tests were performed at the other two calibration test points. As shown in Figure 16, a dominant peak frequency value of 7.9 KHz can easily be seen in the frequency spectrum. This frequency component corresponds to the reflections of the P-waves from the bottom side of the concrete slab. A substitution of this frequency value and the known slab thickness of 9.0 inches into Equation (2), as shown above, can result in a P-wave propagation velocity of approximately 140,000 in/sec that was used throughout the remaining IE tests at the bridge site.

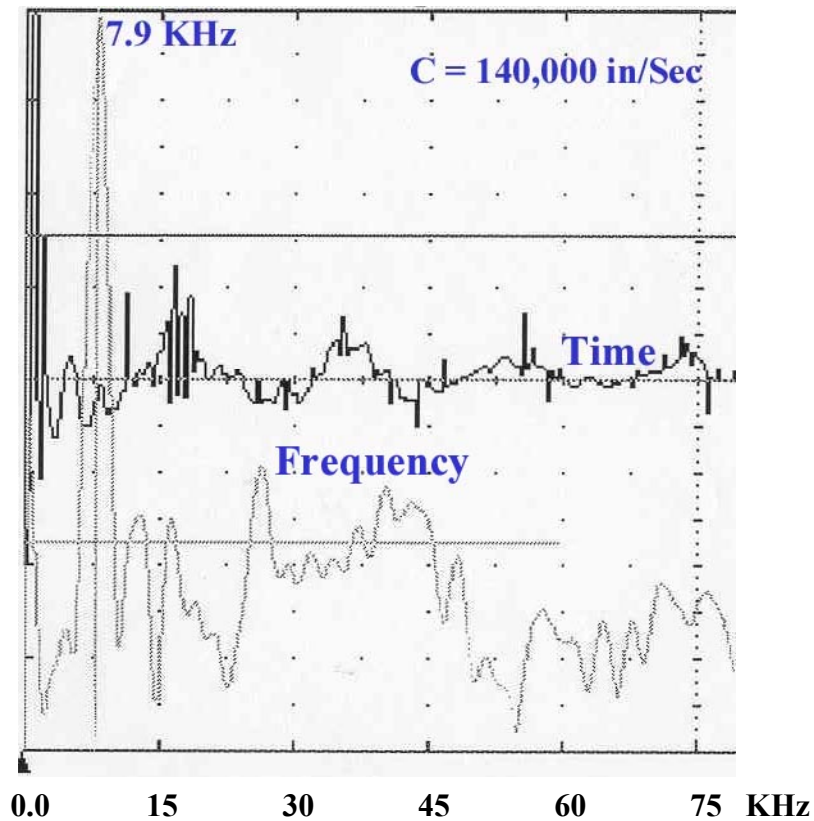


Figure 16 – IE test results for the calibration site in segment 50

The first IE tests were performed on a two-foot length of tendons #8 and #10. The test area was to the West of the joint between segments 86 and 87 on the left (North) side of the bridge. A series of tests were conducted in this region to demonstrate the capability of the IE technique at the presence of personnel from the consultant, DMJM+Harris, Inc., and FLDOT as well as others. Four to five IE test points located directly over the centerline of each tendon were used to conduct the tests. The results of the IE tests indicated evidence of grout voids being present inside of tendon #8 in the tested region. No conclusive evidence of grout voids could be seen in the IE test results for tendon #10 in the tested region. Figures 17a and 17b show IE data for two test points on tendons #8 and #10 at the region described above, respectively. As can be seen in the figures, a dominant frequency peak value of 17.1 KHz (Figure 17a) corresponds to a distance of a void interface approximately 4.1 inches from the concrete surface. The dominant peak frequency value in Figure 17b is 7.9 KHz that corresponds to the slab thickness of 8.9 inches.

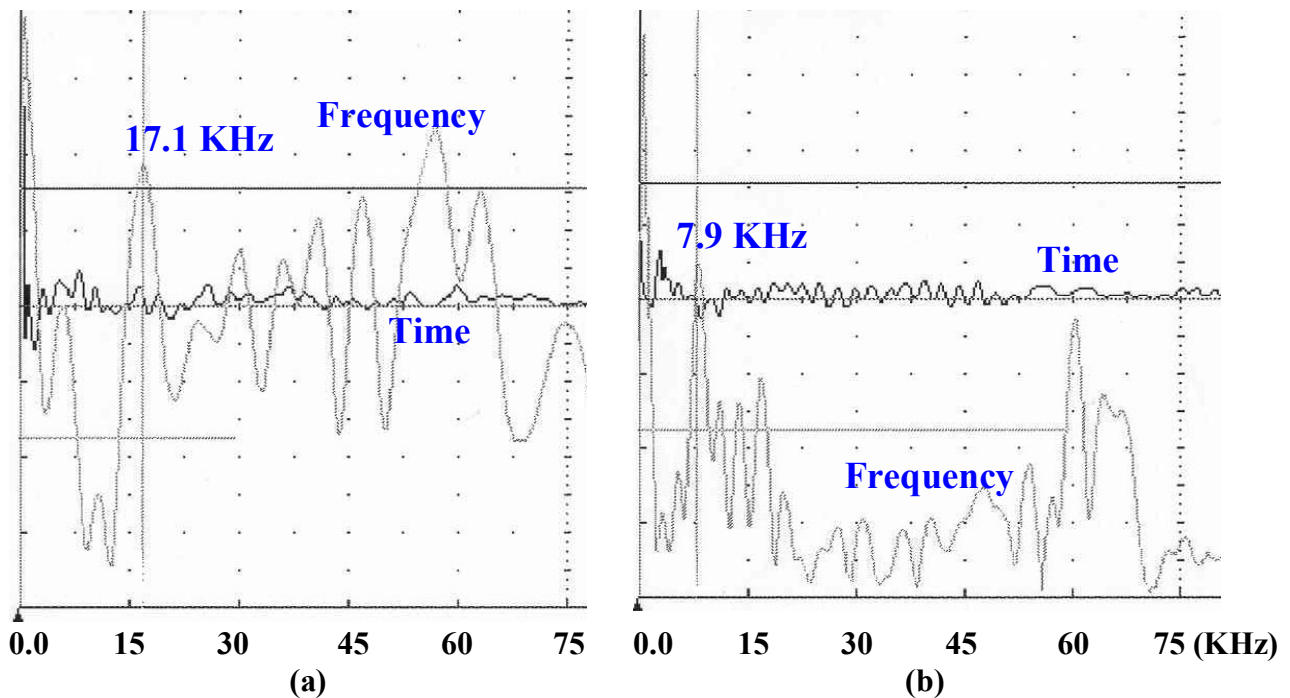


Figure 17 – IE data for tendons #8 and #10 to the West side of the joint between segments 86 and 87

The second area for the Impact-Echo testing was a 3-foot length of tendon #4 on the left (North) side of the bridge and to the East of the joint between segments 68 and 69. Test results indicated evidence of grout voids being present inside of the tendon in the tested region. A dominant peak frequency value of 12.3 KHz was observed. This frequency value indicated that the top of the duct was located at a distance of 5.7 inches from the surface.

The third area that IE tests were performed was in segment 69 on the right (South) side of the bridge. All tendons (a total of 10 tendons) were subjected to IE tests in this

area. Five test points were used along the length of each tendon in the segment, except for tendons #3 and #4 where 4 test points were used. No IE indications for any significant grout voids were observed for tendons #9, #10, #11, and #12. Impact-Echo indications for grout voids were observed for tendons #3, #4, #5, #6, #7, and #8. The IE results indicated partial voids for tendons #3, #4, #5, and #8. The recorded IE test results showed that tendons #3 and #4 are located deeper in the slab. Table 1 shows all dominant frequency values for all IE tests that were conducted in segment 69. In the first column of the table, each value shown within parentheses indicates the location of the test point to the East of the joint between segments 68 and 69. When there are more than one frequency values listed for a test at a specific point, it indicates that more than one strong reflection frequency values were observed in the frequency spectrum for that test. Often for partially grouted P-T ducts, there are at least two dominant frequency peaks in the spectrum. Out of the two peaks, one corresponds to the wave reflections from the top of the duct, if there is a void, and the other is due to the reflections from the opposite face of the slab but with a wave travel path around the duct. Again, it must be noted that a theoretical peak frequency value of 17.8 KHz would correspond to the location of the top of a 2 5/8 inch diameter P-T duct that has its centroid located at 5.25 inches from the concrete surface. For the 9.0-inch thick concrete slab of the bridge, the expected peak frequency value is 7.8 KHz. The frequency values shown in the table vary from the expected value for the reflections from the top of the P-T ducts in the Ramp D Bridge due to variations in the depth of the ducts inside the slab. Figures 18a and 18b show IE results at test point 4 for tendon # 11 (no void) and at test point 4 for tendon # 6 (void).

Table 1 – Frequency values (KHz) for IE test points in Segment 69

Test Points	Tendon ID No.									
	3	4	5	6	7	8	9	10	11	12
1 (1' – 4")	NDP	15.5	15.1/18.0	4.6/14.2	16.1	4.6/16.1	NDP	5.5/10.9	NDP	6.1/14.0
2 (4' – 4")	11.9	13.4	16.1	14.2	14.6	15.4	12.2	NDP	18.0/27.3	7.3/18.2
3 (6' – 8")	13.7	13.7	14.3	13.1	14.3	13.6	12.8	5.5/12.5	21.0	21.5
4 (8' – 8")	NDP	14.3	NDP	16.1	NDP	NDP	NDP	18.7	NDP	19.2
5 (10' – 0")	-	-	17.1	17.1	20.4	NDP	NDP	6.1	26.8	NDP

(NDP = No Dominant Peak)

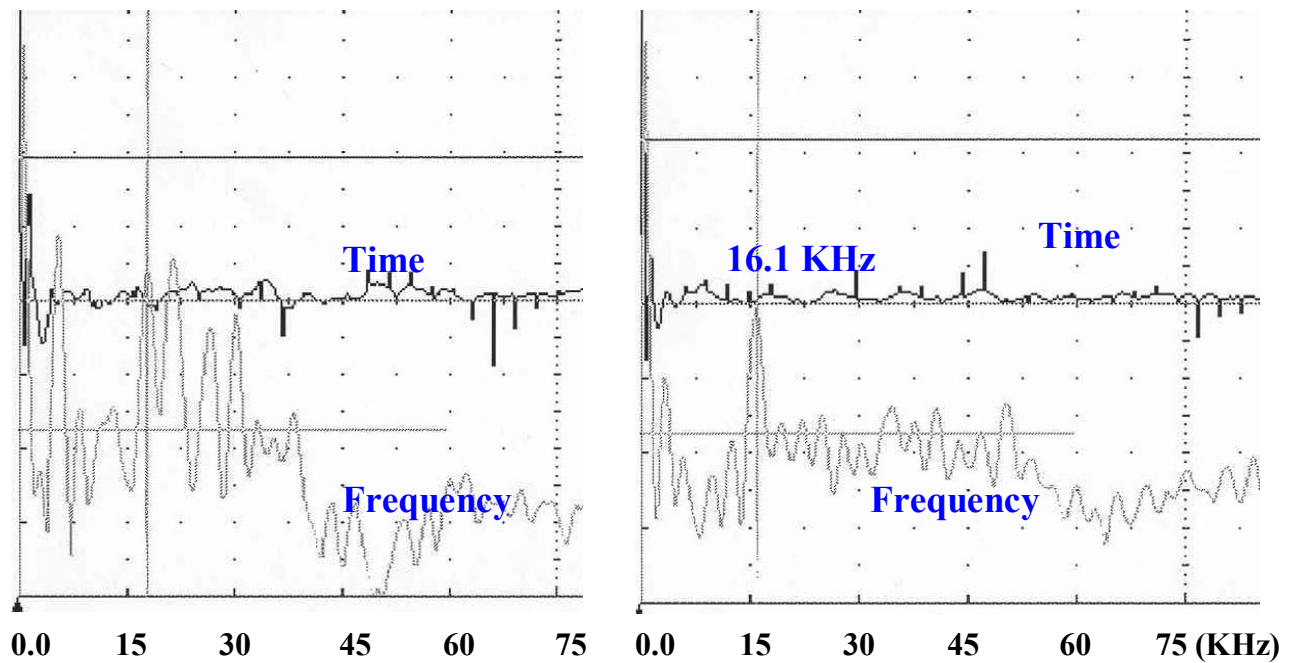


Figure 18 – (a) IE data at test point 4 for tendon # 11 (no grout void) and, (b) at test point 4 for tendon # 6 (grout void).

The fourth IE test area was along tendon #10 on the right (South) side of the bridge in segments 54, 55, and 56. IE tests were performed at several points every 18 inches along the length of the tendon for the three segments. Test results indicated evidence of grout voids being present inside of the tendon in segment 56. In segment 55, there were no strong indications of any significant voids in the tendon. IE indications for partial grout voids were observed for the five-foot length of the tendon adjacent to the joint between segments 53 and 54 (on the East side of the joint). The required time for the IE tests for the three segments was about one hour. Figures 19a and 19b show IE data for tendon # 10 in segments 56 (void) and 55 (no void), respectively.

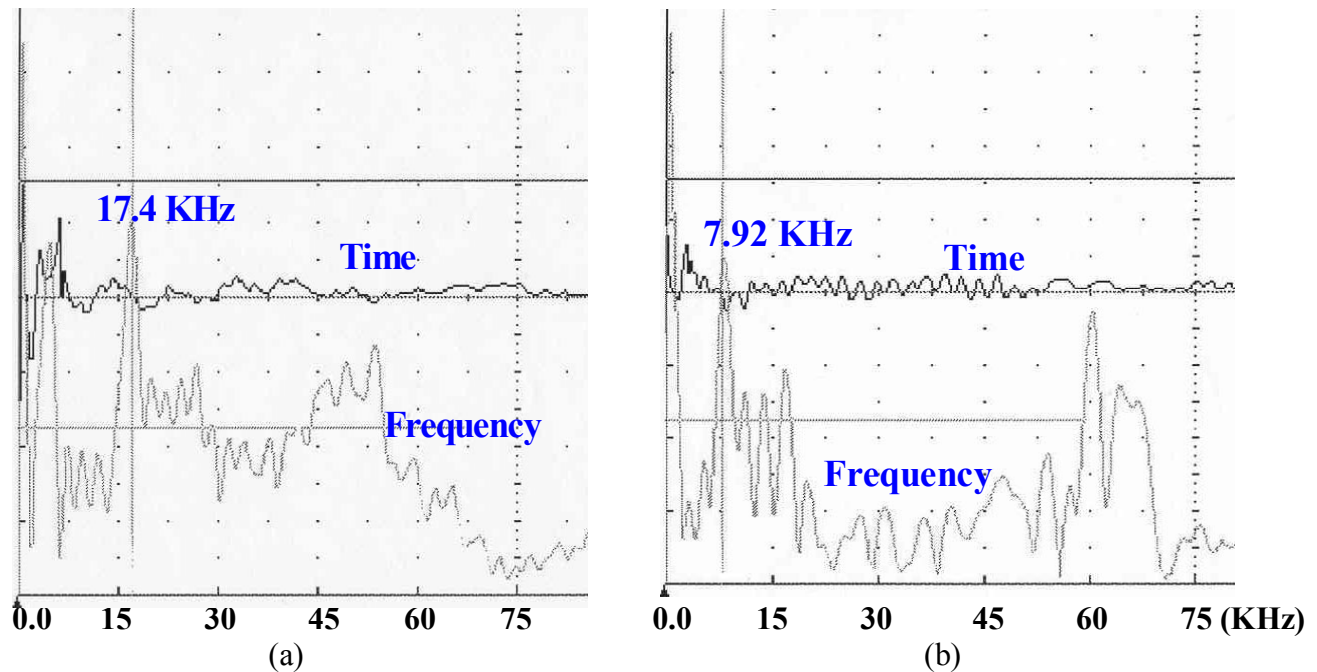


Figure 19 – IE data for tendon # 10 (a) 3'-0" West of the joint between segments 56 and 57 (void), (b) 9'-0" West of the joint between segments 55 and 56 (no void).

C. Conclusion:

The magnetic flux leakage (MFL) equipment was used without any difficulties to test all P-T tendons that were identified for testing at the Ramp D Bridge. The MFL testing at the site produced results that were expected under the existing conditions. The MFL testing of the internal P-T tendons of the Ramp D Bridge did not result in conclusive determination of the status of the tendons due to a number of reasons. These reasons were;

- The tendons were located at a relatively deep distance of 5.25 inches or greater from the deck surface. At the end anchor locations, the tendons were bent deeper into the concrete. This significantly reduced the magnetic flux intensity in the tendons making detection of small flaws not possible. To detect small flaws in the tendons at the stated depth, stronger magnets than those in the existing MFL equipment must be used.
- From the laboratory studies, it was determined that flaws of larger than 33% of the cross section of each tendon could be detected under conditions similar to those for the Ramp D Bridge. This information was made known prior to the field test. It was learned that the man-made flaws produced in the tendons prior to the MFL test were equal to or less than 25% of the cross section of each tendon.
- There were variations in the depth of some of the P-T tendons within the concrete deck.

- Tendon layout in the bridge was geometrically more complicated than typical conditions.
- Locations of the tendons as marked on the deck were not accurate in all areas. This could be verified easily by observing that some of the tendon locations were marked to cross the locations of lifting holes for the segments where there can be no P-T tendons.
- Significant amount of reinforcing steel, transverse P-T tendons, and steel blocks (at end anchors) were located near the tendons and closer to the deck surface. These steel elements caused stronger and frequent magnetic field disturbances that made flaw detection more difficult.

The impact-echo (IE) equipment was used at the bridge site without any difficulties. Although in most areas there were interferences from the nearby steel elements inside the concrete deck, it was possible to make an assessment of the condition of grouting inside of each of the P-T ducts in the areas tested.

References

1. Ghorbanpoor, A., Borchelt, R., Edwards, M., and Abdel Salam, E., "Magnetic-Based NDE of Prestressed and Post-Tensioned Concrete Members – The MFL System," Final Report No. FHWA-RD-00-026, Federal Highway Administration, U.S. Department of Transportation, May 2000, 107 pages.
2. Ghorbanpoor, A., "Evaluation of the P-T tendons of the Mid-Bay Bridge by the MFL Technique," Report submitted to Florida DOT, 2001.
3. Ghorbanpoor, A., "Evaluation of Post-Tensioned Concrete Bridge Structures by the Impact-Echo Technique," Final Report No. FHWA-RD-92-096, Federal Highway Administration, U.S. Department of Transportation, December 1993, 92 pages.

Final Report

Inspection of Post Tension Cables in concrete using High
Energy
X-rays, Ramp D at the Ft Lauderdale Airport

By

Michael Pinna, Consulting Engineer
President of HESCO

April 2002

Final Report

Inspection of Post Tension Cables in concrete using High Energy X-rays, Ramp D at the Ft Lauderdale Airport

By

Michael Pinna, Consulting Engineer
President of HESCO

Scope

To determine High Energy X-rays capability to inspect and detect flaws in post-tension concrete roadways.

Introduction

The system chosen was a Varian Mini-Linatron operated by HESCO Corp. of La Honda, Ca. The equipment utilizes standard s-band technology common to most industrial linacs, and produces the same high radiographic quality through thick sections as can be expected from these fixed units. The overall system has been condensed and repackaged for field use. It consists of a power supply cabled to a small remote control, an R.F. generator and the small linear accelerator itself.

Location and Description

The Ramp D overpass at the Ft. Lauderdale Airport is a Box style overpass made of high tensile strength concrete construction. The roadway is segmented or sectioned and joined together with tongue and groove joints, epoxy, and post tensioning cable. The ramp is a banked and pitched roadway with an approximately 20° downward pitch running south to north. The bottom side of the roadway was accessible thru a man hole at the underside of the box structure.

Site Preparation

Sixteen locations were chosen (8 per side) along a 300 foot long stretch of the roadway. The locations were marked top and bottom in order to align the x-ray source with the film and locations were identified by the segment designations. Locations identified as R for Right were re-identified as S and L for Left was re-identified as SS.

Equipment Set-up

The HESCO 6MV portable linear accelerator (LINAC) was air freighted and trucked to the site. FDOT supplied the "Snoop" man lift, night lighting, and portable generator. The contractor supplied a Gradeall type forklift. The Gradeall type forklift was chosen because it has an articulating head which makes possible the angled shots required for this job.

The x-ray and rf-heads were strapped to the forks and covered for whether protection. The modulator (power unit) and chiller remained in the truck. The control box was moved to a safe area just below the roadway.

Film Identification

The film locations were identified with lead lettering and one steel 2.7 film side penetrometer. Source side wire penetrameters were also placed on the roadway. The locations of the lead lettering were painted on the underside of the roadway for future reference.

X-ray Procedure

Prior to testing, a radiation survey was performed to determine radiation safety compliance, (see Radiation Safety). The testing was conducted by two technicians, one technician positioned and operated the x-ray machine, while the second technician remained inside the box roadway to position the film for each location. The film was placed into position using a telescoping pole and tray which held the film against the underside of the roadway.

Radiation Safety Survey and Procedure

A radiation safety survey was conducted to determine radiation levels in the test area. The x-ray source is collimated to a 30° forward primary beam and is positioned down towards the roadway. A walking survey determined that the radiation levels directly below the x-ray beam was 5 mr/hr, the highest recorded level was at 20 mr/hr, approximately 200 ft away at the adjacent freeway off-ramp leading to the Ft. Lauderdale air terminal.

The Florida Highway Patrol provided road control during testing. Prior to each shot, (x-rays on), the x-ray tech would signal that the roadway be secured. Personnel on site would move to safe locations and the shot would begin. Shot times varied from a couple of minutes to 18 minutes for the thickest angled shot. Closing the roadway was a precautionary measure when taking into consider the recorded levels. A typical inspection would allow traffic to flow through the test area making the following assumptions: Cars traveling at 45 miles per hour or 66 ft/sec would receive a dosage of less then .02 mR total. Cars traveling at 35 miles per hour or 51 ft/sec would receive a dosage of .03 mR total. Even a bicyclist traveling at 10 miles per hour or 14 ft/sec would receive a dosage of .12 mr which is certainly less then the 2 mr/hr requirement.

The x-ray technician inside the box measured readings of less then .15 mr/hr up to 20 ft away from the primary beam.

Film Viewing Results

High energy X-rays has the ability to penetrate and view defects in concrete as small as 1/16" or less. The table below lists all visible defects in the grout, strands, and concrete. The defects listed as ground strands may also be interpreted as voids on top of the strands

The areas that contain the fabricated defects offer an extra layer of interpretation. The exploration and back filling of an area with grout creates its own set of defects and creates density changes due to the difference in material and installation techniques. As an example, the concrete saw cutting lines are visible as sharp lines cutting across the cable. Locations that were not excavated and backfilled, for example segment 79-11B, contain less defects and a uniform film density between cabling, grout, and concrete.

Table 1

Segment	Hole I.D.	Defects	comments	Exposure time (minutes)
89	S1	Broken and cut strands, voids in grout		5
88	SS1	Voids in grout, ground strands		6 1/2
88	13C	voids in conduit at left, voids in concrete		2 1/2
88	13D	Voids in grout, ground strands, strands have been separated, broken conduit casing		18
87	11A	1" x 1/2" void in center of film w/smaller 1/4" voids surrounding, possible broken cable B-B, coil of wire		3.3
86	SS3	Cable has been ground/cut in two, partial pcs of rebar, pulled back conduit sheeting is visible	Shot is off center	4.6
86	SS9	Cable conduit on right contains large void and is ground and cut, cable in center of view is ground and cut, missing sections of cable, strands of center cables or broken at bottom of view. Partial pcs of rebar, large "staple" in lower left also electrical wire, voids in grout	Shot is off center	2 1/2
85	5A	Film moved, not readable	Film or source moved during shot	4 1/2
79	SS9	Saw cut from A to A, cable conduit and some cable cut, missing section of rebar, saw cut from B to B, voids in concrete		2.2
79	5B	Small voids in grout	Shot is off center	4 1/2
79	13A	Large void in concrete by wire IQI, breaks in conduit wall, broken cable strand below "B" on right, voids in grout		3
77	11B	Voids in concrete, cable in center has large strands	Shot is slightly off center	8.3
76	S1	Not tested		
76	SS3	Not tested		
69	11B	Not tested		
56	S5	Not tested		

X-ray Films

The x-ray film used was Kodak AA, size 14" x 17". Shot times varied due to concrete thickness variations.

The x-rays have been sent to Habeeb Saleh for digitization. Habeeb is with the Federal Highway Administration, NDE Validation Center, 6300 Georgetown Pike, Mclean, Virginia, 22101, Phone # 202-493-3123, E-Mail Habeeb.Saleh@igate.fwha.dot.gov. Digitized x-rays should be available early late next week.

Conclusion

High Energy X-rays are a very affective method for inspection of post-tensioned concrete roadways. An x-ray image which is a picture, can be reviewed and discussed, and held for future reference of the specific area or to develop a historical record and case studies to help improve the fabrication process or design of the structure.

Project Notes, Lessons Learned, Improvements

- 1) This project was a coordinated effort between HESCO, DMJM-Harris, Florida Department of Transportation, Federal Highway Administration, and PCL .
- 2) An acceptance/rejection criteria must be established for x-ray interpretation of grouted areas and post tensioned cable.
- 3) Positioning the x-ray machine above approximately equals the time to position and locate the film.
- 4) Road or lane closer of the roadway being inspected is essential for inspection. Closer of adjacent roadways may not be necessary as with this project. Future inspections may be performed with extra lead shielding to limit scatter radiation.
- 5) The cost for inspection of a single overpass is comparatively high since a high percentage of the cost is the transportation of the machine and personnel. Longer-term projects at multiple locations will prove to be more cost effective.
- 6) Road closer coordination took between 25% to 50% of the time for each x-ray location.
- 7) Film review should be closely coordinated with cognizant department of FDOT.
- 8) Digitized x-rays can be put into a computerized format and sent to various locations via E-mail.
- 9) Future advancements in machine portability will allow the x-ray machine to be placed inside the structure, further increasing radiation safety and decreasing the need for time consuming and costly traffic management.
- 10) See Caltrans report attached.

USE OF A PORTABLE LINEAR ACCELERATOR TO RADIOGRAPH BRIDGE COMPONENTS

Philip J. Stolarski and Paul Hartbower
Department of Transportation, State of California
CALTRANS
Sacramento, California

This paper will discuss the characteristics and uses of portable linear accelerator x-ray sources for use in field inspections of bridges and associated structures.

Overview

The advent of a portable source of very high energy x-rays has opened up inspection possibilities in a wide range of environments. Applications have included such areas as concrete and steel bridges, nuclear waste containers, nuclear and fossil power plants, surface and airborne transportation systems, space launch systems and other thick section problems that cannot be imaged using other NDT methods.

CHARACTERISTICS OF PORTABLE LINEAR ACCELERATORS

Topics will include:

1. Portability
2. High Output
3. Thick Section Penetration
4. Short Exposure Times
5. Image Quality/Resolution

PORTABILITY

Perhaps the most notable attribute of these systems is their portability. For example, a typical 6 Mev unit consists of a remote van mounted control and power module and an at-site r.f. generator coupled via flexible wave guide to the accelerator. The accelerator, at 100 pounds in a roughly 12" cube is the actual working point of the system. Compare this to the refrigerator sized, crane mounted units commonly used for indoor radiography and the real value of this new technology is obvious.

HIGH OUTPUT

The output of portable systems matches that of the fixed systems. That means energies of from 1Mev to 11Mev at photon fluxes of from 15 to 3000R/Min/1 Meter. The control and r.f. drive units are basically the same for each energy, with different accelerators being fitted as needed. This gives the user great latitude for developing exactly the system to meet his needs without the large price differences normally associated with an increase in output.

THICK SECTION PENETRATION

As with output, portable systems can match the penetration capability of fixed units in all respects. An important thing to remember is that these energies have never been available in the field before the appearance of these accelerators. That means otherwise uninspectable areas can now be considered as candidates for NDE examination. For instance, a 48" pre-stressed concrete bridge beam with corrosion indications can now be examined for loss of section in it's tensioning members.

SHORT EXPOSURE TIMES

The very short exposure times, most commonly a few minutes or less, characteristic of accelerators make them much less sensitive to effects such as vibration or ambient radioactivity that limit other work. Radiation perimeter control is likewise made much easier and safer because of the very short exposure times.

IMAGE QUALITY/RESOLUTION

In addition to the shorter exposure times and high energy/output, accelerators have very small focal geometry (<2mm). This is less in most cases than that of conventional x-ray systems and certainly much smaller than isotopic sources. This fact produces much smaller geometric unsharpness values at equivalent source to film distances (SFD). Much greater SFD can be used to achieve higher sensitivity (i.e. 1/1T -vs- 2/1T) and finer film resolution (i.e. type M -vs- type AA) than has been otherwise possible.

FIRST USE IN CALIFORNIA

In 1988, failures of vertical suspender cables on the Guy West Pedestrian Overcrossing Bridge in Sacramento prompted a major research effort to determine the condition of other bridges of similar design. The first application was on the

San Francisco Bay Bridge between San Francisco and Oakland. This is a major cable suspension bridge utilizing vertical suspender cable. The failures in the Guy West Bridge had occurred inside the socket by which the cable attaches to the bridge. Isotope radiography was acceptable for examination of these smaller cables but could not image the large cables and sockets on the Bay Bridge.

Tests of the Bay Bridge sockets using a portable linear accelerator gave clear radiographs of the acceptable condition of it's sockets as well as providing base line data for future comparisons.

Other similar inspections have been done on the Golden Gate Bridge, the Vincent Thomas and Gerald Desmond bridges in Long Beach, the Meridian bridge in northern California.]

OTHER APPLICATIONS

The accelerators success has not been limited to steel structures. A number of inspections were done in support of earthquake damage evaluations after the Loma Prieta quake on various structures including bridges and buildings around the San Francisco area.

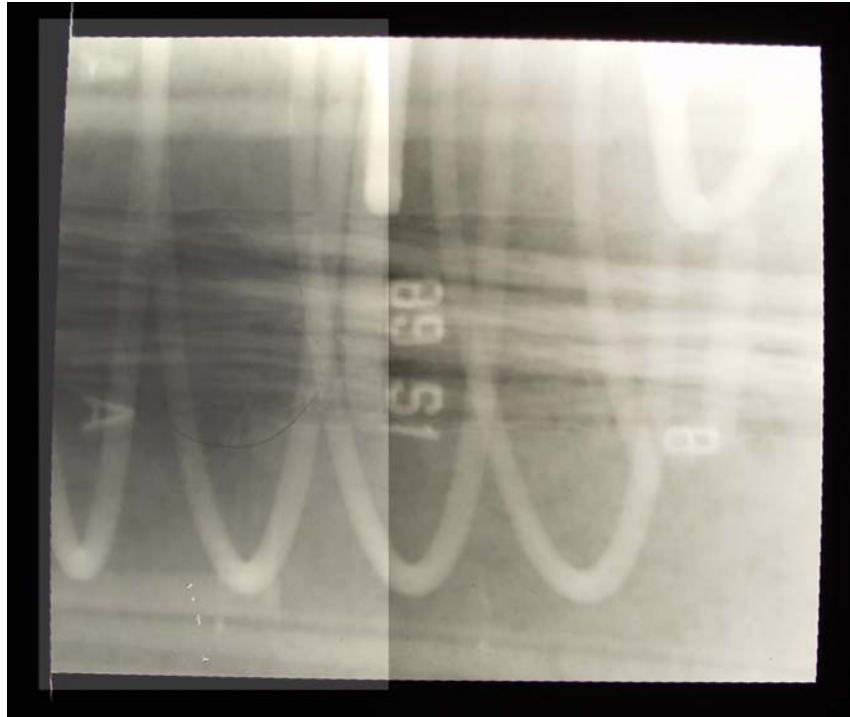
A particularly interesting application was analysis of corrosion indications and collision damage on the Richmond/San Rafael Bridge across the northern end of San Francisco Bay. The accelerator and film were positioned along the bridge from a 21 ft. boat. Radiographs gave clear data on the condition of all suspect tension members.

Caltran's use of the portable accelerator has not been limited to bridges structures. One of the most successful applications was the analysis of a bridge drainage pump associated with the Dumbarton Bridge located near San Jose, Ca.

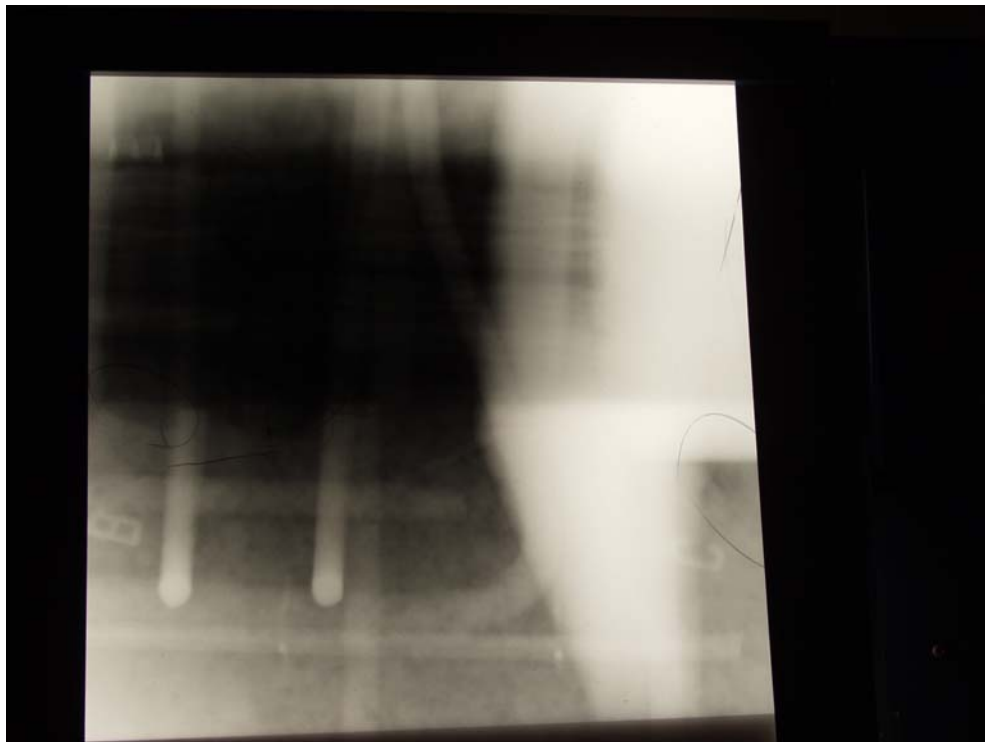
CONCLUSIONS

The experience of Caltrans has shown the portable linear accelerator to be a safe and effective method for radiographic inspection of a wide variety of concerns within the transportation infrastructure of California. The consideration of this technology is recommended for those faced with the examination of large thick section structures that would otherwise defy analysis.

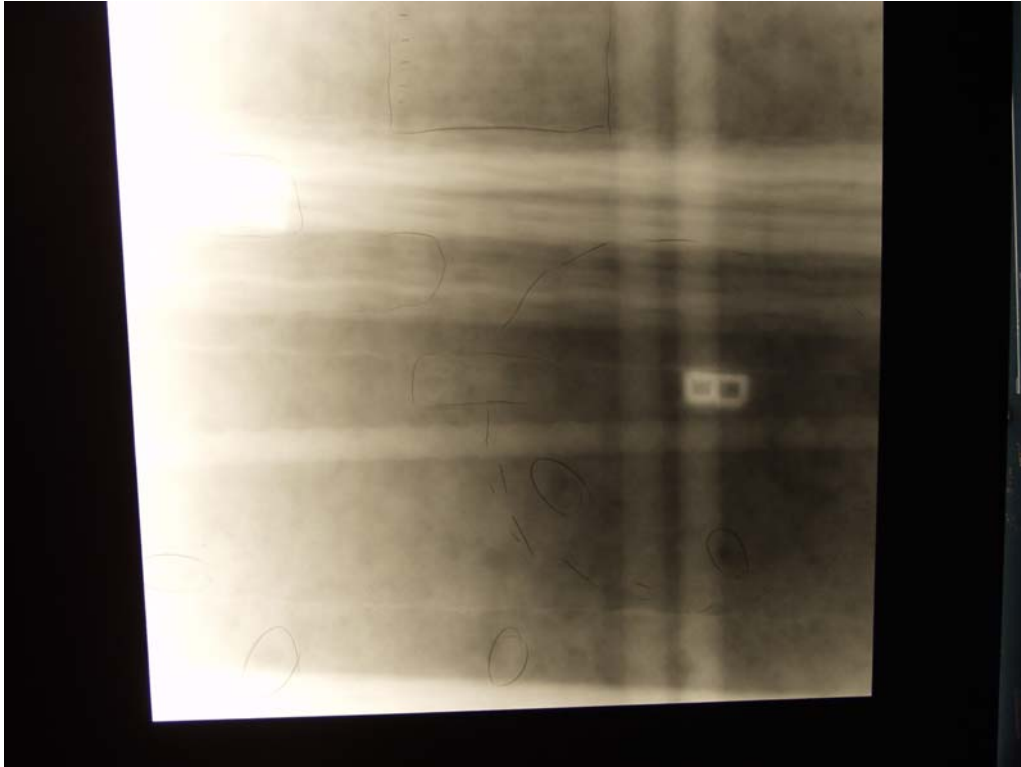
Appendix G – X-Ray Pictures



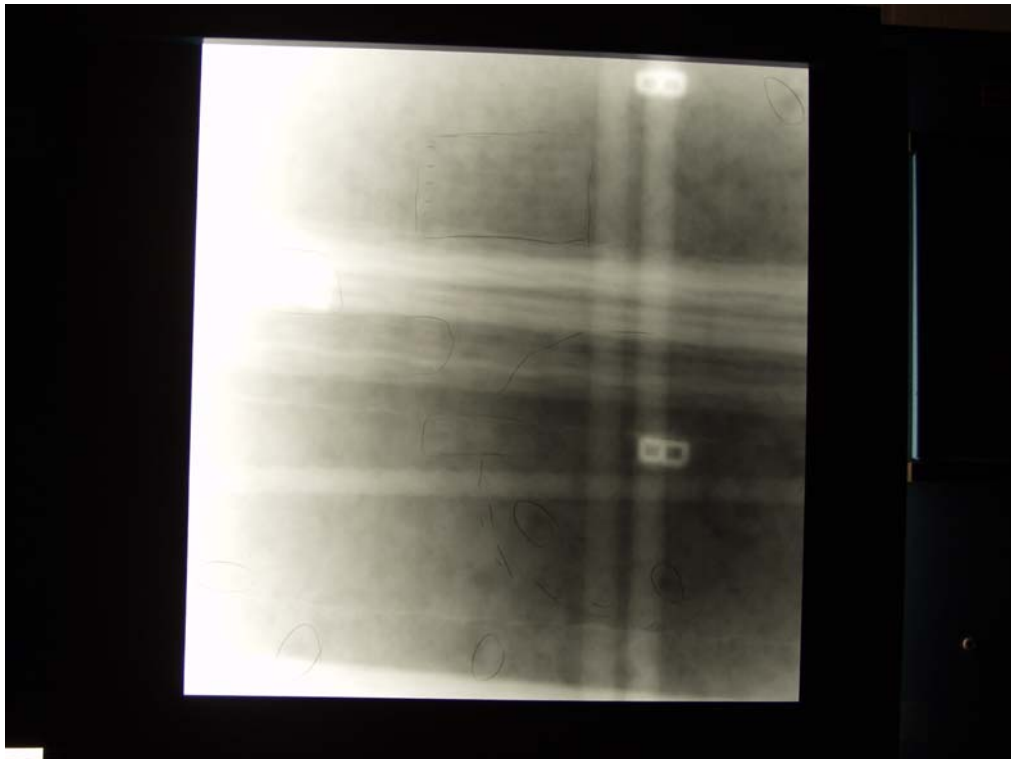
Picture 1 – X-Ray at Segment 89 Hole S1



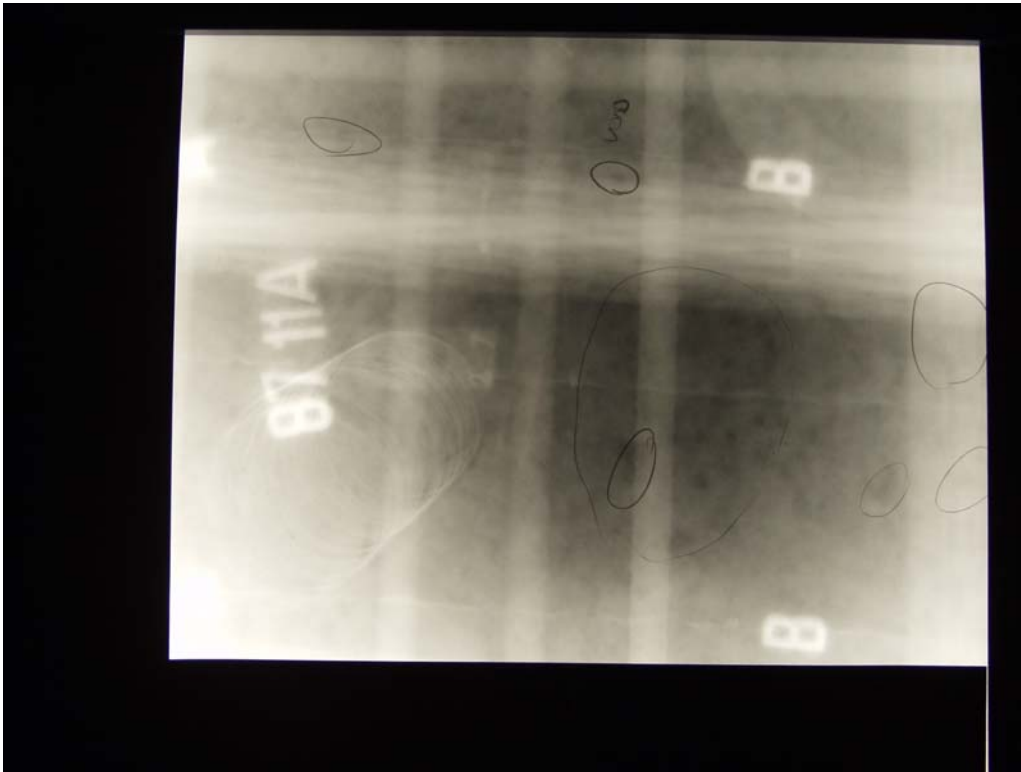
Picture 2 – X-Ray at Segment 88 Hole SS1



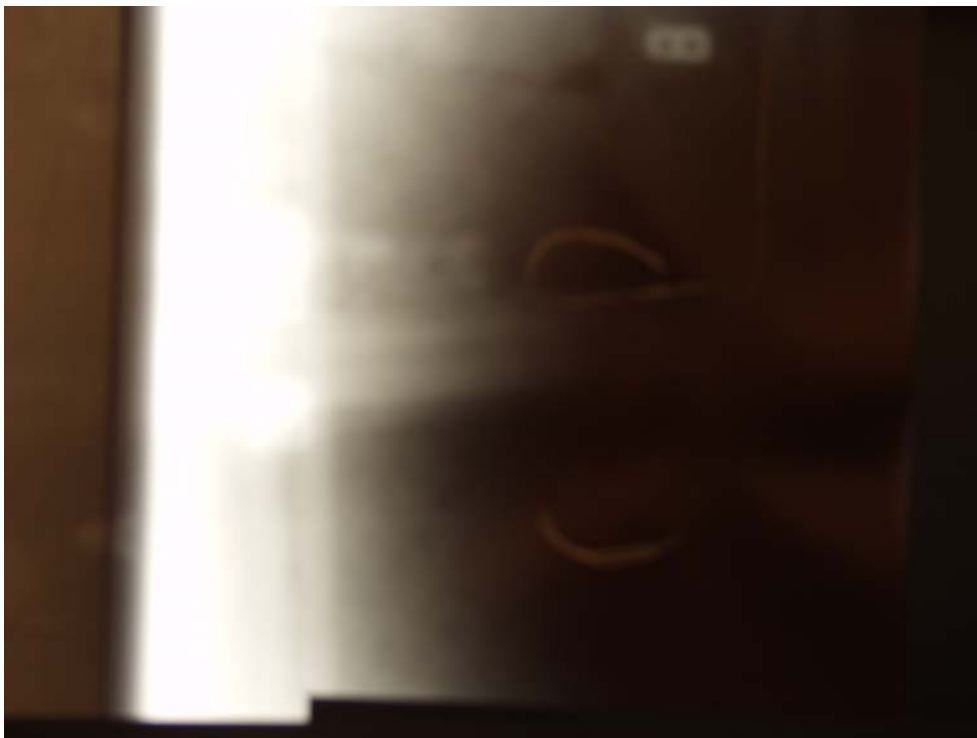
Picture 3 – X Ray of Segment 88 Hole 13C



Picture 4 – X-ray of Segment 88 Hole 13D



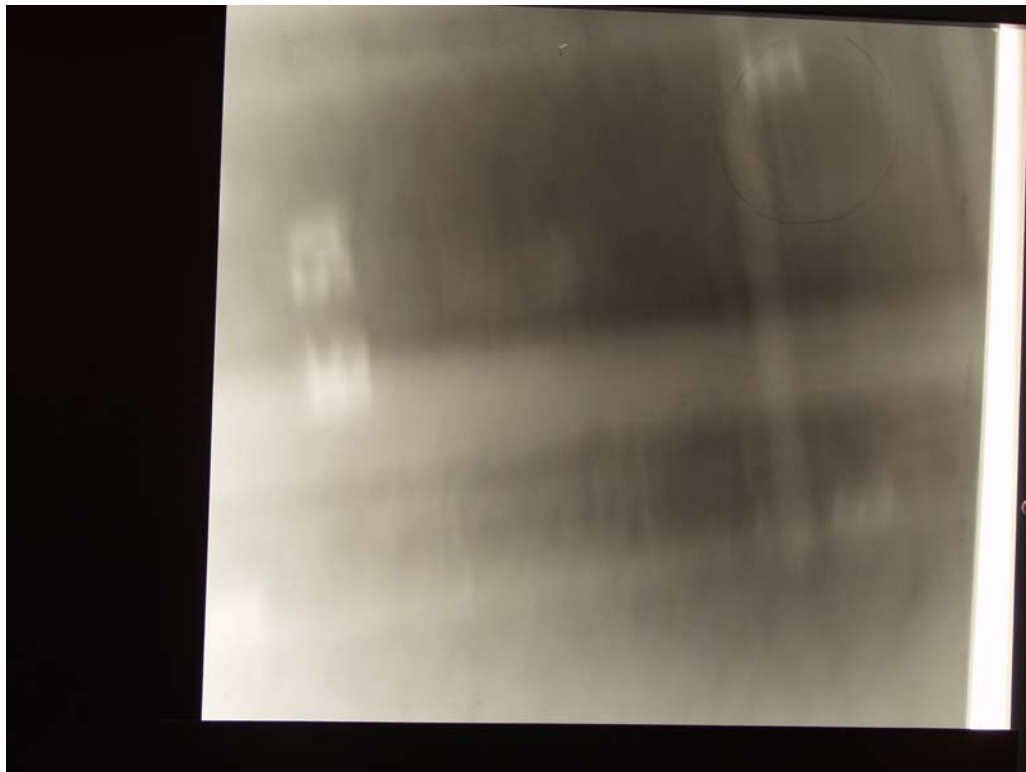
Picture 5 – X Ray of Segment 87 Hole 11A



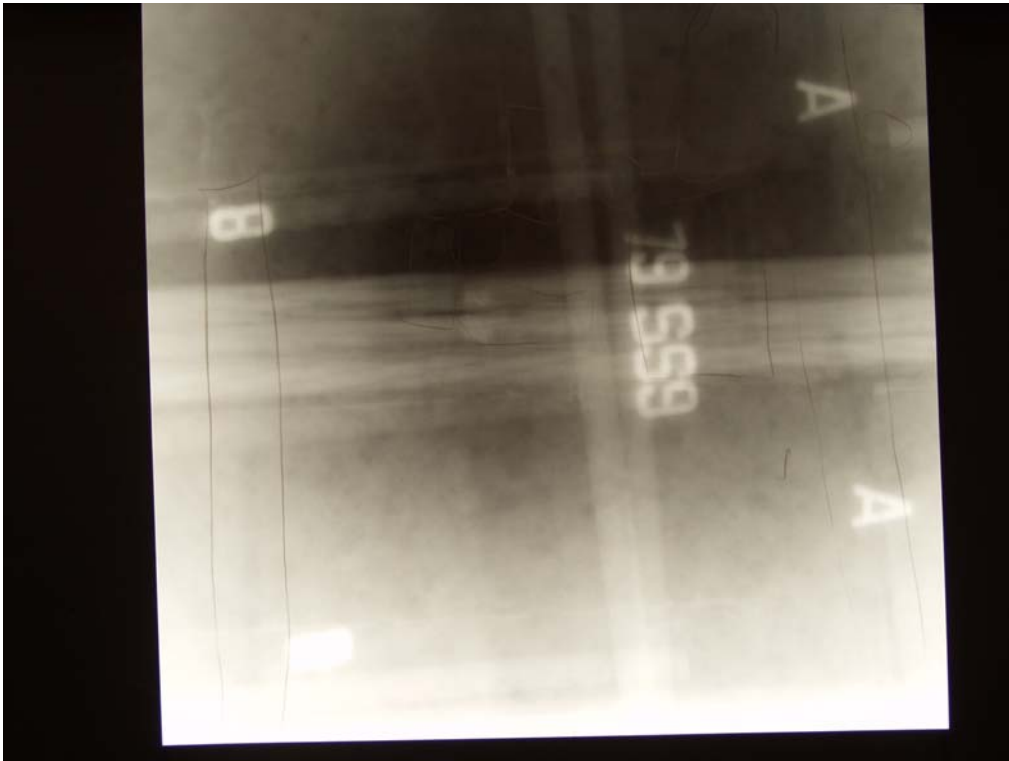
Picture 6 – X Ray of Segment 86 Hole SS3



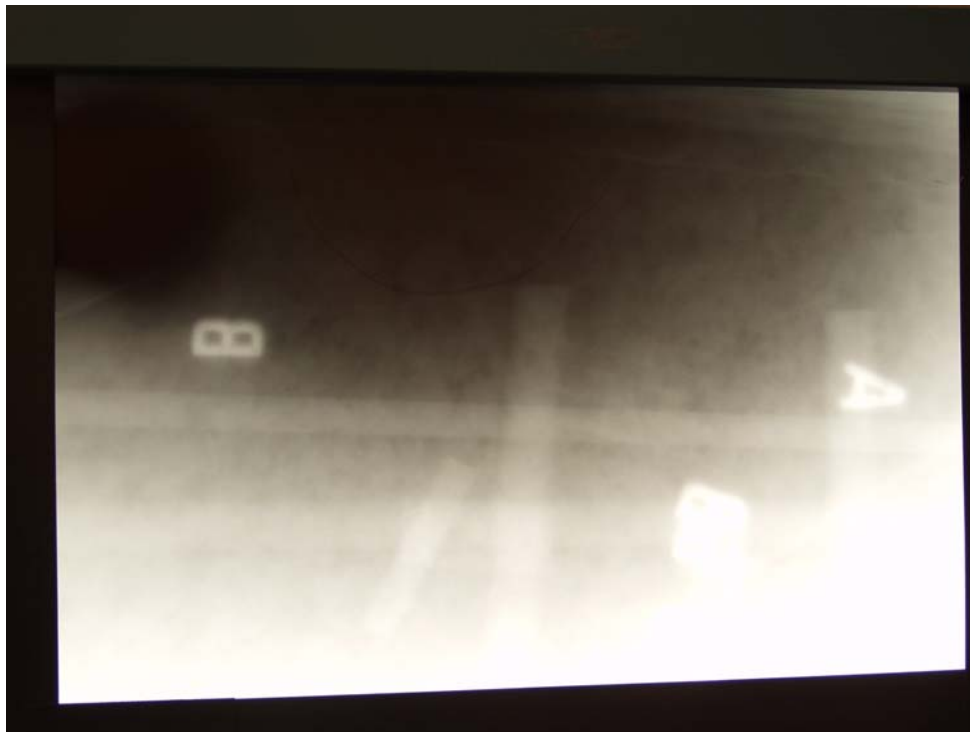
Picture 7 – X Ray of Segment 86 Hole SS9



Picture 8 – X Ray of Segment 85 Hole 5A



Picture 9 – X Ray of Segment 79 Hole SS9



Picture 10 – X Ray of Segment 79 Hole 5B



Picture 11 – X Ray of Segment 79 Hole 13A



Picture 12 – X Ray of Segment 77 Hole 11B

References

1. Timoshenko, S.P. and Goodier, J.N., 1972. *Theory of Elasticity*, 3rd ed. Mc-Graw-Hill.
2. Sansalone, M., and Street, W.B., *Impact-Echo: Nondestructive Testing of Concrete and Masonry*, Bulbrier Press, Ithaca, N.Y., 1997.
3. Abraham, O., and Côte P., Impact-Echo Thickness Frequency Profiles for Detection of Voids in Tendon Ducts, *American Concrete Institute Structural Journal*, May-June 2002.
4. Ghorbanpoor, A., Borchelt, R., Edwards, M., and Abdel Salam, E., Magnetic-Based NDE of Prestressed and Post-Tensioned Concrete Members – The MFL System, *Federal Highway Administration, Publication No. FHWA-RD-00-026*, 2000.
5. Corven Engineering, Inc., Condition Inspection and Maintenance of Florida Post-Tensioned Bridges, *Florida Department of Transportation Report*, Tallahassee, Florida, 2002.